TECTONO-METAMORPHIC EVOLUTION OF THE GRENVILLE FRONT ZONE, SMOKEY ARCHIPELAGO, LABRADOR

JOHN VICTOR OWEN

TECTONO-METAMORPHIC EVOLUTION OF THE GRENVILLE FRONT ZONE, SMOKEY ARCHIPELAGO, LABRADOR

by

© John Victor Owen, B.Sc., M.Sc.A.

A thesis submitted to the School of Graduate Studies in partial fulfillment of the requirements for the degree of Doctor of Philosophy

Department of Earth Sciences
Memorial University of Newfoundland
March, 1985

St. John's Newfoundland

ABSTRACT

The Grenville Front in eastern Labrador coincides with the Benedict Fault, a south-dipping zone of heterogeneously deformed rocks. In the Smokey archipelago, the Benedict Fault transects Paleohelikian plutonic rocks of the Benedict Mountains Intrusive Suite (BMIS). Various members of the BMIS locally contain a north- to northeast-trending pre-Grenvillian planar fabric known as the Makkovik trend. Makkovik trend fabrics are defined by amphibolite-facies mineral assemblages, and their presence characterizes the BMIS as a pre-Grenvillian lithostructural domain, one of three identified in the area. The age of the Makkovik trend is constrained by Rb-Sr (whole rock) dates determined for granulite-facies gneisses ($\geq$ ca. 1.9Ga) intruded by the BMIS, and by a 1676 $\pm$ 77Ma age determined for ferrodiorite-ferrosyenite which intrudes the BMIS.

The White Bear Islands Granulite Complex (WBIGC), a second lithostructural domain, comprises high-grade ortho- and paragneisses, which show evidence of a period of passive retrogression to amphibolite-facies predating the development of Grenvillian fabrics. Relatively high PT-estimates of 830-860 $\pm$ 75°C and 7-8 $\pm$ 1Kbar were determined for the granulite-facies event using the two-pyroxene geothermometer and the Al content of orthopyroxene coexisting with garnet. Relatively low PT-estimates of ca. 685°C and 4.6Kbar were derived using various calibrations of the garnet-orthopyroxene (-plagioclase-quartz) geothermobarometer.

Conditions of pre-Grenvillian retrogression of the WBIGC are estimated at 650 $\pm$ 50°C and ca. 5.5 $\pm$ 1.5Kbar (garnet-cordierite geothermobarometry) assuming P(H2O) $\sim$ 0.4P(total). The garnet-biotite and two-feldspar

geothermometers give variable results which are interpreted to record points on the cooling curve of the WBIGC.

The third lithostructural domain, known as the Bluff Head orthogneiss, consists predominantly of amphibolite-facies granodioritic gneisses typical of the northern Groswater Bay Terrane. Age relations of these gneisses with the BMIS and the WBIGC are uncertain. Both gneissic domains, however, locally contain pre-migmatitic metabasites bearing clinopyroxenes of similar composition, suggesting equilibration under broadly similar metamorphic conditions. The WBIGC and the Bluff Head orthogneiss are thus inferred to have shared a common, early tectono-metamorphic history prior to the emplacement of the BMIS. Pre-Grenvillian retrogression of the WBIGC is most pronounced in the western portion of the study area, and may be transitional into the amphibolite-facies assemblages near Bluff Head. Alternatively, the Bluff Head orthogneiss may record the effects of significant recrystallization during the Grenvillian orogeny; garnet-biotite and two-feldspar temperature estimates for the gneisses are consistent with conditions determined for Grenvillian metamorphism in the area.

A zonal distribution of structural and metamorphic features attributed to the Grenvillian orogeny is apparent from north to south across the Smokey archipelago. Three east-west trending Grenvillian structural domains, separated by major Grenvillian high-strain zones, have been recognized on the basis of contrasting fabric development and metamorphic grade. North of the Benedict Fault, Makkovik trend fabrics are locally retrograded to greenschist-facies assemblages. Greenschist- to lower amphibolite-facies assemblages characterize south-dipping Grenvillian fabrics in a $\sim$3km wide transitional domain to the

south of the Benedict Fault. The Cut Throat Island Fault (CTIF), a south-dipping zone of mylonites, defines the southern extent of the transitional domain. Garnetiferous assemblages of the epidote amphibolite- to lower amphibolite-facies characterize Grenvillian fabrics south of the CTIF. Grenvillian L-S fabrics are most extensively developed in this domain and formed during the second of three phases of folding attributed to the Grenvillian orogeny. Temperatures of Grenvillian metamorphism south of the CTIF are best estimated by low Mn-Ca garnet-bearing mineral assemblages at ca. 550 $\pm$ 30°C (garnet-biotite, garnet-amphibole thermometery). Mineral assemblages suitable for pressure determinations are lacking; however the composition of amphiboles together with the presence of garnet in domain G indicate a southerly increase in lithostatic pressure in the map area.

The Grenville Front zone on the Labrador coast is thus characterized by a southward-increasing Grenvillian metamorphic gradient which has been telescoped across major thrust (or high angle reverse) faults, and by the heterogeneous development of L-S fabrics which overprint pre-Grenvillian structural and metamorphic features. Similar features characterize the Grenville Front zone elsewhere in Labrador, and are consistent with the characterization of this portion of the Grenville Province as a region of significant crustal thickening about 1Ga ago.

ACKNOWLEDGMENTS

This study would not have been possible without the assistance and interest of my supervisors, Drs. Toby Rivers, Brian Fryer, and Tom Calon, and of the staff of the Department of Earth Sciences, Memorial University of Newfoundland. In particular, Dr. Henry Longerich is thanked for instruction on the use of the electron microprobe and for countless hours of informative discussion. Gert Andrews performed all of the wet chemical analyses (A.A.), and Trish Finn prepared half of the Rb-Sr samples, and guided me through the sample preparation procedure for the rest. Pat Browne kept the various financial aspects of the study under control, particularly during the field work. Dr. Charles F. Gower is thanked for his ongoing interest in the project, and for numerous discussions both in and out of the field. Drs. A. Davidson, C.F. Gower, J. Martignole, and D. H. Wilton are thanked for their painstaking review of the thesis. Finally, I thank my friends John Greenough and Sheila Moores for their patience and encouragement over the course of my studies at Memorial.

CONTENTS

TABLES

Page No.

FIGURES

ABBREVIATIONS

The following abbreviations are used in this study:

a_j^i : activity of component "j" in phase "i"

γ_j^i : activity coefficient (component "j" in phase "i")

X_j^i : molar proportion of component "j" in phase "i"

Ab: albite
act: actinolitic amphibole
AIS: Adlavik Intrusive Suite
al: allanite
alm: almandine
amph: amphibole
An: anorthite
ap: apatite
bi: biotite
BMIS: Benedict Mountains Intrusive Suite
cd: cordierite
chl: chlorite
CI: colour index
cpx: clinopyroxene
ct: carbonate
CTIF: Cut Throat Island Fault
cum: cummingtonite
En: enstatite
ep: epidote
fib: fibrolite
Fo: forsterite
Fs: ferrosilite
gros: (or gr) grossularite
gt: garnet
hbl: hornblendic amphibole
ilm: ilmenite
Ksp: K feldspar
ky: kyanite
MgTs: Mg-Tschermak
mt: magnetite
mu: muscovite
ol: olivine
opx: orthopyroxene
Or: orthoclase
PT: pressure-temperature
pfu: per formula unit
pl: plagioclase
py: pyrite
pyr: pyrope
qz: quartz
sil: sillimanite
sp: spinel
spes: spessartine
sph: sphene (titanite)
WBIGC: White Bear Islands Granulite Complex
Wo: wollastonite
zr: zircon
zs: zoisite

CHAPTER 1
INTRODUCTION

1.1 PURPOSE AND SCOPE

Precambrian shield terranes typically have prolonged and complex geologic histories, and the diverse assemblages of rocks that they contain form "provinces" defined by the ubiquitous presence of the latest tectono-metamorphic overprint. Boundary regions between geologic provinces are of particular interest as they provide insight into relationships between earlier tectono-metamorphic effects and the latest orogenic overprint. Evaluation of such boundaries must therefore focus both on the examination of the lithologic characteristics of neighbouring domains, and on the conditions and chronology of the orogenic overprints that characterize each province.

The purpose of this study is to outline the tectono-metamorphic evolution of an area straddling the Grenville Front on the Labrador coast. In this area, the effects of the Grenvillian orogeny have remained a contentious issue in recent years, emphasizing the problems encountered in the regional interpretation of areas marked by a scanty data base. The present investigation is not, however, restricted to a description and evaluation of Grenvillian elements to the exclusion of earlier features. Rather, from the outset of the project, emphasis has been placed on establishing criteria whereby pre-Grenvillian features could be distinguished from those demonstrably of Grenvillian age.

The study is divided into two parts; the empirical portion focuses on five aspects of Grenvillian and pre-Grenvillian geology:

(1) **the distinction and distribution of major rock units straddling the Grenville Front**

(2) the establishment of a structural framework embracing Grenvillian and pre-Grenvillian deformational features

(3) the recognition and distribution of key metamorphic mineral assemblages

(4) the estimation of P-T conditions of metamorphism

(5) the determination of the ages of selected rock units in order to bracket the ages of orogenic events that they record.

The interpretative portion of the study uses the empirical data to model the evolution of the tectonic margin represented by the Grenville Front zone in eastern Labrador.

1.2 LOCATION, ACCESS, AND DESCRIPTION OF THE STUDY AREA

The study area (Fig. 1-1) is centered on the islands of the Smokey archipelago, and is bounded by 54.22'N and 54.42'N, and 56.50'W and 57.39'W. The seasonally occupied hamlet of Smokey is a port of call of CN Marine coastal boats, which run on a weekly basis from July through October between Goose Bay and Nain.

Topographic relief in the Smokey area is subdued, although prominent ridges of mafic dykes (Michael gabbro) are locally evident. The study area is sparsely vegetated; caribou moss, lichens and scrub brush obscure rock exposures inland and in the center of islands in the archipelago. The climate is temperate from mid-June to early September. The prevailing winds are from the northwest, and are frequently sufficiently strong to hamper the piloting of small boats, particularly in the northern and eastern portions of the archipelago.

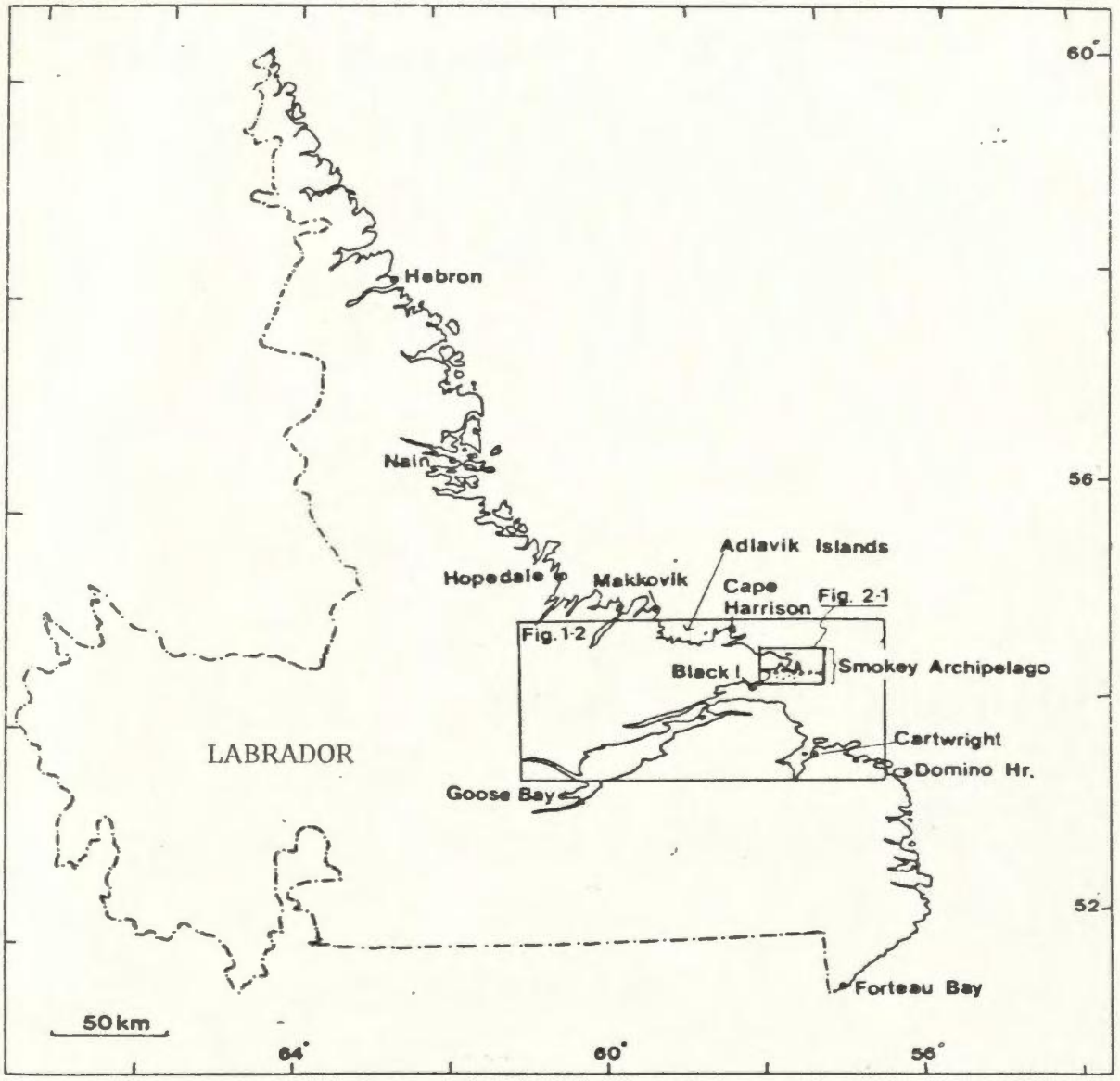

Figure 1-1. Index map showing localities mentioned in the text, and indicating the locations of Figures 1-2 and 2-1.

1.3 REGIONAL SETTING

The Smokey archipelago straddles the junction between the Grenville and Makkovik Provinces (Makkovik Subprovince of Taylor, 1971; see Gower and Ryan, in press) in easternmost Labrador. In this area, the Grenville Front, marking the northern extent of widespread Grenvillian deformation, coincides with the Benedict Fault (Gower et al., 1980), a south to southwest-dipping zone of heterogeneously-strained rocks. In the vicinity of the study area, the Benedict Fault transects Paleohelikian plutonic rocks of the Trans-Labrador batholith (Wardle et al., 1982). The Trans-Labrador batholith is one of three crustal segments recently recognized in eastern Labrador by Gower and Owen (1984). Gower and Owen's tripartite subdivision encompasses, from north to south, the Trans-Labrador batholith, the Groswater Bay Terrane, and the Lake Melville Terrane (Fig. 1-2).

The Trans-Labrador batholith is a composite suite of mafic to felsic intrusions of Paleohelikian age (ca. 1790-1625Ma) extending some 400km westward from the Labrador coast to Churchill Falls, where the batholith merges with similar plutons comprising the north-trending Ungava batholith (Wardle et al., 1982) of the Churchill Province. The Trans-Labrador batholith underlies much of the Smokey area, where it comprises granitoids of the Benedict Mountains Intrusive Suite (BMIS) (Gower, 1981) and a broadly coeval suite of differentiated gabbroic rocks tentatively correlated with the Adlavik Intrusive Suite (AIS) (Gower, 1981). North of the Benedict Fault, some plutons of the Trans-Labrador batholith, particularly granitoids of the BMIS, contain north- to northeast-trending fabrics, termed the "Makkovik trend" (Ermanovics et al.,

1982) after the predominant fabric orientation typifying the Makkovik Province. South of the Benedict fault, east-trending Grenvillian fabrics are generally predominant. The development of Grenvillian fabrics obscures the boundary relations between the Trans-Labrador batholith and gneissic rocks of the Groswater Bay Terrane. Although in places the Trans-Labrador batholith is clearly intrusive into high-grade tectonites (the White Bear Islands Granulite Complex, see below) in the central and eastern portions of the Smokey archipelago, the age of these plutonic rocks relative to amphibolite-facies gneisses of the Groswater Bay Terrane is less certain.

Gneissic rocks of the Groswater Bay Terrane are exposed near Bluff Head in the southwestern corner of the study area. These granodioritic to (quartz) monzonitic gneisses, known as the Bluff Head orthogneiss, are considered to have been derived from igneous protoliths, and presently contain metamorphic mineral assemblages characteristic of the amphibolite facies. Elsewhere in the Groswater Bay Terrane, both para- as well as orthogneisses are prevalent, and comprise mineral assemblages characteristic of both medium- and high metamorphic grade.

Paragneisses in the Groswater Bay Terrane (Gower and Owen, 1984) include relatively high-grade migmatitic muscovite + kyanite + garnet-bearing metapelitic rocks exposed to the northeast of Cartwright (Owen et al., 1983), and lower-grade greywackes and siltstones preserving primary sedimentary textures on Black Island on the north side of Groswater Bay. These lower-grade rocks may postdate the higher-grade paragneiss.

Orthogneisses in the Groswater Bay Terrane are predominantly of tonalitic

to granodioritic composition, and generally contain amphibolite-facies mineral assemblages. In this regard, the orthogneisses in the vicinity of Bluff Head are typical of those exposed elsewhere in the Groswater Bay Terrane.

Tonalitic to granodioritic orthogneisses of the Groswater Bay Terrane have been dated by several methods, yielding ages ranging from ca. 1610-1680Ma (Rb-Sr, Nd-Sm: Brooks, 1982, 1983; U-Pb, zircon: Krogh, 1983). Massive to foliated granitoids which in part intrude these gneisses include K feldspar-megacrystic granodiorite and clinopyroxene-bearing monzonite. Krogh (1983) reports a 1632Ma age (U-Pb, zircon) for a pyroxene-bearing monzonite of the Groswater Bay Terrane.

Several generations of mafic dykes occur in both the Trans-Labrador batholith and the Groswater Bay Terrane. Gneissic rocks of the Groswater Bay Terrane contain pre-migmatitic pyroxene-bearing metabasites which are crosscut by at least three generations of amphibole-bearing mafic dykes also occurring in plutonic rocks of the Trans-Labrador batholith. These later dykes predate a major suite of Neohelikian mafic intrusions known as the Michael gabbro (Fahrig and Larochelle, 1972), which in the study area is restricted to the area south of the Benedict Fault (Gower and Owen, 1984). Including the Michael gabbro, there are thus at least five generations of mafic dykes which were affected by Grenvillian tectono-metamorphic activity.

The structure of the Groswater Bay Terrane is dominated by a major west-plunging antiform with its axial trace passing through George Island (Fig. 1-2). Shallowly west-plunging folds in the area are outlined by deformed gneissic fabrics

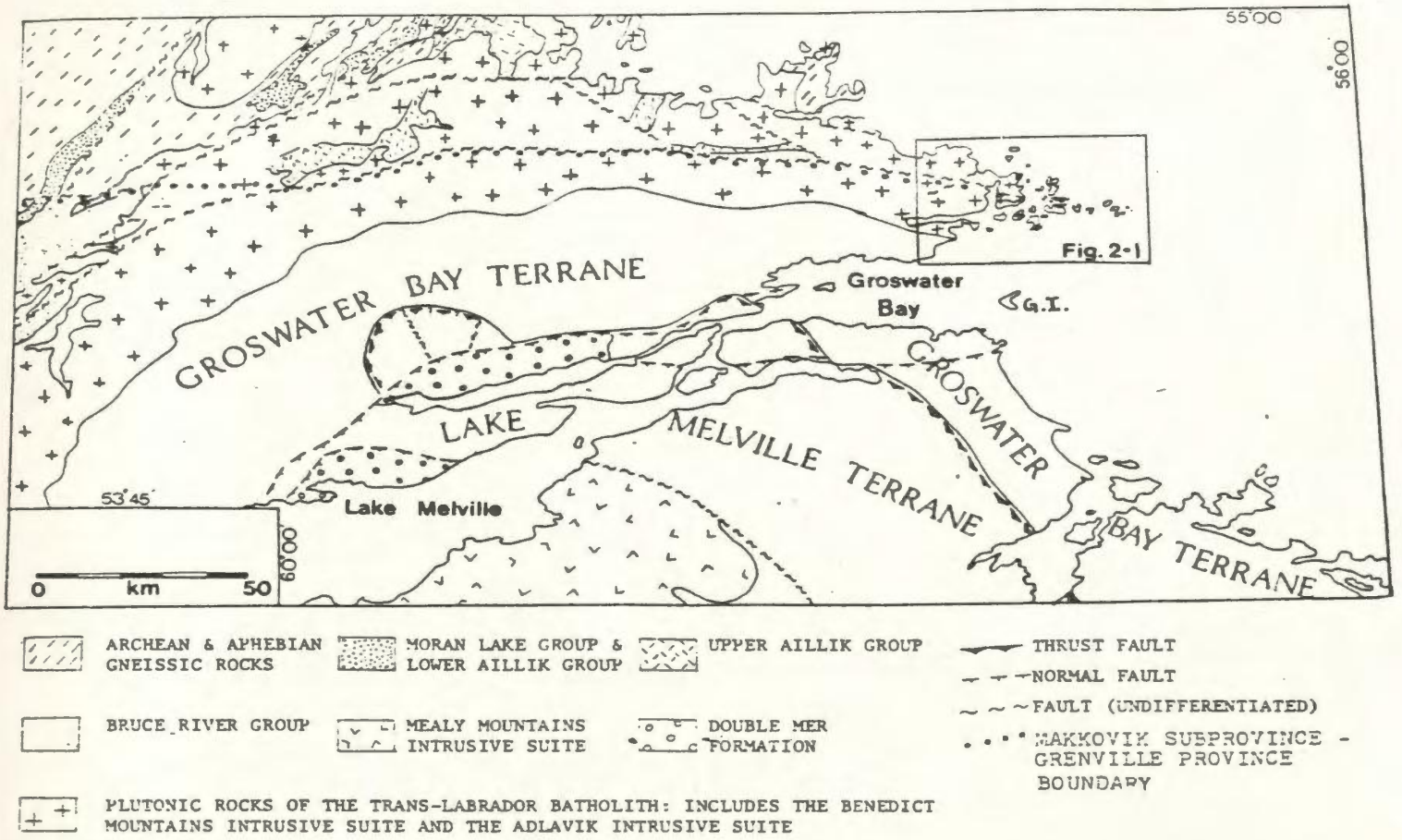

Figure 1-2. Regional setting of the Smokey archipelago, showing the lithotectonic regions described by Gower and Owen (1984). The rectangle shows the location of the study area (cf. Figure 2-1). G.I. = George Island.

and mafic dykes, and are attributed to an early period of Grenvillian deformation. These early Grenvillian folds were subsequently refolded about south- to southeast-plunging axes during the development of Grenvillian L-S fabrics, which are predominant south of the Benedict Fault (Owen and Rivers, 1983).

The junction between the Groswater Bay Terrane and the Lake Melville Terrane coincides with the Rigolet thrust zone, a south-dipping zone of schistose to mylonitic rocks. The Lake Melville Terrane contains both gneissic rocks and massive to foliated plutonic rocks, as does the Groswater Bay Terrane. In the Lake Melville Terrane, however, paragneisses are areally more extensive, and compositionally the orthogneisses are predominantly granodioritic rather than tonalitic to granodioritic as in the Groswater Bay Terrane. The paragneiss includes pyritic psammitic schist, which in places is interlayered with quartzite and metacarbonate, and a variety of pelitic schists. Aluminous metapelites generally contain sillimanite + K feldspar. However, within the Mount Gnat granulite belt, a subdivision of the Lake Melville Terrane, metapelites locally contain orthopyroxene and bear kyanite close to the Rigolet thrust zone. Massive to foliated granitoid rocks in the Lake Melville Terrane include K feldspar-megacrystic granodiorite, quartz diorite to monzonite, and hornblende- and clinopyroxene-bearing quartz syenite to granite.

In contrast to the relatively simple structural trends of the Groswater Bay Terrane, the Lake Melville Terrane is characterized by complex patterns interpreted to be the result of the interference between Grenvillian and pre-Grenvillian structures. Recent mapping in the Paradise River area, south of Sandwich Bay (Gower et al., in press) indicates that the Lake Melville and

Groswater Bay Terranes may have undergone a similar structural evolution, marked by north-directed Grenvillian thrusting. The southwestern margin of the Lake Melville Terrane coincides with a major structural break, possibly a strike-slip fault (C.F. Gower, pers. comm., 1985). Gabbroic, anorthositic, and monzonitic plutonic rocks in the Mealy Mountains (Emslie, 1976; Gower et al., 1982) occur to the southwest of this fault.

The geology of the Smokey archipelago is dominated by plutonic rocks of the Trans-Labrador batholith, although amphibolite-facies orthogneiss of the Groswater Bay Terrane is exposed near Bluff Head, in the southwestern corner of the study area. The amphibolite-facies orthogneiss, referred to as the Bluff Head orthogneiss, of the Groswater Bay Terrane is distinguished from granulite facies para- and orthogneisses exposed in the central and eastern part of the Smokey archipelago. The Trans-Labrador batholith, the Bluff Head orthogneiss, and the White Bear Islands Granulite Complex (WBIGC) comprise a lithostructural subdivision of the Smokey archipelago which recognizes contrasts in pre-Grenvillian metamorphic mineral assemblages and structures between the three groups. This lithostructural subdivision was introduced by Owen et al. (in press) to provide a descriptive framework for the interpretation of pre-Grenvillian features of this part of the Grenville Front zone. It coincides with Gower and Owen's (1984) regional-scale subdivision of eastern Labrador except for the additional distinction of the high-grade tectonites of the WBIGC.

The three lithostructural domains in the Smokey archipelago have been heterogeneously overprinted by Grenvillian structures and metamorphic mineral assemblages. The zonal distribution of these features from north to south across

the area has led to the recognition of three structural domains separated by Grenvillian high-strain zones (see Owen and Rivers, 1983). Details of these two tripartite subdivisions of the Smokey archipelago using structural and metamorphic criteria are presented in Chapter 3.

1.4 PREVIOUS WORK

Initial geological investigation in Labrador was restricted to readily accessible coastal areas. The earliest work has been reviewed by Kranck (1939), who provided a geological sketch map of much of the Labrador coast, from Forteau Bay to Hebron. Two aspects of Kranck's contribution are particularly significant to the present study. The first of these concerns the protoliths of quartzofeldspathic gneisses in the Groswater Bay area. These gneissic rocks were collectively termed the "Domino gneisses" by Lieber (1860), and were interpreted as layered metasediments by Packard (1891) and Daly (1902). Kranck (1939) recognized that this composite unit has a broadly granitic composition in the type locality at Domino Harbour, and attributed the gneissic fabric to the deformation of a heterogeneous assemblage of felsic plutonic rocks.

Kranck's second important contribution stems from his distinction of massive granitoids north of Indian Harbour (part of the Trans-Labrador batholith) from the gneissic rocks exposed to the south (part of the Groswater Bay Terrane).

The merits of Kranck's pioneering work were not fully appreciated by some later workers. Both Douglas (1953) and Stevenson (1970) suggested that the gneissic rocks bordering Groswater Bay were largely derived from sedimentary protoliths, an interpretation refuted by more recent investigations (Gower et al., 1980; Gower, 1981). Stevenson, whose report incorporates the first systematic

attempt at mapping the Smokey archipelago, confirmed, however, the presence of massive granitoids in the Benedict Mountains, and contrasted these with quartzofeldspathic gneisses cropping out to the south. The most comprehensive description of the geology in the general vicinity of the Smokey archipelago is provided by C.F. Gower's report and 1:100,000 scale maps (Gower, 1981; Gower et al., 1983).

The position of the Grenville Front in eastern Labrador has been the subject of considerable controversy in recent years. Criteria for the positioning of the Front have been reviewed by Gower et al. (1980), who adopted Stevenson's (1970) suggestion that the northern limit of widespread Grenvillian deformation coincides with a major high-strain zone, termed the Benedict Fault by Gower, in this area. Gower et al.'s (1980) extrapolation of the position of the Benedict Fault in the Smokey area, has, however, proven to be inaccurate. Their extrapolation placed the Benedict Fault along the north coast of Cut Throat Island, a locality now known to coincide with another distinct, major high strain zone. The present study places the Benedict Fault some 3km to the north of the position suggested by Gower et al. (1980).

Considerable attention was paid by early workers to polyphase suites of mafic dykes occurring in both gneissic rocks and massive granitoid rocks along coastal exposures. Douglas (1953) described five generations of mafic dykes and distinguished pre- and post-migmatization dyke suites. Kranck (1947) postulated that the emplacement of late mafic dykes was controlled by continental rifting. Grasty et al. (1969), seeking dykes of Tertiary age related to the opening of the Labrador Sea, reported instead Helikian and Hadrynian (middle and upper

Proterozoic) dyke ages (K/Ar, whole rock). From these, Grasty et al. (1969) suggested that the Grenville Front passes through the Smokey archipelago.

The significance of the Michael gabbro, originally described as "trapdykes" by early workers (Kranck, 1939, 1953), has recently been reviewed by Emslie (1983). Emslie postulated that the preservation of delicate corona structures in these dykes, and the retention of pre-Grenvillian K-Ar ages in mafic dykes in the Mealy Mountains provided evidence that the Grenvillian orogeny in eastern Labrador was characterized by relatively low metamorphic grade.

1.5 GENERAL FEATURES OF THE NORTHERN MARGIN OF THE GRENVILLE PROVINCE

Recent geological investigations in various regions of the Grenville Province have added immeasurably to our knowledge of this portion of the Canadian Shield. This is particularly true in the case of the Grenvillian geology of Labrador, which has benefitted from cooperative efforts from geological surveys at both federal and provincial governmental levels. The central and northern portion of the Grenville Province is now quite well known in several localities, particularly at Coniston, Ontario, Chibougamau, Quebec, and in western Labrador. Before presenting new data from easternmost Labrador, it is worthwhile to briefly summarize salient features of Grenvillian geology from these regions.

A small area of the Grenville Front zone in the Coniston area has been described in detail by LaTour (1979, 1981). At Coniston, two mylonite zones of differing character mark the sites of metamorphic and structural breaks. The more southerly shear zone juxtaposes lower- to upper amphibolite-facies rocks against greenschist- to epidote amphibolite-facies assemblages farther to the north. The more northerly shear zone, which coincides with Lumbers' (1975) Grenville Front Boundary Fault (GFBF), juxtaposes these latter rocks against greenschist-facies rocks of the Southern Province. LaTour noted that the two mylonite zones differed both in the character of the structures that they contained and in the effect that mylonitization had on earlier metamorphic mineral assemblages. At Coniston, the GFBF spans a zone containing well-developed isoclinal folds, and coincides with the staurolite-in isograd in metapelites, and with the chlorite- and

epidote-"out" isograd in metabasites. In contrast, the more southerly mylonite zone is marked by "swirled", rootless folds and coincides with the garnet isograd in Fe-rich metabasites. According to LaTour's model, the GFBF is the younger of the two shear zones, and developed during late isostatic rebound and cooling of Grenville crust. The other, apparently older shear zone is interpreted to be the root zone of one of a series of nappes responsible for crustal thickening during the Grenvillian orogeny.

The model of foreland-directed thrusting proposed for the Grenville Front at Coniston is consistent with descriptions of the Front elsewhere, particularly in western Labrador (e.g. Rivers, 1983b; Rivers and Nunn, in press; Rivers and Chown, in press), and near Chibougamau (Chown, 1984; Daigneault and Allard, 1984; Kline, 1984; Baker, 1980). Both strike-slip and thrust faults characterize Grenvillian deformation in the Chibougamau area, although some of these faults probably developed along earlier structures. Fault zones marked by sub-greenschist facies mineral assemblages occur to the northwest of greenschist-facies mylonite zones within the Grenville Province (Chown, 1984). The Mistassini Fault, a major thrust zone in the area, separates sedimentary rocks of the Mistassini Basin from basement rocks transposed from the Grenvillian hinterland farther to the southeast.

An important feature common to Coniston, Chibougamau, western Labrador, and, as will be seen, the Smokey archipelago, is the transition from low- to medium-grade Grenvillian mineral assemblages southward across the Front. This suggests that shallow to moderate crustal levels of the Grenvillian crust are exposed at these localities. Elsewhere, Grenvillian metamorphic zones have been

telescoped across major thrust faults (e.g. the Grenville Front), and are presently inverted (see Calon and Hibbs, 1981).

Evidence suggests that high-grade assemblages documented elsewhere along the Front may have been inherited from a pre-Grenvillian tectono-metamorphic event. For example, in western Labrador, a metamorphic sequence comprising low-grade assemblages initially interpreted (Rivers, 1983) to grade into high-grade kyanite + K feldspar parageneses farther to the southeast, is now interpreted to contain both Grenvillian and pre-Grenvillian assemblages (Rivers and Nunn, in press). An appraisal of geochronological data to the north and south of the high-grade assemblages suggests that the kyanite + K feldspar isograd approximately coincides with a major thrust fault, which separates an allochthon of pre-Grenvillian gneisses with ca. 1.65Ga isotopic ages from parautochthonous rocks reworked during the Grenvillian orogeny (Rivers and Chown, in press). The parautochthonous rocks yield Grenvillian (ca. 1Ga) ages in various isotopic systems (Rb-Sr, K-Ar, 40Ar/39Ar), and similar ages are provided by U-Pb data which plot very close to concordia, suggesting significant lead loss resulting from reworking during the Grenvillian orogeny. Upper intercepts on U-Pb concordia diagrams for the same parautochthonous rocks yield Paleohelikian ages, synchronous with the age of contiguous autochthonous rocks in the Grenville Foreland zone (Rivers and Nunn, in press) north of the Grenville Front.

The regional distribution of diachronous isotopic ages in western Labrador and eastern Quebec suggests that there may be a plethora of allochthonous terranes in this portion of the Grenville Province. On the basis of these isotopic dates coupled with reinterpretation of geological data, Rivers and Chown (in

press) have identified a belt of allochthonous rocks lying to the southeast of the Grenville Front zone. This belt coincides with a regional gravity "high", which contrasts with the negative Bouguer anomaly associated with the parautochthonous rocks of the Grenville Front zone (Wynne-Edwards, 1972). The allochthons, individually tens to hundreds of kilometers in diameter, typically define a northward-convex lobate pattern, and have a distinct aeromagnetic signature. Due to poor exposure, sole thrusts at the base of the allochthons have not as yet been identified during mapping in western Labrador. However, Gower (1984) reports the presence of strongly lineated rocks which may correspond to a boundary mylonite zone underlying a lobate extension of high-grade rocks of the Lake Melville Terrane overlying the Groswater Bay Terrane in eastern Labrador (approximately 150km WSW of Smokey).

Pre-Grenvillian ages clustering around 1.65Ga are recorded by Rb-Sr, K-Ar, and some 40Ar/39Ar dating techniques applied to the allochthonous rocks. The predominance of ca. 1.65Ga ages has led several workers in Labrador to postulate a major tectono-metamorphic event at this period, recently termed the Labradorian orogeny (e.g. Nunn et al., 1984; Thomas et al., 1984). No Grenvillian ages have yet been determined in the allochthons; U-Pb diagrams are very close to concordia. The apparent absence of ca. 1000Ma isotopic ages from the allochthons suggests that these rocks were not profoundly affected by the Grenvillian orogeny. The timing of their emplacement is at present uncertain; it is possible that the stacking of crustal slabs (allochthons) provided the elevated lithostatic pressures for Grenvillian metamorphism at depth. In this case, there is a causal relationship between the thrust sheets and the youngest metamorphic event recorded in the underlying rocks.

1.6 FIELD WORK, SAMPLING, AND ANALYTICAL WORK

Mapping in the Smokey archipelago was conducted at a scale of 1:50,000 during the summer months of 1982 and 1983. Although a few foot traverses were made to extend geological contacts inland, most work focused on shoreline exposures, which are wave-washed and virtually continuous. Emphasis was placed on determining the distribution and relative chronology of major rock units and their possible correlation within, and to the north of the Grenville Front, represented in the area by the Benedict Fault (Gower et al., 1982). Representative samples of different rock types were collected for subsequent analytical work in whole rock and mineral geochemistry, geothermobarometry and geochronology. Aspects of the sampling proceedure and sample preparation are discussed in Appendix A.1.

All major rock units were analysed for major elements and for 18 trace elements (Appendix A.2). Average bulk rock compositions of the different units are presented below. In selecting samples for these analyses, emphasis was placed on outlining trends or variations in the chemistry of suites of Paleohelikian plutonic rocks and on determining the influence of bulk rock compositions on the composition of key minerals in Grenvillian and pre-Grenvillian metamorphic rocks. Consequently, only a few individual units or groups of rocks are extensively represented in these analyses; rock units deemed less important in achieving either of these goals are represented by only a few analyses.

Isochrons and (or) errorchrons of seven units dated by the Rb-Sr (whole rock) method are presented in order to place absolute time constraints on the

relative chronology established in the field. Details of the analytical procedures and the isotopic compositions of these three units are presented in Appendix A.3. Errors associated with the isotopic dates reported in this study are expressed at the 2-sigma confidence level.

Estimation of PT-conditions associated with Grenvillian and pre-Grenvillian metamorphism is based on various calibrated geothermobarometers (Chapter 4). Mineral analyses were determined using the electron probe microanalyser (microprobe). Details of the operating conditions, precision, and accuracy of the microprobe are outlined in Appendix A.4.

CHAPTER 2
FIELD RELATIONS, PETROGRAPHY, AND GEOCHRONOLOGY

2.1 PREAMBLE

This chapter outlines aspects of the field occurrence and relative and absolute ages of major rock units, and summarizes important features of their petrography. The distribution of major rock units is shown in a generalized geological map of the Smokey archipelago presented in Figure 2-1. The 1:100,000 scale field map (Map 1), of which Figure 2-1 is a simplified version, and a sample-location map (Map 2) are provided in the pocket at the end of the thesis.

Eight major groups of rocks have been distinguised in the study area. The three oldest groups comprise pre-Grenvillian metamorphic rocks described by Owen et al. (in press):

(i) gneissic to migmatitic granulite-facies paragneiss and orthogneiss, comprising the White Bear Island Granulite Complex (WBIGC);

(ii) gneissic to migmatitic orthogneisses, containing amphibolite-facies mineral assemblages, comprising the Bluff Head orthogneiss (Groswater Bay Terrane);

(iii) Paleohelikian granitoids of the Benedict Mountains Intrusive Suite (BMIS) (Gower, 1981), a part of the Trans-Labrador batholith (TLB).

Younger rocks lacking the mineral fabrics and parageneses characterizing the three groups of pre-Grenvillian metamorphic rocks may themselves be grouped into five broad categories:

(iv) Paleohelikian differentiated gabbroic rocks, tentatively correlated with the Adlavik Intrusive Suite (AIS) (Gower, 1981), which are broadly coeval with (iii), but which lack evidence of a pre-Grenvillian metamorphic

Figure 2-1. Simplified geological map of the Smokey archipelago.

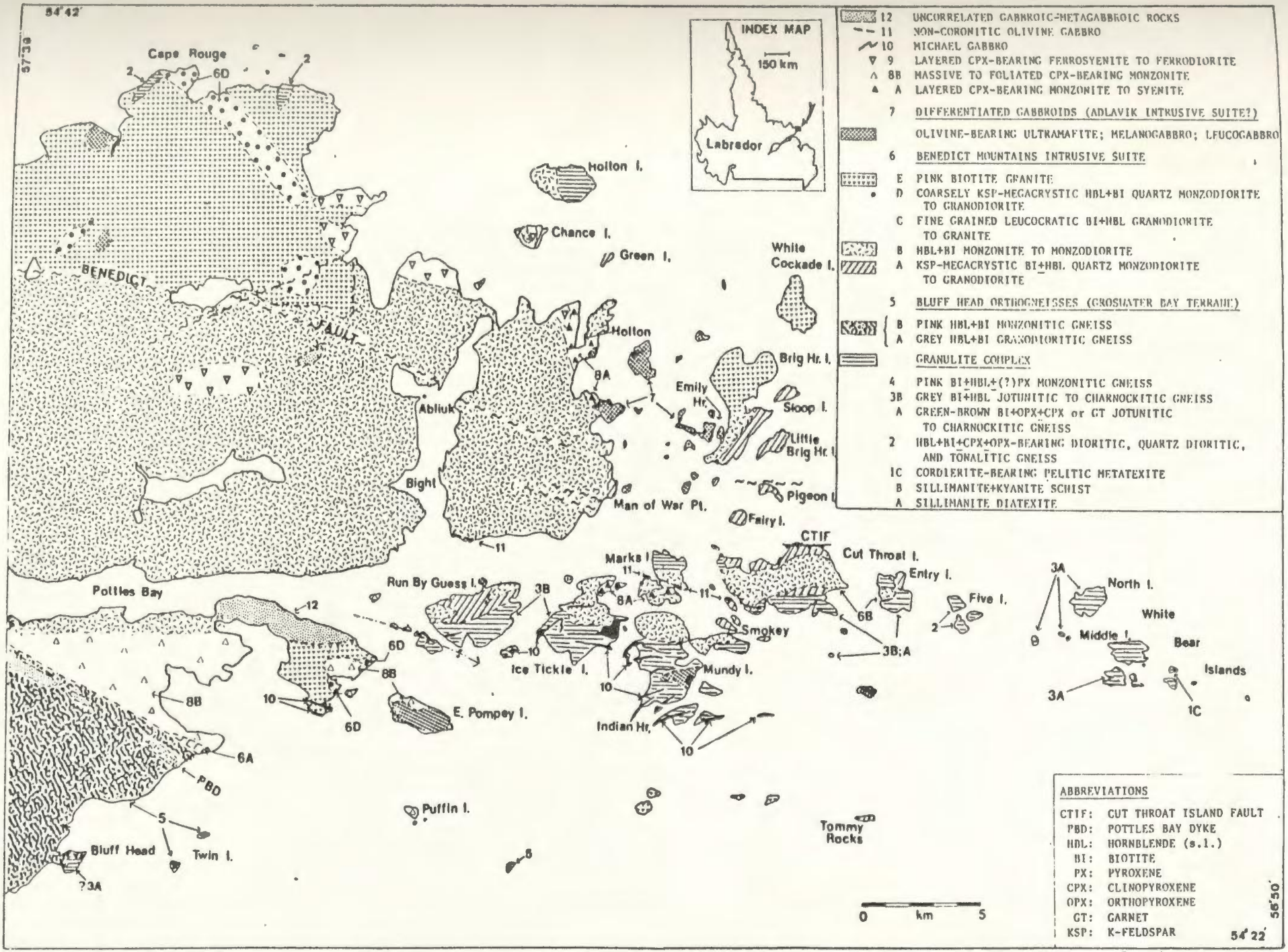
INDEX MAP
150 km
Labrador
12 UNCORRELATED GABBROIC-METAGABBROIC ROCKS
11 NON-CORONITIC OLIVINE GABBRO
10 MICHAEL GABBRO
9 LAYERED CPX-BEARING FERROSYENITE TO FERRODIORITE
8B MASSIVE TO FOLIATED CPX-BEARING MONZONITE
A LAYERED CPX-BEARING MONZONITE TO SYENITE
7 DIFFERENTIATED GABBROIDS (ADLAVIK INTRUSIVE SUITE?)
OLIVINE-BEARING ULTRAMAFITE; MELANOGABBRO; LEUCOGABBRO
6 BENEDICT MOUNTAINS INTRUSIVE SUITE
E PINK BIOTITE GRANITE
D COARSELY KSP-MEGACRYSTIC HBL+BI QUARTZ MONZODIORITE TO GRANODIORITE
C FINE GRAINED LEUCOCRATIC BI+HBL GRANODIORITE TO GRANITE
B HBL+BI MONZONITE TO MONZODIORITE
A KSP-MEGACRYSTIC BI±HBL QUARTZ MONZODIORITE TO GRANODIORITE
5 BLUFF HEAD ORTHOGNEISSES (GROSWATER BAY TERRANE)
B PINK HBL+BI MONZONITIC GNEISS
A GREY HBL+BI GRANODIORITIC GNEISS
GRANULITE COMPLEX
4 PINK BI±HBL±(?)PX MONZONITIC GNEISS
3B GREY BI±HBL JOTUNITIC TO CHARNOCKITIC GNEISS
A GREEN-BROWN BI+OPX+CPX or GT JOTUNITIC TO CHARNOCKITIC GNEISS
2 HBL+BI+CPX+OPX-BEARING DIORITIC, QUARTZ DIORITIC, AND TONALITIC GNEISS
1C CORDIERITE-BEARING PELITIC METATEXITE
B SILLIMANITE+KYANITE SCHIST
A SILLIMANITE DIATEXITE
ABBREVIATIONS
CTIF: CUT THROAT ISLAND FAULT
PBD: POTTLES BAY DYKE
HBL: HORNBLENDE (s.l.)
BI: BIOTITE
PX: PYROXENE
CPX: CLINOPYROXENE
OPX: ORTHOPYROXENE
GT: GARNET
KSP: K-FELDSPAR
0 km 5
54°42'
57°30'
56°50'
54°22'
Cape Rouge
Holton I.
Chance I.
Green I.
White Cockade I.
BENEDICT
FAULT
Holton
Brig Hr. I.
Emily Hr.
Sloop I.
Little Brig Hr. I.
Abliuk
Bight
Man of War Pt.
Pigeon I.
Fairy I.
CTIF
Cut Throat I.
Marks I.
Entry I.
Five I.
Run By Guess I.
Pottles Bay
Smokey
Ice Tickle I.
Mundy I.
E. Pompey I.
Indian Hr.
North I.
White
Middle I.
Bear
Islands
Puffin I.
Tommy Rocks
Bluff Head
Twin I.
?3A

Figure 2-1.

fabric;

(v) clinopyroxene-bearing monzodiorite to monzonite;

(vi) ferrosyenite to ferrodiorite;

(vii) dykes of coronitic olivine gabbro, referred to as the Michael gabbro (Fahrig and LaRochelle, 1972);

(viii) uncorrelated mafic rocks, of uncertain age relative to the Michael gabbro.

With the possible exception of some rectiplanar mafic dykes, all rocks in the study area predate the Grenvillian orogeny, and all units exposed in the southern half of the study area heterogeneously bear the effects of Grenvillian tectonism and metamorphism.

Owen and Rivers (1983) grouped all rocks interpreted to predate the TLB into a basement complex. Since this initial assessment, it has become apparent that various members of the BMIS preserve pre-Grenvillian metamorphic mineral assemblages defining north- to northeast-trending fabrics characteristic of the Makkovik Province (Ermanovics et al., 1982), and represent a distinct group of pre-Grenvillian metamorphic rocks. Furthermore, continued mapping in the Smokey archipelago revealed the presence of two groups of gneissic rocks, one comprising amphibolite-facies orthogneiss (of the Groswater Bay Terrane), the other comprising granulite-facies para- and orthogneisses (of the WBIGC). Owen and Rivers' initial grouping of early gneissic rocks is thus an oversimplification, and a revision of their scheme was deemed necessary by Owen et al. (in press). Prior to discussing details of Owen et al.'s pre-Grenvillian lithostructural subdivision of the area (see section 3.2), a description of field aspects and the petrography of important lithologies is in order. The following descriptions are presented on a unit-by-unit basis under the headings outlined in the legend of the

geological map presented in Figure 2-1.

Modal compositions of the different units are visual estimates from thin sections and stained rock slabs. Classification of hypersthene-free granitoid rocks follows Streckeisen's (1976) nomenclature scheme. The classification of hypersthene-bearing granitoid rocks is discussed below. Mineral compositions, determined by the electron microprobe, are expressed in mole percent of pure end-member components. The sample number is specified for each composition cited in the text.

2.2 FIELD OCCURRENCE AND PETROGRAPHY OF GNEISSIC ROCKS

The term "White Bear Island Granulite Complex" (WBIGC) refers to high-grade metamorphic rocks in the central and eastern part of the Smokey archipelago. The Granulite Complex is particularly well exposed in the White Bear Islands, and comprises both paragneiss (units 1A, 1B, 1C) and orthogneiss (units 2, 3A, 3B, 4). Gneissic rocks of the northern Groswater Bay Terrane are exposed near Bluff Head, and are hereby referred to as the Bluff Head orthogneiss. No paragneiss has been recognized in the Bluff Head orthogneiss (units 5A, 5B). The WBIGC will be described first.

2.2.1 Paragneisses of the White Bear Islands Granulite Complex

Three varieties of paragneiss occur in the Smokey archipelago. All are pelitic and are probably lithological variants of one metasedimentary sequence. The paragneisses generally occur as screens or rafts in orthogneiss. Crosscutting relations with the enclosing rocks are not preserved, and both the para- and orthogneisses share a common fabric. It is therefore not clear whether the paragneiss predates or postdates the orthogneiss.

Sillimanite-bearing diatextite (unit 1A) crops out on an islet between Ice Tickle and Mundy Islands. The rock is medium-grained (1-4mm), pink, and variably rusty weathering, consisting of quartz (30-40%), microcline (35-45%), plagioclase (An32; 10-15%), biotite (2%), and sillimanite (1-5%), with minor garnet (pyr 14%; alm 55%; spess 27%; gros 4%; sample V524-2). Sillimanite occurs as oriented sheaths of acicular crystals. Fibrolitic sillimanite is also present, occurring along the contacts between feldspars. Grenvillian fabrics transecting the unit are characterized by the development of ribbon quartz and by the partial replacement of sillimanite by muscovite. A discontinuous 5cm wide calcsilicate layer in the diatexite consists of garnet (alm 46%; spess 4%; gros 50%; sample V71-4), epidote, and quartz, with subordinate normally-zoned plagioclase (An43-->33). The calcsilicate rock probably represents a primary compositional layer (e.g. bedding) within the pelitic sequence.

A screen of white weathering, buff-coloured sillimanite-kyanite schist (unit 1B) occurring within orthogneiss (unit 3B, see below) on Entry Island represents the second variety of metapelitic rocks in the area. This exposure was first identified by Stevenson (1970), and the presence of kyanite in the unit is portrayed on the "Metamorphic Map of the Canadian Shield" (Fraser and Heywood, 1978). The unit is quartz-rich (>50%), and contains clusters of 0.5mm bladed kyanite (15-30%), acicular sillimanite (1-5%), and accessory blue tourmaline and retrograde muscovite (after the aluminosilicates). Textural relations suggest that sillimanite replaces kyanite. The sillimanite-kyanite schist is virtually homogeneous except for rare cm-scale magnetite-bearing layers, probably

representing primary compositional bands. The lack of development of a gneissic or migmatitic fabric may be attributed to the relatively refractory nature imparted to the unit by the absence or paucity of feldspars (e.g. Mehnert et al., 1973; Busch et al., 1974).

The third class of metapelites in the study area comprises cordierite-bearing metatexites (unit 1C) occurring in the White Bear Islands. Unlike unit 1A, which lacks relicts of metapelitic paleosome, this pelitic metatexite is characterized by well-defined paleosome and neosome components. The paleosome consists of relatively biotite-rich and biotite-poor bands interlayered on a centimeter- to decimeter-scale, probably reflecting primary compositional variations (e.g. bedding) in the sequence. Cordierite, where present, is restricted to the biotite-rich bands, and to the leucosomes.

The neosome component of the rock consists predominantly of coarse-grained beige to pink granitic (s.l.) leucosomes. Melanosomes, where present, are represented by thin (1-5mm), discontinuous biotite-rich selvages isolated within the leucosome or separating the leucosome from the paleosome. A variety of morphologies of leucosomes are present in the metatexites. With respect to the paleosome gneissosity, both concordant and discordant leucosomes occur, a significant feature of the unit since the localization of the neosome (cf. Mehnert, 1968) may be related to dilatant structures within the paleosome. Concordant leucosomes form conspicuous layer-parallel veins within the paleosome, and are typically bounded by biotite-rich selvages. Discordant leucosomes, which occur as veins or pods up to approximately 70cm in diameter, generally lack melanosome seams, but not uncommonly have offshoots of layer-parallel veins.

Both types of leucosomes share a common mineralogy, as follows: plagioclase (An32-An36; 25-50%), quartz (10-20%), antiperthitic K feldspar (5-20%); biotite (1-5%); garnet (0-15%); cordierite (0-15%); orthopyroxene (0-5%); sillimanite (0-2%); magnetite (1-5%); ilmenite (1%); green spinel (0-2%). Paleosome plagioclase compositions fall in the same range as mentioned above. The paleosomes, however, are virtually free of garnet and orthopyroxene, but contain cordierite (extensively pinitized) in biotite-rich layers.

The leucocratic and melanocratic compositional layering characterizing the paleosome has been modified by the development of a layer-parallel gneissosity, chiefly by the segregation of biotite into mm-thick selvages. In addition to plagioclase (An32-36), fine bead perthite, and quartz, the leucocratic layers contain biotite + magnetite $\pm$ ilmenite $\pm$ green spinel. Fibrolite is locally present along feldspar boundaries. Melanocratic layers contain abundant biotite + (pinitized) cordierite + magnetite $\pm$ ilmenite $\pm$ green spinel. Garnet poikiloblasts enclosing variably oriented acicular sillimanite + biotite + quartz are locally present, indicating the coexistence of these minerals prior to garnet nucleation. Four textural associations of garnets have been observed in pelitic metatexite: (1) garnets replaced by cordierite, or by (2) biotite $\pm$ quartz $\pm$ sillimanite; (3) garnets showing two-stages of growth, and (4) coarse-grained garnet poikiloblasts, generally situated in leucosomes.

In places, relict garnet is enclosed within cordierite in melanocratic biotite-rich layers of paleosomes. These 0.5mm garnets are xenoblastic, and have been extensively replaced by the cordierite. Despite extensive pinitization of the host cordierite, the garnets are fresh and have not been hydrated. Other garnets have

been replaced by biotite ± quartz ± sillimanite, and are enclosed by intergrowths of these minerals. The third type of garnet provides evidence of two phases of garnet growth. These garnets have idioblastic cores (0.2-0.5mm in diameter) with thin (0.1mm) mantles of xenoblastic garnet or clusters of small (0.05-0.1mm) subidioblastic garnets. In places the garnet is enclosed in cordierite or biotite ± quartz ± sillimanite.

In the leucosomes, garnet forms a stable paragenesis with hypersthene and, in places, with biotite. Elsewhere, garnet is partially replaced by biotite + quartz ± sillimanite. Cordierite replaces garnet and(or) biotite + sillimanite, and is itself replaced by sillimanite and pale green phyllosilicate (pinite). Orthopyroxene is commonly replaced by intergrowths of biotite ± quartz.

2.2.2 Orthogneisses of the White Bear Islands Granulite Complex

Three types of orthogneiss (units 2, 3 and 4) locally contain granulite-facies mineral assemblages. Along with the metapelitic gneisses (units 1A,B,C), these comprise the WBIGC (see section 3.4). The average major element geochemistry of the various orthogneissic rocks of the WBIGC is listed in Table 2-1, and normative quartz, plagioclase and K feldspar contents of each member are plotted in Figure 2-2.

The first group comprises an apparently continuous series of dioritic, quartz dioritic and minor tonalitic compositions (unit 2) predominating on Five Islands, and occurring as xenoliths in younger Paleohelikian plutonic rocks throughout the study area (Owen and Rivers, 1983). The second group (unit 3) consists of hypersthene-bearing quartz monzodiorite to granite gneiss occurring in a swath from Run By Guess Island to the White Bear Islands. The relative ages of units 2

Table 2-1. Major element geochemistry of orthogneissic rocks of the Granulite Complex.

	Unit 2		Unit 3A		Unit 3B		Unit 4	
SiO_2	63.4	(9.0)*	62.8	(4.5)	66.1	(3.8)	68.8	(2.3)
TiO_2	0.82	(0.52)	0.58	(0.17)	0.52	(0.24)	0.30	(0.00)
Al_2O_3	15.1	(2.5)	17.5	(2.1)	16.1	(1.6)	15.6	(1.1)
**Fe_2O_3	5.66	(3.38)	4.92	(1.92)	3.35	(0.75)	2.65	(0.57)
MnO	0.08	(0.04)	0.07	(0.02)	0.05	(0.00)	0.04	(0.00)
MgO	2.80	(1.75)	1.79	(0.73)	1.21	(0.46)	0.74	(0.12)
CaO	4.28	(2.60)	4.25	(1.12)	2.96	(0.84)	2.45	(0.37)
Na_2O	3.10	(0.78)	4.32	(0.86)	3.91	(0.66)	3.84	(0.51)
K_2O	2.81	(1.54)	3.36	(0.88)	4.20	(1.02)	4.37	(0.50)
P_2O_5	0.22	(0.28)	0.19	(0.11)	0.13	(0.02)	0.10	(0.01)
LOI	0.65	(0.34)	0.49	(0.22)	0.64	(0.34)	0.82	(0.19)
	98.92		100.27		99.17		99.71	
# of analyses	8		7		3		3	

Table 2-2. Major element geochemistry of the Bluff Head orthogneisses.

	Unit 5A	Unit 5B
SiO_2	73.7	65.5
TiO_2	0.20	0.42
Al_2O_3	13.9	16.9
**Fe_2O_3	1.97	2.82
MnO	0.08	0.07
MgO	0.19	0.80
CaO	0.90	1.88
Na_2O	4.60	4.06
K_2O	4.17	7.16
P_2O_5	0.02	0.10
LOI	0.48	0.50
	100.21	100.21
# of analyses:	1	1

( )* = one standard deviation

** all iron as Fe_2O_3

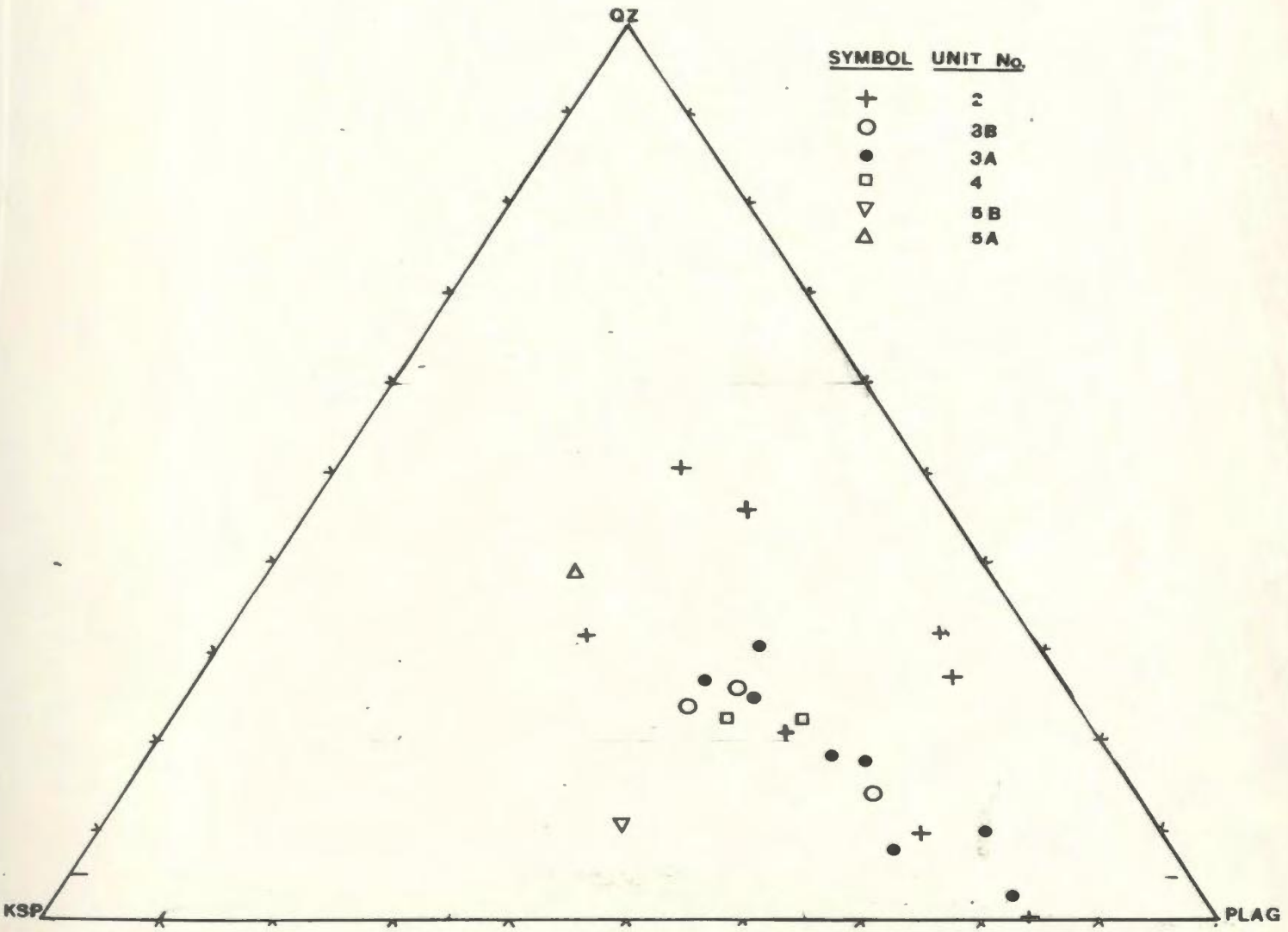

Figure 2-2. Normative quartz, K feldspar, and plagioclase contents of orthogneisses of the White Bear Islands Granulite Complex and the Bluff Head orthogneiss.

and 3 are unknown from either field relations or their isotopic compositions. The charnockite nomenclature of Lof (1983) is adopted for the classification of these granulite-facies orthogneisses. This scheme is based on the modal abundance of quartz, K feldspar, and plagioclase in hypersthene-bearing granitoid rocks. In Lof's (1983) classification, hypersthene-bearing (quartz) monzodiorite is termed jotunite, hypersthene-bearing (quartz) monzonite is termed mangerite, and hypersthene-bearing granite is termed charnockite. It should be emphasized that this nomenclature implies neither the normative mineralogy nor aspects of the major element geochemistry of these rocks. The jotunitic end-member is dominant in unit 3.

The third group (unit 4) of granulite-facies metaplutonic rocks is represented by pink, gneissose, quartz-bearing monzonite exposed near Run By Guess Island, near Smokey, and on Marks Island and Cut Throat Island. At the latter locality, the monzonites are associated with jotunitic gneiss, and southeast of Smokey, enclaves of retrograded (unit 3B) jotunite occur in unit 4.

The dioritic member is dominant in the first group of granulite-facies orthogneisses (unit 2), and consists of plagioclase (An25-An42; 35-50%), quartz (0-10%), hornblende (10-25%), biotite (5-20%), orthopyroxene (0-3%), clinopyroxene (0-3%), and magnetite-ilmenite (2%). Tonalitic compositions have a higher proportion of biotite/hornblende, and contain up to 15% microcline, and 15-25% quartz. Pyroxenes occur locally in the dioritic-tonalitic gneisses, and appear to be restricted to the eastern portion of the study area. A sample (V581-1) of dioritic gneiss from the White Bear Islands contains orthopyroxene and clinopyroxene, and a sample of tonalitic gneiss from Five Islands contains traces of clinopyroxene. In both samples, pyroxenes are partly replaced by

hornblende, and coexist stably with biotite. Unit 2 has been dated (Rb-Sr, whole rock; see section 2.8.1) at 1923 $\pm$ 148Ma.

The jotunitic member is dominant in the second group of granulite-facies orthogneisses (unit 3). It has yielded a Rb-Sr age of 1899 $\pm$ 187Ma (see section 2.8.1), identical, within the specified errors, to that determined for unit 2. The unit occurs as a swath from Run By Guess Island through to the White Bear Islands, and consists of plagioclase (An26-An33; 45-65%), variably antiperthitic orthoclase (5-20%), quartz (5-15%), red-brown biotite (5-8%), orthopyroxene (2-5%), hornblende (0-5%), clinopyroxene (0-3%), garnet (0-5%), magnetite (1-2%) $\pm$ ilmenite (0-2%), and traces of apatite and zircon. Where hornblende is present, invariably it is seen to partially replace orthopyroxene. Two-pyroxene assemblages are common, but orthopyroxene coexists with garnet in only one location (an islet 1km southwest of North Island, see Map), and garnetiferous two-pyroxene assemblages have not been found. K feldspar may occur both as megacrysts and as a groundmass phase, and the jotunitic member grades into charnockitic gneiss as the proportion of this mineral increases at the expense of plagioclase. Apart from the different proportions of K feldspar/plagioclase, the mineralogy of the jotunitic and charnockitic members of this suite are similar.

The granulite-facies jotunitic-charnockitic gneiss becomes extensively retrograded to amphibolite-facies rocks westward within the study area, a feature also noted in unit 2. Incomplete retrogression of this suite leads to the common occurrence of patches of greenish-brown orthopyroxene-bearing gneiss enclosed within its grey-coloured retrograded equivalent (Owen and Rivers, 1983, Fig. 19.7). Textures of the granulite-facies assemblage were faithfully preserved during

this period of passive retrogression, contrasting it with the dynamic retrogression associated with Grenvillian high-strain zones (Owen and Rivers, 1983). Retrograded portions (unit 3B) of the jotunitic-charnockitic suite are distinguished from their granulite-facies equivalents (unit 3A) in Figure 2-1.

Pink monzonitic gneiss (unit 4) is associated with tonalitic gneiss on Marks Island and with jotunitic gneiss on Cut Throat Island. Aggregates of brown and green-brown biotite + altered pyroxene(?) $\pm$ hornblende, which impart a streaky texture to the rock, coexist with plagioclase (An23; 25-45%), microcline (15-35%), and quartz (10-20%). Although no fresh pyroxene has been observed in the monzonite, boudinaged two-pyroxene-bearing metabasites occur in the unit on Cut Throat Island, testifying to the attainment of granulite facies.

2.2.3 Pre-Migmatitic Metabasites

Granulite facies, two-pyroxene-bearing metabasites are also well-represented in pelitic metatexite (unit 1C) and jotunitic gneiss (unit 3A) in the White Bear Islands. The metabasites are characterized by a granoblastic texture. Pyroxenes in two metabasite samples (V194-2, V580-8) show similar textural relationships to those seen in the jotunitic gneiss (unit 3A); where in contact, clinopyroxene partly encloses, but does not replace orthopyroxene. Biotite forms a stable paragenesis with both pyroxenes, and sample V580-8 contains trace amounts of retrograde hornblende. West of the White Bear Islands, pre-migmatitic metabasites have been pervasively retrogressed to amphibolite-facies, and contain hornblende, subordinant biotite, and ilmenite-magnetite. Both pyroxenes (where present) in the retrograded metabasites are mantled by olive-green hornblende.

Clinopyroxene coexists with (retrograde) hornblende and biotite in a

distinctive pre-migmatitic microcline-bearing rock occurring as boudinaged layers in the jotunitic gneiss (units 3A,B). These have also been identified in granodioritic gneiss (unit 5A) near Bluff Head, and serves as a useful, albeit rare, marker of the early metamorphic history of both rock units.

2.2.4 The Bluff Head Orthogneiss

Orthogneisses lacking granulite-facies mineral assemblages are dominant in the southwest corner of the study area, and collectively comprise the Bluff Head orthogneiss (see Fig. 3-1 and section 3.4). Granodioritic (unit 5A) and monzonitic (unit 5B) varieties are prevalent. Since the gneisses are commonly interbanded on a metre- to decametre scale, they have not been distinguished in Figure 2-1. Furthermore, the relative age of units 5A and 5B is unknown. The bulk rock compositions of these orthogneisses are listed in Table 2-2, and the normative quartz, plagioclase and K feldspar contents of both units are plotted in Figure 2-2.

The migmatitic gneisses exposed in the vicinity of Bluff Head are typical of the orthogneisses dominating the northern Groswater Bay Terrane. These gneissic rocks are distinguished from members of the WBIGC since they lack orthopyroxene, and therefore it is uncertain whether these rocks ever attained granulite-facies (cf. section 4.5). Their mineralogy is simple, although these gneisses may have undergone significant retrogression from middle amphibolite facies (at least) to epidote-amphibolite facies. The present mafic mineralogy of the gneisses consists of blue-green hornblende + brown to green-brown biotite $\pm$ garnet $\pm$ epidote $\pm$ white mica. Garnet has locally formed at the expense of biotite, as evidenced by the depletion of the latter mineral around garnet porphyroblasts. The gneissic fabric in both units consists of alternating mm-thick,

leucocratic-melanocratic layering, accentuated by the local development of layer-parallel melanosome (biotite + hornblende)-seamed leucosomes averaging 1-2cm in thickness.

The paleosome of the granodioritic gneiss (unit 5A) is grey to rose, rather fine-grained (1-2mm), and consists of plagioclase (An3-18; 40-65%), quartz (15-25%), microcline (5-15%), biotite (2-6%), hornblende (1-3%), muscovite (1%), and accessory epidote, allanite, apatite, zircon, and Fe oxides. The leucosomes are granodioritic, and occur as well-defined veins bounded by biotite-rich selvages, or form medium-grained (1-4mm) pegmatoid patches diffusely dispersed through the paleosome.

In places the granodioritic gneiss and associated mafic dykes are agmatized by biotite quartz monzodiorite, containing a striking blue-irridescent plagioclase (50-65%; An11), quartz (20-25%), microcline (15%), biotite (6%), and traces of allanite, epidote, and zircon. Quartz monzodiorite identical to this occurs elsewhere in the Groswater Bay Terrane, specifically, near Hare Bay, northeast of Cartwright (Owen et al., 1983).

Associated and interbanded with the granodioritic gneiss is medium-grained (1-4mm), grey to rose (quartz) monzonitic orthogneiss (unit 5B). This unit consists predominantly of microcline (25-45%), plagioclase (An10; 20-40%), quartz (2-10%), blue-green to olive-green hornblende, biotite, and accessory epidote, allanite, zircon and sphene.

In summary, the Bluff Head orthogneiss is a group of granodioritic to (quartz) monzonitic rocks which differs from the WBIGC in predominant

lithologies and metamorphic grade. For this reason, subsequent discussion treats both domains separately. Further discussion of the relationships between the pre-Grenvillian lithostructural domains is presented in section 4.5.

2.3 THE BENEDICT MOUNTAINS INTRUSIVE SUITE

Granitoid rocks of the Benedict Mountains Intrusive Suite (BMIS) are dominant in the northern half of the study area. Five members of the BMIS have been identified. The normative quartz-K feldspar-plagioclase compositions of each has been plotted in Figure 2-3. Compared with the visually estimated modal composition of these rocks, the normative modes are somewhat quartz-rich, particularly for monzodioritic to monzonitic rocks. Figure 2-3 nonetheless delineates broad compositional variations within the BMIS. The average bulk rock compositions of the five members of the BMIS identified within the study area are presented in Table 2-3.

The oldest rock unit grouped in the BMIS in this study is K feldspar-megacrystic quartz monzodiorite to granodiorite (unit 6A), which has been dated (Rb-Sr, whole rock) at 1787 $\pm$ 35Ma (see section 2.8.2). Gower and Ryan (in press) recently have proposed that ca. 1.8Ga granitoids in eastern Labrador may be attributed to a major "Makkovikian" orogenic event characterizing the Makkovik Province, and suggested that ca. 1.65Ga plutonic rocks, including the BMIS, belong to a separate tectonic event known as the Labradorian orogeny. Unit 6A is nonetheless included in the BMIS in the present study since it contains NNE-trending fabrics defined by amphibolite-facies mineral assemblages also observed in relatively young (ca. 1.7Ga) members of the BMIS in the Smokey area.

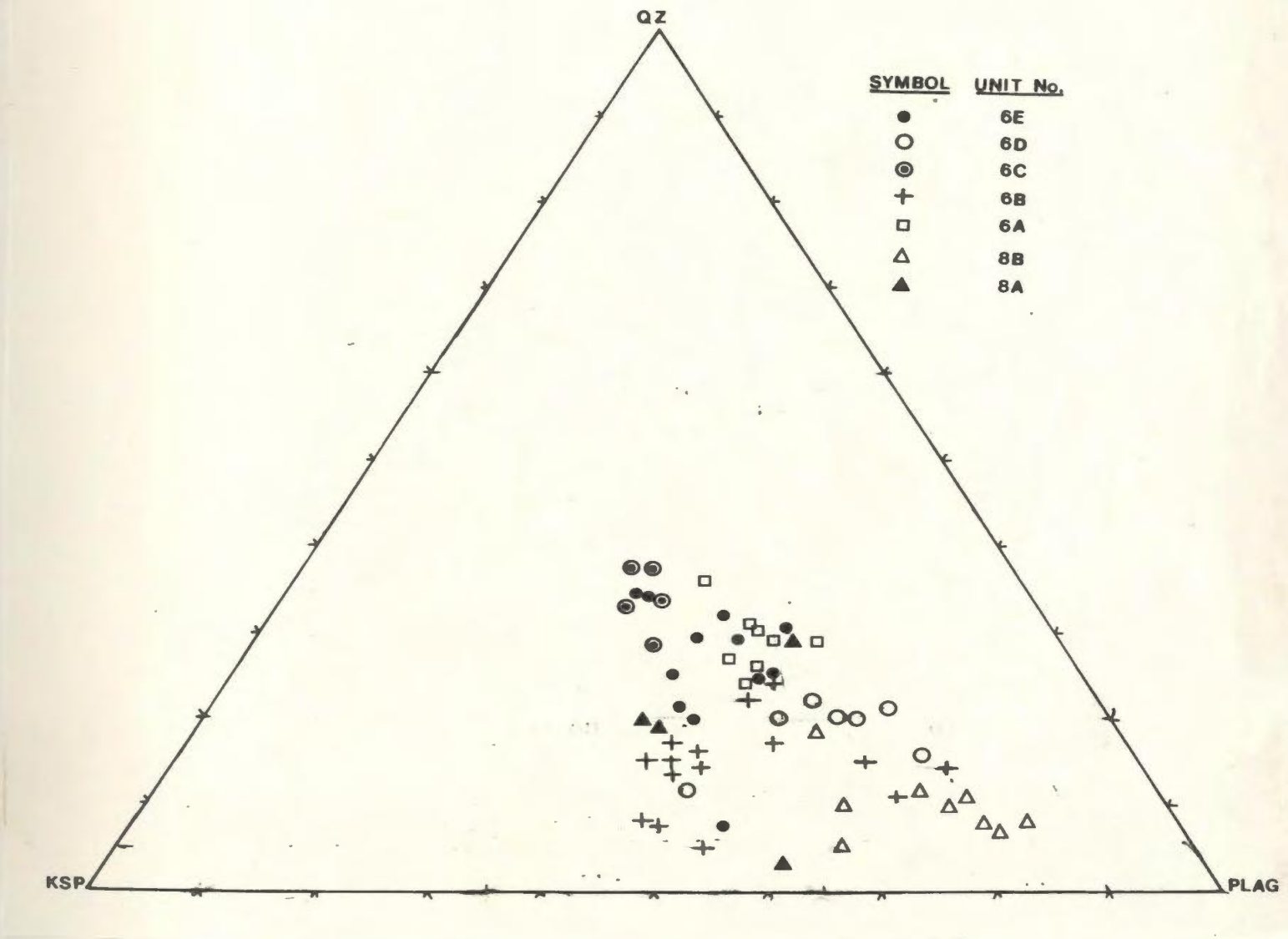

Figure 2-3. Normative quartz, K feldspar, and plagioclase contents of five members of the Benedict Mountains Intrusive Suite, and of clinopyroxene-bearing monzonitic to monzodioritic rocks.

Table 2-3. Major element geochemistry of the BMIS

	Unit 6A	Unit 6B	Unit 6C	Unit 6D	Unit 6E
SiO_2	69.8 (2.5)*	64.5 (2.7)	75.6 (1.7)	65.2 (1.1)	71.8 (2.0)
TiO_2	0.31 (0.10)	0.55 (0.19)	0.09 (0.05)	0.42 (0.14)	0.28 (0.10)
Al_2O_3	15.3 (0.9)	16.3 (1.1)	12.6 (0.8)	16.5 (0.6)	14.1 (0.8)
**Fe_2O_3	2.53 (0.64)	4.78 (1.22)	1.26 (0.40)	3.83 (0.64)	2.22 (0.62)
MnO	0.04 (0.01)	0.09 (0.02)	0.02 (0.00)	0.08 (0.03)	0.05 (0.01)
MgO	0.67 (0.24)	0.88 (0.62)	0.16 (0.06)	1.39 (0.23)	0.39 (0.25)
CaO	2.09 (0.49)	2.51 (1.03)	0.67 (0.21)	3.13 (0.50)	1.26 (0.42)
Na_2O	3.96 (0.37)	4.28 (0.35)	3.30 (0.21)	4.34 (0.45)	4.04 (0.57)
K_2O	4.38 (0.69)	5.44 (1.40)	5.62 (0.31)	3.90 (1.26)	5.02 (0.72)
P_2O_5	0.11 (0.09)	0.13 (0.06)	0.03 (0.02)	0.15 (0.03)	0.05 (0.05)
LOI	0.53 (0.53)	0.56 (0.26)	0.64 (0.32)	0.74 (0.41)	0.69 (0.26)
	99.72	100.02	99.99	99.68	99.90
# of analyses:	16	15	5	7	12

( )* = one standard deviation

** all iron as Fe_2O_3

Owen and Rivers (1983) distinguished this unit from schistose, but otherwise similar granodiorites exposed in the central portion of the study area. These latter rocks were grouped along with the gneissic rocks described above into Owen and Rivers' medium- to high-grade basement complex. Subsequent mapping has demonstrated, however, that Owen and Rivers' early granodioritic unit actually comprises both early orthogneisses (retrograded jotunite, unit 3B) as well as megacrystic granodiorite (unit 6A). The field distinction of these units, although hampered by the pervasive development of schistose Grenvillian fabrics, is possible due to the local preservation of orthopyroxene in incompletely retrogressed jotunite. The megacrystic granodiorites (unit 6A) to the north and south of the Cut Throat Island Fault (CTIF) have identical compositions (Table 2-4), a feature which supports the areal extent of the unit as presently portrayed in Figure 2-1.

The quartz monzodiorite to granodiorite of unit 6A consists of plagioclase (An22-25; 25-45%), microcline (10-25%), quartz (15-25%), biotite (1-5%), hornblende (1-5%), with accessory apatite, and opaques. This unit locally contains garnet associated with Grenvillian fabrics south of the CTIF (Fig. 2-1), a feature also noted in other members of the BMIS. North of Cut Throat Island, the unit exhibits a well-defined north- to northeast-trending ("Makkovik trend") schistose to gneissose fabric, which is overprinted by east-trending Grenvillian L-S fabrics in the southern portion of the study area. Gneissose fabrics in unit 6A are particularly well exposed north of Man of War Point, and are defined by hornblende- and (or) biotite-rich segregations and by lens-shaped amphibolite enclaves.

Table 2-4. Statistical comparison of major element chemistry of quartz monzodiorite-granodiorite (unit 6A) to the north and to the south of the Cut Throat Island Fault (CTIF). Samples to the north of the CTIF are unfoliated or bear Makkovik trend fabrics, while those to the south have a Grenvillian fabric (GS2, see Chapter 3). The t-test shows that compositions of the two sample groups are statistically indistinguishable at the 0.05 level of significance except for MnO and K2O, which are statistically identical at the 0.025 level of significance.

	North of CTIF			South of CTIF					
	$\bar{Y}$	σ	$(Yi - \bar{Y})^2$	$\bar{Y}$	σ	$(Yi - \bar{Y})^2$	s^2	s	t
SiO2	70.0	2.73	44.62	69.7	2.55	52.09	6.91	2.63	0.19
TiO2	0.28	0.11	0.08	0.34	0.09	0.06	0.01	0.10	1.19
Al2O3	15.28	0.80	3.85	5.33	1.04	0.06	0.89	0.94	0.15
Fe2O3*	2.48	0.69	2.85	2.57	0.64	3.33	0.44	0.66	0.27
MnO	0.05	0.02	0.00	0.04	0.01	0.00	0.00	0.01	1.98
MgO	0.71	0.28	0.28	0.64	0.20	0.34	0.06	0.24	0.58
CaO	2.05	0.42	1.07	2.12	0.56	2.56	0.26	0.51	0.02
Na2O	4.04	0.43	1.12	3.90	0.34	0.93	0.14	0.38	0.73
K2O	4.04	0.38	0.89	4.64	0.77	4.76	0.40	0.63	1.89
P2O5	0.09	0.05	0.02	0.12	0.12	0.12	0.01	0.09	0.66

* all iron as Fe2O3
$\bar{Y}$ = mean
σ = population standard deviation
$(Yi - \bar{Y})^2$ = sum of squares of deviations
s^2 = variance
s = sample standard deviation
t = Student's t (comparing two means)
critical value of t (n=16) at 0.05 level of confidence is 1.753
critical value of t (n=16) at 0.025 level of confidence is 2.131

Samples north of the CTIF:
V40, V192, V333-1, V340, V427, V428, V766
Samples south of the CTIF:
V260, V274-1, V294, V393-1, V546-1, V628, CG-79-344, CG-79-366, CG-79-377

Monzodiorite to monzonite (unit 6B) exposed in the vicinity of Abliuk Bight (and elsewhere) constitutes the most voluminous member of the BMIS exposed in the Smokey archipelago. This unit intrudes jotunitic gneiss (unit 3A) of the WBIGC on the west side of Entry Island, however, crosscutting relationships with megacrystic granodiorite (unit 6A) were not observed, hence the relative age of these two units is not known directly from field relations. A Rb-Sr (whole rock) age of 1697 + 41Ma (see section 2.8.2) obtained for the monzodiorite nonetheless demonstrates that the monzodiorite postdates the megacrystic granodiorite.

The monzodiorites are rose to grey, medium to coarse-grained and consist of plagioclase (An12-24; 30-50%), variably antiperthitic microcline (40-55%; 20-40%), and lesser amounts of quartz (0-10%), hornblende (4-8%), biotite (1-3%), and accessory apatite, zircon, and, in places, garnet. North of the Benedict Fault, the monzodiorites, along with younger members of the BMIS (units 6C, 6D, 6E), are generally massive, however Makkovik trend fabrics are developed locally along zones up to ~1km wide.

Buff- to rose-coloured, fine-grained (1-2mm) granodiorite to granite (unit 6C) comprises the third member of the BMIS. These rocks occur as small (m-scale) tabular or lensoid bodies scattered throughout the study area, and locally intrude or contain inclusions of monzonite (unit 6B), megacrystic granodiorite (unit 6A), and clinopyroxene-bearing monzonite (unit 8B, see below). Despite the range of compositions represented by this unit, the rocks are consistently fine- to medium-grained (1-3mm), leucocratic (CI=1-3), and characteristically have patches of rusty-weathering iron sulphides. Microcline and sodic plagioclase (An1-12) contents vary from 20-60% and 15-40%, respectively, with the

remainder of the rock consisting of quartz (15-25%) and minor amounts of biotite, hornblende and pyrite.

The fourth member of the BMIS is a coarse megacrystic granodiorite (unit 6D) exposed at Cape Rouge. Microcline megacrysts up to 6cm in diameter typically constitute from 15-35% of the rock, and are set in a plagioclase (An17-24) and quartz-rich groundmass, which contains $\leq$5% K feldspar, hornblende (2-5%), biotite (1-4%), accessory apatite, sphene, and, in places, epidote.

The age of unit 6D relative to the first three members of the BMIS is unknown. Inclusions of this unit occur in medium-grained (2-5mm), pink biotite granite (unit 6E) in Bluff Head Cove, and large (km-scale), tabular to ovoid bodies of the granodiorite occur in the granite (unit 6E) in the vicinity of Cape Rouge. Just east of this locality, the contact between the two units is exposed, and the grain size of the granite decreases from 3mm to less than 1mm within two metres of the granodiorite. This observation is interpreted as a chilling effect and implies a marked temperature contrast between the granite magma and its host rocks, and suggests that at least late plutons of the BMIS were intruded at high crustal levels.

The biotite granite (unit 6E) is dominant at Cape Rouge, and consists of microcline (30-45%), plagioclase (An16-22; 20-40%), quartz (20-25%), biotite (1-4%), hornblende (0-2%), and may include accessory sphene and apatite. The age of biotite granite (unit 6E) relative to megacrystic granodiorite (unit 6A), hornblende-biotite monzodiorite (unit 6B), and biotite-hornblende leucogranite

(unit 6C) is unknown from field relationships. Unit 6E yields a Rb-Sr (whole rock) age of 1725 $\pm$ 31Ma (see section 2.8.2), within-error of the ca. 1697Ma age determined for unit 6B.

2.4 POSSIBLE CORRELATIVES OF THE ADLAVIK INTRUSIVE SUITE

Gower (1981) correlated differentiated mafic to felsic plutonic rocks around and to the north of Groswater Bay with similar rocks at Adlavik Bay, some 100km west-northwest of the study area. These latter gabbroids, first described by Stevenson (1970) and Clark (1979), have been termed the Adlavik Intrusive Suite (AIS) by Gower (1981).

In the study area, a heterogeneous assemblage of layered gabbroic rocks similar to those described by Stevenson (1970) and Clark (1979) occurs between Holton and Emily Harbour (Unit 7; Fig. 2-1). Layering in the gabbros is defined largely by variations in the proportion of plagioclase to mafic phases, although granulometric layering is also present in a hornblende (s.l.)-megacrystic variety of the suite (see below). The igneous layering generally strikes to the NNE, and dips moderately to the west. Variations in lithologies across the body suggest that the intrusion youngs towards the west or northwest (Gower, 1982). Identical layered gabbroic rocks occur sporadically throughout the western half of the study area (e.g. on Mundy and East Pompey Islands).

Three lithological varieties of mafic rocks correlated with the AIS have been recognized; these are: an olivine-bearing ultramafic rock, hornblende-megacrystic mesogabbro, and non-megacrystic meso- to leucogabbro. Of these, only the third is volumetrically important, and the variants are not distinguished in Fig. 2-1. All gabbroic rocks tentatively correlated with the AIS are collectively referred to as

unit 7. Their average bulk rock compositions are listed in Table 2-5.

Olivine-bearing ultramafic rocks form the basal member of the intrusion, and are exposed at Emily Harbour and on Mundy Island. At these localities, the unit appears to be at most a few tens of metres thick, and, in the Emily Harbour occurrence, grades westward through olivine-bearing gabbro, and olivine-free mesocratic to leucocratic gabbro near Holton. The ultramafic rock typically contains amphibole (35-45%), clinopyroxene (10-25%), orthopyroxene (0-20%), and olivine (10-15%), and may include accessory amounts of biotite, plagioclase, white mica, and ilmenite. Approximately 0.6km up-section (west) of Emily Harbour, olivine occurs with plagioclase in a sample (V635-1) of gabbro also containing clinopyroxene, orthopyroxene, biotite and ilmenite (see section 4.4).

Two types of olivine-free gabbro have been recognized. The first is a conspicuously hornblende-megacrystic mesogabbro (CI=25-45). Idiomorphic hornblende megacrysts up to 3cm in diameter are commonly restricted to 5-100cm thick, relatively melanocratic layers, intercalated with non-megacrystic mesogabbro. Clinopyroxene and minor biotite occur throughout the rock. With a decrease in the proportion of hornblende megacrysts, the unit grades into hornblende + clinopyroxene + biotite mesogabbro and leucogabbro, comprising the bulk of the AIS within the study area. In places, the mesogabbro contains up to ~5% interstitial K feldspar. Nowhere, however, has the gabbro been seen to grade into intermediate compositions of plutonic rocks.

Except for primary igneous layering, the gabbros are generally massive, and lack any tectonic fabric. However, greenschist-facies assemblages occur locally,

Table 2-5. Major element geochemistry of gabbroids tentatively correlated with the Adlavik Intrusive Suite.

	-1-		-2-	-3-	
SiO_2	46.6	(2.2)*	49.5	48.9	(3.95)
TiO_2	0.30	(0.14)	0.64	0.95	(0.64)
Al_2O_3	5.4	(1.4)	11.6	18.18	(4.97)
**Fe_2O_3	10.01	(1.94)	9.54	10.24	(5.10)
MnO	0.16	(0.02)	0.17	0.14	(0.05)
MgO	22.52	(3.63)	11.51	6.09	(3.24)
CaO	11.75	(3.64)	11.88	10.16	(2.12)
Na_2O	0.73	(0.22)	2.09	2.62	(0.82)
K_2O	0.39	(0.18)	0.94	1.44	(0.79)
P_2O_5	0.04	(0.02)	0.15	0.20	(0.17)
LOI	1.45	(0.29)	1.10	1.28	(0.96)
	99.35		99.12	100.20	
# of analyses:	4		2	5	

( )* = one standard deviation

** all iron as Fe_2O_3

-1- = ultramafites

-2- = amphibole-megacrystic gabbroids

-3- = mesocratic to leucocratic gabbroids

and are attributed to Grenvillian metamorphism. Contacts between the AIS and surrounding rocks are rarely seen, although the gabbroids crosscut quartz monzonitic orthogneiss (unit 4) in the southeast corner of Abliuk Bight. Age relations with various members of the BMIS are less clear, however. Enclaves of medium-grained mesogabbro within megacrystic granodiorite (unit 6A) on the south shore of Brig Harbour Island have been tectonized, and may either be deformed inclusions or remnants of a disrupted dyke of the AIS. Xenoliths of a similar mesogabbro occur in unstrained monzodiorite (unit 6B) south of Emily Harbour. Relations with other members of the BMIS are unknown. Gower (1981) suggested that intrusion of the gabbroids in part overlapped with emplacement of the BMIS. Unfortunately, the unit has not yielded a satisfactory age using the Rb-Sr method; Rb-Sr isotopic compositions of ultramafic to leucogabbroic samples of unit 7 define a scattered quasi-linear array of points defining an "age" of 1747 $\pm$ 310Ma (see section 2.8.2).

2.5 CLINOPYROXENE-BEARING PLUTONIC ROCKS

2.5.1 Monzonite

Two varieties of monzonitic-syenitic rocks of uncertain affinities occur within the study area. Both contain clinopyroxene, a mineral not observed in the BMIS in the study area, but typifying many of the monzonitic rocks of the Groswater Bay terrane (Gower and Owen, 1984) and gabbros correlated with the AIS. The two clinopyroxene-bearing monzonites have contrasting bulk rock compositions (Table 2-6), and have differing normative quartz, plagioclase and K feldspar contents (Fig. 2-3).

Unit 8A, is a grey to beige quartz-bearing monzonite to syenomonzonite,

which forms an ovoid body between Ice Tickle and Cut Throat Islands (Fig. 2-1), and which intrudes the western flank of the AIS exposed near Holton. It is locally characterized by a well developed igneous lamination, defined by variations in the proportions of mafic minerals to feldspars, and is composed of variably perthitic microcline (40-60%), plagioclase (An30; 15-25%), quartz (2-10%), hornblende (8-12%), clinopyroxene (Wo42, En37, Fs21; sample V621) (0-5%), biotite (1-3%), and accessory zircon, apatite, and ilmenite-magnetite. The clinopyroxene is typically mantled by hornblende.

Unit 8B is a grey to purplish-grey clinopyroxene- and quartz-bearing monzodiorite to monzonite exposed in the vicinity of Bluff Head Cove. Unlike unit 8A, this unit lacks igneous lamination. It typically consists of medium-grained (2-5mm) plagioclase (An30; 30-50%) and microcline (20-45%), with lesser clinopyroxene (Wo45, En40, Fe15; sample V453-1; 2-6%), biotite (1-4%), hornblende (0-4%). In places, the monzonite contains up to 10% blue quartz. Clinopyroxene is typically mantled by hornblende.

Field evidence for the relative ages of units 8A and 8B and the BMIS and AIS is ambiguous. Inclusions of a monzonitic rock similar to unit 8B occur within hornblende-biotite monzonite (unit 6B) on an islet off the headland near East Pompey Island, but contacts with the AIS are not exposed. However, near Holton, quartz-bearing monzonitic rocks of unit 8A intrude the AIS, and are themselves crosscut by hornblende-biotite monzonite (unit 6B) on Cut Throat Island.

The above observations indicate that both the AIS and the clinopyroxene-

bearing monzonites predate younger members of the BMIS. Although age relations between unit 8B and the AIS are unknown, unit 8A clearly postdates these gabbroids. Both the gabbroic rocks of the AIS and the monzonites-syenomonzonites of unit 8A commonly show well-developed igneous layering, and may be part of the same differentiated sequence. This supposition is supported by the occurrence of unit 8A along the western ("upsection") flank of the body of AIS gabbroic rocks between Emily Harbour and Holton, and by the relative ages of both units. Nowhere in the study area, however, have gabbroic rocks been seen to grade directly into potassic rocks. This may be a result of rapid compositional changes within the AIS. For example, layered ca. 1610Ma (Rb-Sr, whole rock; Brooks, 1983) gabbroic rocks at Grady Island (Owen et al., 1983), northeast of Cartwright, grade into monzonitic-syenitic rocks over the distance of a few metres. In the absence of continuous exposure, such rapid compositional changes would hinder the recognition of these rocks as part of a continuous differentiated sequence.

2.5.2 Ferrodiorite to Ferrosyenite

A distinctive group of layered quartz-bearing syenitic to dioritic plutonic rocks (unit 9) occurs in the northwestern portion of the study area (Fig. 2-1). The unit is distinctly ferruginous (Table 2-6), and is chemically distinct from the granitoids of the BMIS (Table 2-3) and the clinopyroxene-bearing monzonites of units 8A and 8B (Table 2-6), particularly with regard to incompatible trace elements such as Nb, Y, Zr, and Ce. Inclusions of hornblende-biotite monzonite (unit 6B) occur in ferrosyenomonzonites on Chance Island, and dykes of unit 9 crosscut the pre-Grenvillian north-northeast "Makkovik trend" fabric

Table 2-6. Major element geochemistry of clinopyroxene-bearing plutonites.

	Unit 8A		Unit 8B		Unit 9	
SiO_2	64.7	(4.2)*	58.2	(2.8)	62.2	(2.2)
TiO_2	0.64	(0.22)	0.93	(0.50)	0.77	(0.29)
Al_2O_3	15.2	(1.3)	17.0	(0.9)	14.4	(0.7)
**Fe_2O_3	5.26	(1.91)	6.83	(1.21)	8.44	(1.50)
MnO	0.10	(0.04)	0.12	(0.02)	0.22	(0.05)
MgO	0.64	(0.20)	3.05	(0.98)	0.50	(0.42)
CaO	2.33	(0.79)	5.50	(1.40)	2.43	(0.39)
Na_2O	4.19	(0.68)	4.34	(0.54)	4.60	(0.51)
K_2O	5.80	(0.37)	2.94	(0.87)	5.46	(0.16)
P_2O_5	0.17	(0.08)	0.34	(0.16)	0.15	(0.15)
LOI	0.48	(0.23)	0.58	(0.24)	0.42	(0.27)
	99.51		99.83		99.59	
# of analyses:	4		12		7	

( )* = one standard deviation

** all iron as Fe_2O_3

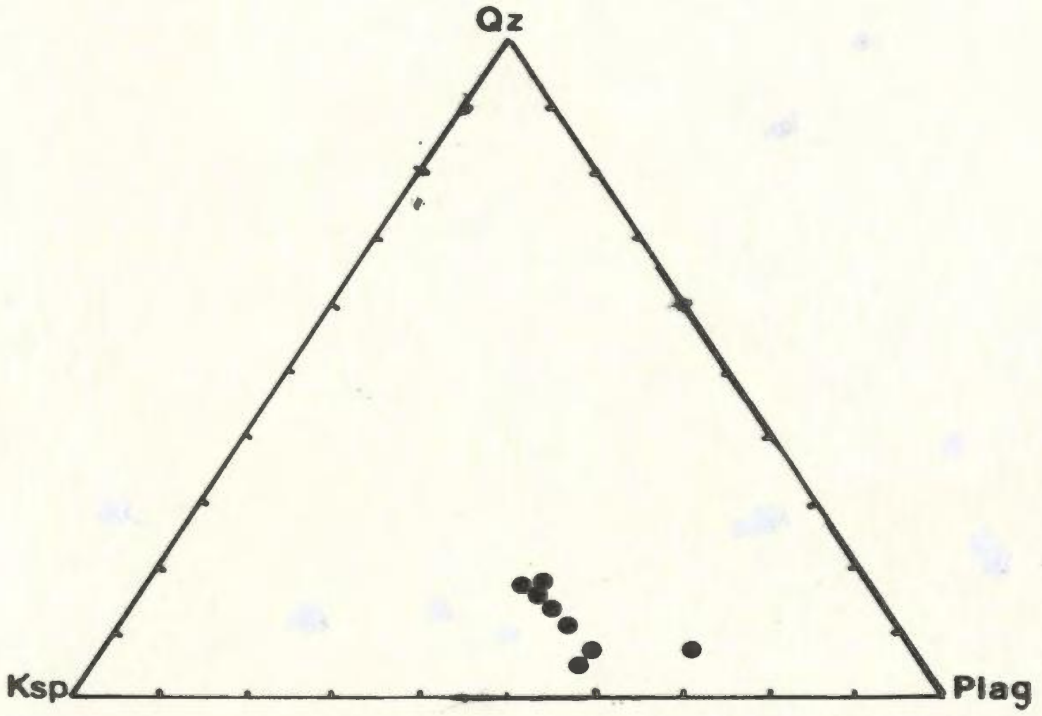

Figure 2-4. Normative quartz, K feldspar, and plagioclase contents of ferrodiorite-ferrosyenite (unit 9)

characterizing the BMIS. These observations demonstrate that the ferrosyenite-ferrodiorite postdates the BMIS, a conclusion supported by the younger, albeit overlapping Rb-Sr (whole rock) age of 1676 $\pm$ 77Ma determined for the unit (see section 2.8).

Although a wide range of compositions of unit 9 is represented in the study area, intermediate (Fig. 2-4) to potassic members are dominant, and are particularly well exposed on Chance Island and mid-way between Holton and Cape Rouge. These rocks are extensively weathered, and consist of antiperthitic microcline (35-70%), sodic plagioclase (An1-5; 5-20%), quartz (2-15%), clinopyroxene (Wo46, En3, Fs51; sample V341-1) (5%), biotite (0-5%), hornblende (1-6%), Fe(Ti) oxides (1-3%), commonly with accessory zircon. Layering, where present, is defined by cm-scale variations in the proportion of mafic minerals to feldspars.

The dioritic member of the suite is exposed west of Abliuk Bight. This is the only known occurrence of the unit south of the Benedict Fault within the study area. The rock consists of plagioclase (An41), microcline (5-15%), clinopyroxene (Wo43, En28, Fs29; sample V693) (4%), biotite (3%), and Fe(Ti) oxides (2%). Oriented plagioclase laths up to 8mm in length define a well-developed fabric, but igneous layering is not evident.

2.6 MICHAEL GABBRO

Dykes of homogeneous, coronitic olivine gabbro exposed in the southern half of the study area are part of a suite of olivine tholeiite intrusions referred to as the Michael gabbro (unit 10). Individual dykes range up to about 100m in thickness. The dykes lack any Grenvillian fabric except where transected by

minor (<5m-wide) Grenvillian shear zones. As a consequence, primary igneous textures are well preserved. In outcrop, the Michael gabbro has a characteristic bronze weathered surface, always with distinct, 1-10cm thick fine-grained chilled margins.

Emslie (1983) reported that plagioclase, augite, and olivine are the dominant minerals in the Michael gabbro. Accessory red-brown biotite, apatite and ilmenite may be present, and hypersthene occurs to the exclusion of olivine in the cores of some thick dykes.

The Michael gabbro intrudes all rocks in the study area except for ferrosyenite-ferrodiorite (unit 9). The latter is exposed largely in the northwestern portion of the study area, while the Michael gabbro has not been identified north of the Benedict Fault (Gower and Owen, 1984). The Michael gabbro is considered to postdate the ferruginous plutonic rocks of unit 9 since the gabbro has yielded Neohelikian isotopic ages using both the Rb-Sr and K-Ar methods. The Rb-Sr (whole rock) ages of 1461 $\pm$ 96Ma (Fahrig and Loveridge, 1981) and ca. 1383Ma (Brooks, 1982) are broadly consistent with K-Ar (whole rock) ages of 1348 $\pm$ 120Ma and 1323 $\pm$ 52Ma (Wanless et al., 1972, 1973, both cited in Fahrig and Loveridge, 1981) determined for the unit.

The significance of the K-Ar ages determined for the Michael gabbro are difficult to ascertain, since they record the time through which the dykes cooled past the blocking temperature of argon (in different minerals) rather than the age of intrusion itself. The possible presence of excess radiogenic argon, particularly in the northern Grenville Province (e.g. Dallmeyer and Rivers, 1983) must also be

considered when evaluating these K-Ar dates.

The Rb-Sr ages determined for the Michael gabbro are also suspect. Fahrig and Loveridge (1981) selectively sampled felsic material occurring as veinlets in what they describe as the Michael gabbro. Compared with their mafic host rock, these veinlets are enriched in silica and alkalis, and are depleted in iron, magnesium and calcium (Fahrig and Loveridge, 1981). The localization of these veinlets in tensional fractions, into which "volatile low temperature constituents" (Ibid, p. 101) are concentrated, suggests that they may contain extraneous material derived from the host rocks into which the gabbro was emplaced. Isotopic dates determined from such material should thus be regarded with caution. The ca. 1383Ma age determined by Brooks (1982) is based on only three samples, and must be regarded as a preliminary age determination. In conclusion, a reliable age for the intrusion of the Michael gabbro is presently lacking, although the available data suggest an age of ca. 1.4Ga.

2.7 MISCELLANEOUS GABBROIC INTRUSIVE ROCKS

A ~12km long, 20m-wide rectiplanar dyke of olivine gabbro (unit 11) trending east-southeast from Abliuk Bight through Marks Island to Cut Throat Island has been distinguished from the Michael gabbro in Figure 2-1. It is massive, brown weathering, with well defined chilled margins. In contrast with the Michael gabbro, however, this dyke is undeformed and non-coronitic, and therefore is interpreted to belong to a generation of olivine diabases postdating the Michael gabbro. East-trending rectiplanar mafic dykes dated at ca. 950Ma occur in the Cape Aillik area (Gower et al., 1982). Since these dykes have an orientation similar to the rectiplanar olivine gabbro (unit 11) in the study area, it

is possible that they belong to the same suite of post-Grenvillian mafic intrusions.

The Pottles Bay dyke (Fig. 2-1) is a discontinuous 1km wide ridge of layered mesocratic to leucocratic pyroxene- and garnet-bearing metagabbroic rocks trending WNW from Pottles Bay Cove. It has characteristics of both the Michael gabbro and the AIS, and is grouped with uncorrelated gabbroic intrusive rocks (unit 12). The Pottles Bay dyke is locally intruded by granitic pegmatites. In these areas, the gabbroids are characterized by abundant hornblende and biotite, the presence of which are indicative of hydration and alkali metasomatism associated with pegmatoid intrusion. Two similar decametre-scale dykes with chilled margins crosscut the granodioritic gneisses (unit 5A) 1km west of Bluff Head. Layering in these dykes, a feature not observed in dykes of the Michael gabbro as mapped in this area, is defined by variations in the proportion of mafic/felsic minerals. Unit 12 comprises a wide range of intrusive mafic rocks not readily correlable with members of the AIS, Michael gabbro, or the olivine diabase of unit 11. The largest mass of uncorrelated mafic rocks occurs on the south side of Pottles Bay. It consists of massive, medium to coarse grained amphibolite, containing amphibole, plagioclase $\pm$ biotite $\pm$ (clino?)pyroxene. Samples of this body have not been examined in thin section.

Only relatively large bodies of mafic rocks are indicated in Figure 2-1. Two generations of small-scale ($<$1m wide) mafic dykes not depicted in Figure 2-1 are: (1) hornblende-megacrystic metabasite, which is crosscut by (2) plagioclase-phyric metabasite. The hornblende-megacrystic metabasite dykes typically trend N75E, and consist of hornblende (as a 1-2mm megacrystic phase and in the groundmass) + biotite + plagioclase (An24) $\pm$ epidote $\pm$ quartz. The plagiocase-phyric dykes

(see Owen and Rivers, 1983, Fig. 19.3) trend N75E to N140E, and contain 1-5mm clusters of saussuritized plagioclase (An20-25) set in a groundmass of hornblende + plagioclase + biotite ± epidote. Crosscutting relations between these dykes are exposed on the south shore of the islet 1.5km to the west of East Pompey Island. Although other, fine-grained metadiabase dykes occur in the study area, these two megacrystic dyke suites are the most easily recognized, and serve as useful stratigraphic markers (Table 2-7). These minor mafic bodies of various ages are important indicators of changing metamorphic conditions, and are considered in some detail in Chapter 4.

Narrow (<2m wide), intermediate to felsic dykes locally crosscut K-feldspar megacrystic granodiorite (unit 6A) and hornblende-biotite monzodiorite (unit 6B). These dykes were observed on Cut Throat, Marks, and Run By Guess Islands. The dykes consist predominantly of microcline, plagioclase (An 7-17, with normal zoning of up to 5 mol.% An), and quartz, but are rather melanocratic, and contain up to 25% mafic minerals including hornblende, biotite ± garnet ± allanite ± epidote. They range in composition from quartz monzodiorite to granite, but the field term "intermediate dykes" is retained here to emphasize their variable composition and melanocratic character.

2.8 RUBIDIUM-STRONTIUM GEOCHRONOLOGY

Seven major rock units have been isotopically dated by the Rb-Sr (whole rock) method. For ease of reference, this absolute chronology is compared with the relative field-based chronology of major rock units in Table 2-7. Regressed data yielding MSWD values ≤3 are considered to be isochrons, otherwise they are considered to be errorchrons (Brooks et al., 1972). The dated units are: dioritic-

Table 2-7. Age relations and metamorphism of major rock units of pre-Grenvillian lithostructural domains. Rock units post-dating the Makkovik trend are not critical to the definition of the lithostructural domains, and record only the effects of the Grenvillian orogeny.

Table 2-7.

Post-Makkovik Trend Rock Units

----> olivine gabbro dykes (11)* [6B]*

-polyphase Grenvillian deformation-

----> Michael gabbro 1461 ± 96Ma [6B]

Ferrosyenite to Ferrodiorite (9) [6A,6B]
(1676 ± 77Ma)

Age Relations of Major Rock Units, Pre-Grenvillian Litho-structural Domains

	TRANS-LABRADOR BATHOLITH BATHOLITH	GROSWATER BAY TERRANE Bluff Head Orthogneiss	GRANULITE COMPLEX
		W.B.I.	
?AIS	(8A) Cpx Syenomonzenite	<(8B) Cpx. Monzonite>*	
AIS	(7) Gabbro, Leucogabbro, Ultramafic rocks		
	*---->C	*---->C	*---->C
BMIS	(6E) Bio. Granite [6D] (1725 ± 31Ma)		
	(6D) Megacrystic Granodiorite		
	(6C) Leucogranite [6B]		
	*---->B	*---->B	*---->B
	(6B) Monzodiorite [3A] (1697 ± 40Ma)		
	(6A) Granodiorite [2] (1787 ± 35Ma)		
		*---->A	(4) monzonitic gneiss
		(5) Granodioritic-Monzonitic	*---->A
			(3) Jotunite (1899 ± 187Ma)
			(2) Dioritic-Tonalitic gneiss (1923 ± 148Ma)
			(1) Metapelitic gneiss

Pre-Grenvillian Fabrics & Metamorphic Mineral Assemblages

Pre-Grenvillian Fabrics & Metamorphic Mineral Assemblages		
(1) Present Orientation: N-NE (Makkovik Trend)	E-W**	variable, generally ENE
(2) Metamorphic Grade: Amphibolite Facies	Amphibolite Facies**	Granulite to Amphibolite Facies
(3) Metamorphic Conditions Unknown	ca. 500C**	Granulite facies P = 7-8 ± 1kb T = 830-860 ± 75C retrograded to: P ~ 5.5 ± 1.5kb T ~ 650 ± 50C
(4) Probable Age: ca. 1.9-1.6Ga	ca. ?1.65Ga	Granulite facies event prob. ≥1.9Ga Retrogression ca. ?1.8-1.65Ga

( )* = unit number; [ ]* = unit intruded by ( )
< >* plutonic rock typical of the Groswater Bay Terrane
*--->Mafic dyke rocks: (minimum relative ages) C = Plagioclase-phyric metabasite; B = Hornblende-megacrystic metabasite A = Hornblende + clinopyroxene + microcline + plagioclase rock

**Probable significant Grenvillian imprint
Note: metamorphic PT-estimates are summarized from Chapter 4.

tonalitic gneiss (unit 2); jotunitic-charnockitic gneiss (unit 3A); K feldspar-megacrystic quartz monzodiorite-granodiorite (unit 6A); hornblende + biotite monzodiorite-monzonite (unit 6B); biotite quartz monzonite-granite (unit 6E); and clinopyroxene-bearing ferrodiorite-ferrosyenite (unit 9).

These units represent three broad groups of rocks. Units 2 and 3A belong to the WBIGC, and would be expected to yield dates older than members of the BMIS, barring a tectono-metamorphic disturbance of Rb-Sr systematics in these rocks. Units 6A, 6B and 6E span the intrusive sequence of the BMIS as preserved in the study area. Each of these plutonic rocks locally contains the Makkovik trend fabric which postdates the gneissic fabric of the WBIGC, and predates the intrusion of the ferrodiorite-ferrosyenite (unit 9). An age of crystallization of the latter unit would thus place an upper limit on the time of development of the Makkovik trend.

Isotopic data used in the age determinations are presented in Appendix A.3, along with a description of the analytical methods employed in this study. Errors in the age and initial ratio (I.R.) specified for each date are expressed at the 2-sigma level of uncertainty.

2.8.1 Geochronology of the White Bear Islands Granulite Complex

Isotopic data for both members of the WBIGC dated in this study define errorchrons yielding ages predating but within-error of the ca. 1787Ma age determined for the oldest member of the BMIS (unit 6A; see below). An age of 1923 $\pm$ 148 Ma (I.R. = 0.7026 $\pm$ 0.0005) has been determined for the dioritic to tonalitic gneisses of unit 2 (Fig. 2-5).

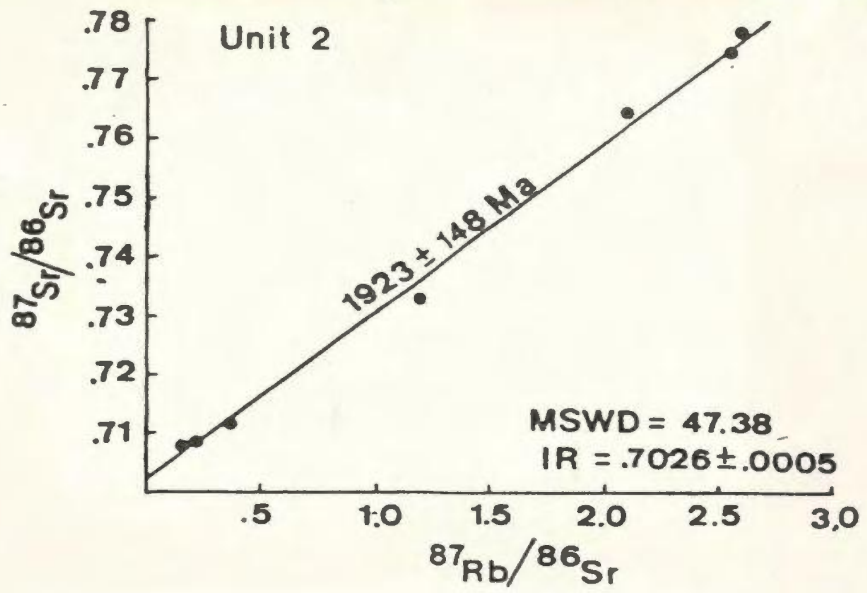

Figure 2-5. Rb-Sr (whole rock) seven point errorchron of dioritic-tonalitic gneiss (unit 2) of the White Bear Islands Granulite Complex.

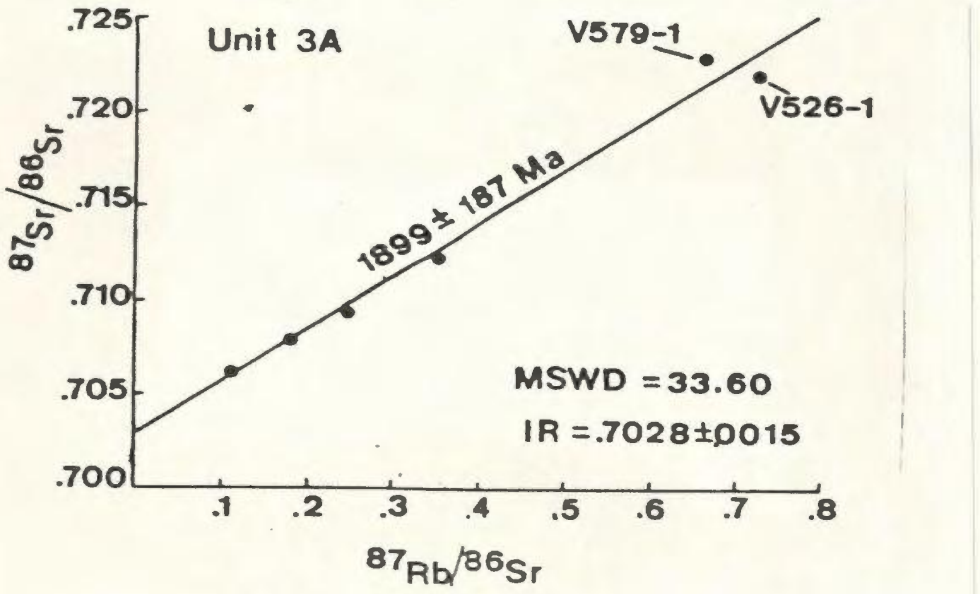

Figure 2-6, Rb-Sr (whole rock) six point errorchron of jotunitic-charnockitic gneiss (unit 3A) of the White Bear Islands Granulite Complex

An analytically identical age of 1899 ± 187Ma (I.R. = 0.7028 ± 0.0015) is determined from samples of jotunitic-charnockitic gneiss (unit 3A). In some respects, unit 3A is well suited to isotopic dating by the Rb-Sr method because it shows minimal retrograde features, and may show marked lithological and compositional variations on an outcrop scale. For example, specimens of both jotunitic gneiss (V193) and relatively K feldspar-rich charnockite (V193-3) were sampled a few metres apart from an outcrop in the White Bear Islands (see Map 2, in pocket). However, the Rb-Sr age determined for unit 3A has a very large error, which stems from divergent 87Sr/86Sr ratios determined for the two samples (V579-1, V526-1) of highest Rb/Sr ratios (Fig. 2-6). Both samples are orthopyroxene-bearing quartz monzodiorites (jotunites), V579-1 also contains garnet, and V526-1 clinopyroxene. Specimen V526-1 was sampled from a decameter-scale patch of unretrogressed jotunite from Run By Guess Island. Despite extensive hydration of the enclosing gneisses, this sample is free of amphibole, shows no signs of retrogression in thin section, and retains mineral compositions similar to other specimens of jotunitic gneiss sampled elsewhere in the WBIGC.

Specimen V579-1 comes from an islet southwest of North Island, and is from the only known locality in which texturally stable garnet + orthopyroxene coexist in the jotunite gneiss. Although lacking amphibole, retrograde biotite-quartz symplectites replace both orthopyroxene and garnet in this sample, suggesting that reequilibration has had a more profound effect on V579-1 than on V526-1 during cooling of the WBIGC. Omitting V526-1 from the errorchron presented in Figure 2-6 yields an age of 1968 ± 231Ma (I.R. = 0.7028 ± 0.0008; MSWD =

31.38) while omitting V579-1 instead provides an age of 1772 ± 66Ma (I.R. = 0.7033 ± 0.0002; MSWD = 3.15). The latter age is similar to that provided by the four point errorchron (1756 ± 122Ma, I.R. = 0.7033 ± 0.0004; MSWD = 4.53) defined when both samples are excluded. Neither sample, however, shows evidence of significant hydration. Consequently, disturbance of Rb-Sr systematics related to metasomatism (e.g. Field and Raheim, 1980, 1981) is likely negligible in these samples, and there is no justifiable reason for omitting either V526-1 or V579-1 from the errorchron presented in Figure 2-6.

The isotopic compositions of retrograded jotunitic-charnockitic gneiss (unit 3B) have not been determined. In contrast, all samples of dioritic-tonalitic gneiss (unit 2) have been retrograded to amphibolite-facies (e.g. hornblende + oligoclase ± clinopyroxene). Despite this retrogression, unit 2 yields an age (ca. 1.92Ga) similar to that determined for unit 3A (ca. 1.90 Ga), although both ages have very large errors. The available data are not amenable to determining the likelihood that either or both dates have been isotopically reset, consequently the isotopic ages determined for units 2 and 3A are inferred to provide an upper limit on the time of granulite-facies metamorphism in the area, which is estimated to be ca. ≥ 1.90Ga B.P.

2.8.2 Geochronology of the BMIS and the Age of the Makkovik Trend

Three of the five members of the BMIS identified in the study area have been dated isotopically. These are: (1) biotite ± hornblende quartz monzodiorite-granodiorite (unit 6A); hornblende-biotite monzodiorite (unit 6B); and biotite ± hornblende quartz monzonite-granite (unit 6E). Biotite ± hornblende

leucogranodiorite-granite (unit 6C) and megacrystic hornblende-biotite granodiorite (unit 6D) have not been dated.

On the basis of field relationships, it is known that unit 6B predates unit 6C, and that unit 6D predates unit 6E. Unit 6A is inferred to be the oldest member of the BMIS in the area since in this unit, the Makkovik trend fabric is most pervasively developed, and includes gneissose as well as schistose variants, the latter being more typical of younger members of the BMIS. It is worth noting that the relative ages of units 6B and 6E are unknown from field relationships.

Biotite $\pm$ hornblende quartz monzodiorite-granodiorite (unit 6A), yields the oldest age (1787 $\pm$ 35Ma; I.R. = 0.7033 $\pm$ 0.0002) (Fig. 2-7). This age determination, along with the pervasive development of the north-northeast "Makkovik trend" in these granodiorites suggest that the unit is synkinematic with respect to the Ketilidian orogeny (ca. 1.8 Ga; Allaart, 1966). It may be tentatively be concluded that the peak development of the Makkovik trend occurred about this time, although waning stages of this event are manifest in rocks up to approximately 100Ma younger. For example, hornblende-biotite monzodiorite-monzonite (unit 6B) locally bears north-northeast trending fabrics and this unit yields an age of 1697 $\pm$ 41Ma (I.R. = 0.7040 $\pm$ 0.0005) defined by the errorchron presented in Figure 2-8.

The only member of the BMIS from the study area isotopically dated in a previous study is biotite granite (unit 6E) from the southeast shore of Byron Bay. Wanless et al. (1972, p. 88) suggested that the K-Ar (biotite) age of 1425 $\pm$ 50Ma determined for a sample of the biotite granite demonstrated that the last period of

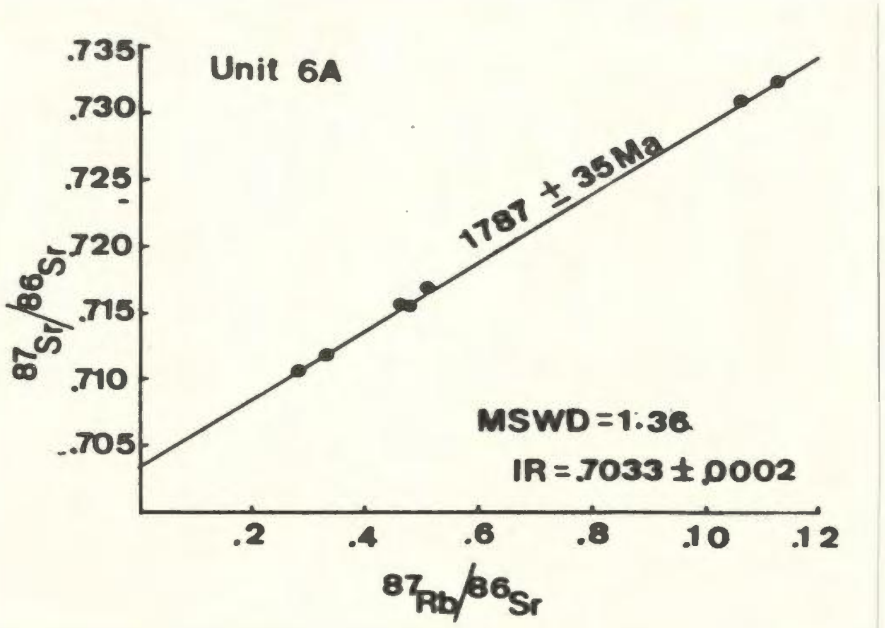

Figure 2-7. Rb-Sr (whole rock) seven point isochron of K feldspar-megacrystic granodiorite (unit 6A) of the BMIS.

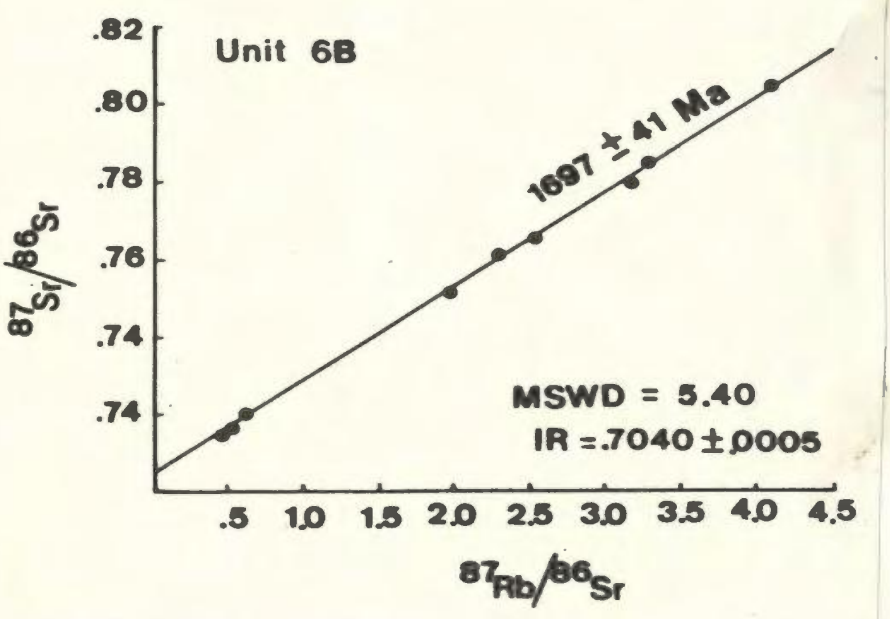

Figure 2-8. Rb-Sr (whole rock) nine point errorchron of hornblende-biotite monzodiorite (unit 6B) of the BMIS.

orogenic activity in the immediate area occurred during Elsonian times, and that the location of the sample (at Byron Bay, immediately west of Cape Rouge) did not lie within the Grenville Province. A four-point Rb-Sr (whole rock) isochron (Fig. 2-9) for the granite (unit 6E) defines a much older age of 1725 $\pm$ 31Ma (I.R. = 0.7032 $\pm$ 0.0006), and suggests that Wanless et al.'s K-Ar age does not record the time of intrusion of the unit. The Rb-Sr date falls within-error of those determined for both K feldspar megacrystic granodiorite (unit 6A) and hornblende-biotite monzodiorite (unit 6B), and the relative age of these units can not be ascertained from the available data. For the purposes of the present study, however, the relative and absolute ages of either unit are not critical. More important is the observation that both units contain Makkovik trend fabrics only locally, and where present these fabrics are schistose rather than gneissose, as is locally the case in the older hornblende-biotite granodiorite (unit 6A). These dates suggest that the waning stages of tectono-metamorphic activity associated with the Ketilidian orogeny continued up to $\sim$100Ma after the development of the penetrative fabrics in the synkinematic (?) granodiorite (unit 6A). This is supported by similar, amphibolite-facies mineral assemblages in metabasites outlining the Makkovik trend in both units 6A and 6E (see section 4.2.3).

An upper age limit on the development of the Makkovik trend is provided by discordant ferrodiorite-ferrosyenite (unit 9). This unit yields an age of 1676 $\pm$ 77Ma (I.R. = 0.7020 $\pm$ 0.0013) (Fig. 2-10). This date is consistent, although overlapping, with the isotopic dates determined for units 6B and 6E of the BMIS.

Rubidium-strontium isotopic compositions determined for a series of ultramafic to leucogabbroic rocks of unit 7 (AIS?) define a scattered quasi-linear

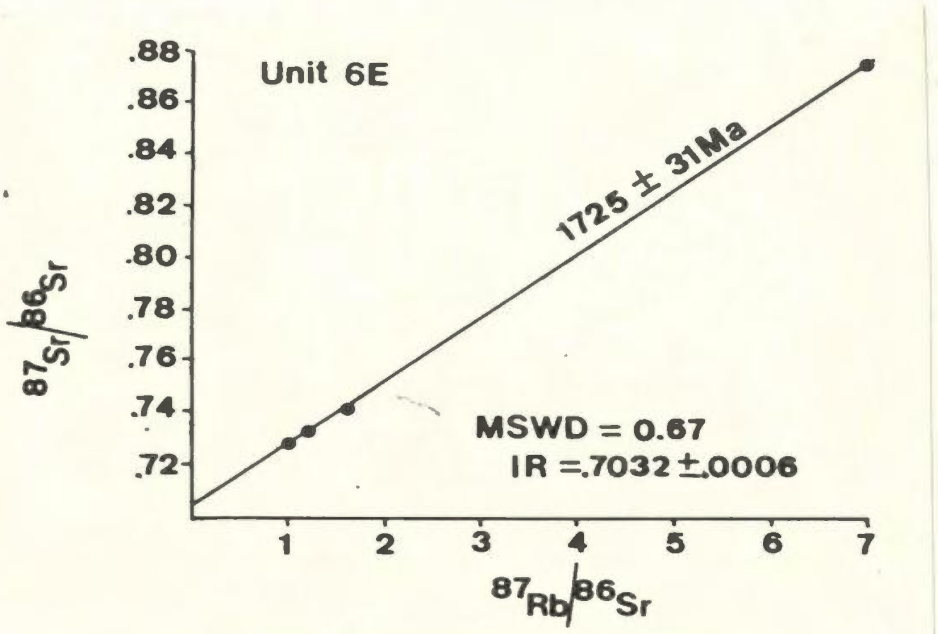

Figure 2-9. Rb-Sr (whole rock) four point isochron of biotite granite (unit 6E) of the BMIS.

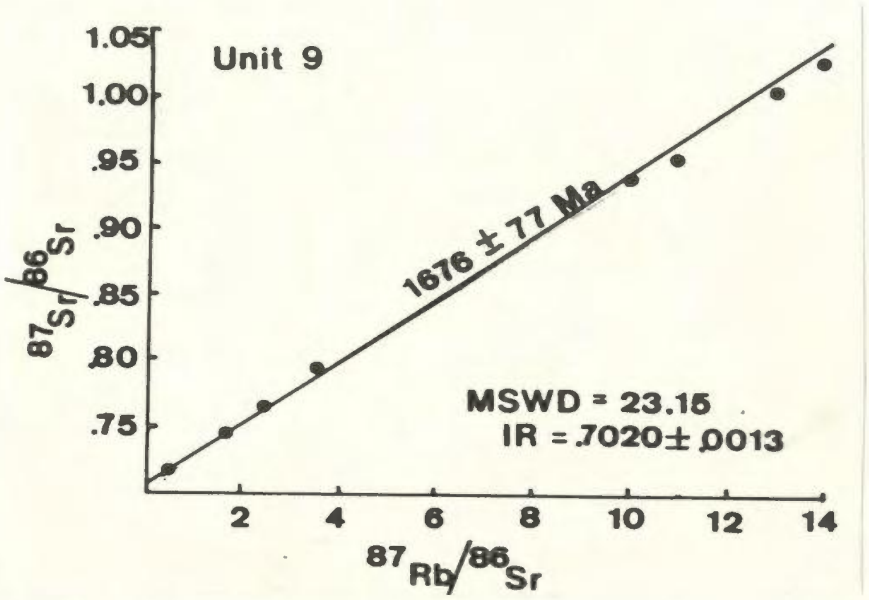

Figure 2-10. Rb-Sr (whole rock) seven point errorchron of clinopyroxene-bearing ferrosyenite-ferrodiorite (unit 9).

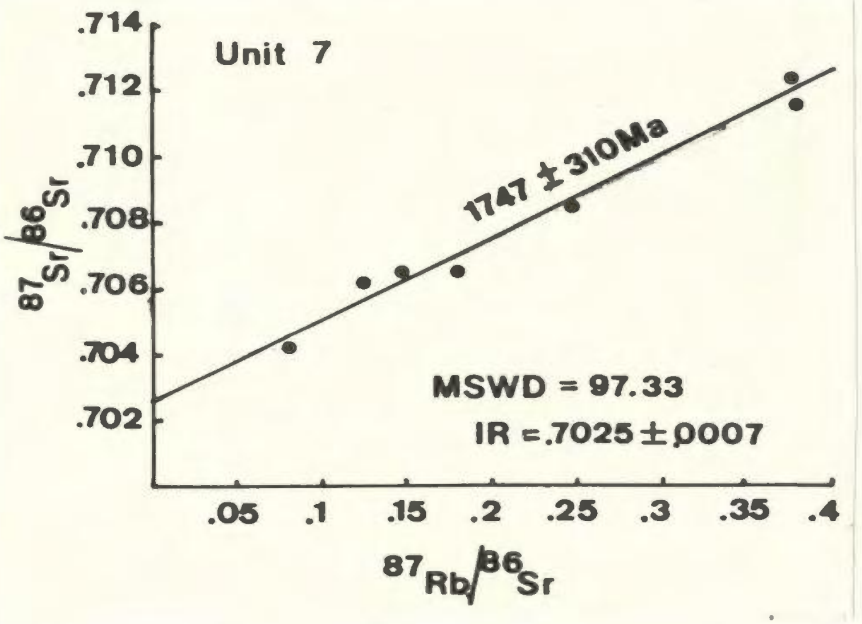

Figure 2-11. Rb-Sr (whole rock) seven point errorchron of mafic-ultramafic rocks (unit 7) tentatively correlated with the Adlavik Intrusive Suite.

array (Fig. 2-11) which yields an "age" of 1747 $\pm$ 310Ma (I.R. = 0.7025 $\pm$ 0.0007). Although consistent with field evidence indicating a broad temporal overlap between these gabbroic rocks and the granitoids of the BMIS, the large error associated with this date preclude meaningful interpretation of relationships between the two suites. The temporal relationship between the gabbroic rocks of unit 7 and specific members of the BMIS thus remains unclear.

Taken together, the Rb-Sr isotopic dates constrain the age of granulite facies metamorphism of the WBIGC to ca. $\geq$ 1.9Ga B.P., and the development of the Makkovik trend in the BMIS to 1.9-1.6Ga.

CHAPTER 3
STRUCTURE

3.1 PREAMBLE

The first step in the structural interpretation of polydeformed geological terranes is the recognition of different generations of structures. Whether an individual fabric is a product of a discrete deformational episode or formed as part of a deformational continuum is a separate problem that is best dealt with following the establishment of a descriptive structural framework. Such a framework should emphasize the relative chronology of structural elements as deduced on the basis of various structural overprinting criteria, and may include the age of igneous intrusions and metamorphism relative to a particular deformational episode. Once the framework has been established, particular generations of structural elements or temporally distinct groups of structures may be found to characterize certain rock units, which may then be grouped as separate structural domains for comparative and interpretative purposes. Although there may be several reasons for contrasts between such domains, there are two general cases: (1) neighbouring domains share a common structural evolution, with contrasting structural styles reflecting marked differences in the rheological behaviour of their respective component lithologies, and (or) abrupt changes in the degree of development of fabrics (e.g. due to heterogeneous strain); or (2) neighbouring domains have, at least in part, independent structural histories, either as a result of diachronous deformation, or due to the tectonic juxtaposition of discrete crustal blocks (allochthons), or both.

Igneous intrusions of a known absolute age provide useful time markers for

distinguishing deformational events in geological terranes. For example, dykes of the ca. 1.4Ga Michael gabbro have been used to distinguish Grenvillian from pre-Grenvillian deformational and metamorphic features in the Smokey archipelago.

3.2 STRUCTURAL AND LITHOSTRUCTURAL SUBDIVISION OF THE SMOKEY ARCHIPELAGO

The distinction of Grenvillian from pre-Grenvillian structural and metamorphic features has led to two tripartite subdivisions of the Smokey archipelago. Three structural domains have been identified by the variable degree of development of fabrics related to the Grenvillian orogeny in a north-south transect across the study area. The Grenvillian structural domains are also characterized by the metamorphic grade of Grenvillian fabrics within them. The three pre-Grenvillian lithostructural domains have been defined principally on the basis of specific rock assemblages and their metamorphic grade, and, to a lesser degree, by the orientation of pre-Grenvillian fabrics.

The heterogeneous development of Grenvillian fabrics in a section from north to south across the study area led to the recognition of the three east-trending Grenvillian structural domains. These domains, first described by Owen and Rivers (1983), and presented in revised form in Figure 3-1, comprise a northern domain (M = Makkovik) dominated by north- to northeast-trending pre-Grenvillian fabrics (Fig. 3-1A, Makkovik trend; Ermanovics et al., 1982), a southern domain (G = Grenville) dominated by east-trending Grenvillian fabrics (Fig. 3-1C), and a transitional domain (T) in which structural orientations characteristic of domains M and G are well represented (Fig. 3-1B).

The three lithostructural domains are the White Bear Islands Granulite

Figure 3-1. Structural and lithostructural subdivision of the Smokey archipelago. The structural subdivision consists of three domains (M, T, and G) separated by Grenvillian high-strain zones. The lithostructural subdivision consists of three groups of pre-Grenvillian metamorphic rocks (White Bear Islands Granulite Complex, Bluff Head orthogneiss, and the Benedict Mountains Intrusive Suite). The region outside of the areas marked "W.B.I. Granulite Complex" and "Bluff Head orthogneiss" is dominated by the plutonic rocks of the Benedict Mountains Intrusive Suite.

A = Domain M, 38 poles to Grenvillian and pre-Grenvillian planar structures

B = Domain T, 40 poles to Grenvillian and pre-Grenvillian planar structures

C = Domain G, 98 poles to Grenvillian schistose planar structures

D = White Bear Islands Granulite Complex, 52 poles to pre-Grenvillian gneissic planar structures

E = Bluff Head orthogneiss, 20 poles to pre-Grenvillian gneissic planar structures.

Note: "N" and "S" show the position of the schematic north-south transect portraying the distribution of Grenvillian metamorphic mineral assemblages in Figure 4-14 (p. 200)

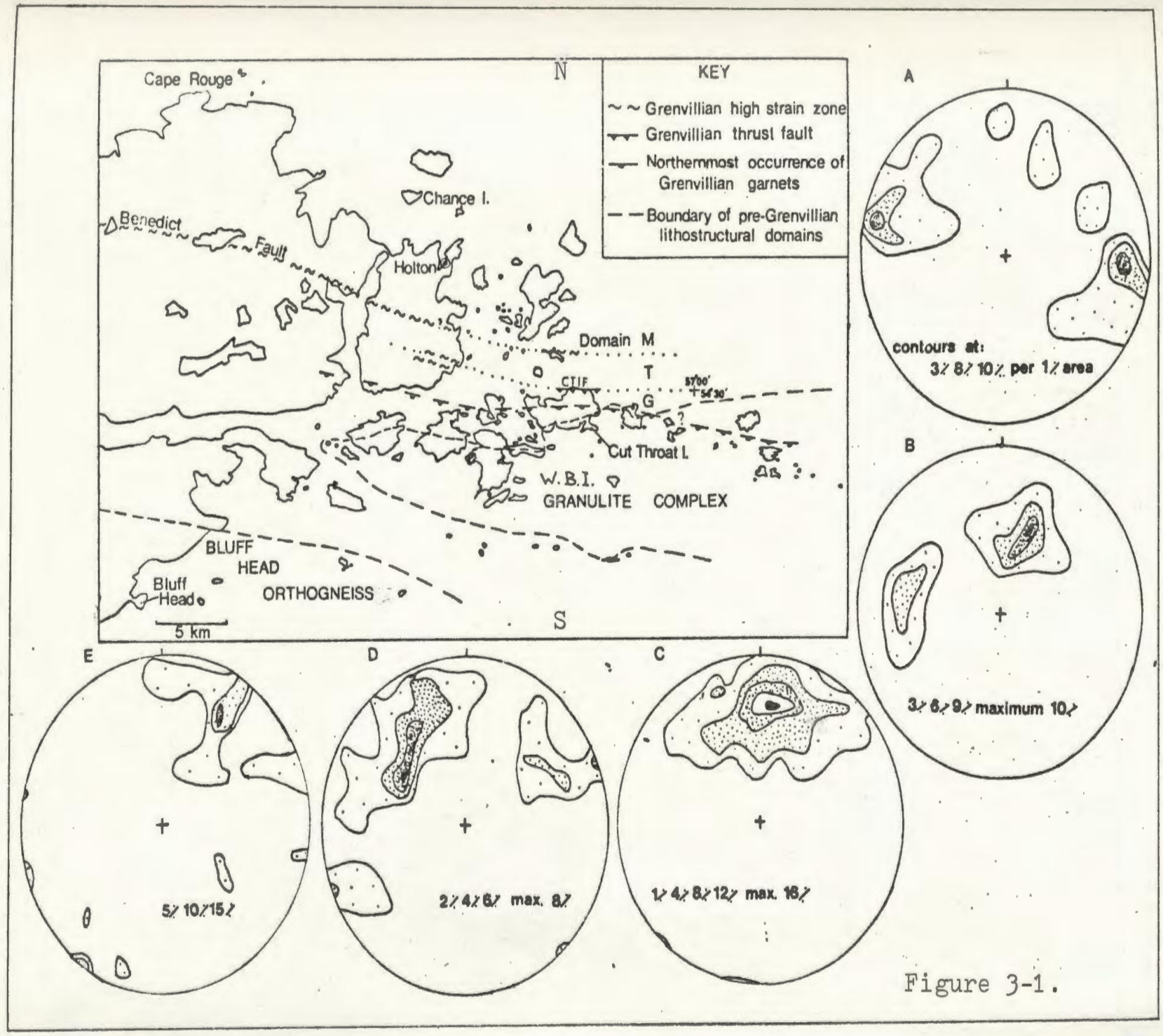
Cape Rouge
N
KEY
Grenvillian high strain zone
Grenvillian thrust fault
Northernmost occurrence of Grenvillian garnets
Boundary of pre-Grenvillian lithostructural domains
Chance I.
Benedict
Fault
Holton
Domain M
CTIF
T
G
Cut Throat I.
W.B.I.
GRANULITE COMPLEX
BLUFF
HEAD
Bluff Head
ORTHOGNEISS
5 km
S
A
contours at:
3% 8% 10% per 1% area
B
3% 6% 9% maximum 10%
C
1% 4% 8% 12% max. 16%
D
2% 4% 6% max. 8%
E
5% 10% 15%

Figure 3-1.

Complex (WBIGC), the Bluff Head orthogneiss, and the Benedict Mountains Intrusive Suite. Key features of each domain have already been summarized in Table 2-7.

The boundaries of the Grenvillian structural domains coincide with major east-trending Grenvillian high-strain zones. The northern and southern boundaries are, respectively, the Benedict and Cut Throat Island faults. Neither fault coincides with discernible linear features on 1:50,000 scale aerial photographs, and there is no recognizable aeromagnetic signature associated with the faults. Both faults were thus identified only during systematic mapping in the area.

The Benedict and Cut Throat Island faults are represented by rocks with schistose to mylonitic fabrics having a pronounced linear component. These strongly deformed rocks grade abruptly into their less highly strained protoliths (e.g. Owen and Rivers, 1983, Fig. 19.6B). The Benedict Fault is well exposed on the north side of Pigeon Island and on the shoreline of Abliuk Bight. Its position as portrayed in Figures 2-1 and 3-1 lies some 6km to the north of Gower's (1981) extrapolation of the fault to the Labrador coast. The schistose to mylonitic fabrics associated with the Benedict Fault are developed within a moderately (30°-65°) south-dipping zone that is $\leq$0.5km wide (or $<$0.4km thick, measured perpendicular to the mylonitic fabric).

The Cut Throat Island Fault (CTIF) is at least 50m thick, and is represented by a series of anastomosing, metre-scale zones of mylonite. The mylonites grade abruptly (over a few cm) into lineated ($L \leq S$), moderately (30°)

south-dipping schistose fabrics. The CTIF is extrapolated WNW along-strike to two decametre-scale mylonite zones near Man of War Point, for a combined "length" of ~13km. The extent of the CTIF westward from the Man of War Point mylonites is not known; mylonites along-strike in Abliuk Bight were not observed. It is possible that the mylonite zone narrows towards the west. This is observed, for example, in the Benedict Fault, which varies in width from a few tens of metres (e.g. on the west side of Abliuk Bight) to upwards of 0.5km (south of Cape Rouge, and on Pigeon Island), and consists of only a few, variably oriented, minor (<5m wide) high strain zones south of Holton. Both the Benedict and Cut Throat Island faults are described in more detail in section 3.3.3.

East-trending planar fabrics are developed only locally north of the Benedict Fault (domain M). These fabrics, which lack a linear component, are attributed to the Grenvillian orogeny because: (1) they have an orientation similar to planar fabrics south of the Benedict Fault which developed during the deformation of the Michael gabbro, and (2) an east-trending shear zone north of the Benedict Fault, and west of the study area, has yielded an age of 1004 $\pm$ 5Ma (40Ar/39Ar, biotite; Archibald and Farrar, 1979). Grenvillian S-fabrics in domain M are best exposed in the vicinity of Cape Rouge, and are considered to be related to the Adlavik Brook Fault (Gower, 1981). These narrow (<5m wide) high-strain zones are marked by epidote veins and the non-penetrative development of a preferred dimensional orientation of quartz and biotite in granitoid rocks, and of chlorite in deformed mafic rocks. They are east-striking, with variable (but generally southerly) dip directions, and overprint but do not obliterate pre-Grenvillian fabrics (e.g. Makkovik trend). A 30cm-wide mafic dyke on an islet ENE of Cape

Rouge is transected by a narrow (20cm) high-strain zone and shows a dextral displacement of ~1m. The deformed dyke (sample V725-2) contains albite, and actinolite-mantled hornblende, but lacks a well-defined schistose foliation discernable in thin section.

The 3km wide transition zone (Domain T) between the Benedict and Cut Throat Island faults appears, on the basis of limited measurements, to be characterized by a bimodal distribution of planar fabric orientations (Fig. 3-1B). The orientation pattern comprises a south- to southwest-dipping Grenvillian foliation, which only locally contains a linear component, developed along high-strain zones. The Grenvillian foliation overprints penetratively developed ESE-dipping pre-Grenvillian foliate, schistose to gneissose "Makkovik trend" fabrics (cf. Owen and Rivers, 1983, Fig. 19.6C). It is clear from Figure 3-1B that pre-Grenvillian planar fabrics in domain T have not been reoriented into parallelism with the SSW-dipping Grenvillian S-fabrics. Similarly-oriented pre-Grenvillian planar fabrics with variable dip directions characterize Domain M, north of the Benedict Fault (Fig. 3.1A).

The south-dipping L-S fabric typifying the Grenvillian orogeny in the area is most extensively developed south of the CTIF (domain G; Fig. 3-1C). Minor (<5m wide) Grenvillian high-strain zones in domain G typically show dextral offset as recorded by displaced layering (e.g. mafic dykes). These high-strain zones are best developed in granitoid rocks, but are poorly represented in mafic rocks such as the Michael gabbro and gabbros correlated with the AIS.

3.3 GRENVILLIAN DEFORMATION

3.3.1 Chronology of Grenvillian Deformational Episodes

Three phases of deformation attributed to the Grenvillian orogeny have been recognized. These are referred to, from oldest to youngest, as GD1, GD2, and GD3, and are associated with three phases of folding, termed GF1, GF2, and GF3, respectively. Measurable GF1 folds have been observed in Grenvillian structural domains G and T, whereas measurable GF2 and GF3 folds have been observed only in domain G. No measurable Grenvillian folds were observed in domain M.

Planar mineral fabrics developed during GD1 and GD2 are referred to as GS1 and GS2, respectively. Both GS1 and, in particular, GS2, are typically lineated; their respective mineral lineations are referred to as GL1 and GL2. No mineral fabric associated with GD3 has been recognized. For ease of reference, salient features of the three phases of Grenvillian deformation are summarized in Table 3-1.

3.3.2 Field Aspects and Geometry of Grenvillian Structural Elements

The first period of Grenvillian deformation resulted in the development of east-trending, inclined folds (GF1; Fig. 3-2) with moderately to shallowly west-plunging or doubly-plunging fold axes (Fig. 3-3A). GF1 folds are non-cylindrical, and are seen to deform pre-Grenvillian gneissic fabrics. They refold pre-Grenvillian folds, and are outlined in massive Paleohelikian plutonic rocks by deformed mafic dykes (including the Michael gabbro). GF1 folds are best exposed in the vicinity of Bluff Head, where they are upright and open to tight. Within

Table 3-1. Salient features of polyphase Grenvillian deformation in the Smokey archipelago.

Phase	Distribution*	Fold Geometry	Components	Typical Profile
GD3	G,T	cylindrical, inclined	no APS**	tight, Z-shaped
GD2	G,T	cylindrical, reclined	GS2=APS GL2<20° to GF2	tight, S- or Z-shaped
GD1	G,T	non-cylindrical, generally upright	GS1 along attenuated fold limbs GL1 to GF1	open to tight

* see Figure 3-1
** APS = axial planar schistosity

Figure 3-2. Shallowly west-plunging, upright GF1 folds developed in granodioritic gneiss (unit 5A) 5km northeast of Bluff Head.

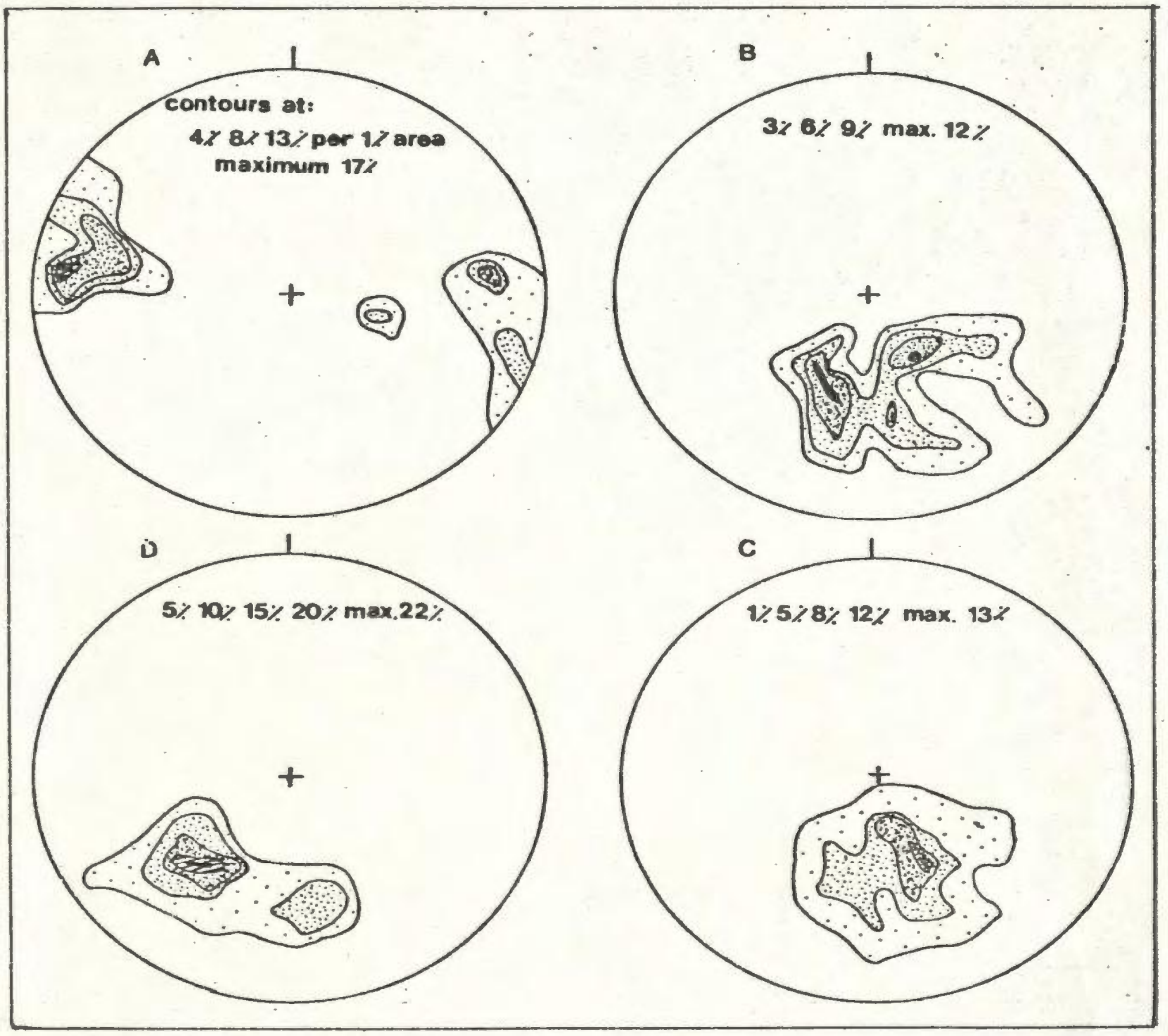

Figure 3-3. Orientation of Grenvillian fold axes and linear fabrics.

A = GD1, 23 fold axes
B = GD2, 32 fold axes
C = GD2, 81 linear structures
D = GD3, 18 fold axes

the study area, GF1 folds have wavelengths ranging from ca. 10cm to >10m, and in some cases are mappable at the 1:100,000 scale. For instance, an upright antiformal GF1 fold with a decametre-scale wavelength deforms a dyke of Michael gabbro about a moderately ESE-plunging axis on an islet southwest of Run By Guess Island, (see Map 1, in pocket).

A regional-scale GF1 fold is exposed on George Island, south of the study area. This fold was first recognized by Gower (1981), and is considered to be a major structural feature of the Groswater Bay Terrane (Gower and Owen, 1984).

The complex orientation pattern of deformed gneissosity observed in outcrops of the granodioritic gneisses near Bluff Head is interpreted to be the result of refolding of pre-Grenvillian structural elements along shallowly west-plunging GF1 axes. Along and immediately to the south of the CTIF, GF1 folds are tight and are north-verging.

A GS1 fabric has been identified only locally. It is a schistose to mylonitic planar fabric with a variably strong linear component. GS1 is typically developed along the attenuated limbs of GF1 folds. Where present, the stretching lineation is at a high angle to the GF1 axis, suggesting that this generation of folds developed by flexural flow (Donath and Parker, 1964). Although mylonite zones related to GD1 are generally south-dipping, a north-dipping shear zone was noted at one locality in the White Bear Islands. This mylonite has detached the lower limb of the associated shallowly west-plunging GF1 fold (Fig. 3-4), and may represent either a backthrust, or the overturned lower limb of a major nappe-like GF1-fold. Similar north-dipping Grenvillian high-strain zones are also associated with the

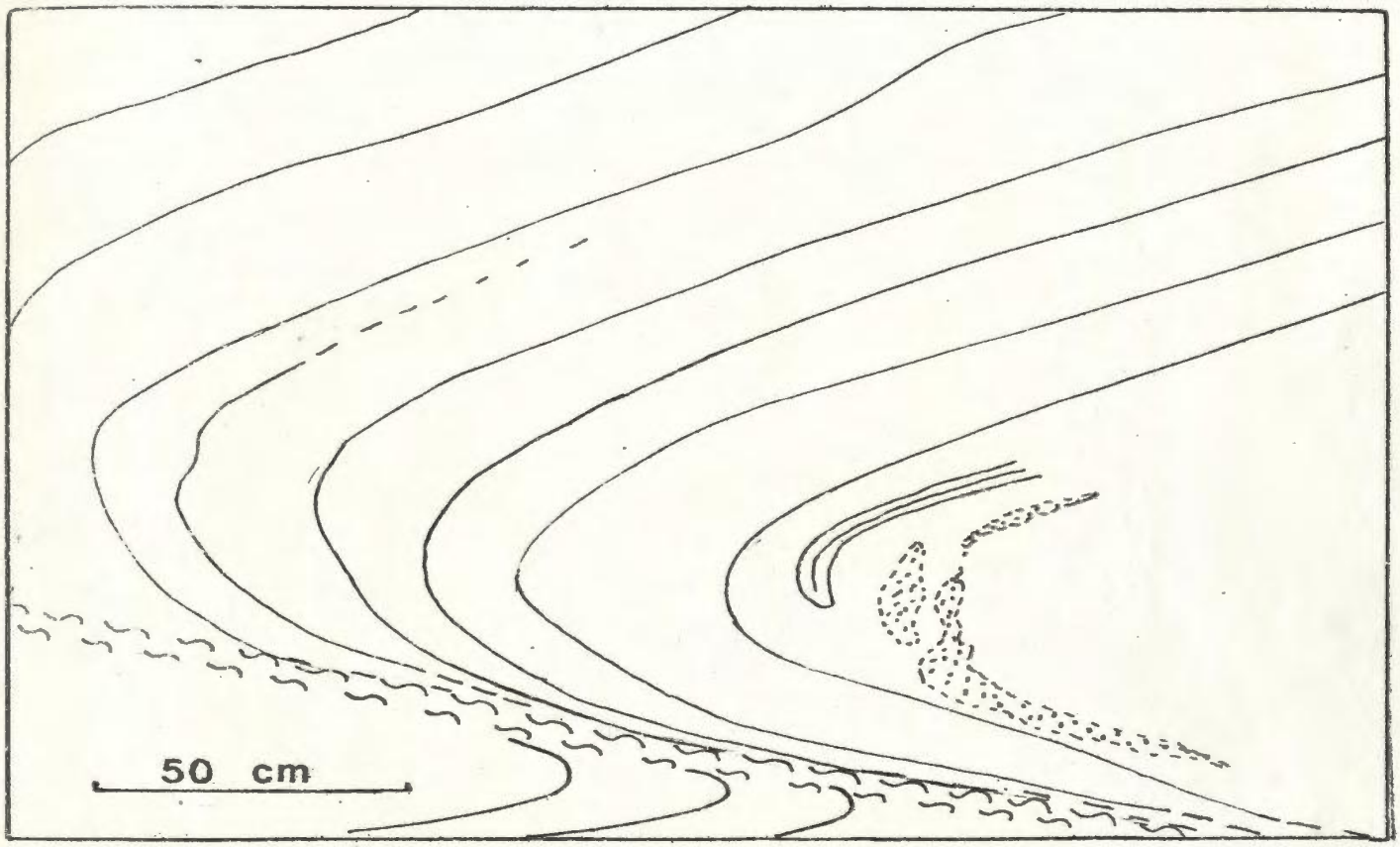

Figure 3-15. North-dipping Grenvillian shear zone displacing the lower limb of a GF1-fold deforming pelitic metatexite (unit 1C). Note folded leucosomes (stippled) and the refolded pre-Grenvillian metabasite in the GF1 fold hinge. Sketched from a photograph; viewed from the east, White Bear Islands.

major antiformal GF1 fold at George Island (Gower et al., 1983) south of the study area.

The second period of Grenvillian deformation produced SE- to SSW-plunging, open to tight reclined folds (GF2; Figs. 3-3B, 3-5). GF2 folds are typically asymmetric. Folding was accompanied by the development of a penetrative south-dipping axial planar foliation (GS2). This foliation coincides with the regional SSE-to SSW-dipping Grenvillian schistosity (Owen and Rivers, 1983), and contains a well-developed mineral lineation (GL2) typically defined by thin (1-2mm), elongate, biotite-rich aggregates. These mineral lineations have a range of orientations similar to that shown by GF2 fold axes (Figs. 3-3B,C). In 21 locations (Fig. 3-6), the planar and linear components of the GD2 fabrics have been measured along with GF2 fold axes. The angle between GL2 and GF2 fold axes as measured in the axial surface (GS2) ranges between 3° and 19°, and averages 9°. The kinematic significance of these data is considered in section 3.3.

GF2 folds are best exposed between Run By Guess and Cut Throat Islands. On Marks Island, a SSE-plunging GF2 fold deforms GF1 folds outlined by both a mafic dyke and a thin (10cm) mylonitic fabric attributed to GD1 (Fig. 3-7). In this outcrop, GS2 forms a penetrative schistose to mylonitic fabric parallel to the GF2 axial surface and locally subparallel to the axial surface of GF1 folds. The angle between the GF2 fold axis and the stretching lineation measured within the GS2 plane is approximately 10°.

Refolded folds are represented on a larger scale by polydeformed dykes of Michael gabbro on the southern portion of Mundy and Ice Tickle Islands (Fig.

Figure 3-5. Southeast-plunging reclined GF2 fold with a well-developed axial planar schistosity (GS2) developed in retrograded jotunitic gneiss (unit 3B). The GS2 fabric contains a strong mineral lineation (GL2). The angle between GL2 and the GF2 axis is 15°. Note the variable development of GS2 in this outcrop. Peninsula on the south shore of Ice Tickle Island. Viewed from the west.

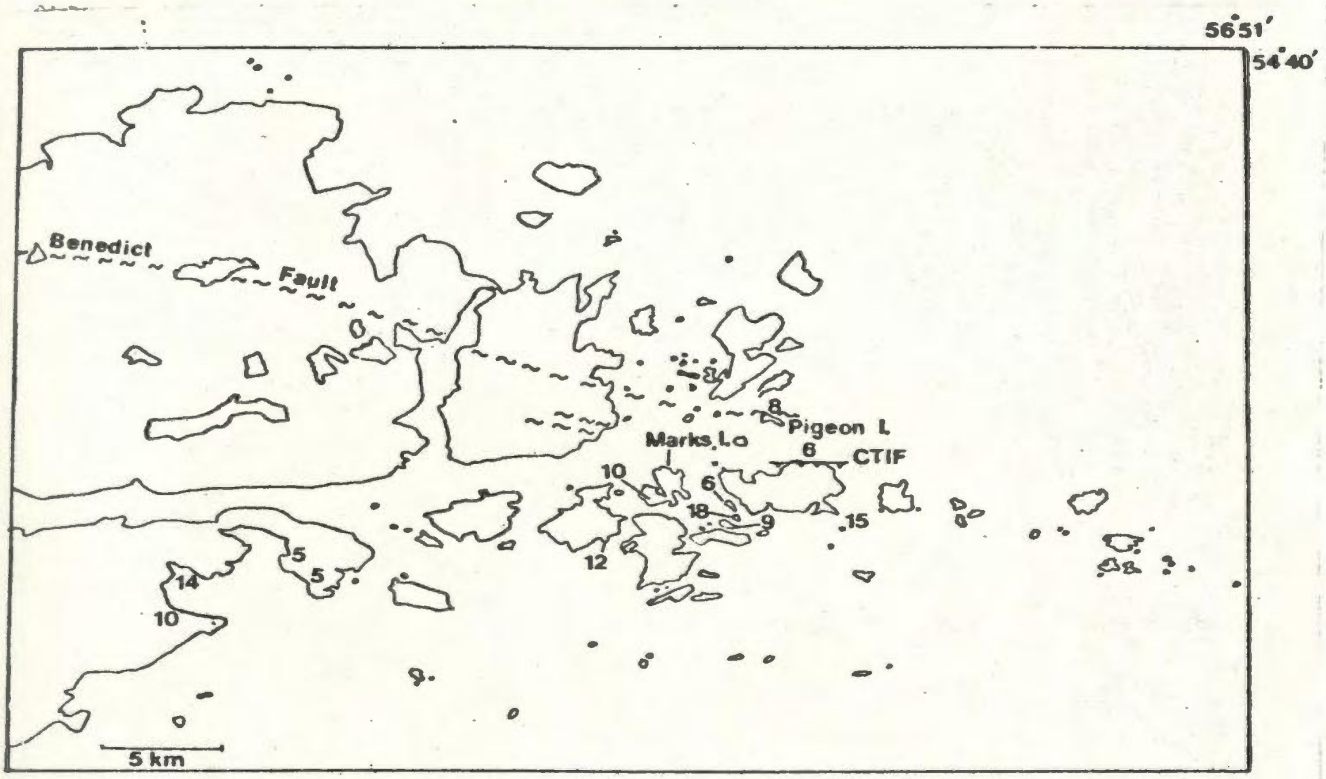

Figure 3-6. Angle between GF2 fold axes and GL2 lineations as measured within GS2 at various locations within the study area. Values recorded at Pigeon Island and along the Cut Throat Island Fault are averages of 4 and 5 measurements, respectively.

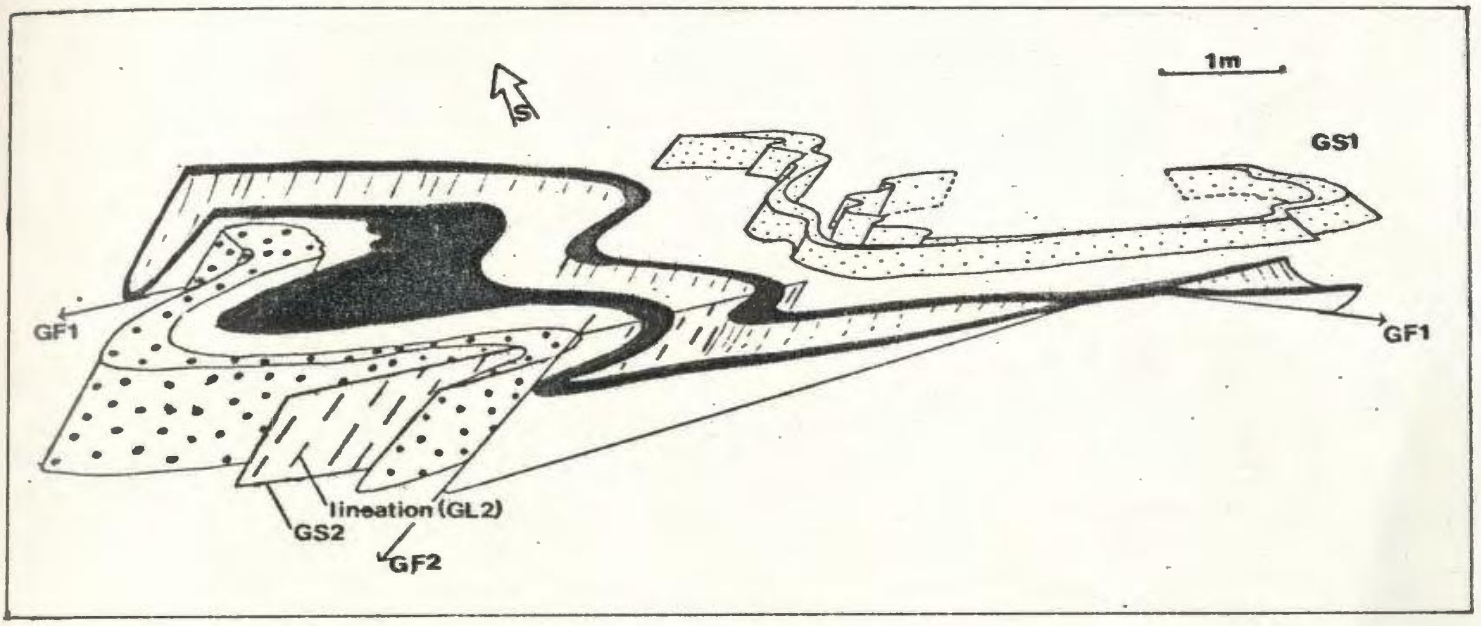

Figure 3-7. Gently doubly-plunging GF1-fold deformed about a moderately ESE-plunging axis during DG2. Folds are outlined by mafic dykes (black-hornblende + epidote bearing metabasite; heavy dots-hornblende + epidote + garnet bearing intermediate dyke, cf. sample V257-8) and by a deformed band of mylonite (GS1, fine stippling). The fold axes of GF1 and GF2 folds are shown, as is the orientation of the lineated GS2 fabric. This interpretation suggests that the intermediate dyke postdates GD1 and antedates GD2, or, perhaps more likely, pinches out. Host rock of the dykes is hornblende + biotite monzodiorite (unit 6B). Viewed from north-northeast, Marks Island.

3-8). Rigorous structural analysis of these folds is hampered by the tendency of the relatively competent Michael gabbro to resist development of fabrics associated with Grenvillian deformation, and by the poor exposure of host rocks in the interior of these islands. These refolded folds are interpreted to represent interference between GF1 and GF2 folds.

Although generally east-trending, GS2 shows considerable variation in strike direction (Fig. 3-1C). This may in part be attributed to its braided or anastamosing character, where schistose to mylonitic fabrics wrap around relatively low strain, lozenge-shaped domains (Fig. 3-9) up to ~1km in length (e.g. on Marks Island, see Map 1, in pocket).

Elsewhere, the range of orientations of GS2 can be attributed to the effects of a third period of Grenvillian deformation (GD3). Locally GS2 fabrics are deformed into open to tight SSW-plunging (Fig. 3-3D) folds with south-dipping axial surfaces. No fabric associated with GD3 has been noted within the study area. GF3 folds (Fig. 3-10) generally have Z-shaped profiles, indicative of dextral offset (Fig. 3-11), and may be associated with the dextral offset noted along Grenvillian high-strain zones in the area (Gower, 1981).

3.3.3 Kinematics of Grenvillian Deformation

A relatively simple pattern of the structural evolution of this portion of the Grenville Front Zone emerges from the observations described above, albeit not as kinematically rigorous as desirable.

The geometric and orientation patterns of the GD1 structural elements provide few indications about the nature of the strain field (i.e. pure shear vs

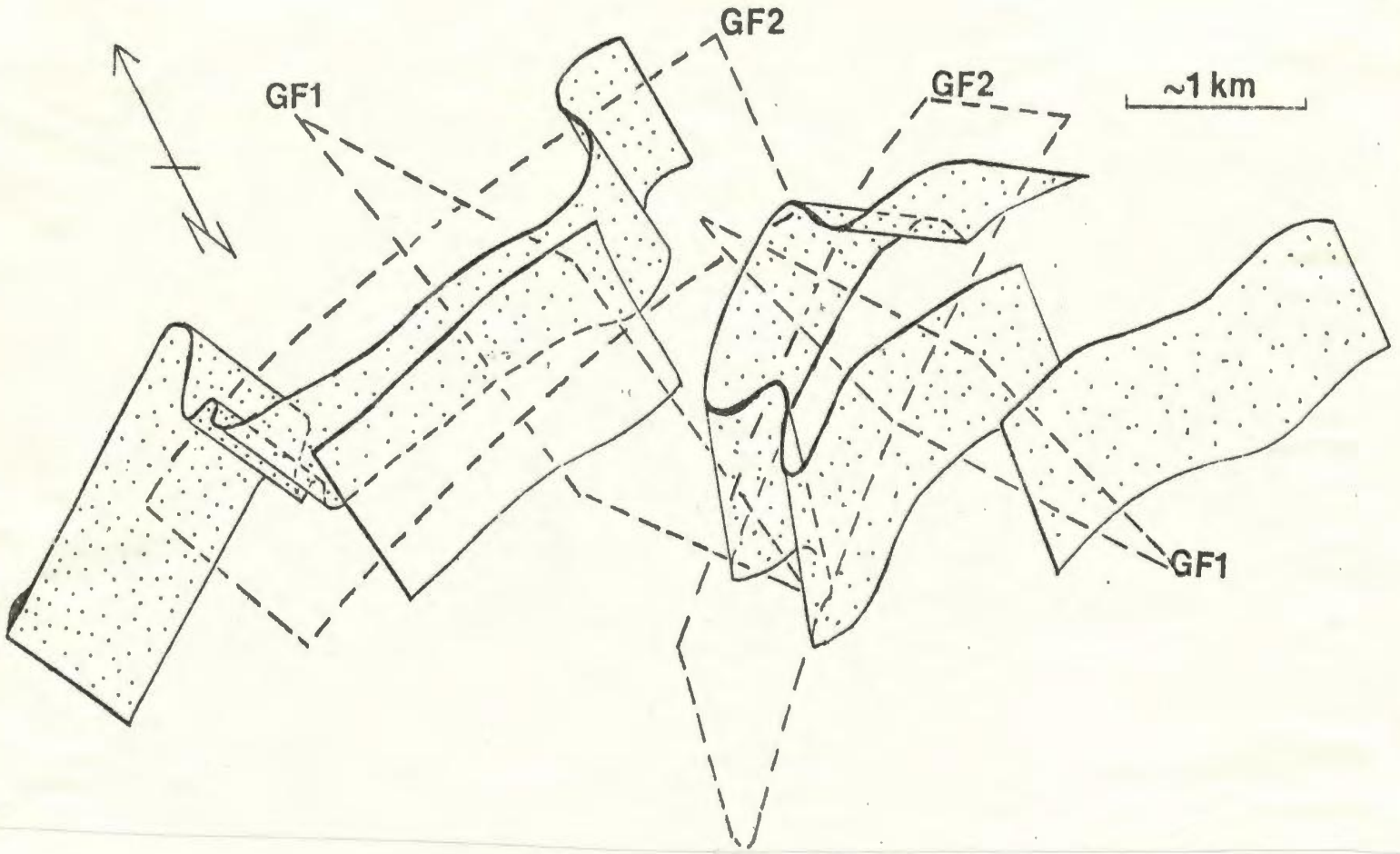

Figure 3-8. Interpretative three-dimensional sketch of polydeformed dykes of Michael gabbro (stippled) on Ice Tickle and Mundy Islands. The fold pattern is interpreted to be the result of interference between GF1 and GF2 folds. Note the similarity with the folds depicted in Fig. 3-7. The axial surfaces of GF1 and GF2 folds are indicated by dashed lines.

Figure 3-9. Lozenge-shaped, 3.5m long, low-strain domain ("tectonic fish") enveloped by mylonitic GS2 fabric developed in megacrystic granodiorite (unit 6A) along the CTIF.

Figure 3-10. SSE-plunging GF3 fold deforming GS2 fabric (and metabasite and pegmatite layers) in clinopyroxene-bearing monzonite (unit 8B); 7km northeast of Bluff Head

Figure 3-11. Deflection of pre-Grenvillian gneissose fabric in retrograded jotunitic gneiss (unit 3B) by Grenvillian high strain zone (GS1?) showing late (GF3) folds. Inset shows refolding of earlier Grenvillian isoclinal folds deformed about the south-west plunging GF3-fold axes. Sense of shear indicated by these late Z-folds is consistent with the dextral offset shown by the pre-migmatitic metabasite (lower left). East shore, Run By Guess Island.

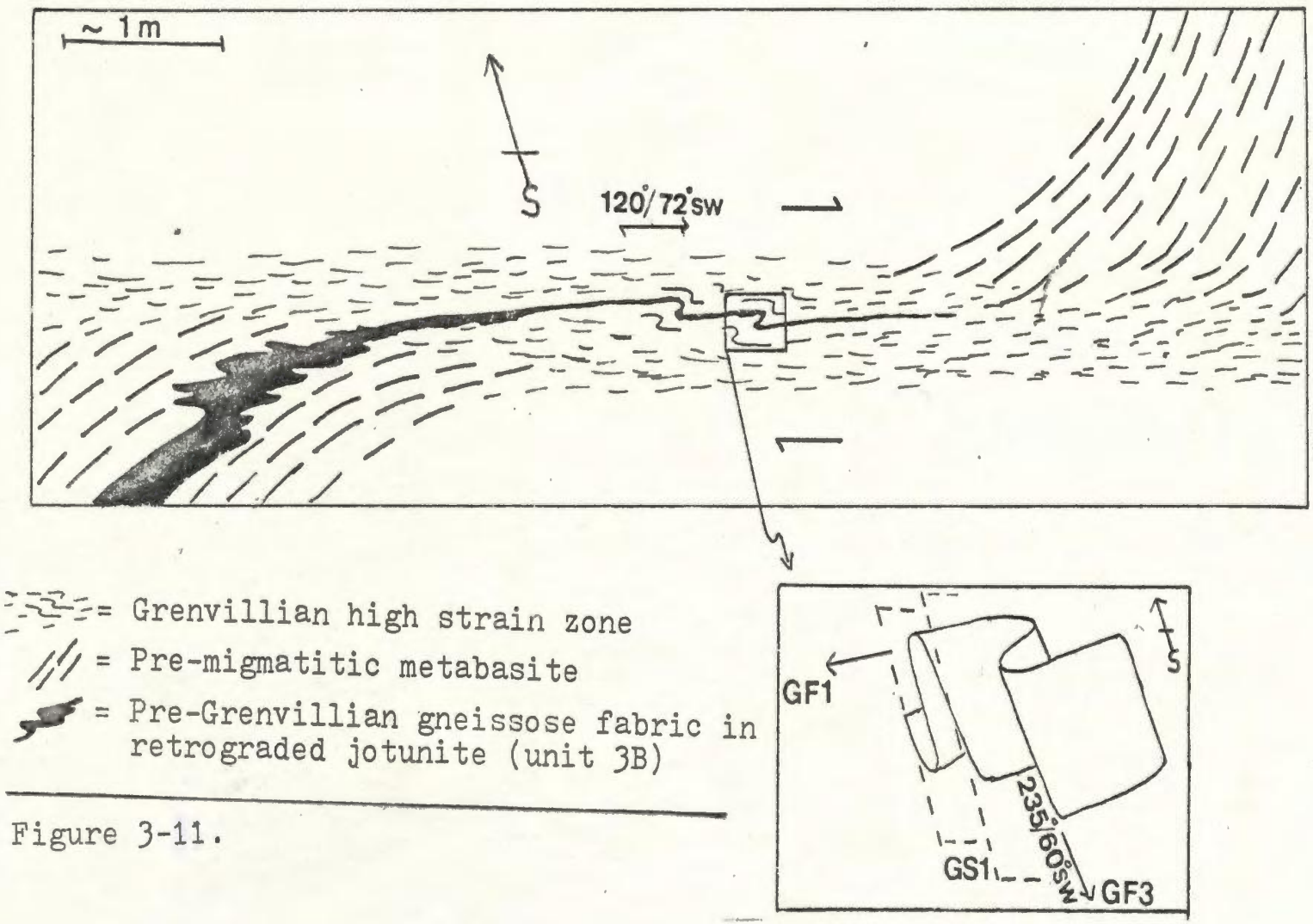
~ 1m
S
120°/72°SW
= Grenvillian high strain zone
= Pre-migmatitic metabasite
= Pre-Grenvillian gneissose fabric in retrograded jotunite (unit 3B)
GF1
S
235/60°SW
GS1
GF3

Figure 3-11.

simple shear) in which GD1 structures developed. The recognition of a few GD1 shear zones that are clearly associated with GD1 fold development suggests that simple shear may have been important during GD1 deformation. As noted previously, the north-dipping shear zone depicted in Figure 3-4 may either represent a hinterland-directed backthrust or it may be part of a foreland-directed large-scale fold nappe system (Ramsay et al., 1982), with the mylonite and associated fold being situated on the overturned limb of the nappe.

Initial Grenvillian deformation involved the development of upright GF1 fold sets in the south. These folds tighten and locally become overturned to the north, particularly near and within GD2 high-strain zones in the central portion of the map area. It should be emphasized that this is not the general case; for example, upright GF1 folds have been observed immediately ($\sim$100m) to the south of the Benedict Fault on the west side of Abliuk Bight. On the north side of Cut Throat Island, however, tight GF1 folds with amplitudes up to $\sim$3m, and wavelengths $<$1m, are overturned to the north. The overturned position of these folds may be an original (GD1) feature. Alternatively, these folds may owe their present orientations to rotation and flattening during GD2. If the overturned folds preserve an original orientation, it may be inferred that during the evolution of GD1 strain path the XY-plane of the GD1 strain field rotated from an upright position in the south to an inclined position farther to the north. Rotation of the XY-plane is a logical consequence of the kinematic evolution of ductile simple shear zones, and would indicate for the present area a northward increase in shear strain (Ramsay, 1981; Ramsay et al., 1982).

The argument that tight, overturned GF1 folds along the CTIF were

displaced during GD2 must be related to a consideration of the nature of GF2 folds and their associated planar and linear structures. The following discussion, which focusses on possible effects of the GD2 strain field on earlier (GF1 folds) and contemporaneous (GF2) fold orientations, concludes that: (1) GF1 folds have been tightened and overturned toward the north only within major GD2 high strain zones; (2) negligible rotation of GF1 fold axes occurred during GD2; (3) GF2 folds may have been originally reclined, and the coincidence of GF2 axes and GL2 stretching lineations reflects the combined control of the GD2 strain field and pre-Grenvillian fabric orientations.

Shearing during GD2 was directed toward the north, as evidenced by the sense of asymmetry of small-scale GF2 folds (Fig. 3-12A), and the sense of rotation of deformed feldspar megacrysts (Fig. 3-12B; see also Simpson and Schmid, 1983, Fig. 1). The rotation axes of these deformed megacrysts are at a high angle to GL2 (cf. Davidson et al, 1982; Davidson, 1984). The development of GS2 fabrics with strong linear fabric components within high-strain zones in originally isotropic rocks demonstrates that GL2 is a stretching lineation and not an intersection lineation. Although some controversy exists as to the origin and kinematic significance of stretching lineations (e.g. Lister and Price, 1978), such mineral lineations are generally considered to coincide with the X-axis of the strain ellipsoid (where $X>Y>Z$) (e.g. Bell, 1978). The rotation of fold axes into approximate parallelism with the X-direction of the finite strain ellipsoid (e.g. as recorded by stretching lineations) is well documented in many ductile simple shear belts (e.g. Ramsay, 1979; Williams, 1978; Rhodes and Gayer, 1977; Bryant and Reed, 1969). This rotation is generally progressive across the shear belt, and the

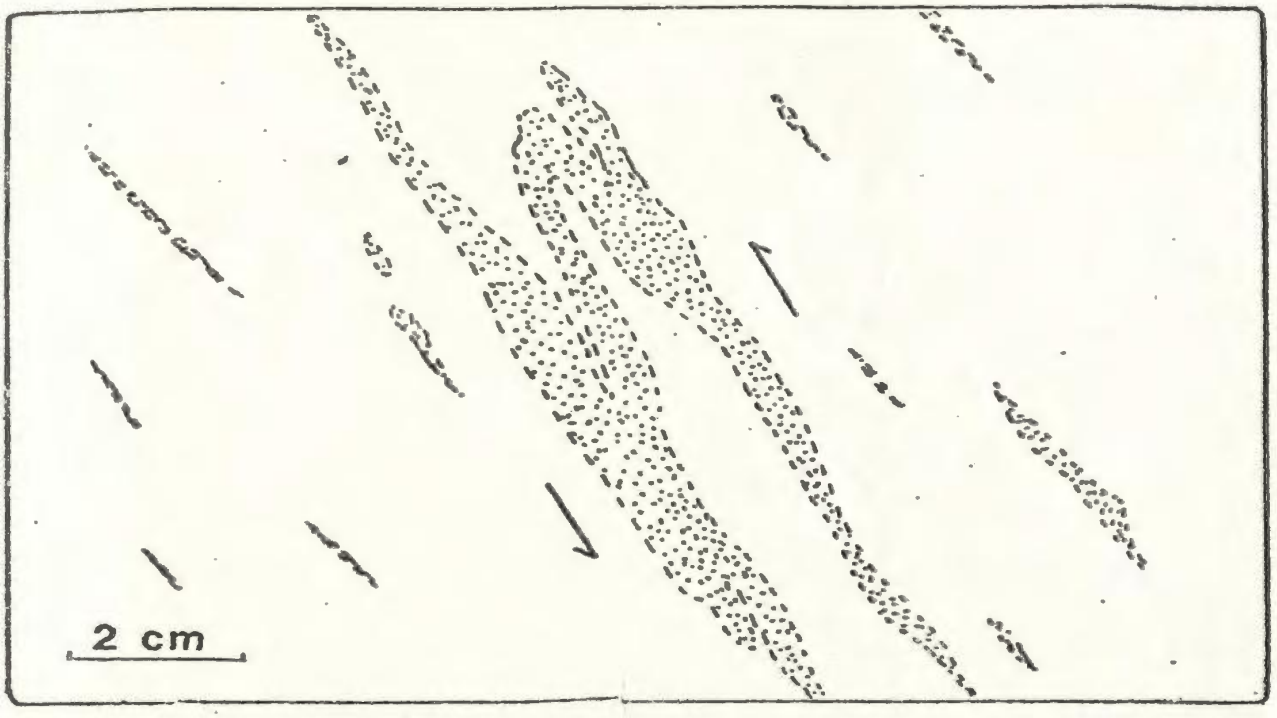

Figure 3-12A. Small-scale asymmetric intrafolial fold outlined by a leucosome vein in megacrystic granodiorite (unit 6A) deformed along the CTIF. Arrows indicate the sense of movement associated with folding. Sketched from a photograph; viewed from the west.

Figure 3-12B. Rotated, "tailed" K feldspar-megacryst in granodiorite (unit 6A) deformed along the CTIF. The sense of rotation indicates translation upwards to the left (north).

angle between fold axes and stretching lineations varies directly with the amount of strain attained in the shear zone. In the Smokey area, however, the angle between GL2 and GF2 axes is $<20^{\circ}$, and averages $\sim 9^{\circ}$ (see Fig. 3-6), and would suggest a high and rather homogeneous GD2 strain gradient, at least south of the CTIF. Since this observation is inconsistent with the variable development of GS2 fabrics, even within domain G, the kinematic significance of the uniformly small angle between GF2 axes and GL2 is not immediately obvious.

In order to rigorously evaluate the possibility that GF2 axes were progressively rotated towards X during heterogeneous simple shear, it is necessary to specify: (1) the attitude of GF2 at the onset of GD2 fold development (possible only in domains of extremely low GD2 strain); (2) quantitative strain data to control the position of regional-scale strain gradients between and within domains G, T and M; and (3) changes in angular relations between GF2 and GL2 compatible with these strain gradients. Since none of these data are available, the classical "rotation of fold axes into the X-direction" model provides only a hypothetical explanation for the observed angular relationships between GL2 and GF2. As it stands, the data depicted in Figure 3-6, in comparison with various structural observations, present a contradictory image of the nature of GD2. Evidence for the existence of large GD2 strain gradients in the area is provided by: (1) the variable degree of development of GS2 fabrics (see Figs. 3-7, 3-13), which culminate only locally in mylonitic rocks even within domain G; and (2) the lack of rotation of GF1 fold axes (see Figs. 3-3, 3-7) even in high strain domains. These observations are at odds with a pattern of relatively high and homogeneous strain that must be deduced from the uniformly small ($<20^{\circ}$) angle between GL2

Figure 3-13 Heterogeneous development of GS2 schistosity on an outcrop scale. Note the constant orientation of lineations (shown as dots) in this outcrop, and the refolded metabasite in the GF2 fold hinge. South side, Marks Island.

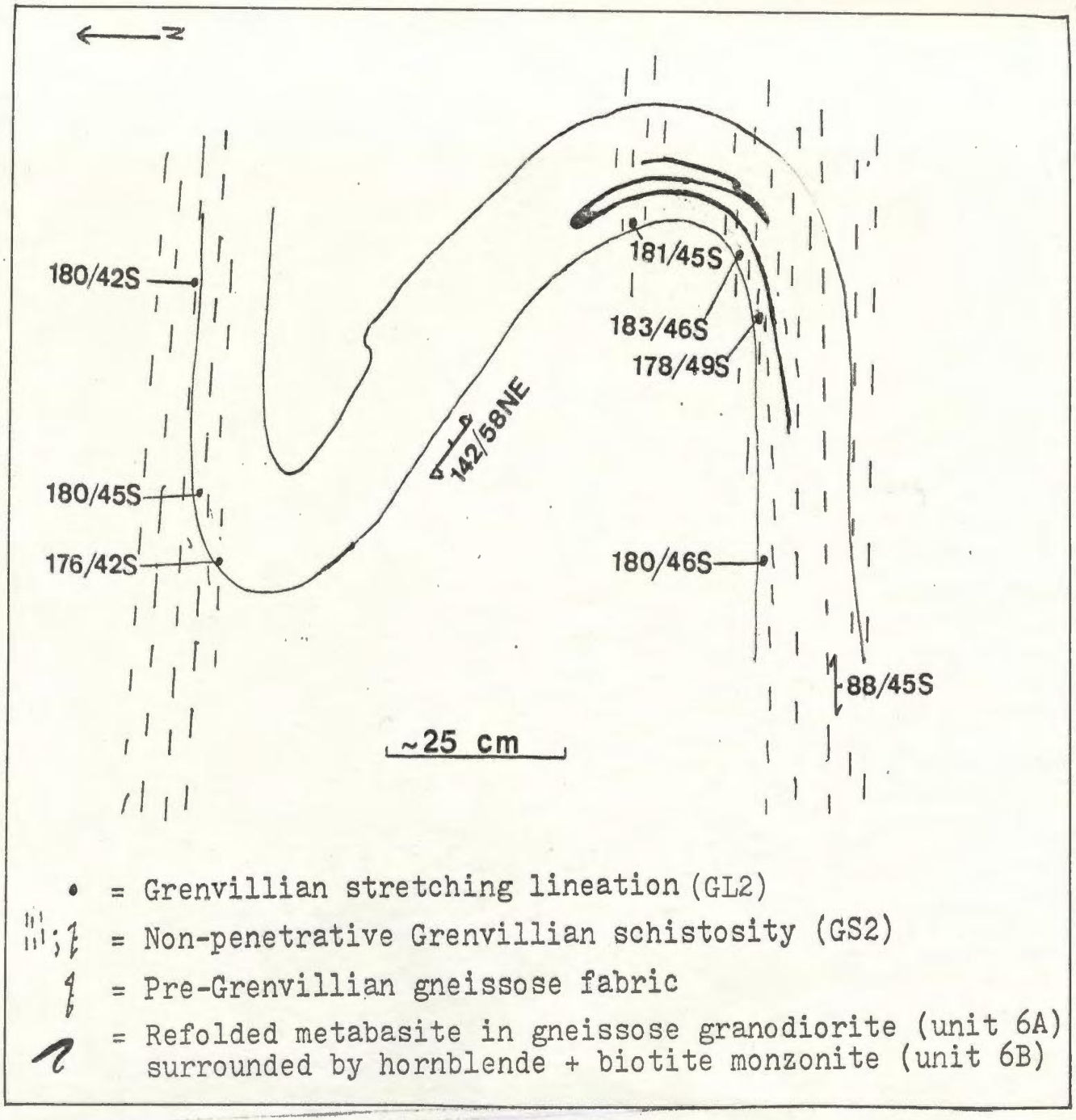
N
180/42S
180/45S
176/42S
181/45S
183/46S
178/49S
142/58NE
180/46S
88/45S
~25 cm
• = Grenvillian stretching lineation (GL2)
= Non-penetrative Grenvillian schistosity (GS2)
= Pre-Grenvillian gneissose fabric
= Refolded metabasite in gneissose granodiorite (unit 6A) surrounded by hornblende + biotite monzonite (unit 6B)

Figure 3-13.

and GF2 axes in domain G. The interpretation of the angular relationships between GL2 and GF2 and the nature of formation of the reclined folds warrants consideration of alternative kinematic models.

Two alternative models may be postulated: (1) GF2 folds were rotated toward reclined positions during GD3; or (2) GF2 folds initially formed in reclined positions with axes subparallel (<20) to GL2 during GD2 deformation.

The similar orientation of GF2 and GF3 axes (Figs. 3-3B,D) suggests that these fold phases were reclined and broadly coaxial from the onset of GD3; the orientation data for GF2 do not indicate that GF2 axes were rotated into their present orientation during GD3. A corollary of this is that GF3 is a continuation of the GD2 strain field, and should not be regarded as a separate deformational event. Given that the first model is untenable, the second model should be considered instead.

The coincidence of the intersection between GS2 (=XY of the finite strain ellipsoid) and Makkovik trend S-planes with both GF2 axes and GL2 (Fig. 3-14) suggests that GF2 folds were initially reclined, and had SSE-plunging fold axes. The absence of measurable GF2 folds in domain T (where the orientation of pre-Grenvillian fabrics is largely preserved) precludes the possibility of proving this model, since it cannot be demonstrated from the available data that pre-Grenvillian fabrics in domain G had NNE-trends prior to the Grenvillian orogeny.

In summary, the reclined nature of GF2 folds and the similar attitudes of GF2 axes and GL2 should not automatically be attributed to the rotation of GF2 axes into approximate parallelism with the X-direction of the finite strain

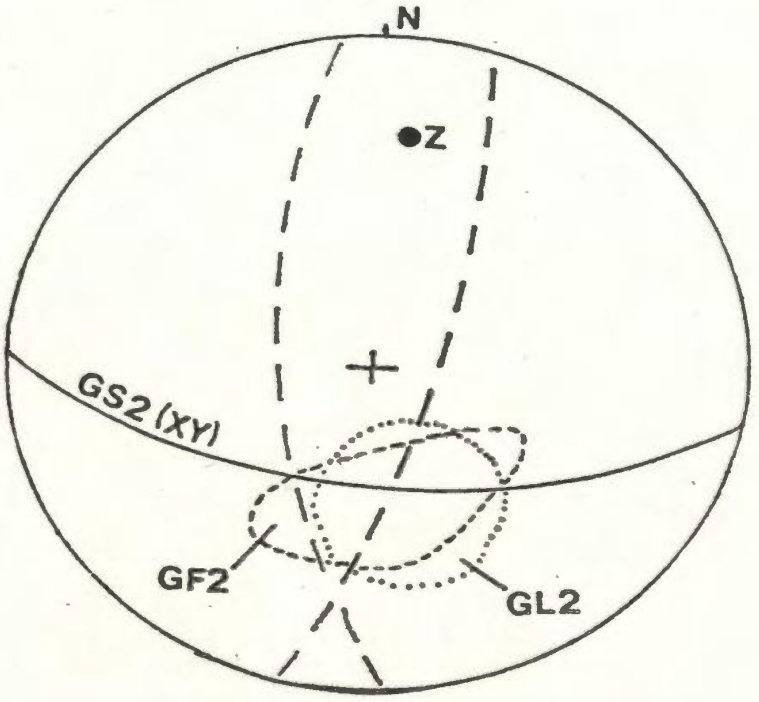

Figure 3-14. Lower hemisphere, equal area projection of Makkovik trend S-planes (dashed lines), GF2 axes and GL2 stretching lineations, and the Z and XY (=GS2) components of the GD2 strain field. Note the coincidence of orientations between GF2 axes, GL2, and intersections between GS2 and Makkovik trend S-planes. See text.

ellipsoid. Although fold axis rotation is characteristic of many ductile shear belts, contrary evidence to the model includes the uniformly small angle between GF2 and X (GL2), and the general lack of rotation of GF1 axes in domains where GD2 structures are prevalent. The preferred alternative model attributes the reclined nature of GD2 folds to the controls that the attitude of pre-Grenvillian fabrics of the Makkovik Province and the attitude of the XY-plane (and hence Z) of the GD2 strain field exert on GD2 fold geometry.

The relative age of translation along the Benedict and Cut Throat Island faults is unknown. That foreland-directed thrusting occurred along both faults is suggested by the kinematic indicators described above, and the observation that these high-strain zones are metamorphic (see section 4.3) as well as structural breaks.

During GD3, dextral movement occurred preferentially along GD1 and GD2 high-strain zones. Dextral strike slip movements have previously been suggested by Gower (1981) for both the Benedict and Adlavik Brook Faults. Gower (1981) estimated dextral offset along the latter fault, a major high-strain zone some 6km north of the Benedict Fault to the west of the study area, to be approximately 16km. However, Gower had insufficient data to estimate the extent of the dextral offset along the Benedict Fault.

The Benedict Fault transects a large body of gabbroic rocks occurring between Emily Harbour and Holton (Figs. 2-1, 3-15). There is no detectable evidence of dextral offset of this body at the 1:50,000 scale of mapping employed, suggesting insignificant strike-slip movement along the Benedict Fault in this

area.

Dextral offset associated with GD3 along minor (<5m wide) shear zones appears to be limited to a few tens of metres (Fig. 3-11). Given this, and the argument outlined above, it is likely that GD3 dextral motion along the Benedict fault zone does not exceed several hundred metres within the study area.

It is not certain that translation along the Benedict Fault, or other high-strain zones in the area, terminated during GD3. A NE-trending shear zone interpreted to be unrelated to the postulated north-directed thrusting along the Benedict fault occurs west of Abliuk Bight (Figs. 3-15; 2-1). This shear zone, characterized by a SE-dipping schistose fabric and the local presence of pseudotachylite, transects an ovoid body of coarsely megacrystic granodiorite (unit 6D) without any offset evident at the scale of mapping. If this fault and the Benedict Fault define a conjugate set (i.e. moved contemporaneously), then the position of the acute angle ($\sim 40^{\circ}$) between the faults (see Fig. 3-15, inset) suggests that the orientation of the maximum compressive stress axis of the stress field under which the faults operated lies roughly in an east-west direction; movement senses on the NE-trending fault in this case would be dextral, with concomitant sinistral movement along the Benedict Fault. Since evidence for this is lacking, the preferred conclusion is that the northeast-trending fault is unrelated to (postdates?) the stress field responsible for foreland-directed thrusting and subsequent dextral shear along the Benedict Fault.

The available kinematic indicators described above suggest an approximately NNW-SSE-oriented direction of maximum compression during

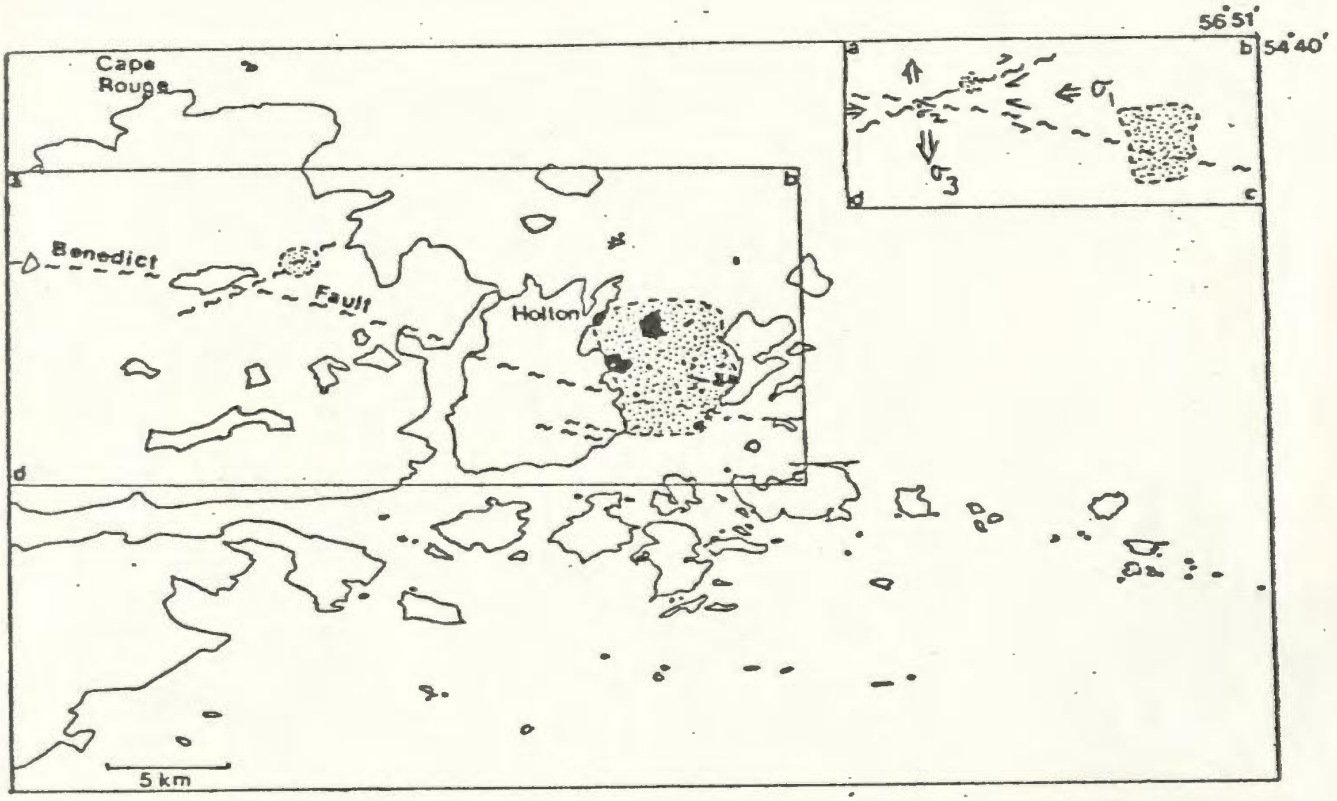

Figure 3-15. Evidence for insignificant dextral displacement along the Benedict Fault. Inset shows the expected direction of maximum compression given the acute angle between the Benedict Fault and an ENE-trending fault which transects, but does not offset, a body of megacrystic granodiorite (unit 6D). The lack of offset of the granodiorite, and independent indications of dextral (rather than sinistral) shear within the Benedict Fault suggest that the two faults are unrelated, and were not contemporaneously active under the stress field (with the resultant offsets indicated for both faults) indicated in the inset.

GD1 and GD2, which culminated in significant north-directed thrusting along both the Benedict and Cut Throat Island Faults. A corollary of the characterization of both faults as thrusts is that Grenvillian structural domains M, T and G contain metamorphic mineral assemblages of contrasting grade. Given sufficient differential crustal uplift along the thrusts, such contrasts would be discernable by differing mineral assemblages in similar rock types, and by variations in the compositions of particular mineral species. Both types of contrasts are described in Chapter 4.

3.4 PRE-GRENVILLIAN LITHOSTRUCTURAL DOMAINS

A variety of pre-Grenvillian structural elements is represented in the study area. The White Bear Islands Granulite Complex and Bluff Head orthogneiss are characterized by gneissic fabrics. The southern border of Gower et al.'s (1980) Grenville Front zone approximately coincides with the junction between the Bluff Head orthogneiss and the BMIS, however, the relative age of the two domains is not known directly from field relations (see section 4.5). Penetrative N-NE-trending (Makkovik trend) planar fabrics in the BMIS are delineated by the preferred dimensional orientation of feldspar megacrysts and mafic minerals, generally with little if any mineralogical segregation.

Evaluation of the three-dimensional geometry of pre-Grenvillian structures is severely hampered by the rounded contours of outcrops of the older gneisses. In many cases, only the strike direction of pre-Grenvillian planar fabrics could be measured with any confidence, and many of these structural elements have been reoriented during the Grenvillian orogeny. Consequently, only general statements regarding the early structural history of the study area are possible. The descriptions that follow focus on the similarities and contrasts of pre-Grenvillian structural elements in each of the three lithostructural domains depicted in Fig. 3-1.

3.4.1 Structures of the White Bear Islands Granulite Complex

Several periods of pre-Grenvillian deformation can be inferred from the limited data at hand: these include the formation of a pervasive gneissosity (Fig. 3-16), followed by one, or possibly two periods of folding prior to migmatization. Gneissic fabrics of the WBIGC presently strike northeast, and dip moderately

Figure 3-16. Disrupted mafic dykes with chilled margins in retrograded jotunitic gneiss (unit 3B). The gneissic fabric in the jotunite trends northeast, and is displaced by a dextral, south-dipping Grenvillian high-strain zone (GS2) (top of photograph). Southwest shore, Run By Guess Island.

toward the southeast (Fig. 3-1D).

The earliest deformational event recognizable on a mesoscopic scale resulted in the development of the gneissic to migmatitic fabrics which characterize the granulites. Petrographic evidence suggests that this gneissosity might not be the earliest S-fabric in the WBIGC. For example, oriented inclusions of sillimanite in garnet porphyroblasts probably are relicts of a pre-gneissosity fabric. These textures are described in more detail in Chapter 4, and only field observations will be summarized here.

Different members of the WBIGC developed contrasting structural styles during high-grade metamorphism. However, despite their variation in appearance, these fabrics are invariably parallel to the contacts between different granulite-facies lithologies, hampering the establishment of a relative chronology of these units in the field.

The gneissic fabric in dioritic to tonalitic gneisses (unit 2) consists of simple melanocratic-leucocratic banding on a mm- to cm-scale. This gneissic layering in places is diffusely infiltrated by medium-grained leucosomes. The pervasive gneissosity developed in the dioritic to tonalitic gneiss contrasts with the predominantly foliated texture defined by oriented feldspars and lenses of mafic minerals characterizing the jotunitic to charnockitic gneiss (unit 3). Locally, however, unit 3 contains foliation-parallel pyroxene-bearing pegmatitic rocks which impart a gneissic aspect to the rock (e.g. Owen and Rivers, 1983, Fig. 19.7).

Fabrics and structural elements preserved in migmatitic metapelites (unit 1C) provide most information about the early structural evolution of the WBIGC.

Gneissosity in the metapelites parallels centimetre- to decimetre-scale layering attributed to primary compositional variations (e.g. bedding, see section 4.2), and has been folded at least once, and probably twice, prior to being disrupted and infiltrated by relatively coarse-grained granitic leucosomes of local derivation. Two periods of pre-migmatization folding are suggested by the agmatization of refolded screens of gneissic metapelite, and by the presence of mushroom-shaped (Type 2; Ramsay, 1967) pre-migmatitic (?) interference patterns in the paleosomes (Fig. 3-17).

There is no evidence of the development of a new fabric concomitant with migmatization. The coarse-grained leucosomes crosscut differentiated gneissic fabrics, and except where transected by Grenvillian high-strain zones, appear to be unfolded. Their non-rectiplanar, vein-like to pod-like form reflects the control of dilational structures (e.g. interboudin dilational zones) on their localization.

3.4.2 Structures of the Bluff Head Orthogneiss

Pre-Grenvillian structural elements in the orthogneisses in the vicinity of Bluff Head have been significantly overprinted by early Grenvillian folding (GD1; Fig. 3-18). The rocks themselves are characterized by gneissic fabrics which commonly contain foliation-parallel leucosomes and patchy leucosomes which diffusely overprint or agmatize the gneissic paleosome. The vein-type leucosomes outline folds locally crosscut by the Michael gabbro, and subsequently deformed by GF1. This evidence for pre-Grenvillian gneissic fabric development and subsequent migmatization has also been noted in the WBIGC (see above). This raises the interesting possibility that both domains may share a common early orogenic history despite the apparent absence of granulite-facies assemblages in

Figure 3-17. Pre-Grenvillian type 2 (Ramsay, 1967) interference pattern outlined by the polydeformed gneissosity in pelitic metatexite (unit 1C). White Bear Islands.

Figure 3-18. Pre-Grenvillian fold refolded about an east-west axis (right-left in photo) during GD1. The folds are outlined by amphibolite layers in granodioritic gneiss (unit 5A). Twin Islands.

the typical granodioritic and monzonitic gneisses near Bluff Head (see section 4.5)

The prevalence of shallowly west-plunging Grenvillian folds (GF1) in the Bluff Head orthogneisses produces complex structural patterns, obscuring pre-Grenvillian interference patterns as noted in the WBIGC. Gneissic fabrics in this area have southwesterly dips (Fig. 3-1E), reflecting the effects of the early Grenvillian folding which may be responsible for the presently divergent fabric orientations noted in the WBIGC and Bluff Head orthogneiss.

Only one pre-Grenvillian fold in the Bluff Head area could be measured. This example, outlined by a deformed metabasite concordant to the host rock gneissosity, is a shallowly north-plunging, west-verging fold, which has been warped about an east-west axis during initial Grenvillian deformation (GD1). Similar styles of folds are pervasive in the southwest corner of the map area, but are generally visible only in two dimensions and are typically deformed by GF1.

3.4.3 Structures of the BMIS

Planar fabrics characterizing the Makkovik trend occur along discrete north- to northeast-trending zones up to approximately 1km wide in various members of the BMIS. The Makkovik trend planar fabric is typically represented in the BMIS by a preferred dimensional orientation of feldspars, biotite and hornblende, and is commonly defined by lens-shaped mafic enclaves or inclusions of gneissic metadiorite correlated with the dioritic-tonalitic gneisses (unit 2) of the WBIGC. Folds associated with the Makkovik trend occur very locally (cf. refolded metabasite in Fig. 3-13), and no fold axes were measurable.

Although all members of the BMIS locally contain N-NE-trending planar

mineral fabrics, the Makkovik trend is most pervasively developed in K feldspar-megacrystic granodiorite (unit 6A), the oldest member of the BMIS recognized in the study area. These granodiorites are foliated to gneissose, with the local development of hornblende- and biotite-rich restites. North-northeast trending mafic enclaves occurring in the granodiorite and younger members of the BMIS (both to the north and south of the Benedict Fault) contain hornblende + oligoclase. This demonstrates that the Makkovik trend was developed during a period of amphibolite-facies metamorphism. Inclusions of (retrograded) gneissic diorite-tonalite (unit 2, see Owen and Rivers, 1983, Fig. 19.2) and jotunite (unit 3A) in the BMIS indicate that this period of metamorphism postdates the granulite-facies event. Furthermore, the Makkovik trend is crosscut by the Michael gabbro, and is transposed along Grenvillian high-strain zones, demonstrating that the north-northeast trending fabrics are pre-Grenvillian in age. Gower (1981) and Owen and Rivers (1983) postulated that the Makkovik trend either developed during late Ketilidian metamorphism (ca. 1.8Ga; Allaart, 1976) or records a previously unknown Paleohelikian orogeny (Labradorian?; ca. 1.65Ga, Nunn et al., 1984; Thomas et al., 1984).

CHAPTER 4
METAMORPHISM

4.1 PREAMBLE

The effects of Grenvillian metamorphism have been distinguished from those of pre-Grenvillian age which characterize gneissic rocks of the White Bear Islands Granulite Complex (WBIGC), the Bluff Head orthogneiss and the foliated plutonic rocks of the Benedict Mountains Intrusive Suite (BMIS). This distinction is inferred from the relative and absolute chronology of major rock units and their contained fabrics outlined in Chapters 2 and 3.

This chapter comprises four principal sections. The first two sections deal with various aspects of pre-Grenvillian and Grenvillian metamorphism, respectively. Metamorphism of coronitic gabbros (e.g. the Michael gabbro) is described in the third section, while the age of metamorphism and its implications for relationships between the three lithostructural domains in the study area are covered in the fourth section.

The first two sections each commence with a summary of the occurrence, textures, and compositions of metamorphic minerals comprising key parageneses, and conclude with estimates of metamorphic conditions. Emphasis has been placed on mineral assemblages useful as metamorphic indicators. Since pre-Grenvillian mineral assemblages are the more diverse, the applicability of various geothermobarometers is briefly reviewed in the first section. Compositional parameters of mineral assemblages relevant to the PT determinations are summarized in tabular form in the text; mineral analyses and a summary of analytical procedures are presented in Appendix A.4. To facilitate comparison of

various aspects of the mineralogy and mineral chemistry of different rock units, the descriptions that follow summarize these features on an assemblage by assemblage basis.

4.2 PRE-GRENVILLIAN METAMORPHISM

4.2.1 Parageneses of the White Bear Islands Granulite Complex

A number of prograde and retrograde parageneses are preserved in the WBIGC. These may be distinguished both on textural and compositional grounds (see below). Prograde assemblages, which record the granulite-facies event, are described first.

4.2.1A Clinopyroxene-Orthopyroxene

Two-pyroxene-bearing assemblages occur locally in dioritic-tonalitic gneiss (unit 2), jotunitic-charnockitic gneiss (unit 3A), and in some pre-migmatitic metabasites. In each case, the pyroxenes coexist with biotite, and mantles of hornblendic amphibole, clearly a retrogressive phase, occur in some samples.

One sample (V581-1) of dioritic gneiss (unit 2) contains coexisting clino- and orthopyroxene. In this sample, the orthopyroxene occurs in the leucosome, while clinopyroxene (+ biotite + hornblende) is restricted to the paleosome. This observation suggests that the orthopyroxene and clinopyroxene may not in this case represent an equilibrium assemblage, in contrast to two-pyroxene-bearing assemblages in other lithologies.

Two-pyroxene-bearing assemblages occur in four samples (V585, V586, V526-3A, V687) of jotunitic-charnockitic gneiss (unit 3A). In these samples, both pyroxenes are evenly distributed through the rock, and occur both separately and in contact. Grain contacts are regular and sharp, and, although clinopyroxene may in places partly enclose orthopyroxene (Fig. 4-1A), there is no evidence of replacement of the latter phase.

Figure 4-1. Photomicrographs of texturally stable prograde mineral assemblages from the White Bear Islands Granulite Complex.

4-1A. Orthopyroxene (white, horseshoe-shaped) in contact with clinopyroxene (grey) in jotunitic gneiss (unit 3A). Bar scale is 0.1mm. X-nicols; sample V585.

4-1B. Typical aspect of coexisting garnet and biotite in jotunitic gneiss (unit 3A). The subidiomorphic garnet (high relief) encloses an idiomorphic biotite flake, while biotite outside the garnet is subidiomorphic (note the ragged grain boundary on the dark grey biotite, left center) and in places has symplectic quartz intergrowths. Bar scale is 0.2mm. Plane polarized light; sample V579-1.

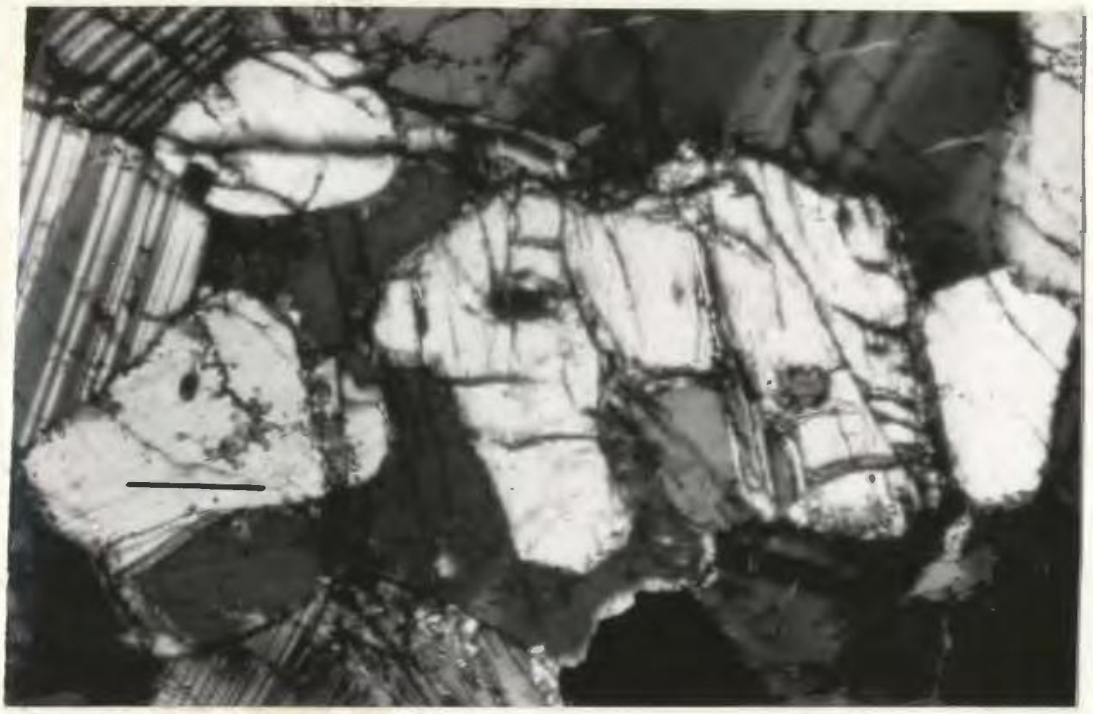

Figure 4-1A

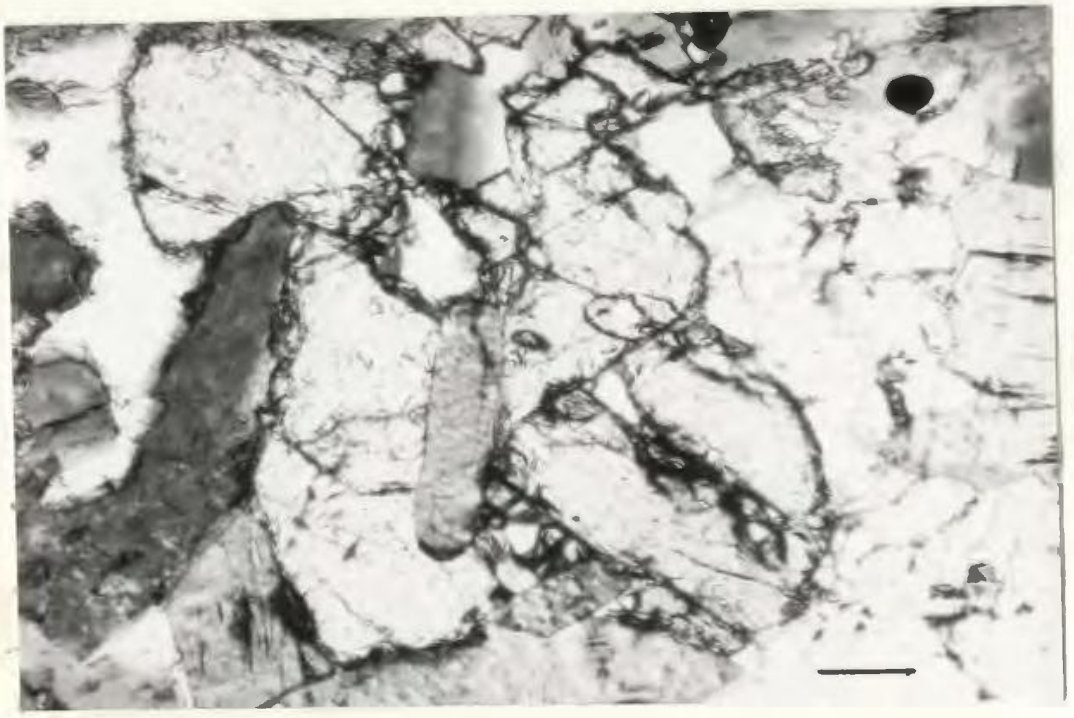

Figure 4-1B

Figure 4-1 (Continued)

4-1C. Orthopyroxene (dark grey, note cleavage) in contact with garnet (left, pale grey) in pelitic metatexite (unit 1C). Bar scale is 0.1mm. Plane polarized light; sample V210-1.

4-1D. Orthopyroxene (grey, note cleavage) in contact with garnet (black) in jotunitic gneiss (unit 3A). Bar scale is 0.2mm. X-nicols; sample V579-1.

Figure 4-1C

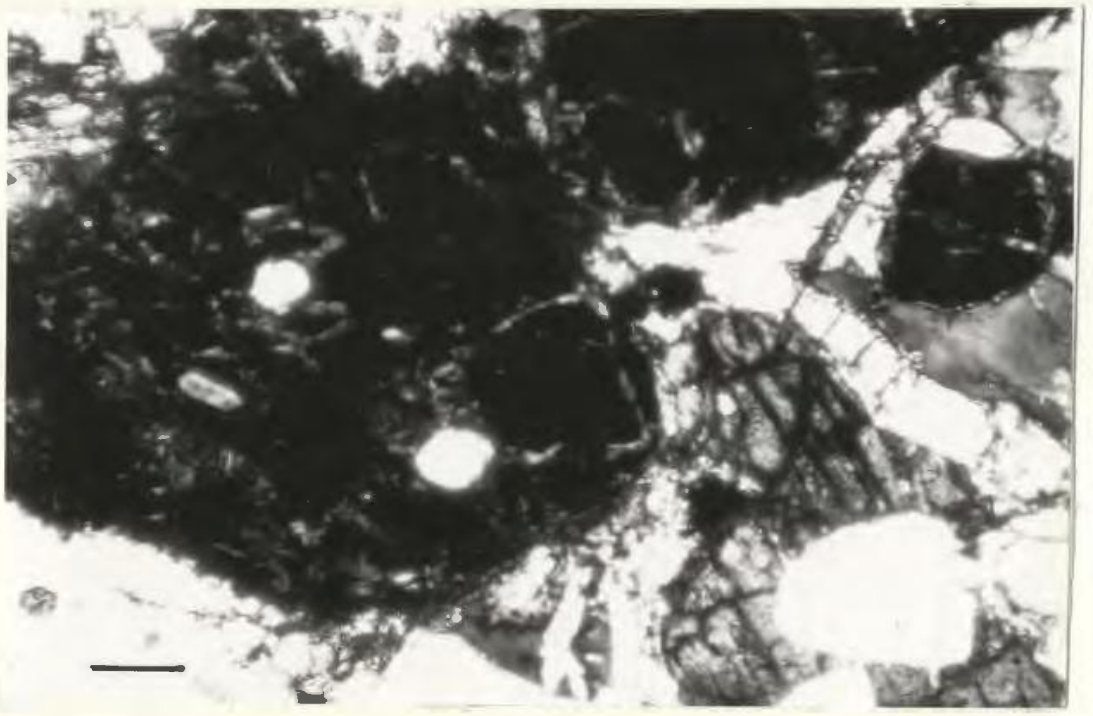

Figure 4-1D

Five pre-migmatitic metabasite specimens (V194-2; V526-3B; V580-7; V580-8; V711-2) variously sampled from jotunitic gneiss (unit 3A), pelitic metatexite (unit 1C) and monzonitic gneiss (unit 4) contain the two-pyroxene + biotite assemblage. These samples are characterized by a granoblastic texture and contain very little (0-2%) amphibole. Specimens V580-7 and V580-8, metabasites sampled from pelitic metatexite, contain calcic plagioclase (An90 and An86, respectively). In contrast, the plagioclase in specimens V526-3B (An25), V194-2 (An34) and V711-2 (An24), all of which were sampled from K feldspar-bearing orthogneissic rocks (units 3A, 3B, and 4, respectively), is considerably more sodic. The pyroxenes together comprise up to approximately 40 vol.% of the metabasites. As in the jotunitic-charnockitic gneiss, the pyroxenes occur both as discrete grains, or are in sharp mutual contact, with clinopyroxene in places partially enclosing orthopyroxene.

Orthopyroxenes from these various granulite-facies metamorphic rocks span a wide range of composition. Most typical in all granulites are ferrohypersthenes to hypersthenes, with Mg/(Mg+Fe) ranging from 0.33-0.61. Eulite (Mg/(Mg+Fe) = 0.15) is present in one sample (V470-2) from the Bluff Head charnockite occurrence (Fig. 2-1). The orthopyroxenes are unzoned, or show slight iron enrichment toward grain rims in contact with clinopyroxene. Compositional variation between grains within the same thin section is less than the resolution of the microprobe.

The broad range in orthopyroxene compositions is directly related to bulk rock compositions (Fig. 4-2). It should be emphasized, however, that whereas the bulk composition controls the iron and magnesium content of this (and other)

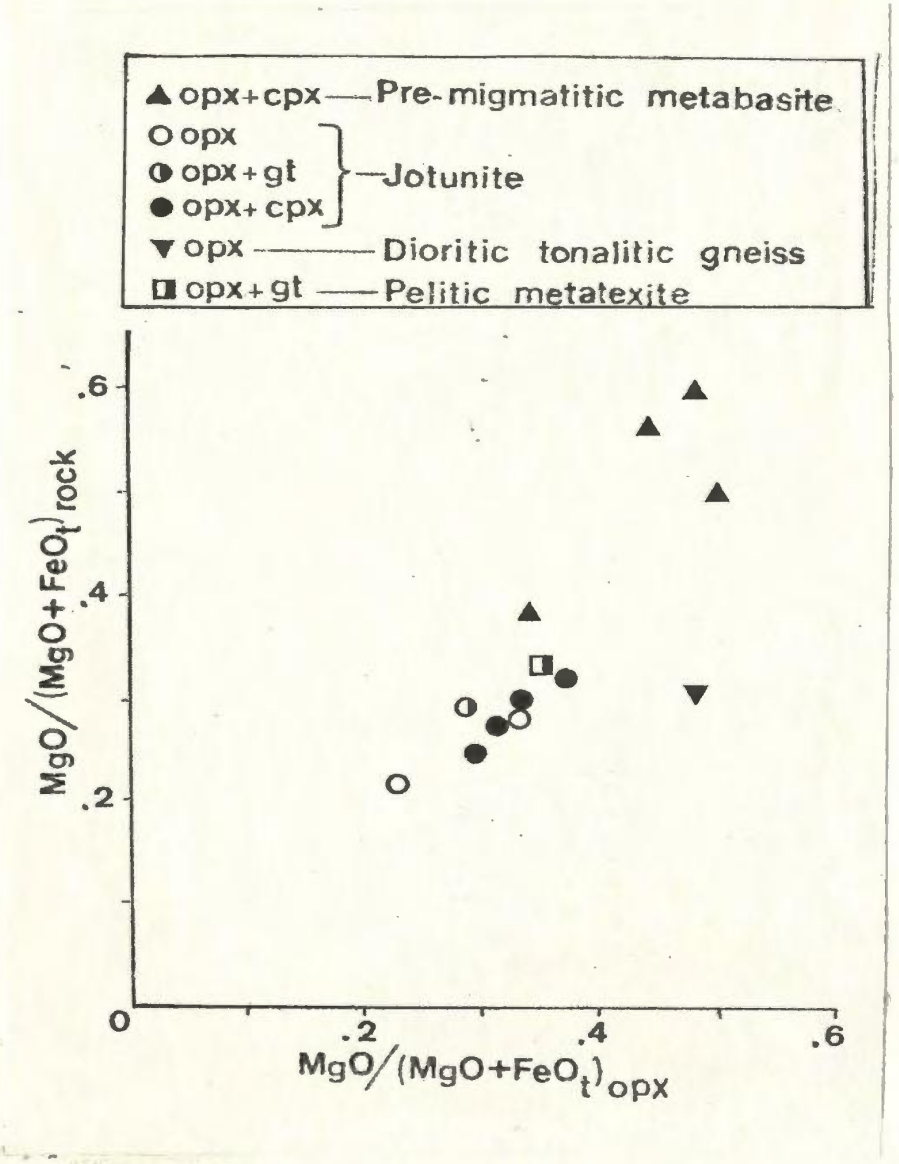

Figure 4-2. Plot of the bulk rock and orthopyroxene $MgO/(MgO+FeO_t)$ content in various members of the Granulite Complex.

mafic mineral(s), it is the grade of metamorphism which controls the distribution of Mg/(Mg+Fe) between ferromagnesian minerals.

The limited data available indicate that the MgO/(MgO+FeO) ratio of orthopyroxene is smaller, although overlapping, in orthopyroxenes coexisting with clinopyroxene or garnet compared with orthopyroxenes coexisting only with biotite. In contrast, the alumina content of orthopyroxene is unrelated to bulk rock composition (Fig. 4-3), but appears to hinge rather on the presence or absence of coexisting garnet or clinopyroxene. Alumina contents are most pronounced in assemblages containing garnet; intermediate values occur in orthopyroxenes associated with clinopyroxene, and the lowest (albeit overlapping) alumina contents occur where biotite is the only other ferromagnesian mineral (Fig. 4-4).

Clinopyroxene in the granulites shows a restricted range of compositions. The typical clinopyroxene contains 43-47mol% wollastonite, 34-44% enstatite, and 10-21% ferrosilite. The clinopyroxenes are unzoned with respect to these end members, and the compositional variation between grains on the scale of a thin section is within resolution of the microprobe. All samples contain orthopyroxene $\pm$ clinopyroxene, except for garnetiferous samples V221 and V579-1 which contain both contain orthopyroxene + garnet.

Clinopyroxenes from orthopyroxene-free metabasites (samples V42-1; V132-2; V541-2) from the WBIGC have compositions similar to those from two-pyroxene-bearing assemblages.

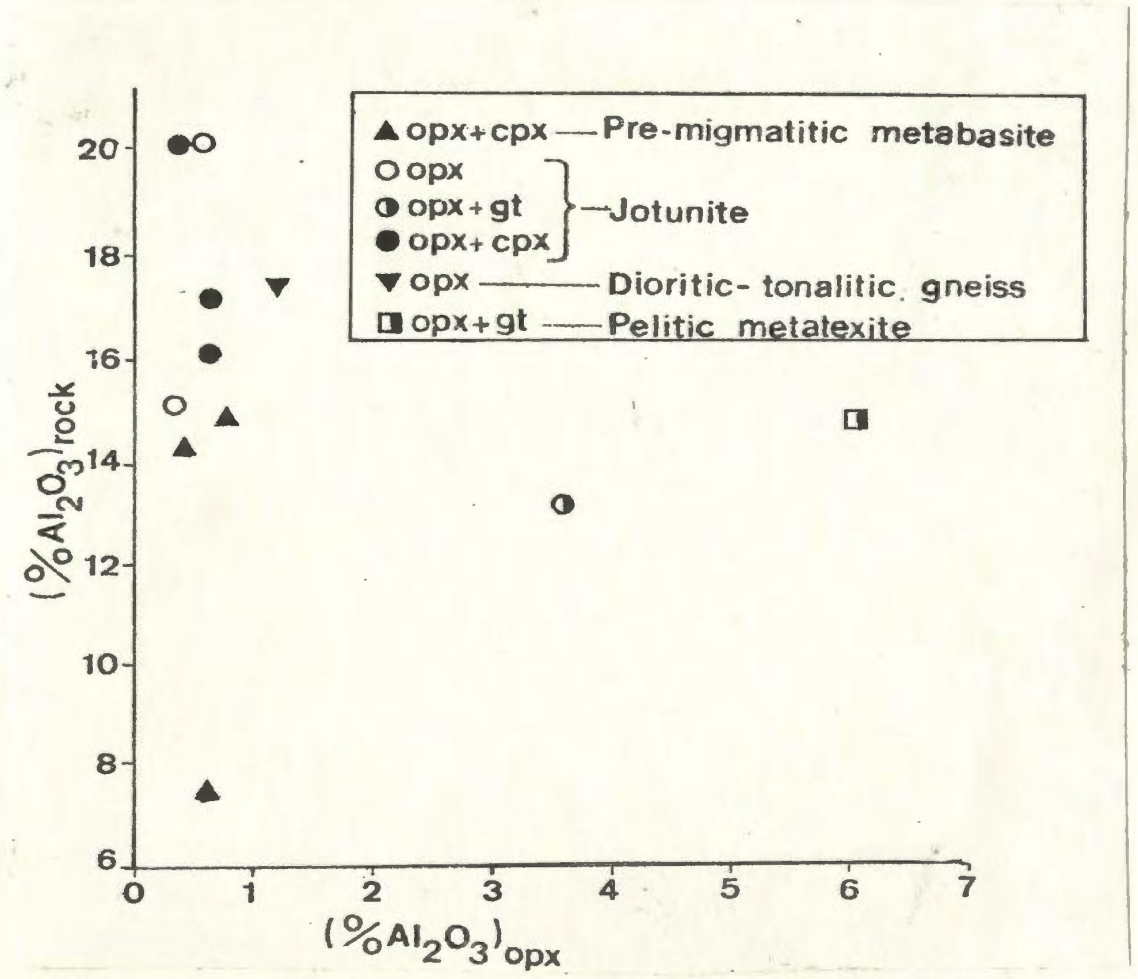

Figure 4-3. Plot of the bulk rock and orthopyroxene Al_2O_3 content in various members of the Granulite Complex.

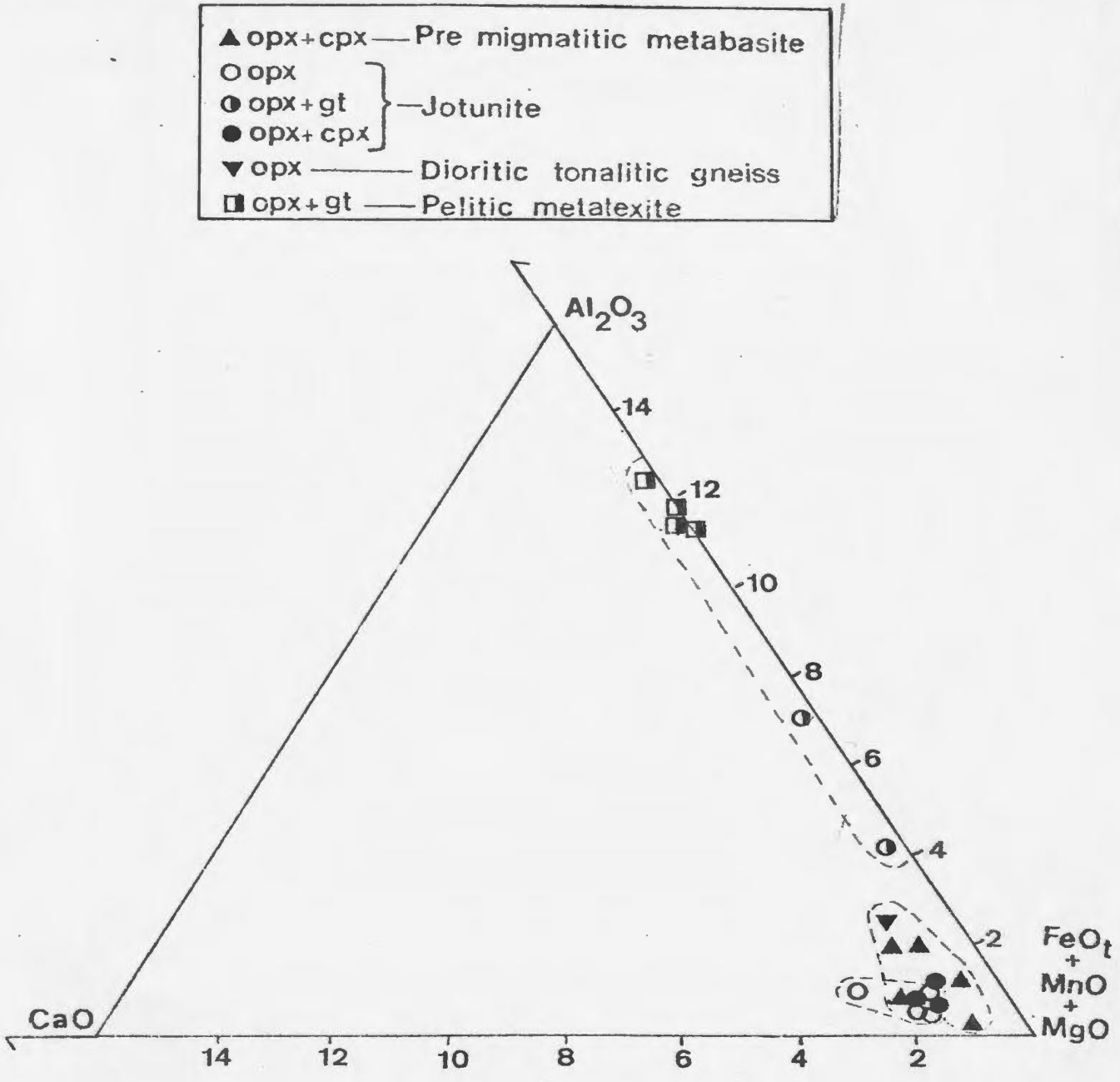

Figure 4-4. Relationship between the Al_2O_3 content of orthopyroxene and coexisting mafic minerals in various members of the Granulite Complex. See text.

4.2.1B Garnet-Biotite

Although biotite is an important constituent of all members of the WBIGC, garnet + biotite-bearing assemblages are rare except in pelitic metatexite (unit 1C), and are unknown in dioritic-tonalitic gneiss (unit 2) and monzonitic gneiss (unit 4). Garnet occurs in jotunitic-charnockitic gneiss in two localities only; the significance of these occurrences is considered in section 4.2.1C.

There are two textural varieties of biotite associated with garnet: (1) idiomorphic biotite inclusions (Fig. 4-1B) in garnet; and (2) subidiomorphic biotite enveloping garnet, and commonly with quartz $\pm$ sillimanite intergrowths in pelitic metatexite (unit 1C).

The latter texture appears to record the progressive retrogression of the assemblage garnet + K feldspar according to the divariant reaction [1]:

gt + Ksp + H2O = bi + sil + qz [reaction 1]

in which the lower grade assemblage is presented on the right hand side of the expression.

Although individual biotites are unzoned, biotite may show a considerable range of compositions on the scale of a thin section (see below), even for particular textural occurrences of the mineral. Equilibrium may have thus not been attained on a local scale. For this reason, thermometry using garnet-biotite pairs in these samples would not be expected to faithfully record the contrast in temperature between peak granulite-facies metamorphism and subsequent pre-Grenvillian retrogression of the WBIGC.

Subidiomorphic brown to reddish-brown biotite stably coexists with garnet in orthopyroxene-bearing jotunitic gneiss (unit 3A; samples V221; V579-1), although symplectic biotite + quartz intergrowths locally replace orthopyroxene.

No significant between-grain compositional variations have been detected in biotite in this unit.

The determination of mineral compositions by the electron microprobe is hampered by the inability of the probe to distinguish the oxidation states of iron. Furthermore, the possible presence of site vacancies in the biotite structure renders the stoichiometric estimation of oxidation ratios (= $Fe3^+$ /($Fe3^+$ + $Fe2^+$)) untenable (Percival, 1983). Previous workers have noted, however, low ferric iron contents in biotite, particularly from medium- and high-grade rocks. Stevenson (1979) reported biotites with oxidation ratios ranging from 0.01-0.07 and 0.02-0.09 in paragneisses at amphibolite and granulite-facies, respectively. Chinner (1960) presented analyses of biotites from medium-grade metapelites with oxidation ratios of 0.06-0.20 (avg. 0.10). Chinner attributed the differences in the ferric iron content of biotite to variations in pre-metamorphic bulk rock compositions.

The above data suggest that biotites in medium- to high-grade gneisses typically have oxidation ratios of approximately 0.10 or less. For purposes of illustration only, the latter value has been assumed for biotites from pre-Grenvillian garnetiferous metamorphic rocks in the Smokey archipelago. These have been plotted on Troger's (1971) (Alvi+$Fe3^+$+Ti+Cr) - Mg - ($Fe2^+$+Mn) diagram (Fig. 4-5). Biotites in granulite-facies rocks are more magnesian and cluster in the field of meroxene, while biotites from amphibolite-facies granodioritic gneisses fall in the lepidomelane-sideromelane fields. There is, however, direct evidence that at least some biotites from the WBIGC have higher oxidation ratios, exceeding 0.10. Biotite separated from sample V210-1 (pelitic

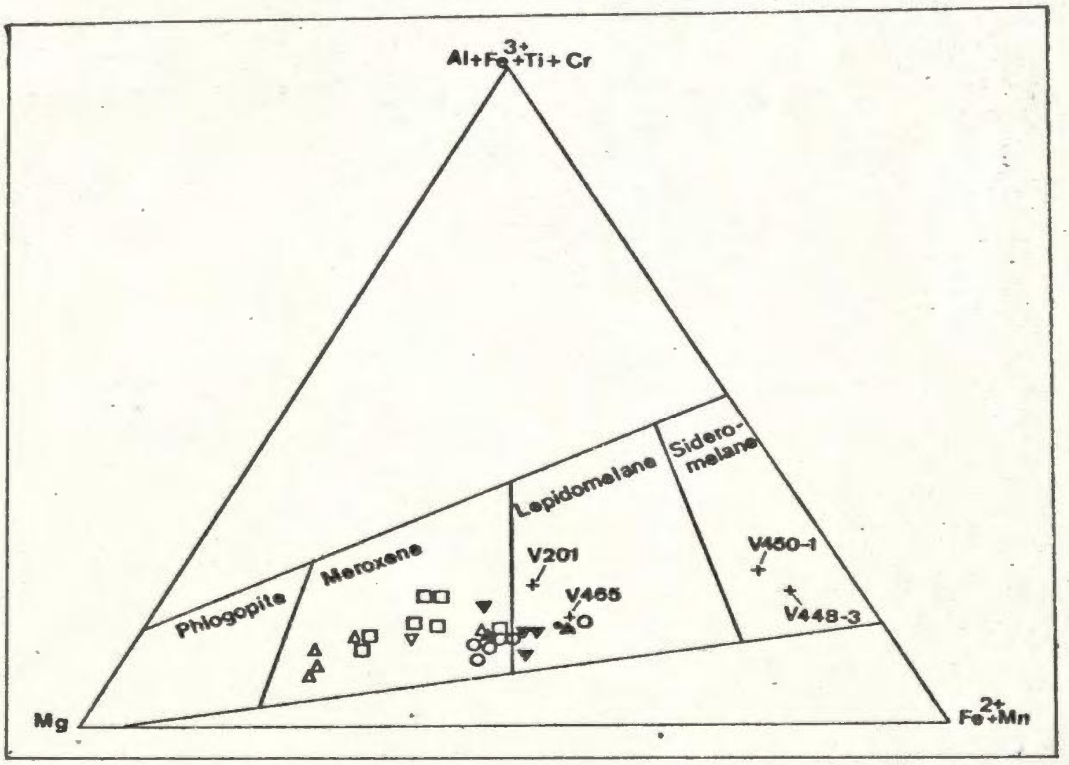

Figure 4-5. Compositions of biotites from pre-Grenvillian metamorphites plotted on Troger's (1971) diagram. For illustrative purposes, the biotites are plotted assuming an oxidation ratio of 0.1 (see text). Symbols: squares-pelitic metatexite (unit 1C); crosses-granodioritic gneiss (sample numbers are indicated); open triangles: upright-pre-migmatitic metabasites; inverted-dioritic-tonalitic gneiss (unit 2); black triangles: upright-Makkovik trend metabasites; inverted-retrograded dioritic-tonalitic gneiss; circles-jotunitic gneiss (unit 3A).

metatexite; unit 1C), has an oxidation ratio of 0.23 (Appendix D). It should not be assumed that this oxidation ratio is representative of biotite from the WBIGC, or even from unit 1C in particular. Sample V210-1 contains a variety of biotite textures, and the analysis presented in Appendix D is the average of a range of biotite compositions in the specimen.

The TiO2 content of the reddish-brown biotites associated with the granulite-facies rocks ranges from 3-6 wt.%, versus 1.5-3.5 wt.% in most biotites retrograded to amphibolite-facies. The TiO2 content of biotites thus increases with metamorphic grade, a conclusion consistent with observations by Dallmeyer (1974) and Dymek (1983).

Between-grain variations in biotite compositions in individual samples are negligible in the jotunitic-charnockitic gneiss (unit 3A). As might be expected, however, there is considerable between-grain variation in biotite composition in the layered pelitic metatexite (unit 1C), although no zoning has been detected within individual crystals. The variability of biotite and garnet compositions present in pelitic metatexite paleosomes has been documented in four samples. One of these (CG-79-347) consists of a texturally complex, biotite- and pinitized cordierite-rich mesosome, while sample V580-16 is a coarse-grained leucosome containing cordierite-mantled garnet porphyroblasts. The remaining two samples (V210-1, V580-12) contain well defined paleosome and leucosome components.

Analyses of six biotites and garnets from various textural occurrences in sample CG-79-347 are presented in Table 4-1. In this sample, Mg/Fe(t) in biotite ranges from a minimum of 1.15 for green-brown biotite replacing garnet to a

Table 4-1. Compositional parameters and temperature estimates of different textural varieties of garnet and biotite in a sample (CG-79-347) of pelitic metatexite (unit 1C). Analyses 1,3,4,6,9, and 11 are garnets; analyses 2,5,7,8,10 and 12 are biotites.

	DOMAIN 1		DOMAIN 2			DOMAIN 3			DOMAIN 4		DOMAIN 5	
	1	2	3	4	5	6	7	8	9	10	11	12
SiO_2	37.61	37.27	39.02	37.11	37.72	36.53	37.74	36.05	37.08	37.16	40.82	38.30
TiO_2	0.00	3.52	0.00	0.00	0.66	0.02	2.96	5.23	0.01	3.97	0.00	1.96
Al_2O_3	22.78	15.96	20.15	20.25	17.95	20.43	16.30	14.64	20.84	16.86	21.14	16.67
FeO	32.69	14.82	35.60	35.84	15.79	32.42	16.94	18.19	31.66	16.10	28.31	10.89
MnO	0.52	0.03	0.70	0.71	0.03	0.73	0.00	0.04	0.67	0.02	0.44	0.04
MgO	7.39	14.29	4.86	5.28	14.82	6.48	12.53	11.78	7.53	12.42	9.79	18.25
CaO	0.51	0.00	0.72	1.10	0.00	0.83	0.00	0.00	0.87	0.00	0.66	0.00
Na_2O		0.15			0.10		0.11	0.09		0.18		0.25
K_2O		9.82			8.65		10.23	9.67		9.67		8.46
	101.50	95.86	101.05	100.29	95.72	97.44	96.81	95.69	98.66	96.38	101.16	94.82
Si	5.829	5.553	6.158	5.951	5.563	5.944	5.601	5.473	5.923	5.507	6.186	5.578
Aliv	0.171	2.467	-	0.049	2.437	0.056	2.399	2.527	0.077	2.493	-	2.422
Alvi	3.992	0.327	3.908	3.780	0.684	3.863	0.453	0.093	3.849	0.453	3.963	0.437
Ti	0.000	0.393	0.000	0.000	0.069	0.002	0.330	0.597	0.001	0.443	0.000	0.213
Fe*	4.238	1.840	4.700	4.807	1.948	4.412	2.103	2.310	4.230	1.996	3.588	1.325
Mn	0.068	0.004	0.094	0.096	0.000	0.101	0.000	0.005	0.091	0.003	0.056	0.004
Mg	1.707	3.162	1.143	1.262	3.255	1.571	2.772	2.665	1.793	2.743	2.211	3.958
Ca	0.085	0.000	0.122	0.189	0.000	0.145	0.000	0.000	0.149	0.000	0.107	0.000
Na		0.043			0.026		0.032	0.026		0.068		0.052
K		1.860			1.627		1.937	1.873		1.568		1.829
Mol%												
pyr	27.3		20.3	28.3		26.7			30.4		39.0	
alm	70.2		75.8	66.8		69.1			65.5		58.1	
spes	1.1		1.7	2.2		1.7			1.5		1.0	
gros	1.4		2.2	2.7		2.4			2.5		1.9	
Mg/Fe	0.40	1.72	0.24	0.26	1.67	0.35	1.32	1.15	0.42	1.37	0.62	2.99

* all iron as Fe^{2+}. Garnets recalculated to 24 oxygens, biotites recalculated to 22 oxygens

Geothermometry (Thompson, 1976)

DOMAIN 1: analyses 1 & 2, T = 646 C

DOMAIN 2: analyses 3 & 5, T = 522 C
: analyses 4 & 5, T = 540 C

DOMAIN 3: analyses 6 & 7, T = 690 C
: analyses 6 & 8, T = 735 C

DOMAIN 4: analyses 9 & 10, T = 727 C

DOMAIN 5: analyses 11 & 12, T = 609 C

DOMAIN 1: garnet resorbed by brown biotite + sillimanite + quartz. For profile, see Fig. 4-7

DOMAIN 2: two-growth garnet (analysis 3 = idiomorphic core; analysis 4 = ragged garnet mantle) enclosed by symplectic intergrowth of green-brown biotite + quartz

DOMAIN 3: garnet poikiloblast partly resorbed by ragged green-brown biotite (analysis 7). Nearby idiomorphic brown biotite (analysis 8) is enclosed in quartz

DOMAIN 4: garnet poikiloblast in contact with subidiomorphic brown biotite (from leucosome component of pelitic metatexite)

DOMAIN 5: garnet and biotite (coexisting with sillimanite) enclosed and resorbed by cordierite

maximum of 2.99 where biotite associated with garnet has been replaced by cordierite. Magnesium/iron(t) ratios of different textural varieties of garnet range from 0.24 to 0.62 for garnets in association with the biotites just mentioned. These variations in biotite and garnet Mg/Fe ratios suggest that chemical disequilibrium is prevalent at this grade (see section 4.2.4A), but they are nonetheless consistent with the observed preferential partitioning of Mg/Fe in the sequence cordierite > biotite > garnet (e.g. Lonker, 1980).

Compositional parameters of biotites from samples V210-1, V580-12 and V580-16 are summarized in Table 4-2A. The between-grain compositional variations evident in Tables 4-1 and 4-2A are broadly consistent for particular textural occurrences, and may be readily attributed to the diverse origins of biotite in the samples. These data indicate that paleosome biotites, which are equigranular and (sub)idiomorphic, show remarkably little grain-to-grain compositional variations, whereas leucosome biotites, which typically show textural evidence of a retrograde origin (e.g. symplectites), are more heterogeneous with respect to Mg/Fe ratios and Ti and Alvi contents.

Several varieties of garnet have been distinguished in pelitic metatexite. Garnet generally forms 1cm poikiloblasts in leucosomes, which are not uncommonly mantled by cordierite. Garnets are typically replaced by biotite + sillimanite + quartz or by cordierite. In samples CG-79-347 and V210-1, two stages of garnet nucleation are indicated by the local presence of small (0.1-0.3mm) (sub)idiomorphic garnet cores with thin (0.1mm) ragged garnet mantles. The older garnets in both samples are typically clouded by an opaque mineral (magnetite?), which is too fine-grained for analysis with the microprobe.

Table 4-2A. Compositional parameters of various textural varieties of pre-Grenvillian biotites in pelitic metatexite (unit 1C).

	Paleosome Biotite					Leucosome Biotite					
	Grain #:					A.*	B.*	C.*	D.*	E.*	F.*
Sample V210-1	1.	2.	3.	4.	5.						
Mg/(Mg+Fe)	.630	.634	.633			.673	.685	.663	.653	.713	
Ti	.347	.342	.352			.282	.343	.289	.383	.326	
Alvi	.466	.418	.431			.516	.379	.532	.418	.474	
Sample V580-12											
Mg/(Mg+Fe)	.500	.499	.526	.546	.519		.645		.595		.605
Ti	.481	.467	.358	.376	.465		.169		.426		.367
Alvi	.566	.469	.533	.468	.417		.596		.353		.451
Sample V580-16											
Mg/(Mg+Fe)								.645			.559
Ti								.126			.443
Alvi								.000			.466

*A = ragged biotite enclosed in cordierite
*B = symplectic biotite + quartz nucleated on magnetite
*C = biotite + sillimanite + quartz symplectic intergrowth replacing garnet
*D & *E = euhedral (idiomorphic) biotite enclosed in garnet porpyroblasts; *E is enclosed in the garnet presented in Table 4-2B. *F= biotite adjacent to garnet.

Table 4-2 B. Compositional parameters of various textural varieties of pre-Grenvillian garnets in pelitic metatexite (unit 1C).

Sample V210-1	Garnet Porphyroblasts	Garnet Enclosed In Cordierite			Two-Stage Growth Garnets	
		A.*	B.*	C.*	D.*	E.*
$\frac{Mg}{Mg+Fe}$	.281	.392	.378	.323	.298	.321
pyr	25.9 mol%	38.9	38.8	32.4	30.6	31.2
alm	66.2	56.5	56.7	66.2	66.2	61.8
spes	4.6	2.9	2.3	0.8	3.0	4.0
gros	3.2	1.7	2.2	0.6	0.2	3.0

Sample V580-12		
$\frac{Mg}{Mg+Fe}$	.272	.288
pyr	25.8	28.2
alm	70.9	64.0
spes	1.9	4.5
gros	1.4	3.3

Sample V580-16		
$\frac{Mg}{Mg+Fe}$	.365	.349
pyr	34.9	28.5
alm	55.7	66.8
spes	5.7	1.9
gros	3.7	2.8

*A = tiny (0.1mm) garnet enclosed in cordierite
*B = ragged garnets enclosed in cordierite
*C = symplectic garnet + (?) magnetite intergrowth enclosed in cordierite
*D = anhedral (xenomorphic) garnet on which ragged second-generation garnet has nucleated (=*E)

Garnets have been analysed in seven samples of pelitic metatexite (unit 1C). With one exception (V172), all samples contain variably pinitized cordierite, and three (V207, V210-1, V580-12) also contain hypersthene. Compositions of these and other pre-Grenvillian garnets, expressed in terms of garnet end members, are displayed graphically in Figure 4-6. The compositional variations of garnets from samples CG-79-347, V210-1, V580-12 and V580-16 listed in Tables 4-1 and 4-2B appear to be related to the textural occurrences of the garnets. In particular: (1) second-stage growth garnets in samples V210-1 and CG-79-347 have higher pyrope/almandine ratios than the earlier garnets they envelope, suggesting that they crystallized at higher T conditions; (2) garnets replaced by cordierite have higher pyrope/almandine ratios than (first-stage) garnets distant from cordierite.

The garnets in pelitic metatexite are essentially almandine-pyrope solid solutions, with Mg/(Mg+Fe) in garnet cores ranging from 0.17 to 0.39, and with grossular and spessartine contents typically totalling approximately 8 mol.%. To ascertain the effects of marginal reequilibration (i.e. during subsolidus cooling) with other phases, core and rim compositions were determined for garnets in contact with other ferromagnesian minerals. The extent of reequilibration of garnet rim compositions in pelitic metatexite was evaluated by analysing across garnet-hypersthene, and garnet-cordierite interfaces in sample V210-1, and across garnet-biotite interfaces in V210-1 and CG-79-347. Profiles of these analyses are presented in Figure 4-7. They show the garnet cores to be essentially homogeneous with respect to Mg and Fe. Rim compositions of garnets in contact with biotite and cordierite show iron enrichment within less than 0.1mm of the grain edge. With the exception of garnets in sample V172, which show a marked

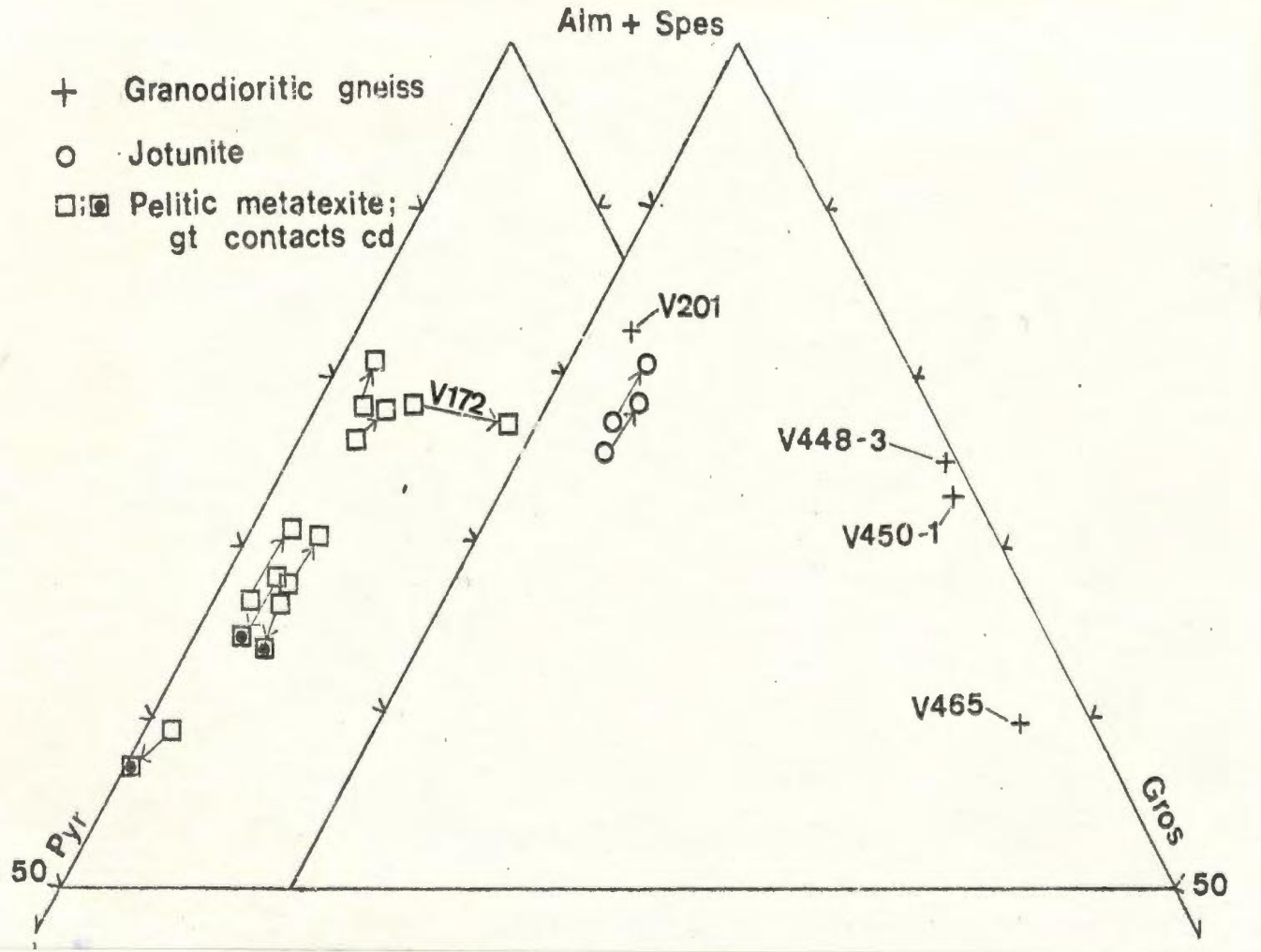

Figure 4-6. Pre-Grenvillian garnet compositions expressed in terms of end members. Arrows show core to rim zoning. Granodioritic sample V201 is from uncorrelated unit in the Granulite Complex; V448-3, V450-1 and V465 are from the Bluff Head orthogneiss; V172 is from pelitic metatexite (unit 1C).

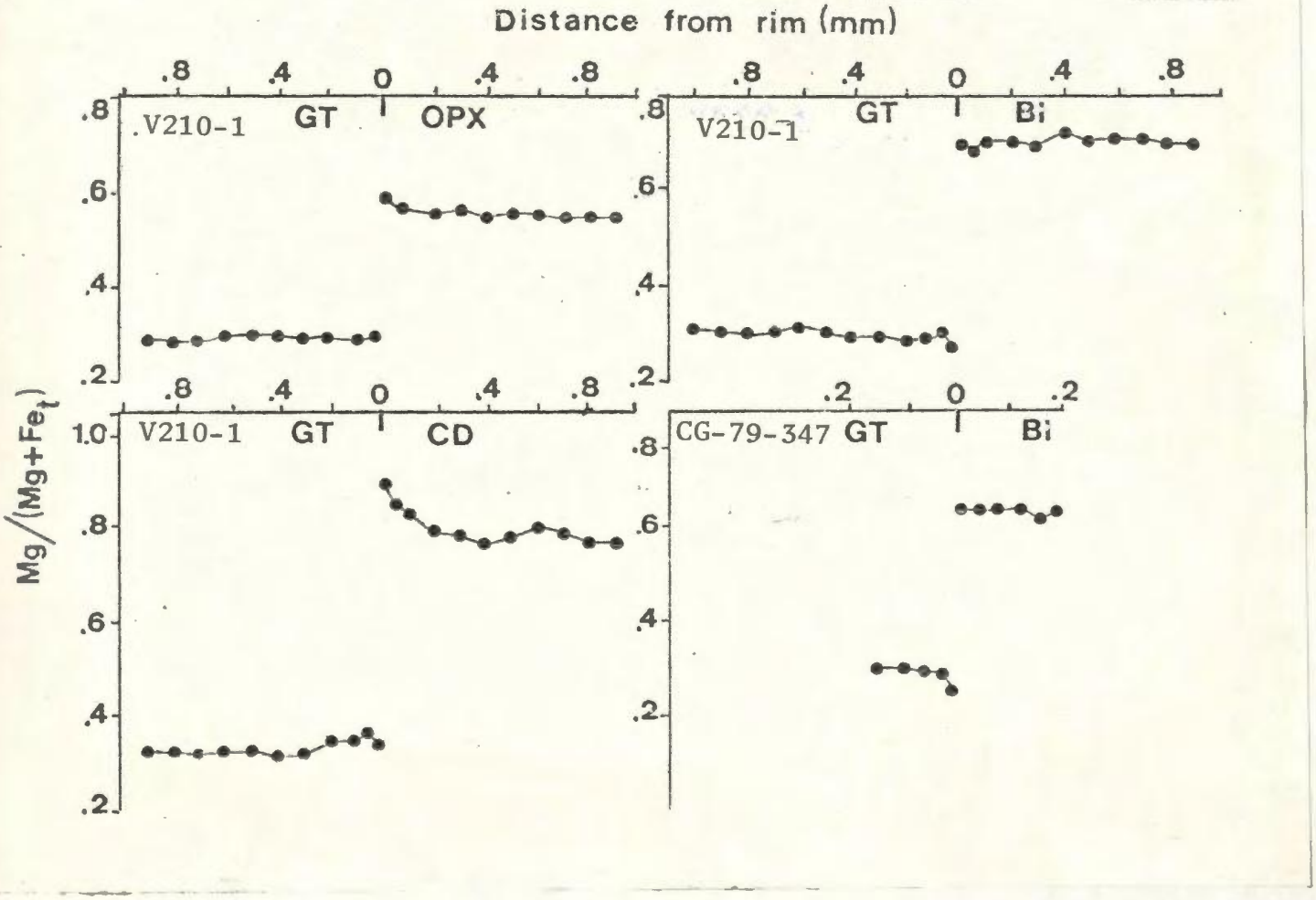

Figure 4-7. Microprobe line traverse analyses across garnet-biotite (samples V210-1; CG-79-347), garnet-orthopyroxene and garnet-cordierite parageneses (V210-1). See text.

increase in the proportion of grossular towards the rim (see Fig. 4-6), zoning of non-femic components is negligible.

Garnets in orthopyroxene-bearing jotunite (samples V221, V579-1) are almandine-rich with a significant pyrope content (15-20mol%) and minor non-femic components (spessartine + grossularite = $\leq$8mol%). Garnet rims are slightly enriched in almandine (76mol%, versus 73-74mol% in cores), and show a corresponding depletion in the pyrope content. Textural evidence suggests that garnet and orthopyroxene stably coexist in these samples. However, textural and compositional features of garnets coexisting with clinopyroxene and biotite in sample V471-2 from the Bluff Head charnockite occurrence are significantly different from those in samples V221 and V579-1. Sample V471-2 is characterized by a relict coronitic texture, in which garnet necklaces mantle iron oxide $\pm$ clinopyroxene aggregates, and are surrounded by brown biotite. Orthopyroxene in this sample is associated with biotite, is partly replaced by amphibole, and is not observed in contact with garnet or clinopyroxene. Although containing similar amounts of pyrope, the garnets in V471-2 contain significantly less almandine (47mol%) and have higher grossular (22mol%) and spessartine (16-18mol%) contents than the garnets in V221 and V579-1. Together with the relatively sodic composition of plagioclase in the sample (An12, versus An30 in V221 and V579-1), these features indicate a retrograde origin for garnet and clinopyroxene at the expense of orthopyroxene and (calcic) plagioclase $\pm$ Fe oxide in sample V471-2 (e.g. Whitney, 1978). Since this is inferred to be a disequilibrium assemblage, it will not be considered further here.

Compositional variation between garnet porphyroblasts within the same thin

section is limited to about ± 4 mol.% pyrope in garnetiferous leucosomes in pelitic metatexite and in garnetiferous jotunitic gneiss. However, in some instances there are marked variations in the compositions of different textural varieties of garnets in the metapelite paleosome. Garnet end-member compositions of four types of garnets from the paleosome of sample CG-79-347 are presented in Table 4-1. Although no significant variation in the grossular and spessartine components of these garnets was detected, pyrope contents vary between 20 and 39mol.% between the different textural types of garnet. Given the heterogeneity of the banded paleosome and the varying degree and nature of garnet replacement, this variation in garnet compositions is not unexpected. Analyses from a profile across the boundary between incompletely replaced garnet and its biotite (+ sillimanite + quartz) host in sample CG-79-347 are presented in Figure 4-7. The rim of this garnet shows a similar pattern of iron enrichment as noted in garnet-biotite and garnet-hypersthene pairs from the leucosome of sample V210-1.

4.2.1C Garnet-Pyroxene

Garnet + orthopyroxene-bearing assemblages occur in three samples (V207, V210-1, V580-12) of pelitic metatexite and two samples (V221, V579-1) of jotunitic gneiss.

As noted in section 4.2.1B, garnets in the jotunitic-charnockitic gneiss are almandine-rich with low ($\leq$8mol%) spessartine and grossular contents. Garnet-orthopyroxene contacts are distinct and sharp (Figs. 4-1C, 4-1D), indicating that these phases comprise an equilibrium assemblage. The iron/magnesium ratios of both phases vary across grains in mutual contact. In samples V221 and V579-1, the Fe/Mg ratio of garnet rims is greater by 20% and 27% (respectively) than in

the cores. A corresponding decrease in this ratio is found in the contiguous orthopyroxenes, which have rim compositions depleted in Fe/Mg by 10% and 16% in these samples (respectively) compared with core compositions.

Garnet-orthopyroxene pairs in pelitic metatexite also exhibit stable grain boundaries (Fig. 4-1C), but core to rim variations in iron/magnesium ratios have been noted only in orthopyroxene (Fig. 4-7A). This suggests that garnet has more fully reequilibrated with respect to these elements in this lithology than in the jotunite.

Garnetiferous assemblages are rare in the jotunitic-charnockitic gneiss (unit 3A). This would suggest, as a first approximation, compositional rather than metamorphic control on the distribution of garnet in this unit.

The significance of garnet in high-grade meta-igneous rocks became a high-profile topic in a series of publications concerning the occurrence of garnet + pyroxene-bearing rocks in the Adirondacks by Buddington (1965; 1966) and deWaard (1965a,b; 1967). DeWaard (1967) demonstrated the importance of bulk rock composition in controlling the distribution of garnet in orthogneisses, and suggested that all rocks containing orthopyroxene and plagioclase generated clinopyroxene + garnet + quartz with increasing metamorphic grade. Martignole and Schrijver (1973) compiled whole-rock analyses from garnetiferous and non-garnetiferous granulite-facies anorthosite-charnockite massifs in the Adirondacks and the Morin Complex of Quebec in order to more clearly ascertain what garnet-forming parameters are prevalent at this grade. They distinguished two compositional suites based on Fe^{2+}/Mg and normative An/Ab; garnet-free

assemblages occur in rocks with relatively low An/Ab and Fe2+/Mg ratios.

Normative An/Ab ratios from seven garnet-free jotunite-charnockite samples from the study area range from 0.33 to 0.51, and average 0.46. Garnetiferous jotunite sample V579-1, with an An/Ab ratio of 0.48, is within this range. In the present study, the bulk rock ferrous/ferric iron ratio is unknown, consequently the possible role of fO2 in the development of garnet in these rocks cannot be evaluated. It is worth noting, however, that FeOt/(FeOt+MgO) between garnet-free and garnetiferous jotunite-charnockite samples, at 0.73 (n=7) and 0.70 (sample V579-1), respectively, are very similar. Clearly, another factor must influence the presence of garnet in this unit. Comparing the average composition of the seven garnet-free samples and that of V579-1 (Table 4-3), it is seen that the two series differ mostly in the CaO/(CaO+MnO+MgO+FeOt) (0.38 and 0.15, respectively) and CaO/Al2O3 (0.24 and 0.18, respectively) ratios. The significance of these contrasting Ca contents becomes clear when the mineralogy of the two series is considered. Clinopyroxene is a common constituent of garnet-free jotunite-charnockite, occurring in 5 of the 7 analysed samples. On the basis of these observations, it may tentatively be concluded that higher CaO/(CaO+MnO+MgO+FeOt) and CaO/Al2O3 ratios in this unit favour the development of clinopyroxene rather than garnet for given (moderate) pressure conditions prevalent during metamorphism of the WBIGC.

4.2.1D Garnet-Cordierite

Cordierite has been identified only in pelitic metatexite (unit 1C). Although it occurs in both the paleosome and neosome components of these migmatites, it has been completely pinitized in paleosomes, and only neosome cordierites have

Table 4-3. Major element geochemistry of garnet-free and garnetiferous jotunitic-charnockitic gneiss

	-1-	-2-
SiO_2	62.8	62.0
TiO_2	0.58	0.99
Al_2O_3	17.50	13.2
**Fe_2O_3	4.92	9.56
MnO	0.07	0.09
MgO	1.79	4.04
CaO	4.25	2.42
Na_2O	4.32	2.73
K_2O	3.36	3.03
P_2O_5	0.19	0.02
LOI	0.49	0.15
	100.27	98.23
	(7)*	(1)

**all iron expressed as Fe_2O_3

( )* = number of analyses

-1- = garnet free jotunitic-charnockitic gneiss

-2- = garnetiferous jotunitic-charnockitic gneiss (sample V579-1)

been analysed with the electron microprobe. The cordierite commonly shows lamellar twinning, and contains zircon inclusions with characteristic orange-yellow pleochroic haloes. Cordierite in most of the samples is optically positive, however optically negative cordierite occurs in V580-16. 2Vx ranges from approximately 65°-80° (visual estimate). Cordierites with high CO2 contents are generally optically positive, with 2Vx angles close to 90° (Armbruster and Bloss, 1982). It is therefore inferred that channel fluids in cordierites in unit 1C contain significant, but variable, CO2 in addition to water.

Cordierite has two modes of occurrence: (1) as partial or complete rims mantling garnet porphyroblasts, and (2) as clusters of 0.3-1.5mm subidiomorphic grains, commonly enclosing xenomorphic garnets $\pm$ sillimanite $\pm$ ragged biotite.

Two cordierite-producing reactions are inferred. The local presence of sillimanite and ragged biotite inclusions in cordierite implies that the divariant reaction (2) has occurred:

bi+sil+qz = cd+ksp+H2O [reaction 2]

This texture is typical of cordierite in the biotite-rich paleosome component of the metapelitic gneiss. Garnet in both paleosomes and leucosomes of this unit is locally mantled by cordierite containing sillimanite inclusions, indicating the divariant reaction (3):

2gt+4sil+5qz = 3cd [reaction 3]

These reactions have also been inferred from similar textures described by Gil Ibarguchi and Martinez (1982), who proposed the net cordierite-forming univariant reaction (4):

sil+bi+gt+qz = cd+ksp+H2O [reaction 4]

Petrographic evidence supporting this net reaction is provided by the local presence of garnet + sillimanite + biotite within cordierite (Fig. 4-8).

In the field, fibrous rims armouring some cordierites were tentatively identified as sillimanite. This has been confirmed in thin section, and implies the replacement of cordierite by sillimanite, and thus reversal ("right to left" direction) of reaction [2].

The degree of pinitization in leucosome cordierites ranges from 5-100% even within the same thin section. Cordierite is most highly pinitized where associated with abundant biotite (as in the paleosome); where cordierite is isolated in quartzofeldspathic domains, generally only the rims of cordierite have been altered.

Cordierites from five samples of pelitic metatexite were analysed with the electron microprobe. As a result of variable alteration of the mineral, core and rim analyses of cordierites were possible only in specimens V210-1, V580-12 and V580-16. They are quite uniform in composition, with Mg/(Mg+Fe) varying from 0.75-0.78, except where in contact with garnet. The Mg/(Mg+Fe) ratio of the cores of cordierites touching garnet falls in the range mentioned above, while this ratio varies between 0.80-0.88 directly adjacent (within 0.20mm; Fig. 4-7C) to garnet. This demonstrates that the effects of cordierite-garnet reequilibration during cooling are limited to the outermost margins of grains, and that cores of all but the smallest cordierite crystals likely retain their higher-grade metamorphic compositions.

For a given temperature, the stability field of cordierite is extended to

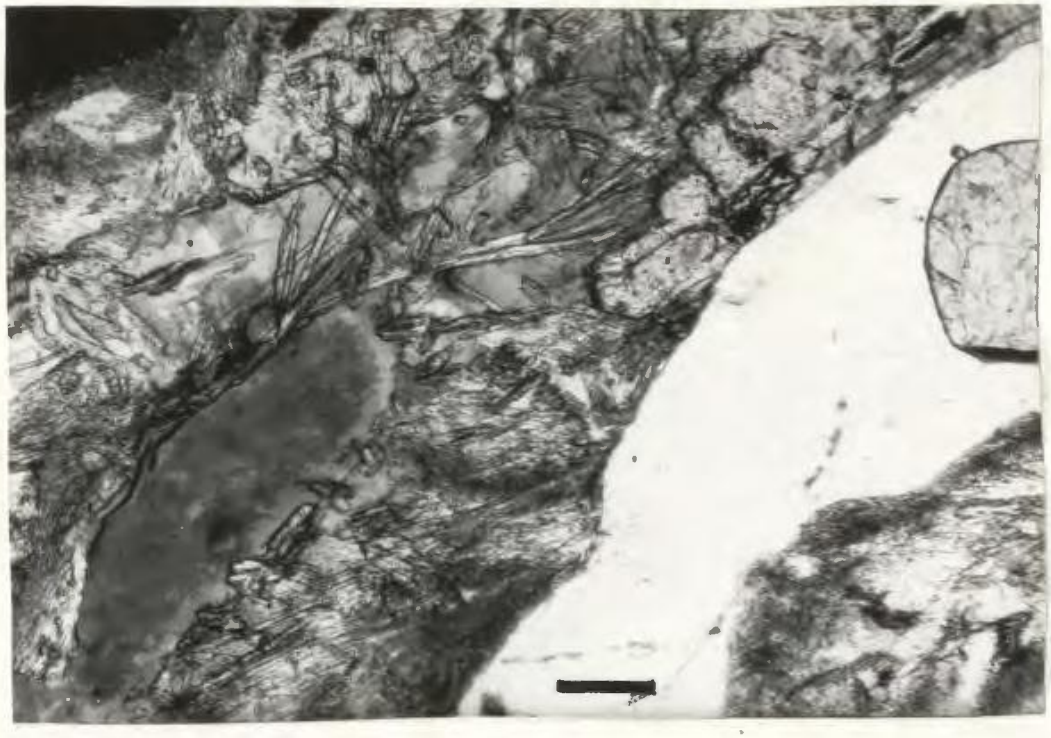

Figure 4-8. Pinitized cordierite enclosing ragged biotite (medium grey), garnet (high relief), and sillimanite needles in pelitic metatexite (unit 1C). Note the idiomorphic garnet (upper right) enclosed in quartz. Biotites enclosed in quartz (not in photo) are also idiomorphic and are compositionally distinct from the ragged biotite enclosed by the cordierite (see text and Table 4-2B). Bar scale is 0.1mm. Plane polarized light; sample CG-79-347.

higher pressures with increased water fugacity (Martignole and Sisi, 1982; Newton and Wood, 1979). An analysis of cordierite is therefore incomplete without a discussion of the magnitude and composition of the fluid phase contained in this mineral.

The content of molecular water accomodated by the cordierite channel structure cannot be directly determined from microprobe analyses. Given an approximate analytical error in the microprobe data of ~1.5%, anhydrous cordierite may be expected to yield totals of 98.5-101.5%. For the data presented in Appendix A.4 (A.4.5) microprobe analysis totals average 97.2%, limiting the probable range of fluid content of these cordierites to ca. 1.3-4.3 wt.%. As reported in the literature, the fluid content of most cordierites is less than 3 wt.%. The variable and often intense degree of pinitization of the cordierites from the study area preclude the possibility of obtaining reasonable estimates of fluid content by gravimetric or by wet chemical analysis of cordierite separates. Consequently, such estimates must be derived by indirect means.

Newton and Wood (1979) developed an ideal mixing model between hydrous and anhydrous Mg-cordierite, and demonstrated the systematic PT dependence of the hydrous end member. For conditions of pre-Grenvillian metamorphism estimated below (section 4.2.4B), isohydrons presented by Newton and Wood (1979, Fig. 2) indicate a water content of approximately 2.1 wt.% or 0.57 mol. water per formula unit. This estimate is consistent with the microprobe analyses, however the optically positive character of cordierite in most samples also suggests significant CO2 in the channel fluid. An important consideration to bear in mind is that the present fluid content of the cordierite may not be

representative of that existing in this mineral during its initial crystallization. Fluids are loosely held in the cordierite channel structure, and the mineral may be dehydrated or rehydrated after the main metamorphic event.

4.2.1E Aluminosilicates

Sillimanite coexists with K feldspar in sillimanite diatexite (unit 1A) and in pelitic metatexite (unit 1C), implying that the second sillimanite isograd was surpassed during pre-Grenvillian metamorphism:

mu+qz = sil+Ksp+V [reaction 5]

Five varieties of sillimanite are present in pelitic metatexite (unit 1C): (a) sillimanite needles up to 0.5mm long occur as inclusions in refractory minerals (garnet, Fe-Ti oxides); and, (b) more commonly, as intergrowths in biotite, while; (c) minute sillimanite needles (fibrolite) occur along grain contacts between feldspars. The significance of the fibrolite (c) in these samples is uncertain. It may represent a retrograde metasomatic reaction (e.g. Ahmad and Wilson, 1982).

In addition, two forms of sillimanite are associated with cordierite: (d) stubby sillimanite grains enclosed in cordierite are inferred to be relics from a cordierite-producing reaction [reaction 4], while (e) sillimanite needles growing in from cordierite grain boundaries are considered to replace this mineral ["reversed" or retrograde reaction 2?]. All five varieties of sillimanite have been observed within an individual thin section of pelitic metatexite.

Assemblages bearing two aluminosilicates occur only in sillimanite-kyanite schist (unit 1B). Textural evidence indicates that kyanite is being replaced by sillimanite. Kyanite has not been observed in any other lithology within the study

area. Its preservation as an apparently metastable phase in unit 1B may be attributed to the small ΔG of reaction associated with the transformation of kyanite into sillimanite, although this does not account for its absence in the other metapelitic rocks. In view of this, an alternate explanation is that the kyanite-schist, which occurs uniquely as a screen within (retrograded) jotunite on Entry Island, may represent a xenolith sampled from depth during emplacement.

4.2.1F Two-Feldspar Assemblages

Plagioclase and K feldspar are essential phases of all pre-Grenvillian metamorphic rocks except metabasites and the dioritic end-member of unit 2 (dioritic-tonalitic gneiss), which both lack essential K feldspar. Despite the pervasive development of exsolution textures (perthite, antiperthite) which characterize feldspars in these rocks, plagioclase and K feldspar show restricted compositional ranges within each lithology (see Chapter 2), and negligible compositional variations within individual thin sections. The feldspars are therefore suitable for use in various calibrated geothermobarometric expressions.

4.2.2 Parageneses of the Bluff Head Orthogneiss

Amphibolite-facies parageneses characterize the granodioritic (unit 5A) and monzonitic (unit 5B) gneisses exposed near Bluff Head in the northern Groswater Bay Terrane. The characteristic mineral assemblage of these gneisses includes biotite + epidote $\pm$ amphibole + sodic plagioclase (An 4-18) + microcline + quartz $\pm$ muscovite $\pm$ allanite. In addition, garnet has been observed locally in unit 5A. Amphibolite-facies mineral assemblages occur in both the paleosome and neosome of these gneisses, and it is unclear whether the rocks were originally migmatized under amphibolite-facies conditions, or whether higher grade

assemblages were obliterated during subsequent retrogression.

4.2.2A Garnet-Biotite

Garnet occurs only sporadically in granodioritic gneiss (unit 5A), and has not been observed in monzonitic orthogneiss (unit 5B). The garnets in unit 5A are invariably enclosed by quartzofeldspathic haloes depleted in biotite, a feature not seen in garnetiferous granulite-facies assemblages, or in garnets associated with Grenvillian fabrics developed in various lithologies (see section 4.3.7A). Biotite-depletion haloes have also been noted in an uncorrelated granodioritic gneiss (unit 5A?; sample V201) from the White Bear Islands. Regardless of the metamorphic grade at which they formed, the haloes demonstrate that the garnet has developed at the expense of biotite.

Garnets from three samples of the Bluff Head granodioritic orthogneiss (unit 5A) (V448-1, V450-1, V465) have been analysed. These garnets are composed of approximately equal proportions of almandine (33-42mol.%), grossular (23-37mol.%) and spessartine (23-41mol.%), with minor (<5mol.%) pyrope. The garnets are similar in composition to garnets associated with Grenvillian fabrics (see section 4.3.7A). In each of the three samples, the garnets are unzoned and there is little between-grain compositional variation on the scale of a thin section.

Biotite in the Bluff Head orthogneiss coexists with garnet, but the two minerals have not been observed in contact. The biotites plot in the lepidomelane and sideromelane fields of Troger's (1971) diagram (Fig. 4-5), and are therefore similar in composition to biotites defining Grenvillian fabrics (see Fig. 4-17). In contrast to the variety of textural occurrences of biotite present in the WBIGC, biotite in these rocks occurs uniquely as brown or greenish-brown subidiomorphic

flakes; symplectic intergrowths with quartz have not been seen.

4.2.2B Amphibole + Epidote + Allanite

Gneissic fabrics in the Bluff Head orthogneiss are defined by the segregation and preferred dimensional orientation of biotite and green amphibole. Details of amphiboles from all pre-Grenvillian metamorphic rocks are presented in section 4.3 ("Grenvillian Metamorphism") in order to facilitate comparison with Grenvillian amphiboles. It is nonetheless worth noting here that amphiboles in units 5A and 5B are hastingsites and hastingsitic hornblendes (Leake, 1978, following the 13CNK normalization scheme described in section 4.3.7C), which contrast with the magnesian hornblendes predominating in retrogressed portions of the WBIGC and foliated members of the BMIS. Amphibole is subordinate to biotite in these gneisses, and coexists with epidote $\pm$ epidote-rimmed allanite $\pm$ muscovite $\pm$ sphene. The hastingsitic hornblendes lack quartz "inclusions" typical of amphiboles developed through the retrogression of pyroxene.

4.2.3 The Makkovik Trend in the BMIS

The Makkovik trend is locally developed in all members of the BMIS in the map area. In younger plutonic phases of the BMIS (e.g. units 6B-6E), it is represented by the development of schistose fabrics along zones up to approximately 1km in width. This schistosity is characterized by the preferred dimensional orientation of feldspar megacrysts, biotite, amphibole and/or by aligned mafic enclaves. The Makkovik trend is most extensively represented in megacrystic granodiorite (unit 6A), where it coincides with a penetrative foliate to gneissose fabric. Descriptions of the Makkovik trend will thus focus on fabric-forming parageneses in the megacrystic granodiorite, and on mafic enclaves within

this, and a younger (unit 6E) member of the BMIS.

4.2.3A. Megacrystic Granodiorite

Both hornblende- and biotite-bearing varieties of K feldspar megacrystic granodiorite are exposed in the study area. The Makkovik trend is typically represented by the amphibolite-facies assemblage hornblendic amphibole + oligoclase + biotite. Neither pyroxene, garnet, nor epidote are associated with the Makkovik trend in this, or any other member of the BMIS. Within this suite, pre-Grenvillian fabrics and parageneses are identical both to the north and south of the Benedict Fault, although south of the Cut Throat Island Fault, the Makkovik trend has been transposed or overprinted during the Grenvillian orogeny.

4.2.3B. Metabasites

Samples of metabasites parallel to the Makkovik trend from the oldest (megacrystic granodiorite, unit 6A) and youngest (quartz monzonite, unit 6E) members of the BMIS have been compared to evaluate possible changes in parageneses associated with the development of the Makkovik trend over time. The metabasites occur as boudinaged mafic interbands, probably representing former mafic dykes. Dioritic gneiss correlated with unit 2 from Cape Rouge was also sampled. The same metamorphic parageneses seen to define the Makkovik trend in megacrystic granodiorite also occur in these diverse mafic rocks. The characteristic assemblage defining the Makkovik trend is thus: hornblendic amphibole + oligoclase (An 20-30) + biotite. Amphibole compositions, considered in some detail in section 4.3.7C, range from ferro- and magnesian hornblendes to magnesian hastingsitic hornblende.

4.2.4 Estimation of Metamorphic Conditions

Both direct and indirect methods have been used by petrologists attempting to estimate conditions of metamorphism. An indirect approach involves imposing metamorphic constraints by plotting mineral assemblages on an established petrogenetic grid (Bowen, 1940) outlining the appropriate inferred mineral reactions on P-T(-X) space. Although visually informative, this technique is limited by the restricted number of metamorphic reactions involving minerals of fixed composition. A more direct approach involves the estimation of P and(or) T conditions from the equilibrium compositions of coexisting minerals. There are two classes of assemblages amenable to this approach: (a) those in which an exchange reaction occurs; and (b) those in which a net transfer reaction occurs. Exchange reactions involve the permutation of two atoms between sites in different minerals with negligible change in the modal amount of the minerals. Such reactions have a low ΔV and a high ΔS and are generally suitable for thermometric calibration. Net transfer reactions generally involve high ΔV and low ΔS, and therefore are more suitable for barometric calibrations. If divariant, net transfer reactions may also incorporate an exchange reaction, and may therefore be sensitive to both T and P.

Several mineral assemblages calibrated for use as geothermometers and geobarometers occur in the study area. Representative examples of these have been sampled and analysed with the electron microprobe. The analyses themselves, estimates of accuracy and precision, and a review of operating conditions of the microprobe are presented in Appendix A.4. Compositional parameters of the various Grenvillian and pre-Grenvillian metamorphic mineral

assemblages are summarized in tabular form in the text. In each case, assumptions pertaining to the relative ages of these assemblages, the degree of attainment of equilibrium and, in certain cases, the influence of bulk rock composition on mineral composition are considered.

The treatment of geothermobarometry in this study is by no means intended to be exhaustive. A number of recent publications have focused attention on testing the internal consistency, accuracy, and precision of various geothermobarometers. Particularly rigorous reviews include discussions of the importance of equilibrium criteria in the application of the garnet-biotite geothermometer (Indares and Martigole, in press), the role of statistical treatment of analytical data in geothermobarometry (Powell, 1985), and evaluations of two-pyroxene geothermometry (Stephenson, 1984) and garnet-orthopyroxene geobarometry (Harley, 1984c). Essene (1982) provided a concise overview of many geothermobarometers which are utilized here.

In this study, an attempt was made to include wherever possible both experimental and empirical calibrations of various geothermobarometers. Only experimental calibrations of the two-pyroxene goethermometer are available. Those employed here (Wood and Banno, 1973; Wells, 1977; Powell, 1978) give determinate errors of known sign, apparently overestimating temperatures by at least several tens of degress (Stephenson, 1984). Newton and Perkins (1982) demonstrated that their thermodynamic calibration of the garnet-orthopyroxene (-plagioclase-quartz) geobarometer yields results consistent with independent pressure estimates when applied to various low- to high-pressure granulite terranes. Similarly, Harley and Green's semi-empirical calibration of the

solubility of alumina in orthopyroxene coexisting with garnet has been demonstrated to yield more reliable results than previous calibrations (e.g. Wood and Banno, 1973) of this geobarometer (Harley, 1984c).

Neither experimental (Goldman and Albee, 1977; Ferry and Spear, 1978; Hodges and Spear, 1982) nor empirical (Thompson, 1976; Indares and Martignole, in press) calibrations of the garnet-biotite geothermometer yield entirely consistent results. This may be a reflection of departures from equilibrium, even within individual thin sections (Indares and Martignole, 1984), or a result of an inappropriate thermodynamic model. More recent calibrations (Hodges and Spear, 1982; Indares and Marrtignole, in press) take account of the presence of minor elements in garnet and biotite, and may be more precise. However, in many cases the results achieved are within error of those obtained by the other calibrations.

Successful application of the garnet-cordierite geothermobarometer largely depends on reliable estimates of nH2O in cordierite. Essene (1982) noted that the Holdaway and Lee (1977) and Martignole and Sisi (1981) calibrations of this geothermobarometer yield approximately correct results for intermediate values of P(H2O).

The data base provided here is insufficient to rigorously test and compare the precision and accuracy of individual calibrations of these, and other, geothermobarometers. However, mineral assemblages are sufficiently diverse, at least in the WBIGC, to quantify the PT conditions of prograde and retrograde metamorphism in the area.

4.2.4A Attainment of Equilibrium

The degree to which equilibrium has been achieved during metamorphism may be inferred from textural and chemical criteria. Although the data indicate attainment of equilibrium during the granulite-facies event, several lines of evidence suggest significant departures from equilibrium during subsequent retrogression of the WBIGC.

Within the WBIGC, it is apparent that the cores of orthopyroxene-bearing assemblages approach equilibrium with other ferromagnesian phases, although the effects of reequilibration during cooling are pervasive along contiguous grain margins. For example, orthopyroxene rims next to garnet are depleted in Al and enriched in Mg. A regular distribution of Mg/(Mg+Fe) ratios typically exists between the cores of garnet-orthopyroxene and orthopyroxene-clinopyroxene pairs (Fig. 4-9), although the data for garnet-cordierite and, particularly, garnet-biotite pairs show a greater spread of Kd values (Fig. 4-9). Furthermore, contacts between the constituent minerals of high-grade parageneses (orthopyroxene-clinopyroxene; garnet-orthopyroxene) are sharp, and individual mineral species generally show a limited range of grain size and of compositions within individual thin sections.

Significant departure from equilibrium during pre-Grenvillian retrogression of the WBIGC is indicated by the following observations:

(1) individual retrograde phases (e.g. cordierite, biotite, sillimanite, amphibole) commonly show a range of grain sizes in similar parageneses;

(2) corona structures and symplectic intergrowths are common textural features;

(3) some phases show marked chemical zonation: cordierite rims adjacent to garnet are

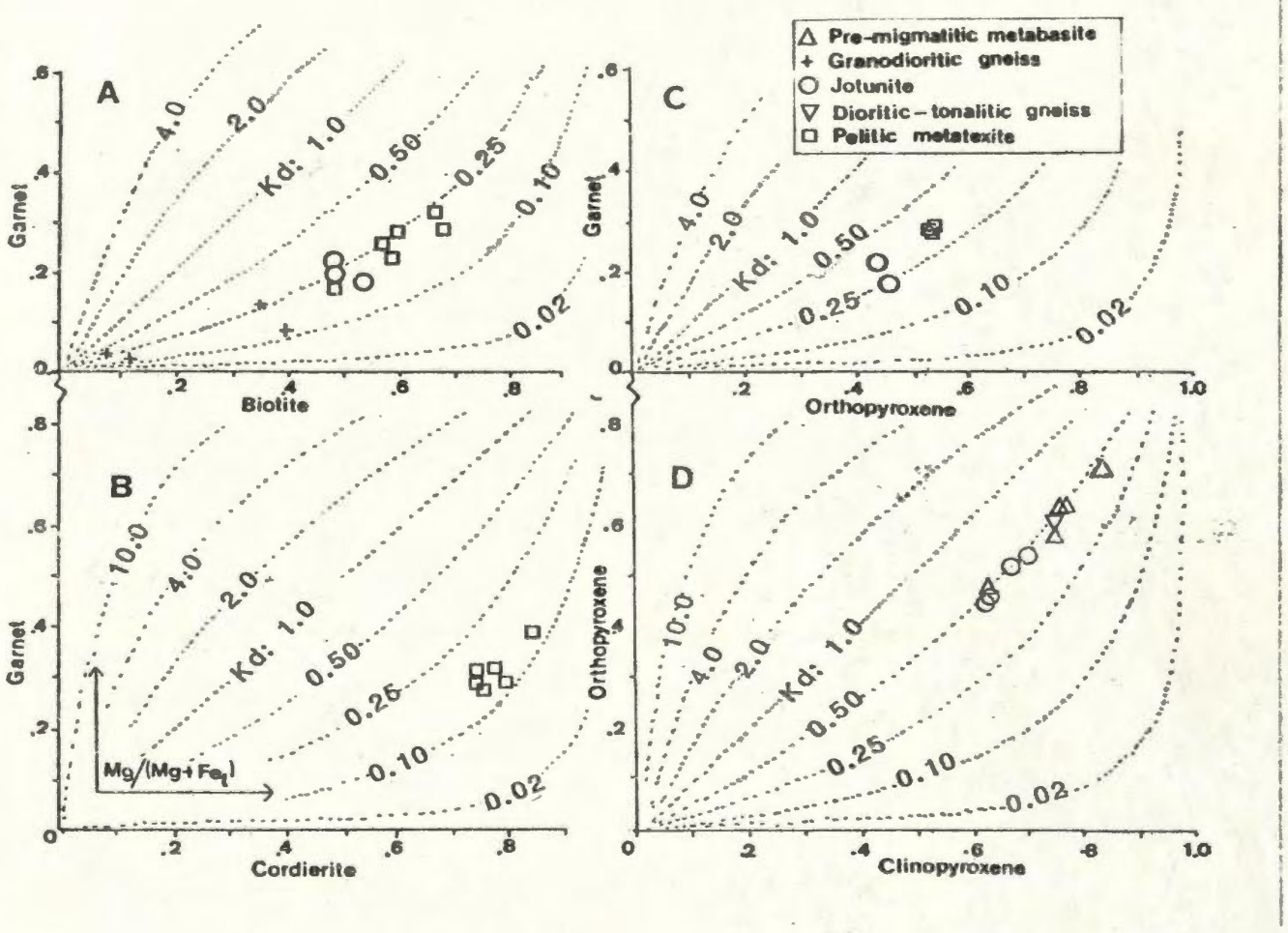

Figure 4-9. Distribution of $Mg/(Mg+Fe_t)$ between coexisting garnet-biotite, garnet-orthopyroxene, garnet-cordierite, and orthopyroxene-clinopyroxene in various members of the Granulite Complex. Kd lines are from Kretz (1961).

enriched in Mg/Fe; relatively non-refractory phases such as biotite, although not zoned, may nonetheless show considerable between-grain compositional variation within individual thin sections (Table 4-1).

The effects of retrogression, typically restricted to the outer 0.1mm of most grains, have been ascertained by determining core and rim compositions of minerals in mutual contact. The cores (/rims) of minerals with reequilibrated rims are considered to be in equilibrium with the cores (/rims) of neighbouring grains. Core (/rim) compositions of contiguous grains or grains coexisting on a domainal (mm) scale are employed in geothermobarometric calculations.

4.2.4B Geothermobarometry of the White Bear Islands Granulite Complex

The pre-Grenvillian PT evolution of the WBIGC has been evaluated by inferring, where possible, specific reactions from textural criteria, and using various calibrated geothermobarometers. A petrogenetic grid presented in Figure 4-10A depicts reactions inferred from the descriptions presented above. For comparative purposes, these reactions are plotted against PT estimates for the granulite facies event and subsequent retrogression determined by geothermobarometery (see Fig. 4-10B). The curve in Figure 4-10B traces granulite facies to retrograde amphibolite facies PT conditions recorded by diverse mineral assemblages in the WBIGC. Temporal aspects of this curve are poorly constrained. The granulite-facies event predates intrusion of the BMIS, and is considered (section 2.8) to date to at least 1.9Ga B.P. It is argued below (section 4.5) that pre-Grenvillian amphibolite-facies retrogression of the WBIGC may coincide with the development of the Makkovik trend in the BMIS, and thus may have occurred as recently as ca. 1.7Ga B.P.

Figure 4-10A. Petrogenetic grid depicting equilibrium curves relevant to the metamorphism of the Granulite Complex. Fields "i" and "ii" are the conditions of granulite facies metamorphism and subsequent retrogression estimated from various geothermobarometers (see below), respectively. Field "ii" falls some 50C below (and 0.5kb above) the lower stability limit of the appropriate composition of cordierite (Fe/(Fe+Mg) = 0.35) from pelitic metatexite (unit 1C). This may indicate that the cordierite crystallized under aH2O conditions differing from those for curve 3 (P(H2O) = 0.4Ptotal). Relatively low retrograde pressures are estimated (for T=650C) by the garnet-plagioclase-Al2SiO5-quartz geobarometer (field "iii"). Sources: Curve [1], Holdaway (1971); [2] Ringwood (1963]; [[3] and [4], both for P(H2O) = 0.4Ptotal, Holdaway and Lee (1977). Conditions for granite melting are shown for aH2O = 1 (curve 5) and for aH2O = 0.4 (curve 6), after Kerrick (1972), cited in Holdaway and Lee (1978).

Figure 4-10B. Schematic representation of pre-Grenvillian PT-evolution of the Granulite Complex. Granulite-facies conditions in field "i" were determined from the two-pyroxene geothermometer (Wood and Banno, 1973; Powell, 1978; Wells, 1977), and from the solubility of alumina in orthopyroxene coexisting with garnet (Harley and Green, 1972). Retrograde conditions are based (1) on the garnet-cordierite geothermobarometer (field "ii"), and (2) on the garnet-plagioclase-Al2SiO5-quartz geobarometer (field iii). The cross centered at 685C and 4.7kb indicates the results of Ca-Mg and Fe-Mg partitioning between coexisting orthopyroxene and garnet. Dimensions of the cross reflect analytical uncertainty associated with the calibrations (Newton and Perkins, 1982; Harley, 1984a). The solid lines defining fields "i" and "ii" indicate the range of PT-estimates determined by various calibrations of the geothermobarometers, while the dashed lines indicate the range of analytical uncertainty with each calibration. The solid arrow traces the interpreted PT-evolution of the Granulite Complex during cooling. The dotted arrow traces an alternative interpretation using the relatively low P estimates derived from the garnet-plagioclase-Al2SiO5 geobarometer.

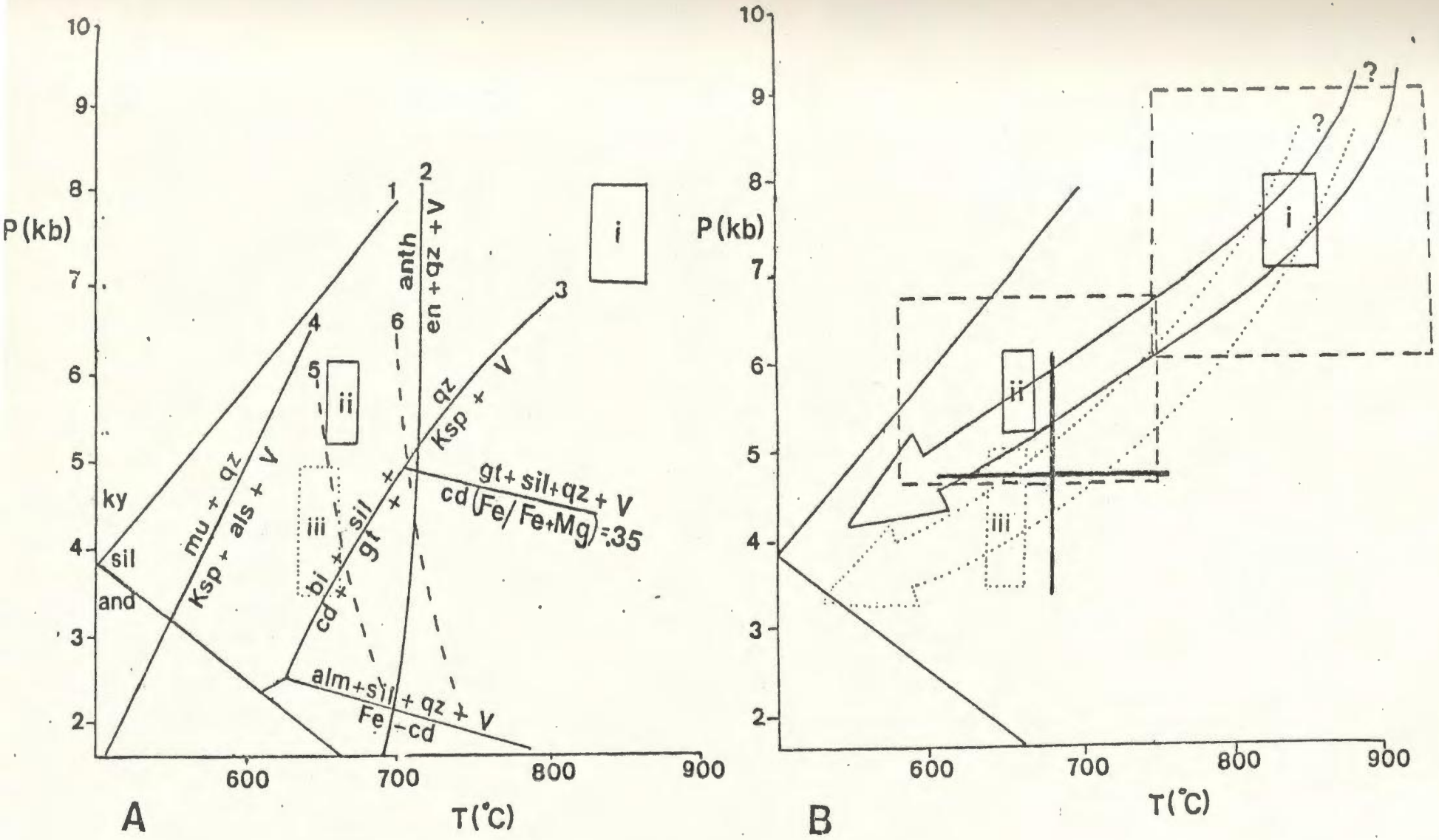
P(kb)
T(°C)
A
B
ky
sil
and
mu + qz
Ksp + als + V
bi + sil +
cd + gt + sil +
alm+sil + qz + V
Fe-cd
anth
en + qz + V
qz
Ksp + V
gt+ sil+qz + V
cd (Fe/ Fe+Mg) =.35
i
ii
iii
1
2
3
4
5
6
?

Figure 4-10.

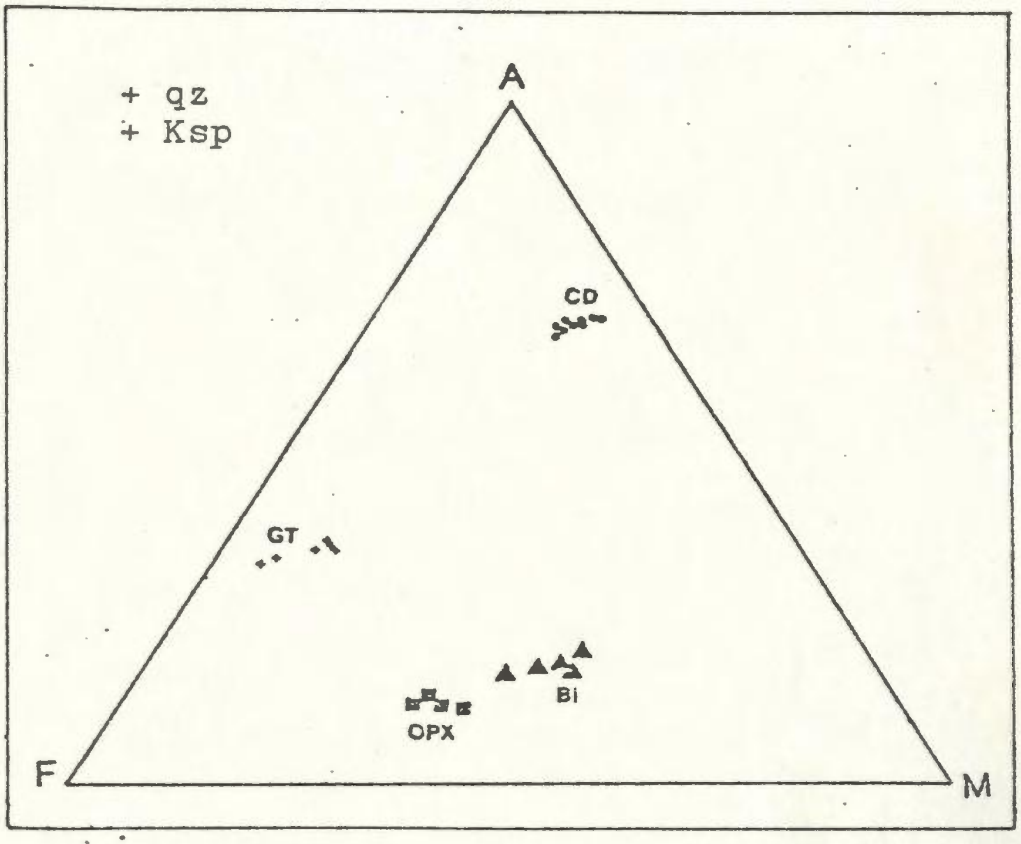

Figure 4-11. AFM diagram depicting the compositions of coexisting garnet, biotite, hypersthene, and cordierite in pelitic metatexite (unit 1C), projected through K feldspar.

Textures and mineral assemblages present in pelitic metatexite (unit 1C) allow utilization of several reaction curves to constrain prograde and retrograde conditions in PT space. Compositions of the various phases in this unit are depicted on an AFM diagram in Figure 4-11.

Application of geothermobarometers to variably retrograded high- to medium-grade metamorphic rocks presents a particular challenge to the petrologist. Although retrograde textures such as corona structures may commonly be distinguished from prograde textures, neither prograde nor retrograde coexisting phases necessarily preserve equilibrium compositions characteristic of their initial crystallization. In samples containing a plethora of textural relations between given mineral pairs, mineral species from different domains in individual thin sections should be analysed in order to determine whether particular textural occurrences of the assemblage consistently have a restricted range of composition. The degree to which equilibrium is approached between such assemblages may vary within an individual thin section, and in some instances, both relatively high- and low-grade texturally and compositionally distinct mineral pairs may coexist in different domains in the same hand sample (e.g. Indares and Martignole, 1984). Where this is not the case, the temptation to assign diverse textural varieties of an assemblage to a particular metamorphic event simply because they are compositionally similar should be avoided. This holds true particularly in the case of the passive, pre-Grenvillian retrogression of the WBIGC, where higher-grade assemblages have been overprinted by lower-grade assemblages without the development of new, mesoscopic mineral fabrics.

4.2.4Bi Two-Pyroxene Geothermometry

Three calibrations of the two-pyroxene geothermometer have been employed. Wood and Banno (1973) and Wells (1977) presented a calibration based on experimental solvus data for the reaction:

$$(Mg_2Si_2O_6)_{cpx} = (Mg_2Si_2O_6)_{opx}$$

Both calibrations assume an ideal two-site solution model, in which a random distribution of Fe2+ and Mg between M2 and M1 is assumed following the allocation of Ca, Na, Mn and Alvi, Cr, Ti, Fe3+, respectively, to these sites. Wood and Banno (1973, Fig. 3) assume a linear relationship between the distribution coefficient of the above reaction and 1/T, an oversimplification which apparently has led both calibrations to overestimate metamorphic temperatures by some 50 to 60C (Raith et al., 1983; Hormann et al., 1980; Evans and Trommsdorf, 1978). or more (Stephenson, 1984).

Powell (1978) presented a polybaric calibration based on Ca-Mg exchange for the reaction:

$$(CaMgSi_2O_6)_{cpx} + (Mg_2Si_2O_6)_{opx} = (CaMgSi_2O_6)_{opx} + (Mg_2Si_2O_6)_{cpx}$$

Compositional parameters and temperature estimates from ten two-pyroxene bearing assemblages are presented in Table 4-4. A pressure of 7.5Kbar (determined using the pressure-dependence of alumina solubility in orthopyroxene coexisting with garnet, see below), has been assumed for the polybaric Powell calibration. The average temperatures determined from the ten samples are:

	RIM (n=7)	CORE (n=11)
Wood + Banno (1973):	826°C(47)*	829 (48)
Wells (1977):	843 (73)	856 (65)
Powell (1978):	769 (59)	844 (32)

( )* = one standard deviation

Table 4-4. Compositional parameters and temperature estimates of the Granulite Complex using the two-pyroxene geothermometer.

$$Kd_1 = (a_{En})_{cpx}/(a_{En})_{opx}; \qquad Kd_2 = ((X^{M2}_{Ca})/(X^{M2}_{Mg}))_{opx} \cdot ((X^{M2}_{Mg})/(X^{M2}_{Ca}))_{cpx}$$

Wood and Banno (1973):

$$T = (-10202)/(\ln Kd_1 - 7.65X^{opx}_{Fe} + 3.88(X^{opx}_{Fe})^2 - 4.6) \quad \pm 70^{o}K$$

Wells (1977):

$$T = 7341/(3.355 + 2.44X^{opx}_{Fe} - \ln Kd_1) \quad \pm 70^{o}K$$

Powell (1978):

$$T = (1600+80P)+(X^{M2}_{Ca}-X^{M2}_{Mg})_{cpx}(6670-88P-1900(X^{M2}_{Fe}))_{opx}/-\ln Kd_2 \quad \pm 75^{o}K$$

note: P for Powell's polybaric calibration was set at 7.5kb in this example.

Table 4-4.

	orthopyroxene						clinopyroxene						A*	B*	C*
	X_{Fe}	M2 X_{Fe}	M2 X_{Ca}	M2 X_{Mg}	M1 X_{Mg}	a_{En}	M2 X_{Ca}	M2 X_{Mg}	M1 X_{Mg}	a_{En}	$-\ln Kd_1$	$-\ln Kd_2$	T°C	T°C	T°C
V581-1	.378	.357	.023	.589	.621	.366	.873	.058	.723	.042	2.165	5.954	847	866	826
V585r*	.534	.509	.022	.444	.463	.205	.897	.042	.645	.027	2.027	6.066	789	825	800
c*	.531	.505	.024	.446	.455	.203	.860	.063	.608	.038	1.675	5.536	831	887	851
V526-3Ar	.464	.441	.021	.509	.531	.270	.894	.051	.698	.035	2.043	6.052	817	851	811
c	.463	.437	.029	.507	.529	.268	.888	.054	.693	.037	2.043	5.661	825	862	879
V586	.482	.456	.021	.490	.513	.251	.872	.053	.651	.034	1.999	5.590	814	851	874
V687	.542	.493	.033	.417	.457	.190	.872	.047	.592	.028	1.915	5.457	798	840	897
V194-2r	.427	.412	.010	.552	.571	.315	.867	.077	.727	.056	1.726	6.432	875	926	711
c	.416	.398	.019	.559	.583	.326	.847	.091	.713	.065	1.612	5.612	896	954	827
V526-3Br	.370	.353	.022	.600	.622	.373	.887	.056	.763	.043	2.160	6.068	853	871	821
c	.373	.355	.021	.597	.626	.374	.880	.069	.761	.052	1.973	5.893	875	904	834
V580-7r	.304	.293	.015	.671	.684	.459	.959	.017	.800	.014	3.490	7.833	741	694	664
c	.305	.291	.026	.664	.680	.451	.950	.025	.807	.020	3.116	6.878	780	744	781
V580-8r	.374	.357	.018	.599	.623	.373	.897	.059	.749	.044	2.137	6.226	853	873	798
c	.381	.365	.019	.592	.614	.363	.880	.074	.712	.053	1.924	5.915	876	909	823
V580-8r	.364	.350	.016	.611	.633	.387	.901	.060	.723	.043	2.197	6.352	852	867	781
c	.362	.345	.025	.609	.634	.386	.896	.058	.729	.042	2.218	5.930	851	864	855
V711-2	.526	.479	.040	.431	.473	.204	.916	.023	.622	.015	2.610	6.062	731	740	841

r*, c* = rim, core compositions

A* = Wood and Banno (1973); B* = Wells (1977); C* = Powell (1978)

The replicate analyses from sample V580-8 (Table 4-4) are within-error of the calibrations, and the average temperatures presented above show reasonably good consistency between samples and between calibrations. Excluding metabasite sample V580-7, which has a higher Kd than the other samples (Table 4-4), from the averaging process increases the above temperatures by $\sim 5^{\circ}C$.

In each case, pyroxene core compositions yield temperature estimates exceeding those derived from rim compositions, and are considered to record peak metamorphic conditions. The Powell calibration yields average temperature estimates similar to those obtained by the Wood and Banno, and Wells calibrations, and all three show a reasonable range of values, expressed at the one standard deviation level. It is concluded that peak metamorphic temperatures in the WBIGC were in the order of 830 to 860 $\pm$ 75°C. There is no direct, independent criterion to evaluate possible overestimation of temperatures by the two-pyroxene geothermometer in the present example. A minimum metamorphic temperature of 710 $\pm$ 10°C, which corresponds to the temperature range under which cordierite is stable under the $\sim$anhydrous conditions (Lee and Holdaway, 1977) prevalent during the granulite-facies event, is, however, suggested by the occurrence of cordierite uniquely as a retrograde phase in the metapelites (unit 1C). In keeping with other workers' observations, the lower temperature of the above range (i.e. 830°C), and a temperature 50°C less than this (i.e. 780°C) will be assumed in calculations involving polythermal geobarometers. It is considered that these two temperatures represent the likely range of metamorphic temperatures of granulite-facies metamorphism in the study area.

4.2.4Bii Garnet-Orthopyroxene Geothermobarometry

Attempts to estimate pressures associated with the granulite-facies event have focused on garnet + orthopyroxene (+ plagioclase + quartz) bearing assemblages. Moderately pressure-sensitive reactions include:

$$CaAl_2Si_2O_8 + Mg_2Si_2O_6 = 1/3Ca_3Al_2Si_3O_{12} + 2/3Mg_3Al_2Si_3O_{12} + SiO_2$$

anorthite + enstatite = grossularite + pyrope + quartz

and,

$$Mg_2Si_2O_6 + MgAl_2SiO_6 = Mg_3Al_2Si_3O_{12}$$

orthopyroxene sol'n = garnet

The first reaction has been calibrated by Newton and Perkins (1982) using measured thermodynamic quantities. In this study, the activities of anorthite in plagioclase and of pyrope and grossular in garnet have been determined using the calorimetric expressions of Perkins and Newton (1981) and Newton and Perkins (1982), respectively. Garnet compositions have been recalculated to 100% excluding spessartine; in all cases, the garnets have $Mn<(Mg/3)$, a necessary requirement since the mixing properties of spessartine are poorly known (Newton and Perkins, 1982). This recalculation procedure slightly increases the activities of pyrope, almandine and grossular, which results in a slight underestimation of P using this calibration. The activity of enstatite in pyroxene has been estimated using the ideal two-site model of Wood and Banno (1973) described above.

Compositional parameters for five garnet + orthopyroxene-bearing assemblages, together with pressures determined by Newton and Perkins' calibration are presented in Table 4-5. Assuming a metamorphic temperature of

Table 4-5. Compositional parameters and pressure estimates of the Granulite Complex using the garnet-orthopyroxene-plagioclase geobarometer.

	pl X_{An}	pl a_{An}	gt X_{Mg}	gt X_{Fe}	gt X_{Ca}	gt a_{gr}	gt a_{pyr}	orthopyroxene M1 X_{Mg}	orthopyroxene M2 X_{Mg}	orthopyroxene a_{En}	-lnKd	P_{bars}
V207	.333	.423	.275	.693	.032	.039	.280	.502	.458	.230	3.460	4988
V210-1r rim	.364	.464	.277	.689	.034	.041	.282	.553	.498	.275	3.667	4188
V210-1r core			.281	.685	.034	.042	.286	.518	.470	.243	3.491	4868
V210-1r r	.364	.464	.276	.691	.033	.040	.281	.576	.534	.307	3.809	3639
V210-1r c			.263	.704	.033	.040	.268	.518	.470	.243	3.670	4176
@V580-12gt1r r	.348	.443	.335	.637	.028	.036	.340	.508	.468	.237	3.228	5885
@V580-12gt1r c			.301	.666	.033	.041	.306				3.308	5575
@V580-12gt2r r	.348	.443	.207	.757	.036	.042	.211	.508	.468	.237	4.028	2793
@V580-12gt2r c			.223	.750	.027	.032	.226				4.162	2275
V221r r	.304	.382	.146	.809	.045	.050	.150	.463	.454	.210	4.267	1869
V221r c			.175	.782	.043	.049	.180	.439	.430	.189	3.817	3608
V579-1r r	.302	.379	.160	.789	.051	.057	.165	.458	.454	.208	3.928	3179
V579-1r c			.206	.745	.049	.057	.212	.421	.407	.171	3.231	5873

a^{pl}_{An} determined by the method of Perkins and Newton (1981)

a^{gt}_{pyr}, a^{gt}_{gr} determined by the method of Newton and Perkins (1982)

a^{opx}_{En} determined by the method of Wood and Banno (1973)

$$Kd = \frac{(a_{gr} \cdot a^2_{pyr})^{gt}}{(a^{pl}_{An} \cdot a^{opx}_{En})}$$

$P = 3944 + 13.070T + 3.5038T\ln Kd \pm 1500bars$
(Newton and Perkins, 1982, equation 12)

@ gt1 = garnet resorbed by cordierite; gt2 = garnet mantled by biotite

T in this example has been set at 830°C

830°C, average pressures (in bars) determined for garnet and(or) orthopyroxene core and rim compositions are:

	RIM	CORE
Newton and Perkins (1982):	3219 (990)*	4631 (975)

( )* = one standard deviation (n = 4)

At 780°C, the Newton and Perkins calibration yields pressure estimates ~200bars less than the above.

Garnet and orthopyroxene form a texturally stable paragenesis in samples V210-1, V221, and V579-1. In the remaining samples (V207, V580-12), the two minerals coexist, but are not in contact. Excluded from the averaging process are the pressure estimates determined for samples V207 and V580-12. In the latter, garnet is replaced by cordierite (V580-12gt1) and is associated with biotite (V580-12gt2). These analyses are presented for comparative purposes only.

The second reaction (see above), based on the pressure-sensive nature of the MgTs content of orthopyroxene coexisting with garnet, has recently been experimentally calibrated by Harley and Green (1982) and by Harley (1984b). These calibrations update earlier work by Wood and Banno (1973) and Wood (1974), whose garnet-orthopyroxene geobarometer was noted by many workers to yield variable pressure estimates, largely as a result of the difficulty in determining the Alvi content of orthopyroxene due to inconsistent SiO2 analysis (e.g. Raith et al., 1983). It should be emphasized that the orthopyroxene coexisting with garnet in the present samples contains up to 6 wt.% Al2O3. The applicability of this geobarometer is therefore not compromised by analytical problems associated with low alumina concentrations in this mineral.

Harley (1984c) recently reviewed the applicability of different calibrations of this geobarometer to various natural rock suites. He found that his more recent (1984b) calibration provided consistent and reliable pressure estimates for very high pressure garnet-peridote and eclogitic rocks, but underestimated pressures of granulites by 0 to 5Kbar compared with Harley and Green's (1982) semi-empirical calibration and with independent data for different suites available in the literature. Accordingly, Harley and Green's calibration, which is based on experiments in FMAS and CFMAS at 800-1200C and 5-20Kbar, has been employed in this study.

Compositional parameters for the five orthopyroxene + garnet-bearing samples and pressure estimates determined using Harley and Green's calibration are presented in Table 4-6. In these calculations, the Al content in the orthopyroxene M1 site has been estimated by averaging Aliv and Alvi (see Wood, 1974; Gasparik, 1984).

These pressure estimates are tightly clustered at 7 to 8Kbar (one standard deviation = 407 bars, n = 13). consistent with the ~8Kbar pressures characteristic of many other granulite-facies terranes (Newton and Perkins, 1982), and may represent a more reasonable result than that provided by Newton and Perkin's (1982) geobarometer based on the assemblage garnet-orthopyroxene-plagioclase-quartz. The divergence between these pressure estimates may reflect: (1) the relative immobility of Al during retrogression compared with Mg-Fe and Ca; or (2) the temperature-sensitive nature of alumina partitioning between garnet and orthopyroxene.

Table 4-6. Compositional parameters and pressure estimates of the Granulite Complex determined from the solubility of alumina in orthopyroxene coexisting with garnet.

	gt X_{Fe}	gt X_{Ca}	opx $X_{Al,M1}$	opx X_{Fe}	$-\Delta Vr$	Kd	P (bars)
V207	.693	.032	.139	.492	204.7	.132	7118
V210-1r*	.689	.034	.129	.492	203.4	.125	6986
c*	.685	.034	.147	.436	205.7	.139	6986
V210-1r	.691	.033	.109	.415	200.7	.125	7029
c	.704	.033	.136	.470	204.3	.130	7059
V580-12r	.637	.028	.137	.471	204.4	.129	7092
c	.666	.033	.137	.471	204.4	.131	7092
V580-12r	.757	.036	.137	.471	204.4	.132	7065
c	.750	.027	.137	.471	204.4	.128	7028
V221r	.809	.045	.027	.529	188.0	.026	7978
c	.782	.043	.049	.553	191.6	.053	7923
V579-1r	.789	.051	.044	.532	190.8	.049	7824
c	.745	.049	.086	.570	197.3	.091	7840

$$Kd = X^{opx}_{Al,M1}(1-X^{opx}_{Al,M1})/(1-X^{gt}_{Ca})^3 \; ; \quad \Delta Vr = -\left[183.3 + 178.98(X^{opx}_{Al,M1}(1-X^{opx}_{Al,M1}))\right] \text{ cal/kb}$$

$$P = \frac{1}{\Delta Vr}(R\ln Kd - 2.93)T + 5650 + 5157(1-X^{opx}_{Al,M1})(1-2X^{opx}_{Al,M1})X^{opx}_{Fe} - 6300(X^{gt}_{Ca}\,X^{gt}_{Fe} + (X^{gt}_{Ca})^2)$$

$\pm$ 1kb (Harley and Green, 1982)

T in this example has been set at 830°C. Pressure estimates are~2kbars lower when T is set at 780°C.

The mobility of Mg and Fe is apparent from core to rim variations in the Fe/Mg ratios in contiguous orthopyroxenes and garnets (see Fe/Mg ratios presented in Table 4-8). The mobility of Ca is apparent from other phases. For example, the mobility of Ca (and alkalis) during retrogression of the WBIGC is suggested by the low (ca. 600°C) temperature estimates provided by two-feldspar geothermometry (see section 4.2.4Bvii) applied to orthopyroxene-bearing jotunitic and metapelitic gneisses.

Given that isopleths for the Al content of orthopyroxene have a slope of about 1°C/40bars for the Harley and Green (1982, p. 700) calibration, overestimation of metamorphic temperatures by 50°C using the two-pyroxene geothermometer would result in the overestimation of metamorphic pressures by ~2Kbar using Harley and Green's geobarometer. Therefore, temperatures in the range of 750 $\pm$ 30°C would yield pressures broadly consistent with those derived from Newton and Perkins' (1981) calibration.

Since there is no indication that the "two-pyroxene" temperatures determined for the WBIGC are overestimates, a pressure of 7.5Kbar will be adopted in polybaric geothermometers used in estimating temperatures associated with granulite-facies metamorphism in the area.

The moderate temperature-dependence of garnet-orthopyroxene equilibria is reflected in two exchange reactions, one based on the distribution of Ca and Mg, the other on the distribution of Fe and Mg between the coexisting garnet and orthopyroxene:

$$\underset{\text{grossular}}{1/3Ca_3Al_2Si_3O_{12}} + \underset{\text{enstatite}}{Mg_2Si_2O_6} = \underset{\text{pyrope}}{1/3Mg_3Al_2Si_3O_{12}} + \underset{\text{diopside}}{CaMgSi_2O_6}$$

and,

1/3Mg3Al2Si3O12 + 1/2Fe2Si2O6 = 1/3Fe3Al2Si3O12 + 1/2Mg2Si2O6
pyrope ferrosilite almandine enstatite

The first reaction has been calibrated for use as a geothermometer by Powell (1978). Application of this geothermometer to the samples listed in Table 4-5 provides a means of evaluating the reliability of the above determined pressure estimates.

Compositional parameters and temperature estimates from the five garnet + orthopyroxene-bearing samples are presented in Table 4-7. The average temperatures so determined are:

	RIM	CORE
Powell (1978):	622 (45)	683 (20)

P is set at 7.5Kbar; T in degrees celsius
( )* = one standard deviation (n = 4; samples V210-1 [includes duplicate], V221, V579-1)

These results may be compared with the temperature estimates derived from the two-pyroxene thermometer reported earlier; in general they are at least 100°C less than the more reasonable temperatures determined using two-pyroxene assemblages.

Similar results to those obtained by the Powell (1978) calibration are provided for the same samples using the experimental geothermometer of Harley (1984a), based on the distribution of Fe and Mg between orthopyroxene and garnet (Table 4-8):

	RIM	CORE
Harley (1984a):	576 (68)	685 (57)

Table 4-7. Compositional parameters and temperature estimates of the Granulite Complex determined from the distribution of Ca and Mg between coexisting garnet and orthopyroxene.

	gt X_{Mg}	gt X_{Ca}	opx $X_{Fe,M2}$	opx $X_{Mg,M2}$	opx $X_{Ca,M2}$	-lnKd	T°C
V207	.274	.032	.486	.458	.003	2.881	630
V210-1r*	.277	.035	.427	.498	.004	2.755	663
c*	.280	.034	.468	.470	.005	2.435	696
V210-1r	.275	.033	.408	.534	.002	3.497	576
c	.263	.033	.459	.470	.005	2.467	697
@V580-12gt1r	.334	.028	.453	.468	.005	2.060	750
c	.300	.033				2.332	713
@V580-12gt2r	.206	.036	.453	.468	.005	2.794	663
c	.222	.027				2.432	710
V221r	.145	.045	.521	.454	.005	3.338	591
c	.175	.043	.542	.430	.007	2.714	657
V579-1r	.159	.051	.522	.454	.009	2.783	657
c	.206	.049	.559	.407	.008	2.493	677

r*, c* = rim, core compositions

@gt1 = garnet resorbed by cordierite; @gt2 = garnet associated with biotite

Orthopyroxene compositional parameters determined assuming ideal two-site model of Wood and Banno (1973)

$Kd = (X^{gt}_{Mg}/X^{gt}_{Ca})(X^{opx}_{Ca,M2}/X^{opx}_{Mg,M2})$; P in this example was set at 7.5kbar

$$T = \frac{7500 + 63P - (2870 + 50P)\,(X^{gt}_{Mg} - X^{gt}_{Ca}) - 1900X^{opx}_{Fe,M2}}{4.58 - \ln Kd - 2.16(X^{gt}_{Mg} - X^{gt}_{Ca})} \pm 75^{\circ}C \quad \text{(Powell, 1978)}$$

P is set at 7.5Kbar; T in degrees celsius
( )* = one standard deviation (n = 4)

The consistent but relatively low temperatures and pressures determined using the Harley (1984a) and Newton and Perkins (1982) calibrations of the garnet-orthopyroxene (-plagioclase-quartz) geothermobarometer may result from indeterminate oxidation ratios in both minerals. Although microprobe analyses of these minerals have been recalculated to electroneutrality, with any charge deficiencies being attributed to the presence of Fe3+ (Percival, 1983), the resulting estimates of ferric iron contents are very small, and the Fe/Mg distribution coefficients between the garnet and orthopyroxene (Table 4-8) are essentially those determined using total Fe.

Alternatively, the PT-estimates derived from Harley (1984a) and Newton and Perkins' (1982) calibrations may accurately reflect conditions of granulite facies metamorphism in the area. This would imply significant overestimation of PT conditions derived by two-pyroxene thermometry and Harley and Green's (1982) calibration of the garnet-orthopyroxene geobarometer. Although, as mentioned above, there is no independent evidence that the two-pyroxene temperatures are overestimates, Stevenson (1984) noted that the Wood and Banno (1973), Wells (1977), and Powell (1978) calibrations are particularly susceptible to overestimating temperatures. Furthermore, indeterminate oxidation ratios in the two-pyroxene assemblages underestimates the temperature estimates by some 10-30C compared with analyses for which the oxidation ratio is known (Bohlen and Essene, 1979).

There is no evidence that pressures of ca. 7.5Kbar determined by Harley

Table 4-8. Compositional parameters and temperature estimates of the Granulite Complex determined from the distribution of Fe and Mg between coexisting garnet and orthopyroxene.

	$(Fe/Mg)_{gt}$	$(Fe/Mg)_{opx}$	X^{gt}_{Ca}	lnKd	T°C
V207	2.529	.967	.032	0.961	749
V210-1r*	2.487	.772	.034	1.170	651
c*	2.446	.882	.034	1.020	720
V210-1r	2.512	.709	.033	1.265	612
c	2.677	.887	.033	1.105	679
V580-12gt1r	1.907	.892	.028	0.760	865
c	2.220		.033	0.912	776
V580-12gt2r	3.674	.892	.036	1.415	557
c	3.378		.027	1.332	584
V221r	5.579	1.123	.045	1.603	500
c	4.468	1.235	.043	1.286	606
V579-1r	4.962	1.139	.051	1.472	542
c	3.616	1.328	.049	1.002	734

r*, c* = rim, core compositions.

$(Fe/Mg)_{gt}$ and X^{gt}_{Ca} are calculated for ternary (Mg + Fe + Ca) garnets.

$$Kd = (Fe/Mg)_{gt}/(Fe/Mg)_{opx}$$

$$T = \frac{3740 + 1400X^{gt}_{Ca} + 22.86P(kb)}{RlnKd + 1.96} - 273 \text{ (in } ^{o}C) \quad \text{(Harley, 1984)}$$

P in this example was set at 7.5kbar

and Green's (1982) calibration are too high. It is nonetheless worthwhile to bear in mind the possible validity of the relatively low PT estimates (ca. 700°C, 4.6Kbar) derived by Harley (1984a) and Newton and Perkins (1982) calibrations. If granulite facies metamorphism in the Smokey area did occur under these conditions, then subsequent retrogression of the WBIGC principally involved hydration rather than a profound decrease in PT. This possibility becomes apparent from the determination of retrograde PT conditions in the area.

Pervasive retrogression of the WBIGC has led to the development of a variety of mineral assemblages useful in estimating PT-conditions subsequent to the granulite-facies event. Since pre-Grenvillian retrogression for the most part appears to pseudomorph granulite-facies textures (e.g. Owen and Rivers, 1983, Fig. 19.7), retrogressed assemblages do not define a distinct preferred dimensional orientation within samples. Reactions (and the relative age) of contrasting or coexisting mineral assemblages must therefore be inferred from symplectic and (or) coronitic textures. Where these are absent (e.g. as in two-feldspar assemblages), geothermometric results similar to those for assemblages characterized by obvious retrogressive textures are assumed to record the effects of the same thermal event.

Estimation of the PT conditions effective during pre-Grenvillian retrogression of the WBIGC focusses on garnet-biotite, garnet-cordierite, and two-feldspar mineral pairs.

4.2.4Biii Garnet-Biotite Geothermometry

As indicated in section 4.1.1B, several textural varieties of garnet-biotite pairs and a range of compositions of both minerals may be present within

individual thin sections. The analyses presented in Table 4-1 lead to a wide range of temperature estimates for sample CG-79-347. Employing Thompson's (1976) calibration of the garnet-biotite thermometer, temperature estimates in this sample range from 522-735°C. This may be attributed to the heterogeneous domainal (mm) scale reequilibration of garnet-biotite pairs in response to cooling of the WBIGC following peak granulite-facies metamorphic conditions.

Compositional parameters and temperature estimates of garnets and biotites from eight samples of pelitic metatexite, three samples of jotunitic-charnockitic gneiss (including the Bluff Head occurrence, V471-2), and the uncorrelated migmatitic granodioritic gneiss (V201) from the White Bear Islands are presented in Table 4-9. With three exceptions (V211-1, V580-16, V201), the analyses presented in Table 4-9 are from the most common garnet-biotite textural type noted in these samples, specifically, where subidiomorphic brown biotite clusters around, and in places is partly enclosed within, subiodiomorphic garnet porphyroblasts. Average temperatures recorded by garnet core and rim compositions for this textural type are as follows:

	RIM	CORE
Goldman+Albee:	534 (63)	562 (65)
Thompson:	618 (47)	653 (67)
Ferry+Spear:	654 (64)	704 (95)
Indares + Martignole:	602 (52)	643 (67)

P is set at 7.5Kbar; T in degrees celsius
( ) = one standard deviation; n = 9

The wide range in temperature estimates between (Table 4-9) and within samples (see Table 4-1) indicates variable reequilibration of coexisting garnet and biotite during cooling of the WBIGC.

Table 4-9. Compositional parameters and temperature estimates of the Granulite Complex using the garnet-biotite geothermometer.

	X^{gt}_{Mg}	X^{gt}_{Mn}	X^{gt}_{Ca}	$\frac{Mn+Ca}{X\ gt}$	X^{bi}_{Mg}	X^{bi}_{Ti}	X^{bi}_{Alvi}	$\frac{Ti+Alvi}{X\ bi}$	Kd_{Mg} gt-bi	G+A'77 T°C	T '76 T°C	---P = 7.5kb-- F+S'78 T°C	I+M T°C
V172r*	.139	.053	.112	.165	.492	.043	.055	.098	.166	497	553	565	582
c*	.174	.041	.053	.094					.217	527	623	662	635
V207r	.387	.020	.031	.051	.607	.069	.049	.118	.251	586	667	725	623
c	.284	.020	.032	.052					.257	593	674	736	634
V210-1r	.285	.046	.032	.078	.683	.042	.042	.084	.186	451	581	604	574
c	.281	.046	.032	.078					.182	447	576	596	567
V211-2r	.212	.182	.020	.202	.604	.023	.142	.165	.177	406	569	587	628
c	.230	.170	.025	.195					.196	407	595	623	662
V580-1Br	.262	.048	.032	.080	.578	.060	.050	.110	.259	598	677	739	672
c	.295	.045	.032	.077					.306	660	733	825	750
V580-12r	.214	.053	.034	.087	.584	.082	.029	.111	.194	506	593	619	537
c	.228	.049	.026	.075					.211	522	616	647	537
V580-16r	.266	.059	.035	.094	.669	.038	.069	.107	.179	546	677	591	568
c	.317	.045	.032	.077					.229	617	639	685	640
CG-79-347r	.262	.009	.018	.027	.579	.080	.070	.158	.258	580	682	736	591
c	.298	.007	.001	.008					.309	628	737	828	656
V471-2r	.197	.142	.191	.333	.548	.093	.015	.108	.202	625	604	634	694
c	.169	.169	.205	.374					.167	582	555	567	648
V221r	.152	.038	.043	.081	.487	.062	.022	.084	.188	471	584	608	555
c	.183	.032	.042	.074					.235	519	647	695	634
V579-1r	.168	.028	.049	.077	.486	.067	.021	.088	.214	498	619	657	592
c	.216	.029	.048	.077					.292	582	717	780	725
V201r	.123	.026	.031	.057	.458	.078	.118	.196	.167	458	555	567	450
c	.136	.025	.024	.049					.186	480	582	604	477

Note: G + A = Goldman and Albee (1977); T = Thompson (1976); F + S = Ferry and Spear (1978); I + M = Indares and Martignole (in press)

Table 4-9. (continued)

KEY

r* = garnet rim

c* = garnet core

$$X_{Mg}^{gt} = \left(\frac{Mg}{Mg+Fe^{2+}}\right)_{gt}$$

$$X_{Mn}^{gt} = \left(\frac{Mn}{Mg+Fe^{2+}+Ca+Mn}\right)_{gt}$$

$$X_{Ca}^{gt} = \left(\frac{Ca}{Mg+Fe^{2+}+Ca+Mn}\right)_{gt}$$

$$\left(\frac{Mn+Ca}{\Sigma X}\right)_{gt} = \left(\frac{Mn+Ca}{Mg+Fe^{2+}+Ca+Mn}\right)_{gt}$$

$$X_{Mg}^{bi} = \left(\frac{Mg}{Mg+Fe_t}\right)_{bi}$$

$$X_{Ti}^{bi} = \left(\frac{Ti}{Mg+Fe_t+Mn+Ti+Alvi}\right)_{bi}$$

$$X_{Alvi}^{bi} = \left(\frac{Alvi}{Mg+Fe_t+Mn+Ti+Alvi}\right)_{bi}$$

$$\left(\frac{Ti+Alvi}{\Sigma X}\right)_{bi} = \left(\frac{Ti+Alvi}{Mg+Fe_t+Mn+Ti+Alvi}\right)_{bi}$$

$$Kd_{Mg}^{gt-bi} = \frac{X_{Mg}^{gt}(1-X_{Mg}^{bi})}{X_{Mg}^{bi}(1-X_{Mg}^{gt})} = \frac{(Mg/Fe)_{gt}}{(Mg/Fe)_{bi}}$$

Goldman and Albee (1977):

$$\ln Kd = -0.177(1000\ln\alpha_M^Q) - 1.22X_{Mn}^{gt} - 2.14X_{Ca}^{gt} + 1.40(1-X_{Mg}^{bi}) + 0.942X_{Ti}^{bi} - 1.59X_{Alvi}^{bi} - 0.492,$$

where $1000\ln\alpha_M^Q = (5570000)/T_K^2$

Thompson (1976):

$$\ln Kd = \frac{-2825}{T_K} + 1.623$$

Ferry and Spear (1978):

$$-\ln Kd = (12454 - 4.662T_K + 0.057P(\text{bars}))/3RT_K,$$

and $\left(\frac{Ca+Mn}{\Sigma X}\right)_{gt} \leq 0.20$; $\left(\frac{Ti+Alvi}{\Sigma X}\right)_{bi} \leq 0.15$

Indares and Martignole (in press)

$$-\ln Kd = \left[\frac{12454+0.057P(\text{bars})+3(-1590X_{Al}^{bi}-7451X_{Ti}^{bi}) - 3(-3000X_{Ca}^{gt}+X_{Mn}^{gt})}{T_K(5.9616)}\right] - 4.662$$

The three samples not included in the above averaging process differ in the textural mode of occurrence of coexisting garnet and biotite. Sample V211-1 contains xenomorphic garnet porphyroblasts partly replaced by symplectic intergrowths of green biotite + quartz + sillimanite. In sample V201, garnet, which is partly replaced by green biotite, is restricted to the leucosome; the biotite analysis recorded in Table 4-9 is of brown subidiomorphic biotite from the paleosome. The biotite from V580-16 described in Table 4-9 is from an idiomorphic flake enclosed in a cordierite-mantled garnet porphyroblast in the leucosome component of pelitic metatexite. The garnet and biotite in samples V211-1 and V201 thus show clear disequilibrium textures. In contrast, the stable grain boundary of the biotite enclosed in garnet in V580-16 is a feature typical of textural equilibrium, and this paragenesis might be expected to record the compositions of both phases developed during peak metamorphic conditions. Surprisingly, temperature estimates for all three samples vary by only $\pm$ 10°C, and are consistent with the average temperature estimates listed above. From the limited data available, this indicates that the compositions of various textural associations of biotite-garnet pairs have pervasively reequilibrated during retrogression of the WBIGC. As in the case of garnets coexisting with orthopyroxene (see above), reequilibration has not been complete; temperature estimates determined using garnet rim compositions are on average some 30-40°C less than those determined from garnet cores.

As noted by several previous workers (e.g. Grew, 1981) Goldman and Albee's experimental calibration, based on oxygen isotopic data from quartz and magnetite coexisting with the garnet-biotite pairs yields temperature estimates

several tens of degrees less than the Thompson, and Ferry and Spear calibrations. This has been attributed to progressive isotopic reequilibration between quartz and magnetite during cooling (Ibid.). The Thompson, Ferry and Spear, and Indares and Martignole calibrations are thus inferred to more closely approximate temperatures of pre-Grenvillian retrogression of the WBIGC. The Ferry and Spear calibration yields garnet core temperature estimates some 40-50°C higher than the Thompson (1976), and Indares and Martignole calibrations, despite the observation that the Ca and Mn content of garnet, and the Ti + Alvi content of biotite are within their prescribed limits. This may be attributed to the fact that the Ferry and Spear calibration is based on synthetic biotite in which all Fe is in the ferrous state. Grew (1981) demonstrated that the Ferry and Spear calibration overestimates metamorphic temperatures by ~50°C when applied to garnet-biotite distribution coefficients calculated using total iron. Grew's results indicate that temperature estimates derived from the Ferry and Spear calibration are consistent with Thompson's calibration when the oxidation ratio of both minerals is known. From this, it may be inferred that the higher temperature estimates yielded by Ferry and Spear's calibration in the present example result from the use of total iron rather than Fe2+ in the determination of the Kd's listed in Table 4-9.

Indares and Martignole (in press) have suggested that Thompson's calibration is particularly applicable to high-grade rocks. The Indares and Martignole calibration provides average temperature estimates similar to those determined from Thompson's calibration, although the calibrations are seen to give widely divergent results for certain samples (Table 4-9).

Variations in temperature estimates obtained from calibrated

geothermometers may be in large part caused by minor elements which contribute to significant departures from ideal solid solution between pure end member compositions. Such variations have been recorded in garnet-biotite geothermometry applied elsewhere in the Grenville Province (e.g. Bohlen and Essene, 1980; Indares and Martignole, in press) and, as suspected by many workers, may result from the presence of Ca in garnet and Ti and Al in biotite. Two recent calibrations of the garnet-biotite geothermometer which account for the influence of these elements on the distribution of Fe and Mg between the two minerals have been presented by Indares and Martignole (in press). The calibrations differ in the manner in which the solubility of Ca in garnet is accounted for. One calibration is based on Newton and Haselton's (1981) thermodynamic model, which ignored (due to a paucity of data at the time of writing) the influence of Mn in garnet equilibria. The other calibration, adopted here, utilizes recent thermodynamic and empirical data presented by Ganguly and Saxena (1984) for ascertaining the mixing properties of both Ca and Mn in garnet.

The wide range of temperatures yielded by each thermometer (Table 4-9) likely reflects significant and varying departures from equilibrium for garnet-biotite pairs, and a better temperature estimate of amphibolite-facies retrogression of the WBIGC may be more uniformly approximated with a different mineral assemblage.

Granodioritic orthogneiss (unit 5A) in the vicinity of Bluff Head is locally garnetiferous. The garnets are almandines with significant Ca + Mn components, and their compositions are more closely analagous to garnets associated with Grenvillian LS-fabrics. Details of the occurrence and compositions of these rocks

are presented in section 4.3, but it is worthwhile to note here that temperature estimates for these samples are in the order of 100C less than those determined for garnet-biotite pairs from the WBIGC, and are consistent with temperatures determined for Grenvillian garnet-biotite pairs. Given this, and the pervasive development of GD1 structures (see Chapter 2) in the vicinity of Bluff Head, it seems reasonable to conclude that garnetiferous assemblages in the northern Groswater Bay Terrane developed or fully reequilibrated during the Grenvillian orogeny.

4.2.4Biv Garnet-Cordierite Geobarometry

Conditions of retrogression of the WBIGC have also been estimated from coexisting cordierite-garnet in pelitic metatexite (unit 1C). The cordierite in this unit is clearly retrograde in origin, and typically partly mantles or encloses garnet ($\pm$ biotite $\pm$ sillimanite). For a given P(H2O), the Mg content of cordierite coexisting with garnet is a function of pressure. Cordierite compositions also show, however, a slight temperature dependence. Since a unique temperature associated with retrogression of the WBIGC could not be determined via garnet-biotite geothermometry, pressures have been calculated for a range of temperatures. Table 4-10 presents compositional data and pressure estimates utilizing the calibrations of Thompson (1976), Holdaway and Lee (1977) and Wells (1979) with temperatures for garnet and cordierite cores set at 750°C and 650°C, and 600°C for rim compositions. These temperatures have been chosen since they span the range of metamorphic temperatures determined from core and rim compositions of coexisting garnet-biotite and garnet-orthopyroxene (see above), in the sequence of decreasing (core to rim) temperatures expected for a cooling metamorphic

Table 4-10. Compositional parameters and pressure estimates of pelitic metatexite (unit 1C) using the garnet-cordierite geobarometer.

	core compositions		*A		**B		***C		rim compositions		*A	**B	***C
	Kd_1	Kd_2	P_{T1}	P_{T2}	P_{T1}	P_{T2}	P_{T1}	P_{T2}	Kd_1	Kd_2	P_{T3}	P_{T3}	P_{T3}
1.	2.887	.374	6511	6574	7590	7594	7579	7267	--	--	--	--	--
2.	3.008	.369	6638	6689	7769	7755	7536	7227	5.289	.330	8224	9858	6770
3.	3.543	.368	7147	7148	8480	8397	7528	7220	3.708	.327	7273	8529	6745
4.	3.281	.394	6908	6932	8145	8095	7745	7417	3.585	.421	7182	8403	7433
5.	2.776	.420	6377	6454	7404	7426	7949	7601	--	--	--	--	--
6.	3.076	.407	6700	6745	7855	7833	7810	7510	3.527	.422	7153	8362	7439
7.	--	--	--	--	--	--	--	--	3.980	.466	7462	8794	7709
8.	3.063	.414	6693	6738	7845	7824	7892	7548	4.419	.407	7743	9186	7330

analysis numbers as in Table 4-13

P_{T1} = 750°C; P_{T2} = 650°C; P_{T3} = 600°C

$Kd_1 = (X_{Fe}^{gt})/(X_{Fe}^{cd})$; $Kd_2 = (X_{Mg}^{gt})/(X_{Mg}^{cd})$

*A = Thompson (1976): $P = (27808-T(15.103-6R\ln Kd_1))/(3.886)$ ± 500bars

**B = Holdaway and Lee (1977): $P = (7631+T(4.287\ln Kd_1-4.59))$ ± 500bars

***C = Wells (1979): $P = (1+(16733+23.67T+6RT\ln Kd_2)/(3.8256)$ ± 400bars

terrane. For core compositions, pressures of ca. 7.5-8.5Kbar (for T=750°C) were derived from the Holdaway and Lee (1977) calibration, while pressures of ca. 6.5-7.1Kbar were determined using Thompson's (1976) field-based calibration at the same temperature. Pressure differences determined using garnet and cordierite core and rim compositions were within indicated calibration errors (<500bars), and the differences in pressure estimates for the assumed temperatures is less than 100bars. These pressures assume that X(H20) = Ptotal, an unlikely assumption considering the ubiquitous preservation of orthopyroxene in the cordierite bearing metapelites and other members of the WBIGC, although as previously noted, cordierite analysis totals average 96.9%, suggesting a significant fluid content incorporated in the cordierite crystal structure. Retrogression of granulite-facies assemblages invariably involved the development of hydrous phases (phyllosilicates, amphiboles), consequently an intermediate value of X(H20) may be assumed for this period of metamorphism. Table 4-11 presents lithostatic pressure estimates (Plith) corrected for different fugacities of water (XH20) at specific values of calculated pressures (Pi) assuming P(fluid) = P(H20) = Ptotal (Treloar, 1981). No independant means is presently available for directly ascertaining the partial pressure of water during retrogression of the WBIGC. This hampers the usefulness of the garnet-cordierite geobarometer in this example. An intermediate (P(H2O) = 0.4Ptotal) has been assumed for purposes of illustration in this study. This value is consistent with the ubiquitous preservation of anhydrous phases despite the widespread development of hydrous phases (biotite, cordierite, amphibole) during retrogression of the WBIGC, and should be considered the upper limit of P(H2O) for the following reasons:

Table 4-11. Lithostatic pressure corrections for variable partial water pressures.

	P_i (bars)							
X_{H_2O}	5000	5500	6000	6500	7000	7500	8000	8500
0.8	4595	5054	5514	5973	6433	6892	7352	7811
0.6	4250	4675	5100	5525	5951	6376	6801	7226
0.4	3954	4349	4745	5140	5536	5931	6327	6722
0.2	3696	4066	4436	4805	5175	5545	5914	6284
0.0	3470	3817	4164	4511	4858	5205	5552	5900

$$P_f = \frac{2.7805P_i}{(4.0061-1.2256X_{H_2O})} \qquad \text{(Treloar, 1981)}$$

P_i = pressure calculated assuming $P_{H_2O} = P_{total}$

P_f = corrected pressure for $P_{H_2O} \leq P_{total}$

(1) there is no evidence for partial melting during retrogression of the WBIGC. At P(H2O) = 0.4Ptotal, the granite minimum melt curve coincides with the Mg/(Mg+Fe) typical of cordierite in pelitic metatexite close to the boundary of the reaction bi + sil + qz = cd + gt + Ksp + V (see Fig. 4-10).

(2) optical evidence suggests variable but significant CO2 in the cordierite channel fluid, which would reduce aH2O.

The assumed partial pressure of water coincides with an estimated pressure of 5.1-5.5Kbar for the pressure range determined by the Thompson calibration, and 5.9-6.7 for the pressure range determined by the Holdaway and Lee (1977) calibration. Cordierite Mg/(Mg+Fe) isopleths presented by Martignole and Sisi (1981) indicate pressures of 5-6Kbar. A pressure of 5.5 $\pm$ 1.5Kbar has been assumed in calculations exploiting the temperature-sensitive nature of garnet-cordierite equilibria. Before this is attempted, however, it is necessary to ascertain the reliability of this pressure estimate.

4.2.4Bv Garnet-Plagioclase Geobarometry

The assemblage garnet + plagioclase (+ sillimanite + quartz) occurring in pelitic metatexite (unit 1C) serves as another potential indicator of pressure conditions prevailing during metamorphism of the WBIGC. The results of application of this geobarometer to the present samples should be interpreted with caution, since it is unclear whether sillimanite forms an equilibrium assemblage with garnet + plagioclase + quartz in the metapelites. Much of the sillimanite (and fibrolite) in these samples appears to be retrograde in origin (section 4.2.1E). In this regard, the pressure estimates derived from this geobarometer may correspond to conditions of retrogression of the WBIGC.

Table 4-12. Compositional parameters and pressure estimates of pelitic metatexite (unit 1C) using the garnet-plagioclase-Al_2SiO_5-quartz geobarometer.

	plagioclase		garnet					T=650°C	T=750°C
	X_{An}	a_{An}	X_{alm}	X_{pyr}	X_{gr}	a_{gr}	-logKd	P(bars)	P(bars)
V207	.333	.460	.695	.273	.032	.040	3.182	3575	4910
V210-1	.364	.502	.695	.272	.033	.042	3.232	3496	4822
V580-1B	.348	.481	.670	.295	.035	.045	3.087	4000	5380
V580-12	.348	.481	.722	.247	.031	.038	3.307	3084	4366
V580-16	.327	.451	.652	.310	.038	.049	2.892	4655	6106
CG-79-347	.225	.289	*.666	.309	.025	.032	2.867	5006	6495
CG-79-347	.225	.289	**.587	.394	.019	.026	3.138	4408	5834

a_{An}^{pl} determined by the method of Perkins and Newton (1981)

a_{gr}^{gt} determined by the method of Newton and Perkins (1982)

$$-\log Kd = -\frac{2551.4}{T} + 7.1711 - \frac{0.2842(P-1)}{T} + 3\log\gamma_{gr}^{gt} - 3\log\gamma_{An}^{pl} \quad \text{(Ghent, 1977)}$$

where $Kd = \dfrac{(a_{gr}^{gt})^3}{(a_{An}^{pl})^3}$;

* = garnet replaced by biotite + sillimanite

** = garnet replaced by cordierite

Ghent et al. (1979):

	T=650°C P(bars)	T=750°C P(bars)
V207	3401	4719
V210-1	3547	4515
V580-1B	3908	4879
V580-12	3485	4453
V580-16	4413	5230
CG-79-347	4256	5230
CG-79-347	3299	4265

The exchange of Ca between garnet and plagioclase coexisting with quartz and an aluminosilicate phase is a low variance assemblage that has been shown to be sensitive to pressure (Ghent, 1976, 1977, 1979). As noted above, several generations and textural occurrences of sillimanite occur in pelitic metatexite. The albite content of feldspars has been reequilibrated at temperatures broadly similar to those determined by garnet-biotite thermometry (see sections 4.2.4Biii; 4.2.4Bvii). Furthermore, sillimanite is a ubiquitous product of the partial retrogression of both garnet, occurring in association with biotite $\pm$ quartz, and of cordierite. Only garnets showing such retrograde features have been used in estimating PT conditions of retrogression. Ghent's (1977) calibration of the garnet-plagioclase (-quartz-Al2SiO5) barometer yields pressure estimates averaging 4.0Kbar and 5.4Kbar at 650°C and 750°C, respectively (Table 4-12). Both pressures have one-sigma errors of ~700 bars. Ghent et al.'s (1979) revised calibration of this geobarometer yields pressures averaging 3.7Kbar and 4.8Kbar at 650°C and 750°C, respectively (Table 4-12).

4.2.4Bvi Garnet-Cordierite Geothermometry

The temperature-sensitive nature of garnet-cordierite equilibria has been exploited in order to constrain possible temperatures associated with retrogression of the WBIGC. Compositional data and temperature estimates determined using the Thompson (1976) and Holdaway and Lee (1977) calibrations are presented in Table 4-13. The average temperatures (in degrees celsius) for garnet ($\pm$ cordierite) core and rim compositions are as follows:

	RIM	CORE
Thompson (1976):	602 (65)*	671 (37)
Holdaway and Lee (1977):	593 (56)	654 (32)

Table 4-13. Compositional parameters and temperature estimates of pelitic metatexite (unit 1C) using the garnet-cordierite geothermometer.

#	X_{Mg}^{cd} rim	X_{Mg}^{cd} core	X_{Mg}^{gt} rim	X_{Mg}^{gt} core	Kd garnet rim	Kd garnet core	*Thompson (1976) T°C garnet rim	*Thompson (1976) T°C garnet core	**Holdaway + Lee (1977) T°C garnet rim	**Holdaway + Lee (1977) T°C garnet core
1.	--	.751	---	.281	---	7.71	---	683	---	663
2.	.864	.761	.285	.281	15.95	8.14	494	666	498	648
3.	--	.801	.262	.295	11.34	9.62	572	616	567	606
4.	.817	.789	.344	.311	8.51	8.27	652	661	636	644
5.	--	.754	---	.317	---	6.60	---	737	---	708
6.	.814	.777	.344	.317	8.34	7.51	658	692	642	670
7.	.848	--	.395	.381	8.54	9.06	651	633	635	620
8.	.851	.779	.346	.323	10.80	7.39	585	679	579	675

*Thompson (1976): $T_K = (2725 + 0.0155P)/(\ln Kd + 0.896) \pm 75^\circ$

**Holdaway + Lee (1977): $T_K = (6150 + 0.0303P)/(R\ln Kd + 2.69) \pm 75^\circ$

The pressure in this example has been set at 5500 bars.

$Kd = (Fe^{gt})(Mg^{cd})/(Mg^{gt})(Fe^{cd})$

#	Sample	Description of Cordierite	(~% pinitization)
1.	V210-1	surrounded by qz + pl	(5)
2.	V210-1	partial mantle on gt	(5)
3.	V580-1B	partial mantle on gt	(60)
4.	V580-12	contains relicts of resorbed gt	(50)
5.	V580-16	surrounded by qz	(5)
6.	V580-16	partial mantle on gt	(5)
7.	CG-79-347	contains relicts of resorbed gt	(90)
8.	V210-1	in contact with garnet	(5)

( )* = one standard deviation (rims, n = 6; cores, n = 8)

These temperatures are broadly consistent with the wide range of temperatures determined by garnet-biotite geothermometry, which yields temperatures some 6 to 8°C less when a pressure of 5.5Kbar is adopted rather than 7.5Kbar (Table 4-9).

4.2.4Bvii Two-Feldspar Geothermometry

Metamorphic temperatures have also been estimated using the two-feldspar geothermometer, based on the exchange of Na between coexisting plagioclase and K feldspar. Two-feldspar assemblages have been analysed in four samples of pelitic metatexite, and one sample each of jotunite and granodioritic gneiss (V201) from the White Bear Islands. K feldspars in the WBIGC are variably perthitic. In order to avoid reintegration problems encountered with coarsely perthitic K-feldspars (e.g. Bohlen and Essene, 1982), only samples containing fine (1-5um albitic blebs) bead perthitic orthoclase were selected for two-feldspar thermometry. In each case, between 7 and 17 analyses were performed on perthitic feldspars using a defocussed (10-15um) electron beam on the microprobe. Albite contents of coexisting plagioclase and (perthitic) orthoclase from these samples straddle the 600°C contour on Stormer's (1978) diagram. For comparative purposes, the data are plotted against the albite contents of Grenvillian two-feldspar-bearing assemblages presented in section 4.3.8 (see Fig. 4-26).

Table 4-14. Summary of metamorphic PT-estimates of the Granulite Complex.

Note: The following PT estimates were determined for the core compositions of different mineral assemblages.

	TEMPERATURE (°C)	PRESSURE (kbar)
Two-Pyroxene		
Wells (1977):	856	
Wood + Banno (1974):	829	
Powell (1978):	844 (7.5kb)	
Garnet-Orthopyroxene-Plagioclase-Quartz		
Newton + Perkins (1982):		4.6 (830°C)
		4.4 (780°C)
Al in Garnet-Orthopyroxene		
Harley + Green (1982):		7.5 (830°C)
Garnet-Orthopyroxene		
(Ca-Mg exchange)		
Powell (1978):	683 (7.5kb)	
(Fe-Mg exchange)		
Harley (1984a):	685 (7.5kb)	
Garnet-Biotite		
Goldman + Albee (1977):	562	
Thompson (1976):	653	
Ferry + Spear (1978):	704	
Indares + Martignole (in press):	643	
Garnet-Cordierite		
Thompson (1976):	671	6.4-7.1* (650°C)
Holdaway + Lee (1977):		7.4-8.3* (650°C)
Wells (1979):		7.2-7.6* (650°C)
Garnet-Plagioclase-Al2SiO5-Quartz		
Ghent (1977)		3.1-5.0 (650°C)
		4.4-6.5 (750°C)
Two-Feldspar		
Stormer (1977):	ca. 600	

*assumes P(H2O) = P(total); pressures are reduced by ~2kbar if P(H2O) = 0.4P(total)

4.2.4C. Summary

The PT estimates determined by the various geothermobarometers applied to the WBIGC are summarized in Table 4-14. The different calibrations yield inconsistent estimates of the conditions of granulite-facies metamorphism of the WBIGC. The two-pyroxene geothermometer yields temperatures averaging 830-860°C, while the alumina content of orthopyroxene coexisting with garnet yields a pressure of 7-8 $\pm$ 1.5Kbar. Relatively low PT estimates of ca. 685°C and 4.6Kbar were determined using the garnet-orthopyroxene (-plagioclase-quartz) geothermobarometer. If the higher PT estimates are valid, then subsequent retrogression of the WBICG (at ca. 650°C, 5.5Kbar, see below) resulted from hydration during cooling and uplift, probably after a significant time interval following the granulite-facies event. If the lower PT estimates are valid, then the retrogression involved hydration only, and likely occurred after a relatively short time interval following the granulite-facies event. Actual conditions of the granulite-facies event were probably intermediate between these two extremes.

Estimation of the conditions of pre-Grenvillian retrogression of the WBIGC has focussed on a variety of geothermobarometers. Garnet-biotite, cordierite-garnet, plagioclase-garnet (-plagioclase-quartz), and two-feldspar assemblages yield PT estimates clustering at ca. 650 $\pm$ 50°C and ca. 5.5 $\pm$ 1.5Kbar.

4.3 GRENVILLIAN METAMORPHISM

Metamorphic mineral assemblages delineating south-dipping S- and L-S fabrics in the Smokey area are associated with polyphase deformation of the Michael gabbro, and are attributed here to the Grenvillian orogeny. Although two phases of Grenvillian fabric development have been identified (see Chapter 3), fabrics associated with second generation Grenvillian folds (i.e. GS2) are the more pervasive.

Description of the effects of Grenvillian metamorphism will be made on a regional scale, following the structural subdivision of the Smokey archipelago depicted in Figure 3-1. The boundaries of the subdivision, the Benedict and Cut Throat Island faults, are metamorphic as well as structural breaks, an observation which supports this tripartite subdivision of the Smokey archipelago.

Grenvillian metamorphic mineral assemblages overprint older tectonic fabrics, and in many cases, similar Grenvillian assemblages occur in diverse rock types. Grenvillian mineral assemblages are best represented in the southern portion of the study area (domain G; see Fig. 3-1), where Grenvillian fabrics are extensively developed, and where the rocks are more diverse. In this domain, Grenvillian assemblages in four bulk rock compositional groups will be described. These are : (1) metabasites; (2) granitoids of the BMIS; (3) orthogneisses in the vicinity of Bluff Head and those of the WBIGC; and (4) metapelites of the WBIGC. Compositions of minerals comprising Grenvillian fabrics were determined by the electron microprobe. The analyses are presented in Appendix A.4 (A.4.8 to A.4.10).

Metamorphic mineral assemblages attributed to the Grenvillian orogeny span upper greenschist-lower amphibolite-facies. The transitional nature of the "boundary" between these two metamorphic series warrants some consideration, and requires a definition of terms employed in the present study.

The terms greenschist and amphibolite facies were first defined by Eskola (1920) on the basis of mineralogical changes observed in rocks of mafic composition. Greenschist-facies assemblages in metabasites characteristically contain chlorite + albite + epidote $\pm$ actinolite (s.l.), whereas the lower amphibolite-facies is characterized by hornblende (s.l.) $\pm$ epidote + oligoclase or more calcic plagioclase. Eskola (1939) grouped assemblages transitional between the two series into the epidote-amphibolite facies (Turner's, 1968, "greenschist-amphibolite transition zone"). Laird (1982) described the epidote-amphibolite facies as comprising assemblages containing hornblende (s.l.) + albite $\pm$ oligoclase, and grouped hornblende (s.l.) + oligoclase-bearing assemblages in the amphibolite facies. The presence of epidote is not considered to be critical in Laird's definition, since the occurrence of this mineral is dependent upon bulk rock and fluid (e.g. X(CO2)) composition as well as metamorphic grade (Laird, 1982). Despite the obvious problems presented by definitions based on negative criteria (e.g. the absence of albite in amphibolite-facies assemblages), Laird's terminology is adopted in the present study.

4.3.1 Grenvillian Parageneses North of the Benedict Fault

Fabrics attributed to the Grenvillian orogeny occur only sporadically north of the Benedict Fault (in domain M), and are best represented along east-trending shear zones at Cape Rouge. At Cape Rouge, Makkovik trend fabrics outlined by

mafic enclaves in foliated granitoids of the BMIS are overprinted but not transposed by epidotized, south-dipping shears which impart a non-penetrative fabric to the rocks. In these zones, mafic enclaves and dykes bearing pre-Grenvillian amphibolite-facies assemblages (comprising hornblende + oligoclase ± biotite) are partly to wholly retrograded to greenschist facies. Three such mineral assemblages have been identified:

(1) chl+ep+pl(An0.2) + ct
(2) act+ep+pl(An0-4)±chl±qz
(3) act+ep+pl(An25-34)±bi±qz

In each example, plagioclase has been extensively saussuritized. In assemblage (1), epidote occurs as irregular grains associated with felty masses of pale green chlorite showing anomalous brown birefringence. No pre-Grenvillian minerals are preserved in assemblage (1). The actinolite in assemblages (2) and (3) occurs as ~1mm (sub)idiomorphic megacrysts (Fig. 4-12A), as 1-2mm pods of fibroradial crystals (Fig. 4-12B), and as thin rinds pseudomorphing hornblende. In places, the actinolite demonstrably replaces hornblendic amphibole attributed to the development of Makkovik trend fabrics. Plagioclase (An25-34) present in assemblage (3) likely reflects relict compositions from the pre-Grenvillian, amphibolite-facies assemblage stable with hornblende, and is considered to coexist metastably with the actinolite.

4.3.2 Parageneses along the Benedict Fault

Specimens of mylonitized metabasite from the Benedict Fault contain the assemblages:

(4) bi+ep+pl(An1-4)±act ± chl
or (5) hbl+bi+ep+pl(An3)+qz

Figure 4-12. Photomicrographs showing different textural varieties of actinolite in metabasites north of the Benedict Fault.

4-12A. Idiomorphic porphyroblast of actinolite in metabasite. Bar scale is 0.1mm. Plane polarized light; sample V608-2.

4-12B. Fibroradial actinolite aggregate in metabasite. Bar scale is 0.1mm. Plane polarized light; sample V608-2.

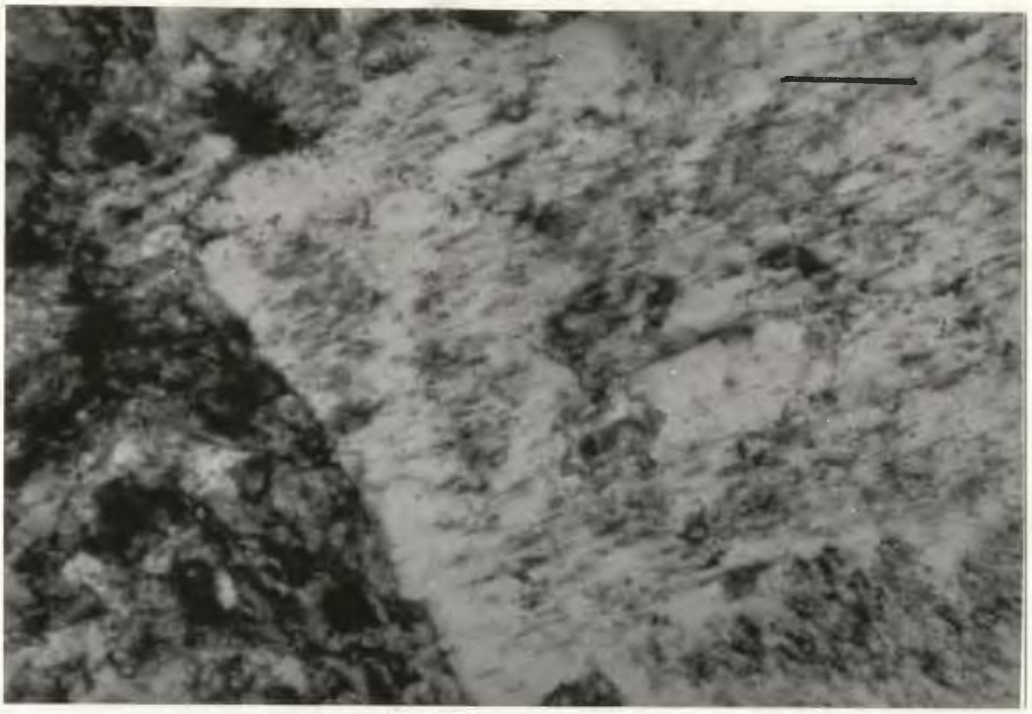

Figure 4-12A.

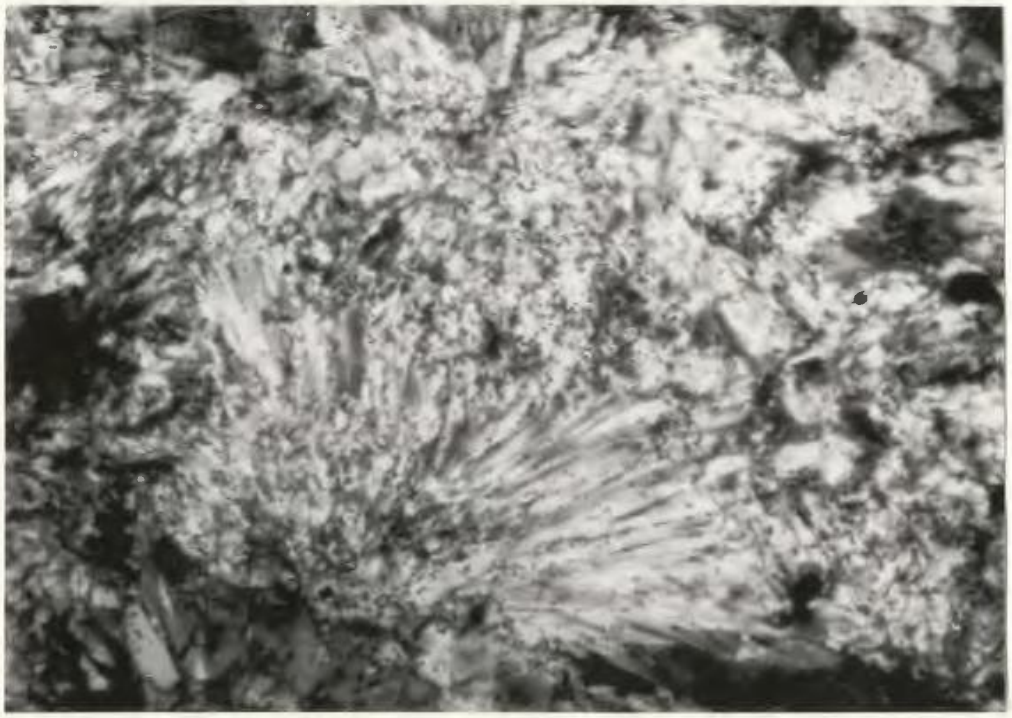

Figure 4-12B.

The former assemblage is assigned to the greenschist-facies due to the presence of sodic plagioclase ± actinolite ± chlorite). Assemblage (5), represented by sample V721-1, is assigned to the epidote amphibolite-facies, due to the stable coexistence of (tschermackitic) hornblende with epidote and albite.

Within the study area, the Benedict Fault transects two members of the BMIS. Mylonitic to schistose Grenvillian fabrics associated with the Benedict Fault are developed in both K feldspar-megacrystic granodiorite (unit 6A) on Pigeon Island, and in hornblende-biotite monzodiorite (unit 6B) in the vicinity of Abliuk Bight. Assemblages in the mylonitized granodiorite comprise white mica, epidote, minor biotite and zircon in addition to K feldspar (microcline), plagioclase (An1-4) and quartz. Thin (5mm), discontinuous layers within the granodiorite, composed of extremely fine-grained epidote and biotite, and studded with porphyroclasts of magnesio-hornblende, probably represent screens of tectonitized metabasite.

Schistose fabrics developed in the monzodiorite (unit 6B) include biotite + epidote ± white mica. Together, the tectonized granitoids are thus characterized by the Grenvillian assemblage biotite + epidote + plagioclase (An1-4) + white mica, which is assigned to assemblage (4).

4.3.3 Grenvillian Parageneses in Domain T

Mineral assemblages characteristic of both the epidote amphibolite- and lower amphibolite-facies occur within Domain T. On Fairy Island, a metabasite layer paralleling the Makkovik trend in megacrystic granodiorite (unit 6A) is characterized by the pre-Grenvillian lower- to middle amphibolite-facies assemblage hornblende + biotite + plagioclase (An38), but lacks epidote. In the

same outcrop, an east-west trending discordant plagioclase-phyric mafic dyke is offset along a narrow Grenvillian GD2 high-strain zone, which is restricted to the dyke (see Owen and Rivers, 1983, Fig. 19.3). The plagioclase-phyric dyke contains the assemblage:

(6) hbl+bi+ep+pl(An24-34)±mu

The presence of fabric-forming calcic oligoclase-sodic andesine and hornblende, and the absence of albite requires that assemblage (6) be assigned to the lower amphibolite-facies.

Granodiorites (unit 6A) of the BMIS deformed along Grenvillian high-strain zones in Domain T contain the greenschist-facies assemblage (4), identical to the granitoid rocks deformed along the Benedict Fault.

4.3.4 Grenvillian Parageneses Along the CTIF

The Cut Throat Island Fault (CTIF) is represented by anastomosing bands of south-dipping mylonite developed in K-feldspar megacrystic granodiorite (unit 6A). The mylonites grade rapidly into less highly strained, lineated, schistose fabrics characteristic of GS2 (see section 3.3).

A sample (V769-3) of mylonitized metabasite from the CTIF contains the assemblage actinolitic hornblende + magnesio-hornblende + biotite + plagioclase (An29) + epidote (assemblage 6). As in sample V721-2 (assemblage 5) from the Benedict Fault, the magnesio-hornblende is a fabric-forming phase which must have crystallized (or reequilibrated) during mylonitization attributed to the Grenvillian orogeny. However, in sample V769-3, the magnesio-hornblende coexists (1) with calcic oligoclase rather than albite, and (2) with 1mm

subidiomorphic crystals of actinolitic hornblende, texturally similar to those occurring along and to the north of the Benedict Fault. Although assemblage (6) is assigned to the lower amphibolite-facies, the specific case of V769-3 is somewhat problematical. Despite the apparent textural stability of coexisting actinolitic hornblende, magnesio-hornblende, and calcic oligoclase in this sample, only the latter two are considered to form a stable paragenesis under conditions of lower amphibolite-facies metamorphism. By analogy with two-amphibole samples along and to the north of the Benedict Fault (e.g. V608-1, from Sloop Island), the actinolitic hornblende likely postdates the more aluminous amphibole, and crystallized during continued, relatively late Grenvillian tectonothermal activity following peak Grenvillian metamorphic conditions. In this sample, however, obvious replacement textures are not preserved.

Tectonized granodioritic rocks (unit 6A) along the CTIF consist of biotite + plagioclase (An30) + K feldspar $\pm$ epidote $\pm$ hornblende, and are assigned to assemblage (6). It is noteworthy that amphiboles are preserved only in relatively coarse-grained, schistose granitoids deformed along the CTIF. Mylonitic fabrics developed in granitoid rocks are defined by biotite.

4.3.5 Grenvillian Parageneses South of the CTIF

Epidote-amphibolite and lower amphibolite-facies parageneses persist in metabasites and granitoids south of the CTIF. Domain G is characterized by the pervasive development of south-dipping, L-S fabrics attributed to the Grenvillian orogeny, which are defined by both garnetiferous and non-garnetiferous mineral assemblages characteristic of the epidote amphibolite- and(or) lower amphibolite-facies. In addition to assemblage (6), a non-garnetiferous assemblage occurs in

some metabasites in domain G. For instance, in V17 and V686, which come from minor (<5m wide) south-dipping high-strain zones south of the CTIF. The assemblage is characterized by the absence of amphibole, and consists of:

(7) **bi+ep+pl(An20)±mu**

The local presence of muscovite in one of these metabasites (V686, sampled from the high-strain zone depicted in Fig. 3-11) implies Ca-K exchange with potassic phases in the granitic (s.l.) host rocks during the development of the high-strain zones.

Garnet first occurs as an additional phase in various rock types approximately 1km south of the CTIF and the high strain zones near Cape Man of War. Garnets occur sporadically in most lithologies and are associated with both GS1 and GS2 fabrics (Figs. 4-13A,B). The typical garnetiferous assemblages in quartzofeldspathic rocks are:

(8) **bi+mu+gt+pl(An22)**
(9) **hbl+bi+ep+gt+pl(An3-12)±sph±mu±al**
(10) **hbl+bi+ep+gt+pl(An17-35)±sph±mu±al**

A fourth garnetiferous assemblage (11; Fig. 4-13A) occurs along a high strain zone transecting the Michael gabbro:

(11) **hbl+bi+gt+pl(An25)+ilm+qz**

Assemblage (8) is represented by one sample (V546-1) of schistose K feldspar megacrystic granodiorite (unit 6A) from Tommy Rocks. More common are assemblages (9) and (10), which occur where Grenvillian fabrics are developed in pelitic metatexite, jotunite, in various members of the BMIS, and in a series of intermediate (quartz monzonitic) dykes cutting the BMIS. Although both assemblages (9) and (10) locally occur within the same outcrop (e.g. (9) in

Figure 4-13. Photomicrographs of garnetiferous Grenvillian parageneses.

4-13 A. Garnet porphyroblast deflecting mylonitic fabric outlined by sheaths of hornblende in deformed Michael gabbro. Bar scale is 0.1mm. Plane polarized light; sample V554-1.

4-13B. Small idiomorphic garnets coexisting with fabric-forming biotite flakes and stubby hornblende (lower left) in deformed hornblende + biotite monzodiorite (unit 6B). Bar scale is 0.1mm. Plane polarized light; sample V257-7.

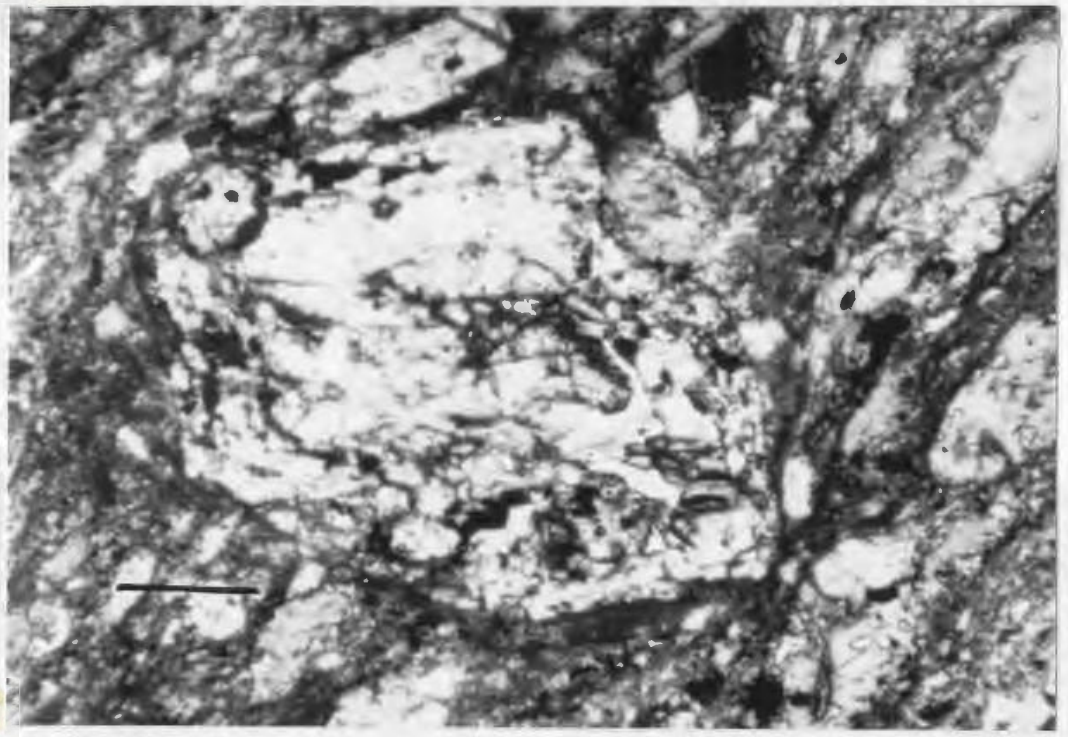

Figure 4-13A

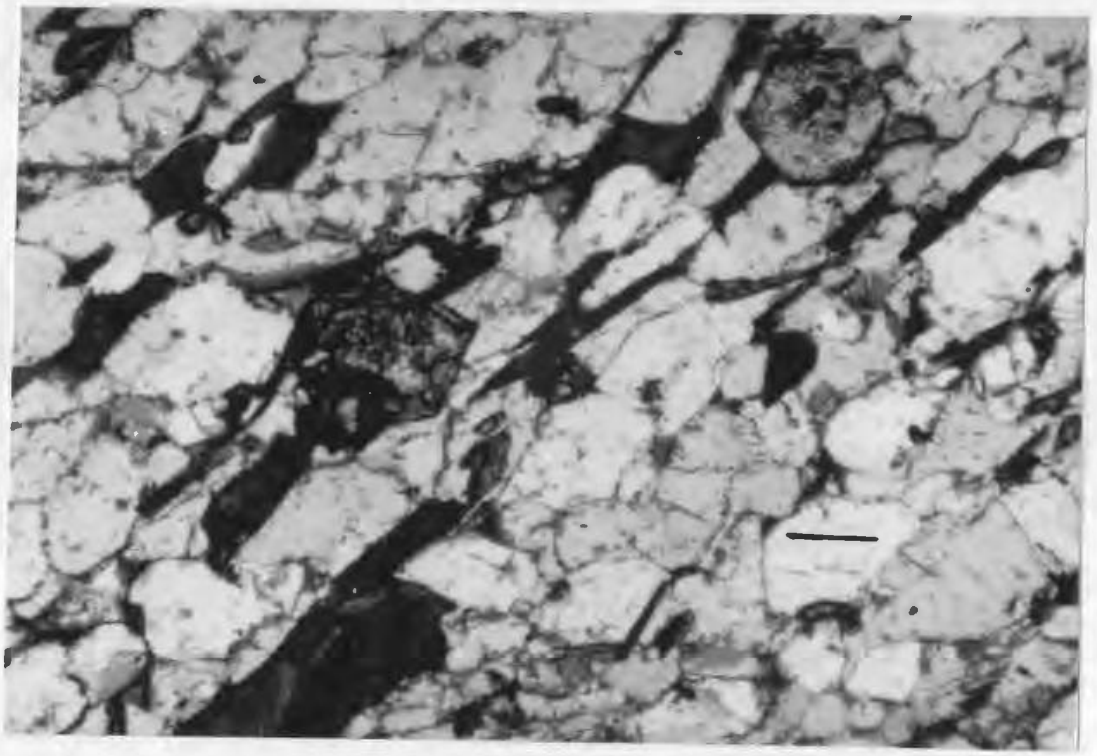

Figure 4-13B

monzodiorite (unit 6B) and (10) in intermediate dykes on Marks Island), albite + oligoclase have not been found within the same thin section. In addition to the minerals listed above, assemblages (8), (9) and (10) also contain quartz and K feldspar (microcline), with variable amounts of zircon, apatite and Fe(Ti) oxides.

Assemblage (11) is restricted to a sample (V554-2) of recrystallized Michael gabbro from Indian Harbour. This lower amphibolite-facies paragenesis differs from the other garnetiferous assemblages insofar as it lacks epidote, and also in that it is the only metabasite observed to contain garnets within the Grenvillian fabric. Given the widespread (albeit not abundant) presence of garnets associated with Grenvillian fabrics in other lithologies south of the CTIF, the absence of garnet in most metabasites may be attributed either to inappropriate $Fe2^{+}$ /Mg ratios in the bulk rock composition (e.g. Binns, 1965), or to oxygen fugacities inappropriate to develop almandine-rich garnets in these rocks (Miyashiro, 1979).

4.3.6 Distribution of Grenvillian Parageneses

The distribution of Grenvillian assemblages (1) to (11) is depicted on a diagrammatic north-south transect through Pigeon and Cut Throat Islands in Figure 4-14. The position of each point on the transect has been determined by projection parallel to the Benedict Fault. Figure 4-14 thus illustrates changes in metamorphic mineral assemblages associated with Grenvillian fabrics across Domains M, T and G. It is readily apparent from this diagram that Grenvillian fabrics in Domain M comprise greenschist-facies assemblages (which locally are seen to overprint pre-Grenvillian parageneses). Non-garnetiferous assemblages of the epidote amphibolite- to lower amphibolite-facies occur along and to the south of the Benedict Fault. Greenschist-facies parageneses and (or) minerals (e.g.

Figure 4-14. Schematic crossection N-S across the Smokey archipelago, transecting Cut Throat and Pigeon Islands. Mineral parageneses attributed to the Grenvillian orogeny are shown for four rock groups: A = metabasites (m-michael gabbro; i-intermediate dykes cutting the BMIS)
B = granitoids of the BMIS
C = orthogneissic rocks of the WBIC and the Bluff Head orthogneiss (northern Groswater Bay terrane)
D = paragneisses of the WBIGC

Abbreviations: CTIF-Cut Throat Island Fault; BF-Benedict Fault; chl-chlorite; sph-sphene; pl-plagioclase; act-actinolitic amphibole; hbl-hornblendic amphibole; ep-epidote; bi-biotite; gt-garnet; mu-muscovite; al -allanite.

Note: "N" and "S" refer to reference line showing the transect on Figure 3-1 (p. 70)

S N

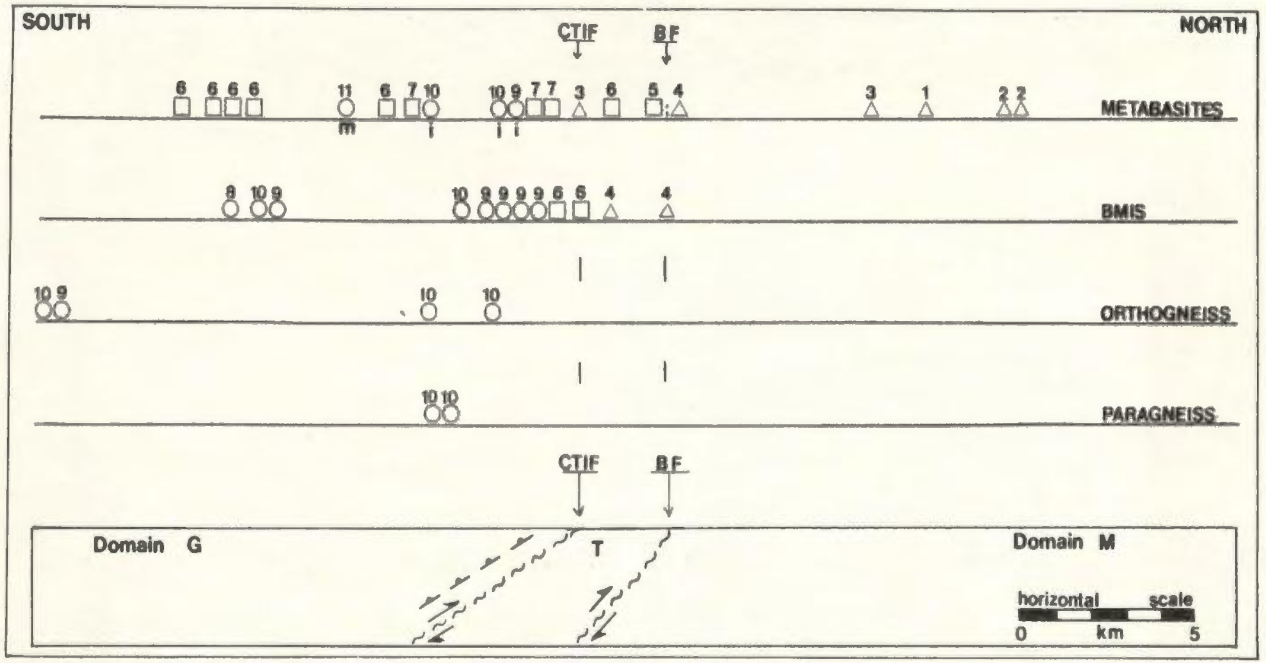

△ GREENSCHIST FACIES

1 chl+ep+pl(An 0.2)+ct
2 act[hbl]+ep+pl(An 0-4)±chl±qz
3 act[hbl]+ep+pl*(An 25-34)±bi±qz
4 bi+ep+pl(An 1-4)±act[hbl]±chl±mu

m = Michael gabbro
i = intermediate dyke rocks
[ ] = metastable phase
* = ?metastable phase

□ EPIDOTE AMPHIBOLE FACIES-LOWER AMPHIBOLITE FACIES (non-garnetiferous)

5 hbl+bi+ep+pl(An 3)+qz
6 hbl+bi+ep+pl(An 17-34)±mu±act*
7 bi+ep+pl(An 20)±mu

○ EPIDOTE AMPHIBOLITE FACIES-LOWER AMPHIBOLITE FACIES (garnetiferous)

8 bi+mu+gt+pl(An 22)
9 hbl+bi+ep+gt+pl(An 3-12)±sph±mu±al
10 hbl+bi+ep+gt+pl(An 17-35)±sph±mu±al
11 hbl+bi+gt+pl(An 25)+qz

— — = northernmost occurrence of garnets associated with Grenvillian fabrics
CTIF = Cut Throat Island Fault
BF = Benedict Fault

Figure 4-14.

actinolitic hornblende in sample V769-3) also occur along the Benedict and Cut Throat Island faults, and presumably record late (or relatively shallow-level) tectono-metamorphic activity along these high-strain zones.

Immediately south of the CTIF, garnet occurs in association with other minerals characteristic of the epidote-amphibolite to lower amphibolite-facies. A plane delineating the northernmost occurrence of these garnets is assumed to be south-dipping since the garnets are associated with, and restricted to, the south-dipping Grenvillian GS2 fabric.

A striking zonation of Grenvillian metamorphic mineral assemblages is thus evident north to south across the study area. This metamorphic zonation coincides with the Grenvillian structural subdivision of the Smokey archipelago (Fig. 3-1), and demonstrates that the Benedict and Cut Throat Island Faults are metamorphic as well as structural breaks. These contrasts in metamorphic grade thus reflect the telescoping of the Grenvillian metamorphic gradient by reverse (south side upwards) movement across these faults, with the effect of exposing progressively deeper crustal levels (depths) towards the south. It is thus inferred that north-directed translation along both faults outlasted peak Grenvillian metamorphism. Evidence for this is provided by the presence of both greenschist-facies and epidote amphibolite- to lower amphibolite-facies mineral assemblages along the Benedict and Cut Throat Island faults, and is supported by the observation that in Domain G, schistose to mylonitic fabrics commonly wrap about garnet porphyroblasts (Fig. 4-13A).

4.3.7 Compositions of Minerals in Grenvillian Parageneses

4.3.7A Garnet

Garnets associated with Grenvillian fabrics typically occur as small (0.05-0.2mm, rarely to 1mm) idiomorphic to subidiomorphic grains. They are usually enveloped by fabric-forming minerals (e.g. biotite), with which the garnets form a texturally-stable paragenesis (see Fig. 4-13B).

The garnets are generally rich in almandine (24-70mol%), and contain significant amounts of spessartine and grossular (totalling 40-75mol%). Pyrope comprises from 0-5% of garnets developed in granitoids, and from 13-15% in pelitic metatexite and Michael gabbro.

Figure 4-15 shows a regular distribution of Mg/(Mg+Fe) between coexisting garnet and biotite associated with Grenvillian fabrics in most samples, although garnet-biotite pairs from deformed Michael gabbro (V554-2) and pelitic metatexite (V580-2, V580-3) have somewhat higher distribution coefficients than those developed in the BMIS, jotunite, and intermediate dyke rocks. Garnet compositions expressed in terms of molecular end-members are plotted in Figure 4-16. The garnets developed in Michael gabbro, intermediate dykes, jotunite and pelitic metatexite show a weak (2-5 mol.%) core to rim increase in the grossular content. Garnets from deformed granitoids of the BMIS, however, show an increase in the almandine content towards the rim, with no systematic zoning in non-femic components (Fig. 4-16; Appendix A.4,A.4.9).

4.3.7B Biotite

Grenvillian biotites are compositionally distinct from biotites associated with pre-Grenvillian fabrics. Most Grenvillian biotites plot in the lepidomelane and sideromelane fields of Troger's (1971) diagram (Fig. 4-17). Biotites from the CTIF (numbered symbols, Fig. 4-17) plot along the boundary between the meroxene and

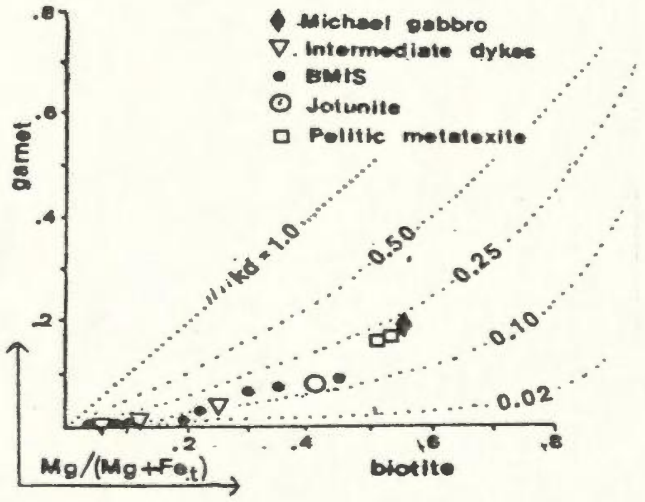

Figure 4-15. Plot showing the distribution of Mg/(Mg+Fe$_t$) between coexisting garnet and biotite associated with Grenvillian fabrics. Kd lines are from Kretz (1961).

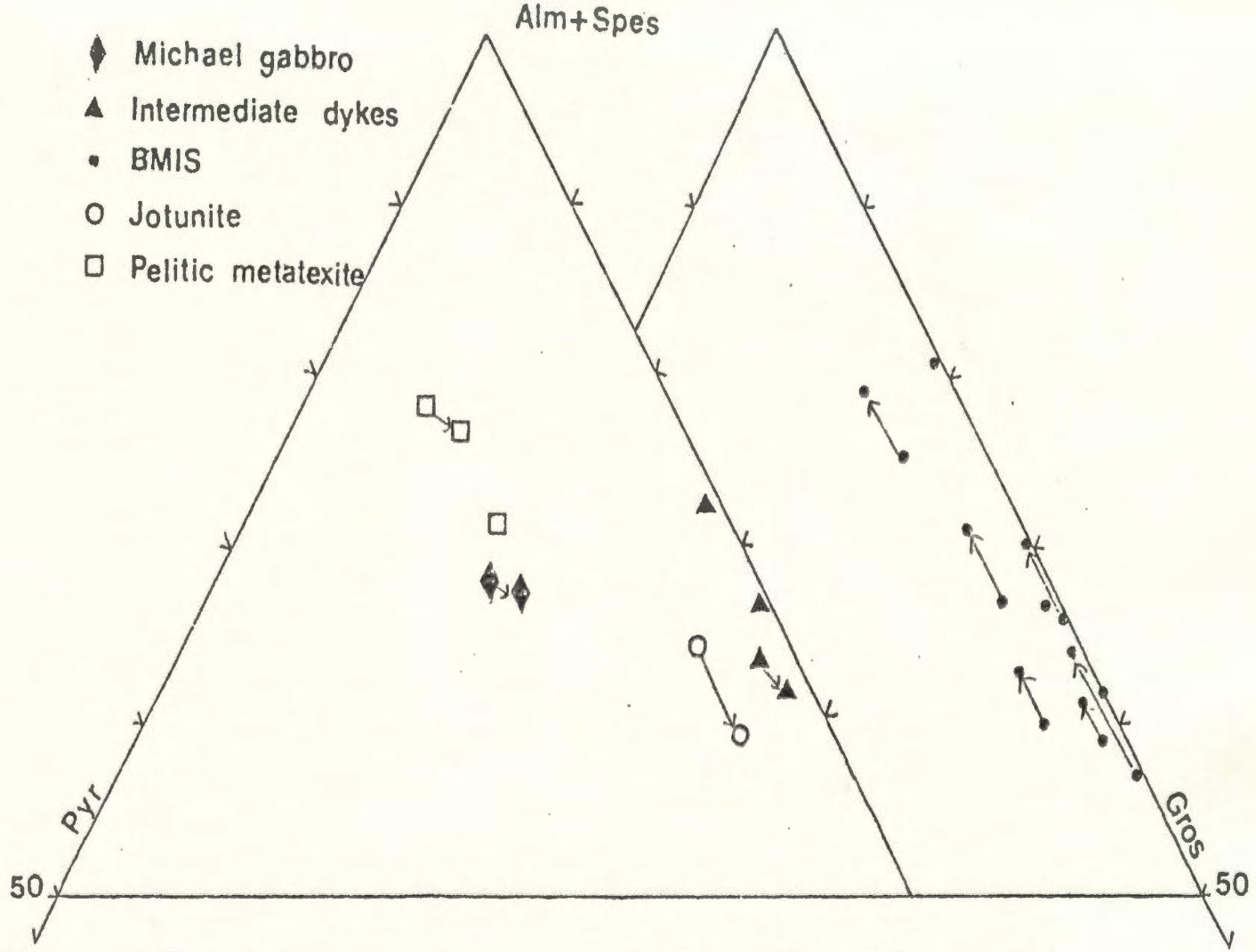

Figure 4-16. Compositions of garnets associated with Grenvillian fabrics, expressed in terms of end members. Arrows show garnet core to rim zoning.

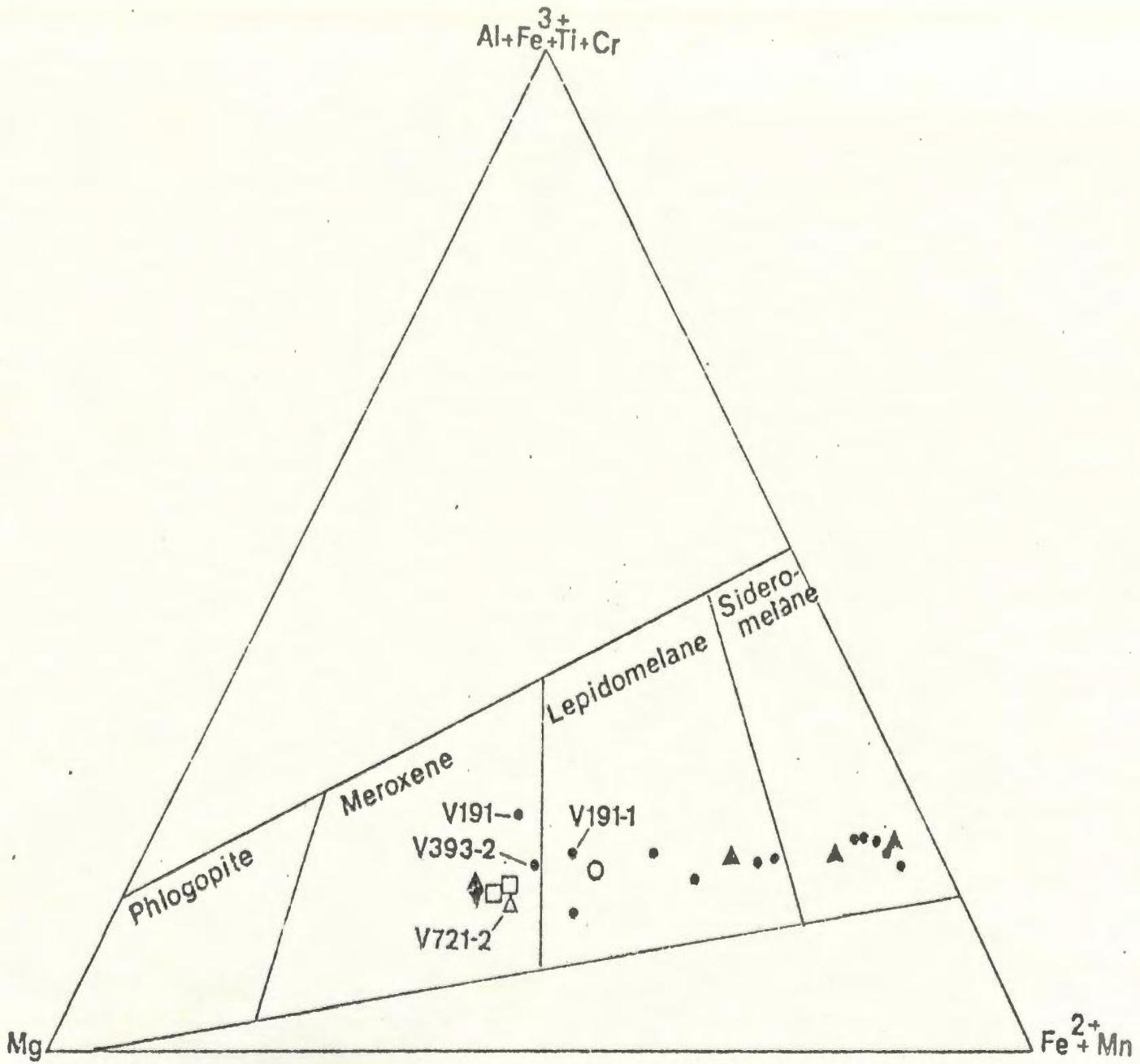

Figure 4-17. Compositions of biotites associated with Grenvillian fabrics in various lithologies plotted on Troger's (1971) diagram. Samples from the Benedict and Cut Throat Island faults are indicated. See text.

lepidomelane fields, however this may reflect bulk rock control on biotite compositions rather than contrasting metamorphic conditions.

Biotites associated with Grenvillian fabrics typically occur as small (0.05-0.5mm) idiomorphic flakes which form a texturally stable paragenesis with coexisting fabric-forming minerals. Grenvillian biotites are brown to greenish-brown in colour, and contrast with the reddish-brown biotites from higher grade, pre-Grenvillian gneissic assemblages. Colour differences noted between biotites from different metamorphic grades have been attributed to differences in the Ti content (e.g. Deer et al., 1971).

4.3.7C Amphibole

In an effort to obtain more information on the Grenvillian metamorphic gradient across domains M, T and G, attention has been focussed on the compositions of amphiboles associated with Grenvillian fabrics developed in metabasites, members of the BMIS, and various gneissic rocks.

Amphiboles have been recognized as sensitive indicators of changing metamorphic conditions since the pioneering studies of Eskola (1914, 1939). As will be seen, however, there is some controversy over which compositional parameters of amphiboles are more sensitive to changes in metamorphic conditions.

In this study, amphibole analyses have been recalculated on the basis of 23 oxygens. Two recalculation schemes are presented for each microprobe analysis (Appendix A.4: A.4.7; A.4.8). The first ("$Fe2^{+}$ ") recalculation assumes all iron to be in the ferrous state. In this calculation, a maximum amount of $Fe2^{+}$ and Mn

is allocated to the M4 site, consequently Na and Ca are maximized in the A site. Amphibole analyses have also been recalculated by normalizing all ions excluding Ca, Na and K to 13 ("13CNK", Appendix A.4: A.4.7 and A.4.8), after which Fe3 is estimated by assuming electroneutrality. This latter scheme has been shown by Robinson et al. (1982, Table 1) to yield the best ferric iron estimate (compared with wet chemical analyses) for hornblendic amphiboles coexisting with epidote.

Since the majority of amphiboles associated with Grenvillian fabrics in the study area coexist with epidote (which generally contains significant amounts of $Fe3^{+}$), the 13CNK recalculation is more suitable for these assemblages, and it has also been adopted in the recalculation of pre-Grenvillian amphibole analyses in order to maintain a consistent basis for comparison.

Although all amphiboles in the study area are calcic and contain between 1.65-1.95 Ca atoms p.f.u. (and less than 0.6 Na atoms p.f.u.), distinct contrasts in amphibole compositions are evident from north to south across the study area.

North of the Benedict Fault, pre-Grenvillian amphiboles, typically magnesio- and tschermakitic hornblendes (using Leake's, 1978, nomenclature) occurring in deformed metabasites outlining the Makkovik trend and in metamorphosed dykes, are replaced by actinolitic hornblende associated with local Grenvillian shear zones. Three modes of occurrence of these actinolitic-pargasitic amphiboles are evident on a domainal scale within individual thin sections of assemblages (2), (3) and (4): (a) They mantle and apparently replace magnesio- and tschermakitic hornblendes (Figs. 4-18A,B) and(or) (b) they occur as randomly

Figure 4-18. Photomicrographs documenting textural evidence for the replacement of pre-Grenvillian hornblendic amphibole by actinolitic amphibole north of the Benedict Fault.

4-18A. Idiomorphic hornblende crystal partially replaced by actinolite (lower right). Bar scale is 0.1mm. Plane polarized light; sample V608-2. Lithology-metabasite

4-18B. Hornblende (dark grey) with a thin rim of actinolite (pale grey). Note the actinolite crystal growing across the hornblende. Bar scale is 0.1mm. Plane polarized light; sample V608-2.

Actinolite and actinolitic hornblende in metabasites north of the Benedict Fault also occur as porphyroblasts and as discrete aggregates of fibroradial crystals. (see photomicrographs, overleaf)

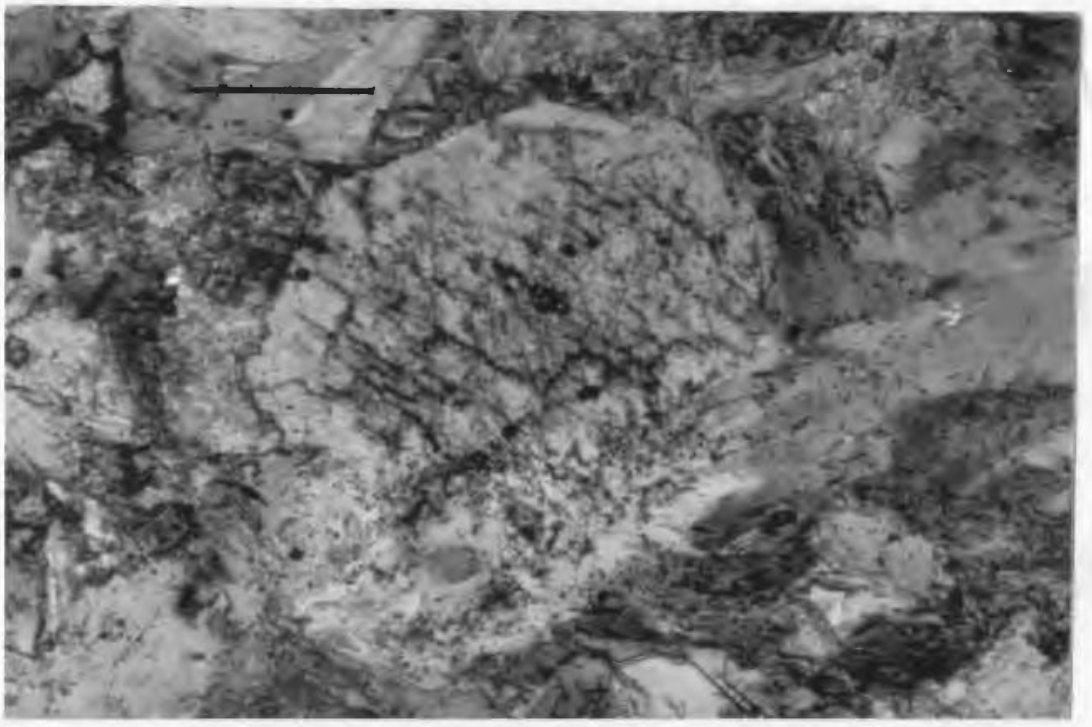

Figure 4-18A

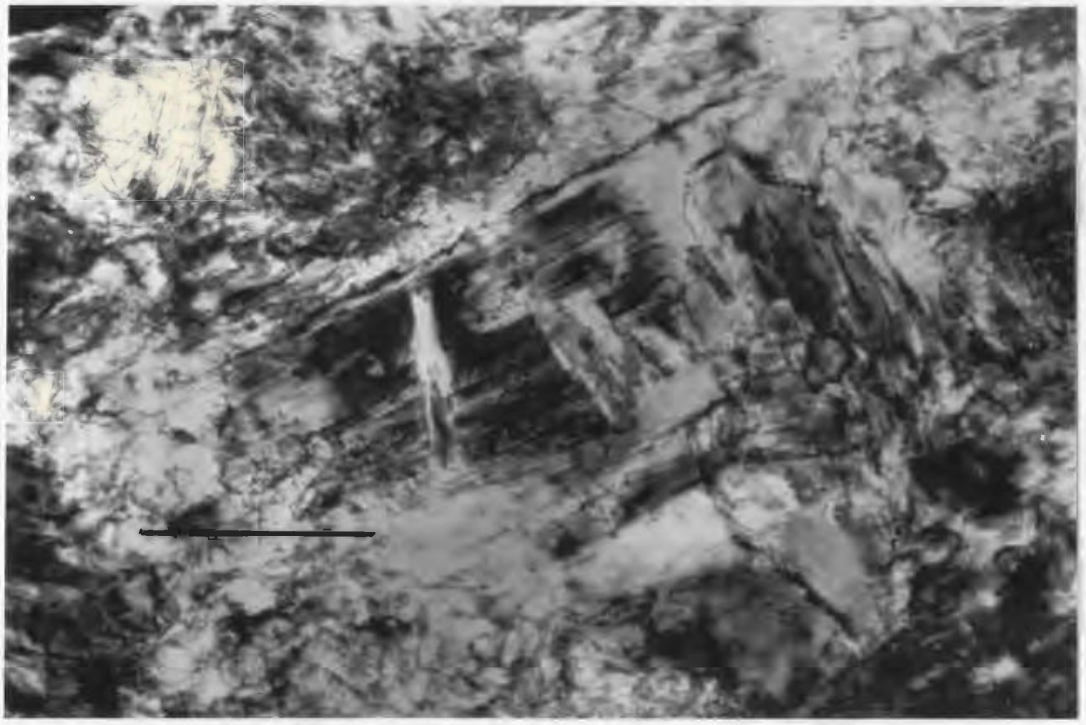

Figure 4-18B

distributed 0.5-1mm (sub)idiomorphic porphyroblasts (see Fig. 4-12A); and(or) (c) they occur as ovoid 1-2mm patches of unoriented or fibroradial crystals (see Fig. 4-12B). These textural varities of actinolitic amphibole have similar compositions in a given thin section, implying that they nucleated under similar PT conditions. Actinolitic to pargasitic amphibole occurs with albite in assemblages (2) to (4), but in assemblage (6) coexists (metastably?) with oligoclase-sodic andesine and magnesio-hornblende in sample V769-3.

Actinolite and actinolitic hornblende are the typical amphiboles in tectonized metabasites along the Benedict and Cut Throat Island Faults. Albitic plagioclase occurs along the Benedict Fault (assemblages 4, 5), whereas oligoclase-sodic andesine (assemblage 6) typifies the CTIF. However, in one mylonitic metabasite sample from each of these faults (V721-2, Benedict Fault; V769-3, CTIF), the stable fabric-forming amphibole is magnesio-hornblende which presumably recrystallized during an early part of the strain history of these shear zones. The CTIF occurrence represents the southernmost extent of actinolitic hornblende noted within the study area. South of the CTIF, the amphiboles characterizing both GS1 and GS2 fabrics are (according to the "13CNK" recalculation scheme) typically ferro-pargasites and magnesio-hornblendes. Despite the limited number of analyses available, contrasts in amphibole compositions are evident between garnetiferous assemblages (9, 10, 11) and garnet-free assemblages (6, 7). Although these contrasts are not sufficient to distinguish their nomenclature by the method of Leake (1978), they become apparent on different formula proportion diagrams.

The occurrence of amphiboles spanning greenschist- to amphibolite-facies

across the Grenville Front provides a means of testing which formula proportion diagrams are most useful in characterizing metamorphic contrasts in this portion of the Grenville Province. In addition, three categories of pre-Grenvillian amphibole associations have been recognized. These are: (1) amphiboles related to the pre-Grenvillian retrogression of the WBIGC; (2) amphiboles associated with the Makkovik trend; (3) amphiboles in metabasites crosscutting the Makkovik trend. Insufficient numbers of analyses are available to permit rigorous comparison between these latter data, but together they are readily contrasted with amphiboles attributed to Grenvillian metamorphism.

Attempts to portray the influence of metamorphic grade on various compositional parameters in amphiboles have met with varying success. Hynes (1982) compared amphibole compositions from medium- and low-pressure metabasites from various metamorphic terranes in order to ascertain whether variations in amphibole compositions were related to pressure changes. He reported that, on the basis of the available data, the two pressure series may not be distinguished by the content of Alvi or Na in the M4 or A sites in amphiboles. Rather, amphiboles which equilibrated at low pressures appear to be characterized by higher Ti/Al ratios. Contrary to Hynes' conclusions, the compilation by Laird and Albee (1981) of amphibole analyses from low-pressure (Abukuma terrane, Japan), medium-pressure (Dalradian terrane, Scotland; Haast River Schist group, New Zealand) and high-pressure (Franciscan terrane, California) belts, together with new data from mafic schists in Vermont, showed that calcic and sodic-calcic amphibole from the different pressure series defined characteristic, albeit overlapping, compositional ranges on various formula proportion diagrams. In

particular, and contrary to Hynes' (1982) findings, they note that amphibole compositions can be grouped according to facies series (as determined independently e.g. from metapelites intercalated with mafic schist) on the basis of a number of compositional parameters. The Na and Al contents of various sites in the amphibole structure appear to be particularly pressure-sensitive, an observation previously made by Raase (1974) and Brown (1977), among others.

There is thus some controversy as to which compositional parameters of amphiboles best serve to characterize metamorphic conditions. This is not unexpected due to the complex character of ionic substitutions in this mineral group. The ability of different formula proportion diagrams to discern compositional variations between amphiboles from contrasting metamorphic environments thus hinges critically on the recalculation scheme adopted for partitioning ions among the different sites in the amphibole structure.

Due to a limited number of samples containing Grenvillian fabrics from domains M and T, specimens from these domains are grouped for comparison with samples from domain G. Figure 4-19 compares Ti/Al ratios of amphiboles associated with Grenvillian fabrics to the north and south of the CTIF. Since the Ti content of amphiboles in the study area appears to be independent of bulk rock composition (Fig. 4-20), systematic Ti variations in amphibole compositions may be attributed to intensive metamorphic variables, probably pressure. North of the CTIF, "Grenvillian" amphiboles are typically actinolitic in composition, whereas Grenvillian amphiboles farther to the south are more aluminous. It is apparent that these amphiboles have higher Ti/Al ratios than amphiboles south of the CTIF (Fig. 4-19). It should be noted that there is considerable overlap in the

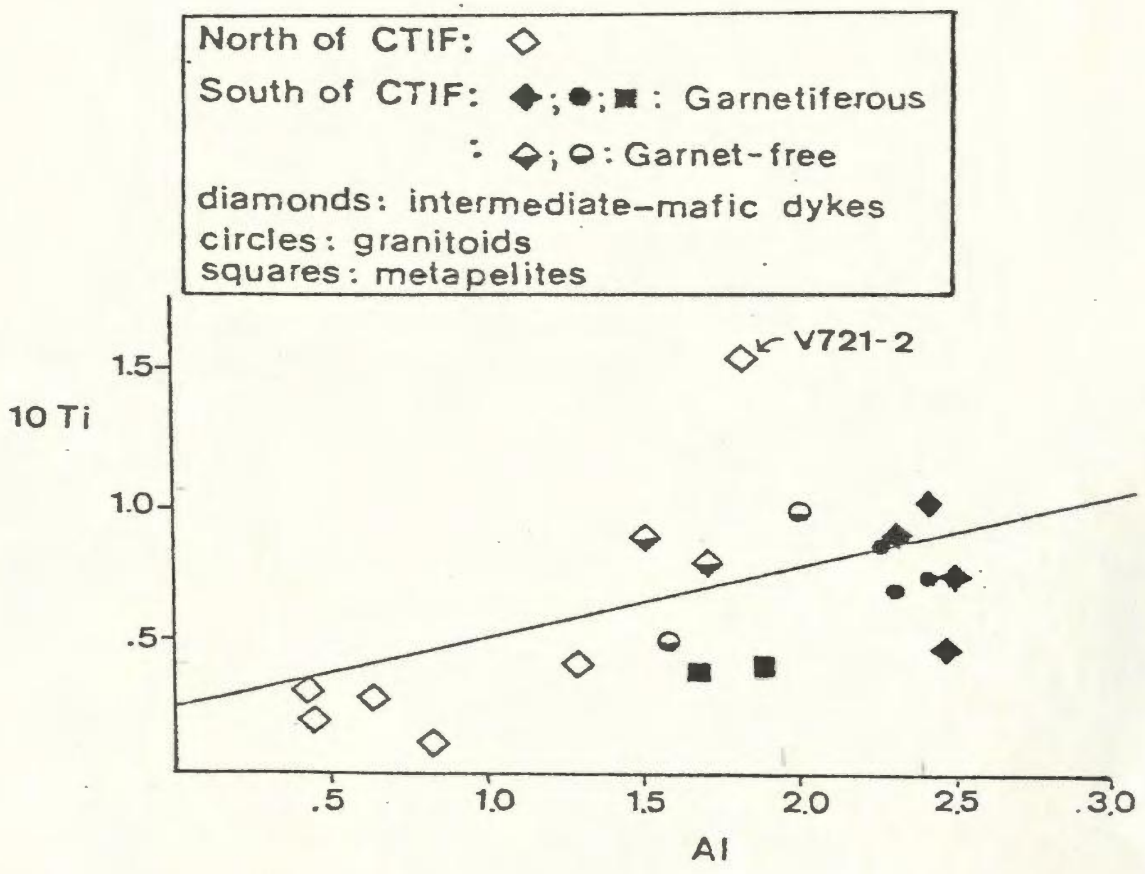

Figure 4-19. Comparison of Ti versus total Al contents of amphiboles associated with Grenvillian fabrics developed in various lithologies north and south of the Cut Throat Island Fault. Sample V721-2 is a metabasite mylonitized within the Benedict Fault. The amphibole in V721-2 is a tschermakitic hornblende, which contrasts with actinolitic amphiboles characteristic of "Grenvillian" amphiboles north of the CTIF. The straight line, taken from Hynes (1982), is for comparative purposes only.

Amphiboles associated with Grenvillian fabrics

- ♦ Michael gabbro
- • BMIS
- ▲ Intermediate dykes
- ● Jotunitic gneiss

Amphiboles predating Grenvillian fabrics

- ⋀ Metabasites discordant to Makkovik trend
- ⋀ Metabasites concordant to Makkovik trend
- ⋀ Makkovik trend in BMIS
- △ Pre-migmatitic metabasites
- ○ Jotunitic gneiss
- ▽ Dioritic gneiss

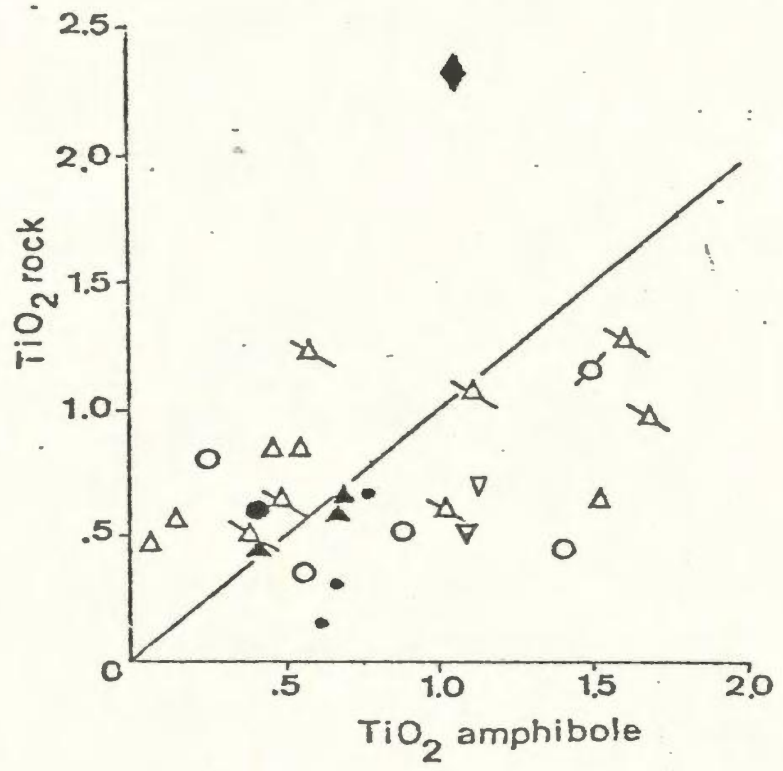

Figure 4-20. Plot of bulk rock and amphibole TiO_2 contents in Grenvillian and pre-Grenvillian tectonites.

Ti/Al ratios of amphiboles from low- and medium pressure terranes (e.g. Hynes, 1982, Fig. 4), and furthermore the presence of sphene may play a crucial role in influencing the Ti contents of amphiboles. Following the results of Laird and Albee (1981), the data depicted in Figure 4-19 are from sphene-free assemblages, consequently amphibole is the sole titaniferous phase in these assemblages (except along and south of the Benedict Fault where biotite $\pm$ ilmenite may also be present). The data depicted in Figure 4-19, although showing transitional variations, indicate that Grenvillian metamorphism is characterized by low- and medium pressure series, north and south, respectively of the CTIF. This observation is in accordance with the restriction of garnetiferous Grenvillian assemblages in Domain G (i.e. to the south of the CTIF), since garnet is also indicative of medium-pressure metamorphism (Laird, 1982).

Additional information may be gleaned from amphiboles, particularly with regard to their edenite, glaucophane, and tschermak contents. Laird and Albee (1981) note that glaucophane substitution

(NaM4, (Alvi+Fe3+Ti+Cr) = Ca, (Fe2+Mg+Mn))

dominates in high-pressure metamorphism, whereas substitutions involving edenite

((Na+K), Aliv = A-site vacancy, Si)

and tschermak

((Alvi+Fe3+Ti+Cr), Aliv = (Fe2+Mg+Mn), Si)

dominate low-pressure metamorphism (see also Holland and Richardson, 1979). Laird and Albee (1981) introduced formula proportion diagrams representing these substitutions in such a way that the ordinate axes record relative pressure increases, while the abcissas record relative temperature increases. The diagrams

thus provide a means of comparing amphiboles from different metamorphic terranes. Since there is considerable overlap in the amphibole compositions from the different pressure series, characterization of pressure series on specific amphibole substitutions alone is reliable only near end-member compositions (e.g. relatively pure glaucophane).

Compositions of "Grenvillian" amphiboles from the study area have been plotted on four of Laird and Albee's diagrams (Fig. 4-21). In all four diagrams, samples from north of the CTIF plot downgrade (closer to the origin) than those from south of the fault. Furthermore, of the samples from south of the CTIF, there is a tendency for garnet-bearing assemblages to plot upgrade of garnet-free assemblages. The best compositional field resolution is shown in Figures 4-21B,C,D. Field resolution is relatively poor for the Na(M4) vs Na(A) plot (Fig. 4-21A), probably because the allocation of Na between the M4 and A sites (the last two sites to be filled) is particularly sensitive to analytical error and to the normalization scheme employed. The compositional field defined by Domain G amphiboles coincides precisely with that defined by Laird and Albee's data from Vermont on the 100Na/(Na+Ca) vs 100Al/(Al+Si) diagram. Data plotted on this diagram are independent of the recalculation scheme, and amphiboles from garnetiferous assemblages cluster "upgrade" (away from the origin) in the same manner in the remaining three normalization-dependent diagrams. As noted by Laird and Albee (1981, p. 148), this indicates that the correlation between amphibole compositions and facies series is largely unrelated to the recalculation scheme. The overlapping of amphibole compositions from garnetiferous assemblages from this study with amphiboles from Vermont (Laird and Albee,

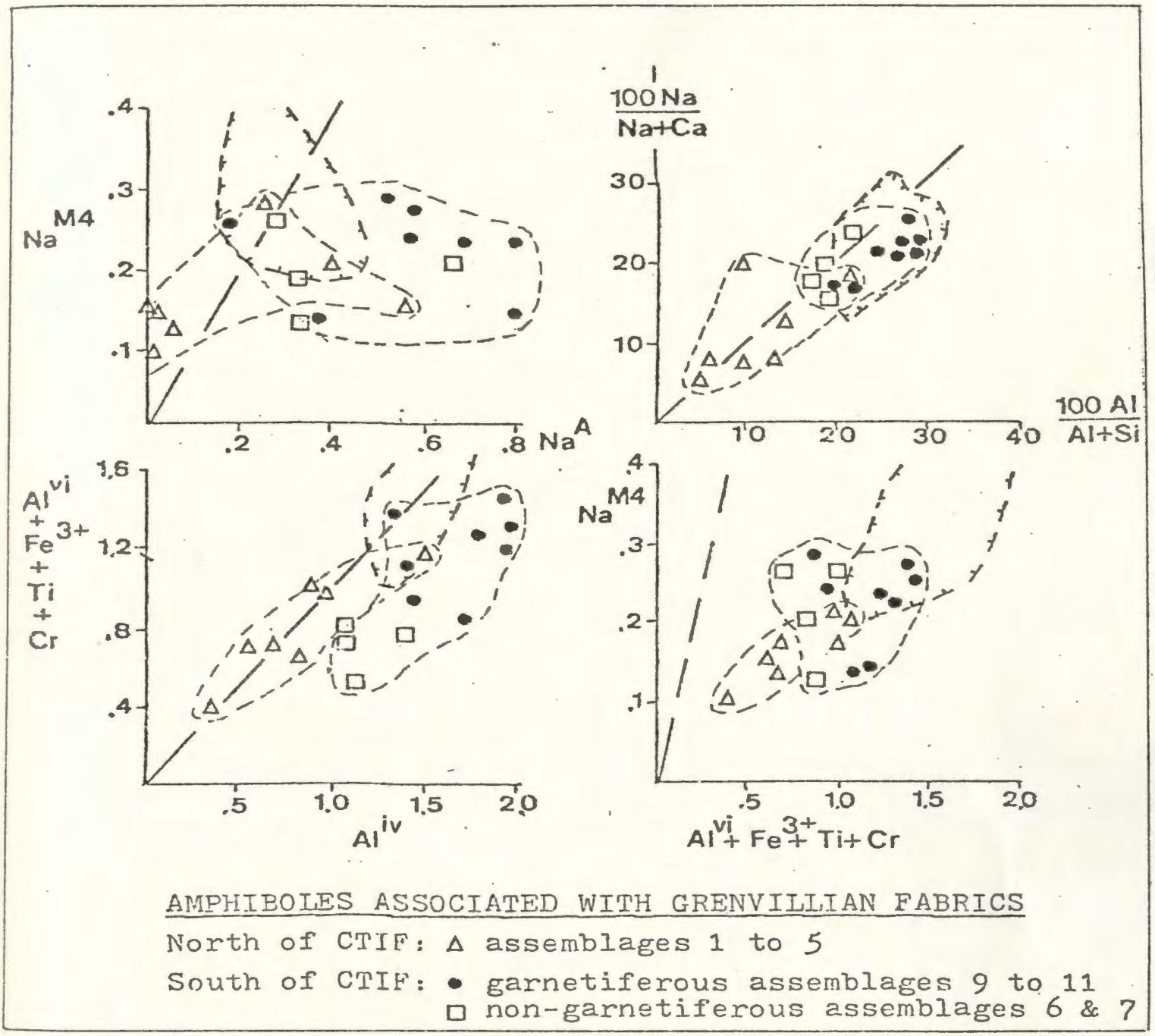

Figure 4-21. Compositions of amphiboles associated with Grenvillian fabrics plotted on various formula proportion diagrams. The "—" symbol encloses the range of amphibole compositions from mafic schist from Vermont, described by Laird and Albee (1981). The straight dashed line equates the scales of the axes of each diagram.

1981) is consistent with similarities in temperatures determined for both medium-pressure terranes. Laird and Albee (1981) report temperature estimates of 500°C and 525°C for rocks from the albite-garnet and oligoclase-garnet zones; temperature estimates (reported below) for both zones in the Smokey archipelago fall on average in the range 550 $\pm$ 30°C.

The data presented in Figure 4-21 thus characterize the regions north and south of the CTIF as belonging to low- and medium-pressure facies series, respectively, consistent with the interpretation of Ti/Al ratios presented in Figure 4-19.

Contrasting relative pressures across the CTIF determined on the basis of "Grenvillian" amphibole compositions are consistent with the structural evidence indicating reverse motion along Grenvillian high-strain zones in the study area. Unfortunately, insufficient amphibole-bearing samples were available to undertake a similar analysis comparing domains M and T; however, metamorphic contrasts across the Benedict Fault have already been demonstrated (see Fig. 4-14).

Metamorphic contrasts resulting from the juxtaposition of the crustal blocks bounded by the Benedict and Cut Throat Island Faults should be reflected by pre-Grenvillian assemblages as well. In order to test this, compositions of amphiboles associated with pre-Grenvillian fabrics sampled to the north and south of the CTIF were plotted on the same formula proportion diagrams as those utilized for "Grenvillian" amphiboles. Compositional variations analagous to those documented in the Grenvillian assemblages are not recorded by pre-Grenvillian amphiboles (Figs. 4-22, 4-23), although the discrimination of

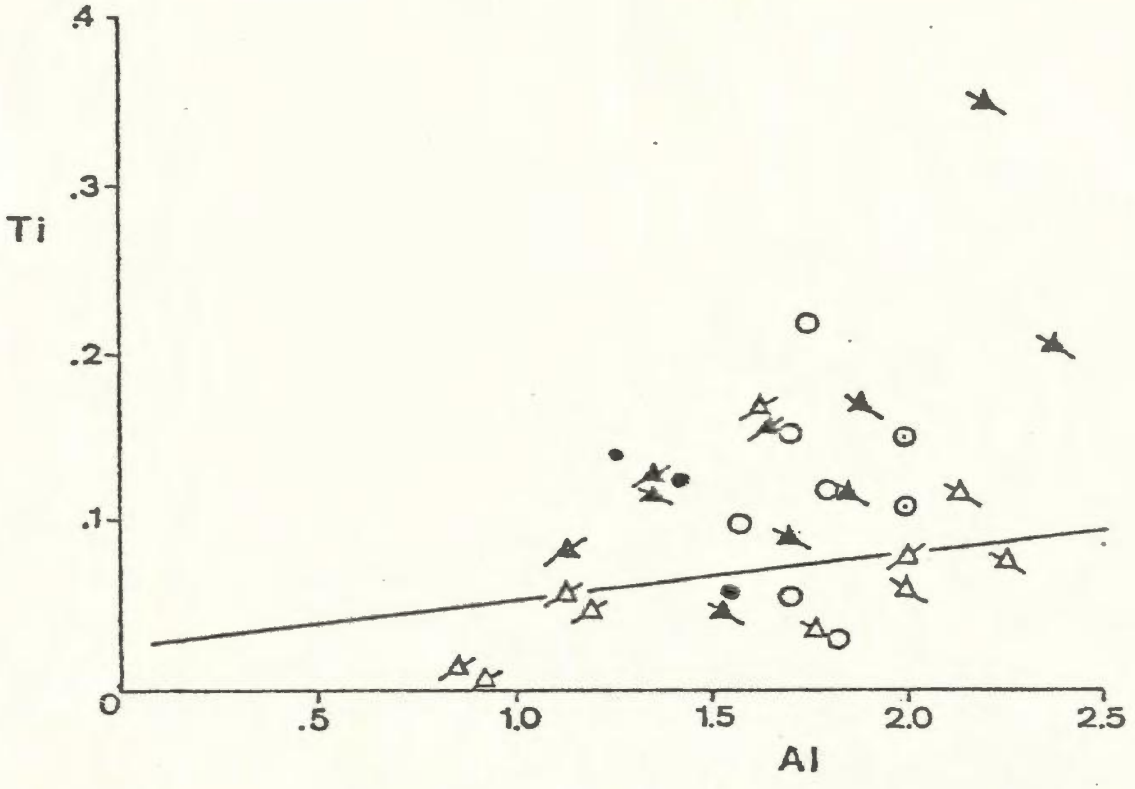

AMPHIBOLES ASSOCIATED WITH PRE-GRENVILLIAN FABRICS

North of CTIF:
- Discordant* metabasite
- Concordant* metabasite
- BMIS (unit 6A)
- Granulite Complex (unit 2)

South of CTIF:
- Discordant metabasite
- Concordant metabasite
- Bluff Head orthogneiss
- Granulite Complex

* with respect to pre-Grenvillian fabric

Figure 4-22. Comparison of the Ti versus Al contents of amphiboles associated with pre-Grenvillian fabrics sampled to the north and south of the Cut Throat Island Fault.

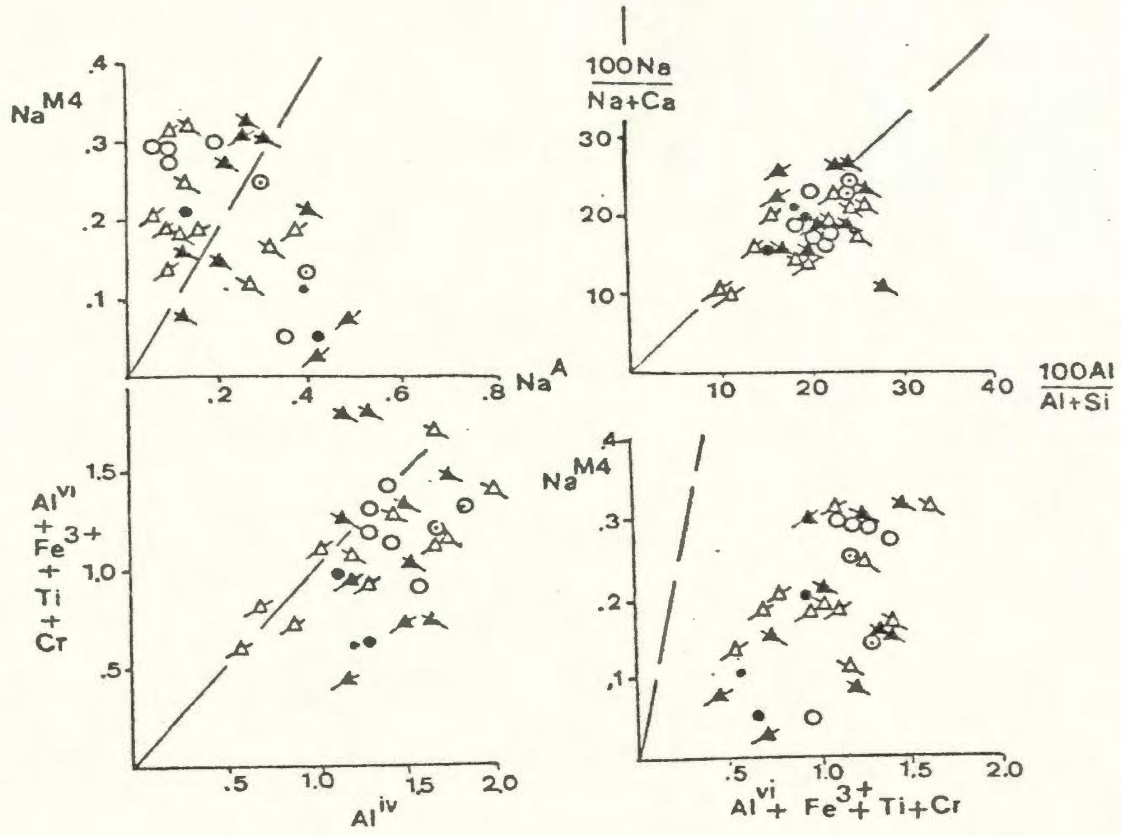

AMPHIBOLES ASSOCIATED WITH PRE-GRENVILLIAN FABRICS

North of CTIF: Discordant* metabasite
Concordant* metabasite
• BMIS (unit 6A)
• Granulite Complex (unit 2)

South of CTIF: Discordant* metabasite
Concordant* metabasite
⊙ Bluff Head orthogneiss
○ Granulite Complex

* with respect to pre-Grenvillian fabric

Figure 4-23. Compositions of amphiboles associated with pre-Grenvillian fabrics expressed on various formula proportion diagrams. The straight dashed line equates the scales of the axes of each diagram.

amphiboles in these diagrams is hampered by a paucity of samples from domains T and M. The four categories of pre-Grenvillian amphiboles (see above, and figure captions) distinguished in these diagrams show a restricted range of compositions and mineralogical association (i.e. with oligoclase-andesine + biotite). From this, it is inferred that reverse movement along the CTIF (and, presumably, the Benedict Fault), although sufficently large to juxtapose contrasting (Grenvillian) amphibole compositions straddling the greenschist- lower amphibolite-facies transition zone, was insufficient to exhume medium-grade amphiboles of compositions sufficently diverse to be distinguished on these diagrams.

Although no systematic variations in "pre-Grenvillian" amphibole compositions are discernable across the Benedict and Cut Throat Island faults, they are likely to show distinct compositional contrasts in comparison with "Grenvillian" amphiboles. Raase (1974) noted that amphiboles from high-pressure terranes are enriched in Si and Alvi compared with amphiboles from low-pressure terranes. Figure 4-24, in which the Si and Alvi contents of "Grenvillian" and "pre-Grenvillian" amphiboles are compared across the study area, shows that the "Grenvillian" amphiboles define a higher, although overlapping, pressure field. This implies burial (e.g. crustal thickening) of that part of the crust now in the Grenville Province following the development of the Makkovik trend, and subsequent uplift later during the Grenvillian orogeny.

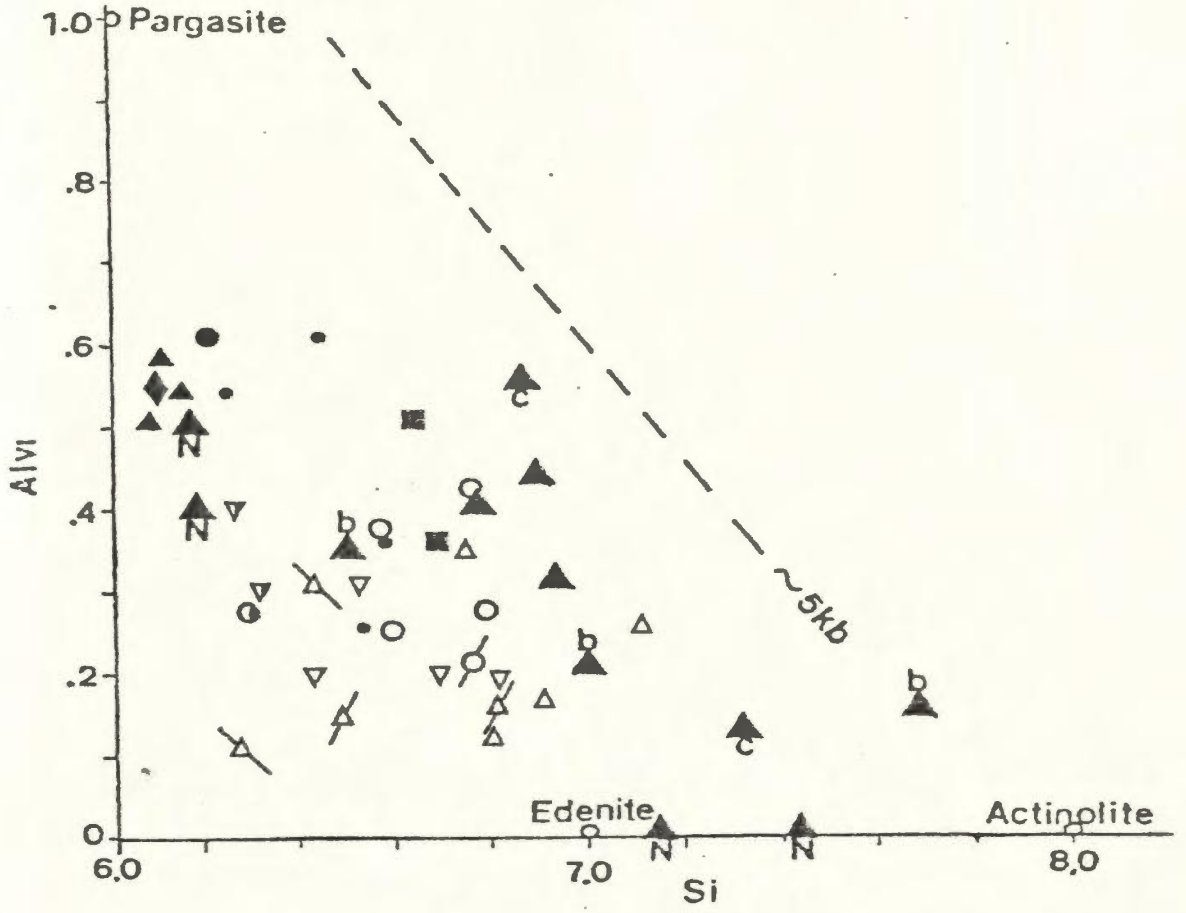

AMPHIBOLES ASSOCIATED WITH GRENVILLIAN FABRICS

▲; ▲c; ▲b; ▲N Metabasites: south of CTIF; along CTIF; along BF; north of BF

▲ Intermediate dykes (garnetiferous); ♦ Michael gabbro

• BMIS

● Jotunite

■ Pelitic metatexite

AMPHIBOLES PREDATING GRENVILLIAN FABRICS

Metabasites discordant to Makkovik trend

Metabasites concordant to Makkovik trend

Makkovik trend in BMIS

△ Pre-migmatitic metabasites

◐ Bluff Head orthogneiss

○ Jotunitic-charnockitic gneiss

▽ Dioritic-tonalitic gneiss

Figure 4-24. Comparison of Alvi versus Si contents of amphiboles associated with Grenvillian and pre-Grenvillian fabrics in various lithologies. See text.

4.3.8 Grenvillian Metamorphic Conditions

The characteristic feature of Grenvillian fabrics is that they are associated with the dynamic retrogression of pre-Grenvillian assemblages. Direct appraisal of Grenvillian metamorphic conditions is most applicable to assemblages south of the CTIF, and the following discussion will be restricted to these.

Critical aspects of the retrogression of pre-Grenvillian medium- to high-grade assemblages are the instability of sillimanite and cordierite along Grenvillian high-strain zones. The former mineral is replaced by white mica (and, presumably, by quartz), and cordierite-bearing gneisses (e.g. pelitic metatexite, unit 1C) are transformed to andesine + biotite + garnet $\pm$ ferrohornblende along Grenvillian shear zones. Since both sillimanite and cordierite were previously stable, with the latter mineral apparently forming exclusively during pre-Grenvillian retrogression of the WBIGC, their instability along Grenvillian high-strain zones indicates that conditions of Grenvillian tectonothermal activity lay outside (e.g. "below") the stability field of both minerals. The range of conditions in which sillimanite and cordierite are unstable defines a broad field in PT space, consequently a more precise estimate of Grenvillian metamorphic conditions must rely on established geothermobarometers.

Unfortunately, in contrast to the plethora of mineral assemblages useful in characterizing pre-Grenvillian metamorphic conditions, only three calibrated thermometric, and no reliable barometric, mineral assemblages are associated with Grenvillian fabrics. The two-feldspar, garnet-amphibole and garnet-biotite geothermometers have been applied to samples south of the CTIF. Garnets do

not occur in domains T and M, and the consistent, but low results (see below) of the two-feldspar thermometer applied to samples from domain G discouraged application of this method from the few two-feldspar bearing samples with Grenvillian fabrics from the northern part of the study area.

Garnets associated with Grenvillian fabrics from most lithologies have significant amounts of grossular and spessartine, which seriously compromises the applicability of various calibrations of the garnet-biotite thermometer. Phase-equilibrium data for garnet-biotite pairs from 16 samples of various lithologies (unit 1C: V580-2, V580-3; unit 3: V194-4; unit 6A: V546-1; unit 6B: V9-2, V164, V257-1,-7, V523, V630; unit 6D: VV772; unit 6E: V434; intermediate dykes: V257-8, V683-3, V710-2; Michael gabbro: V554-2) are presented in Table 4-15. Of these, only three samples (V580-2, V580-3, V554-2) contain garnets of sufficiently low grossular and spessartine contents to warrant application of the Ferry and Spear (1978) calibration. Further problems were encountered due to the extremely high Fe/(Mg+Fe) ratios of the garnets. Unreasonably low (less than approximately 400C) temperature estimates (Table 4-15) determined from garnet-biotite pairs in which garnets contain less than 0.20% MgO may be attributed to analytical error at such low MgO concentrations (e.g. 100Mg/(Mg+Fe) = 0.1 to 1.5). Although temperature determinations were made for all analysed garnet-biotite pairs, analyses were screened prior to averaging the results. If an arbitrary cutoff threshold of 0.35% MgO is chosen, seven of the sixteen garnetiferous samples are rejected from the averaging process (samples V9-2, V164, V257-1, V257-7, V630, all from monzodiorite (unit 6B) ofthe BMIS; and V257-8 and V710-2, both intermediate dyke rocks). Temperatures (degrees celsius) determined

Table 4-15. Compositional parameters and temperature estimates of garnetiferous Grenvillian fabrics developed in various lithologies (see text) using the garnet-biotite geothermometer. Equations and symbols are listed in Table 4-9.

	$100X_{Mg}^{gt}$	X_{Mn}^{gt}	X_{Ca}^{gt}	$\left(\frac{Mn+Ca}{\Sigma X}\right)_{gt}$	X_{Mg}^{bi}	X_{Ti}^{bi}	X_{Alvi}^{bi}	$\left(\frac{Ti+Alvi}{\Sigma X}\right)_{bi}$	Kd_{Mg}^{gt-bi}	(G+A '77)	(T '76)	(F + S 1978)		(I + M in press)	
												3kb	5kb	3kb	5kb
										T^oC	T^oC	T^oC	T^oC	T^oC	T^oC
V546-1r*	7.468	.225	.142	.367	.298	.044	.068	.112	.189	537	586	592	600	729	736
c*	7.433	.204	.179	.383					.188	549	584	590	598	736	743
V9-2r	.328	.136	.279	.415	.063	.045	.080	.125	.044	293	322	269	274	370	375
c	.164	.175	.328	.503					.022	248	246	187	192	302	306
V164	.518	.152	.174	.326	.053	.066	.030	.096	.092	335	431	395	401	465	471
V257-1	.526	.141	.311	.452	.098	.059	.075	.134	.058	329	359	310	316	421	426
V257-7r	.735	.133	.332	.465	.093	.057	.092	.147	.073	364	393	350	356	472	478
c	.505	.139	.398	.537					.050	337	338	288	293	426	431
V523r	3.026	.140	.348	.488	.222	.041	.068	.109	.109	461	463	433	440	609	616
c	2.887	.144	.370	.514					.104	463	454	422	429	609	615
V630r	1.549	.125	.357	.482	.196	.042	.077	.119	.065	362	375	329	335	474	479
c	1.477	.138	.354	.492					.060	363	364	316	321	461	467
V772r	9.183	.293	.277	.570	.450	.053	.033	.086	.123	562	487	463	470	684	690
c	9.176	.283	.290	.573					.123	566	487	463	470	685	692
V434r	7.110	.345	.234	.579	.345	.056	.086	.142	.142	578	517	502	509	719	726
c	7.560	.315	.262	.577					.153	608	532	521	529	746	753
V580-2r	15.681	.061	.099	.160	.519	.042	.083	.125	.172	522	562	560	568	559	574
c	16.493	.073	.074	.147					.183	527	577	581	589	580	588
V580-3r	16.215	.051	.128	.179	.532	.033	.082	.115	.170	538	559	556	564	588	595
c	16.838	.047	.149	.196					.178	562	570	562	579	614	621
V194-4r	8.595	.111	.333	.444	.412	.061	.070	.131	.139	562	512	496	503	635	642
c	8.226	.125	.283	.408					.128	518	495	473	480	590	597
V257-8r	.301	.137	.326	.463	.052	.036	.085	.121	.057	327	356	308	313	444	449
c	.374	.164	.305	.469					.070	350	387	342	348	489	495
V683-3r	3.294	.181	.332	.513	.248	.058	.064	.122	.103	456	452	420	426	585	592
c	3.595	.194	.317	.511					.112	469	468	440	446	609	615
V710-2	1.295	.157	.240	.397	.124	.069	.051	.120	.093	369	433	398	404	493	499
V554-2r	18.238	.063	.178	.241	.554	.074	.045	.119	.180	570	573	575	583	595	603
c	19.559	.073	.162	.235					.196	589	595	605	613	622	630

for garnet core and rim compositions from the remaining nine samples are as follows:

		GARNET RIM	GARNET CORE	
Goldman + Albee:		531 (45)*	539 (50)	
Thompson:		523 (49)	529 (54)	
Ferry + Spear:	3kb	511 (63)	517 (70)	[9 samples]
	5kb	518 (64)	526 (71)	[9 samples]
	3kb	563	582	[low Ca + Mn
	5kb	572	593	garnets, n=3*]
Indares + Martignole:	3kb	633 (62)	643 (63)	
	5kb	641 (61)	650 (63)	
	3kb	581	591	[low Ca+Mn
	5kb	605	613	garnets, n=3*]

( )* = one standard deviation
*low Ca + Mn garnets are from V580-2, V580-3 (deformed pelitic metatexite), and V554-2 (deformed Michael gabbro).

The Goldman and Albee, and Thompson calibrations yield similar results for the Grenvillian garnet-biotite pairs, while Ferry and Spear's calibration, as applied to the three low Ca + Mn garnet samples, estimates temperatures some 50°C higher. Indares and Martignole's calibration, which corrects for Ti and Alvi substitutions in biotite, and for Ca in garnet, was derived for granulite-facies rocks, and is not strictly applicable to the high Mn garnets characterizing medium-grade Grenvillian assemblages in the present example. However, the Indares and Martignole calibration provides temperature estimates for the three low Ca and Mn garnet samples compatible with the Ferry and Spear calibration. Application of Hodges and Spear's (1982) amended calibration of the garnet-biotite geothermometer to two low Mn + Ca garnet samples (V580-2, V580-3) yields an average temperature of ~600°C, consistent with the T estimate derived by the Indares and Martignole calibration for the same samples.

The compositions of garnets and biotites from three samples of granodioritic gneiss (unit 5A) from the vicinity of Bluff Head were also determined, since these minerals are considered to have recrystallized during the Grenvillian orogeny. In each of the three samples (V448-3, V450-1, V465), almandine (33-42 mol.%)-spessartine (23-41%)- and grossular (23-37%)-rich garnets are surrounded by leucocratic haloes depleted in biotite. This texture suggests garnet growth at the expense of biotite, although a comparison of Kd(Mg-Fe) values for the three samples indicates that these phases approach equilibrium. However, the occurrence of depletion haloes is atypical for garnets associated with Grenvillian fabrics developed in the BMIS and metapelitic and jotunitic members of the WBIGC. The garnets, however, are associated with gneissic fabrics rather than the typical Grenvillian schistosity pervasive in other lithologies in domain G. Nonetheless they are interpreted to have recrystallized during Grenvillian metamorphism since: (1) the garnet compositions and garnet-biotite temperature estimates (which range from 389°C to 580°C using Thompson's [1976] calibration; Table 4-16) are closely analogous to those indicated above; and (2) the common presence of early Grenvillian folds (GF1) seen to deform gneissic fabrics in the vicinity of Bluff Head indicates significant recrystallization of the Bluff Head orthogneiss during the Grenvillian orogeny.

The PT-dependence of the distribution of Al between calcic amphibole and plagioclase has recently been evaluated by Plyusnina (1982). This geothermobarometer is applicable to the limiting assemblage Ca-amphibole + chlorite + albite + quartz $\pm$ carbonate $\pm$ mica. Although Ca-amphibole + albite assemblages defining Grenvillian fabrics are not uncommon in the area, none were

Table 4-16. Compositional parameters and temperature estimates of the Bluff Head orthogneiss using the garnet-biotite geothermometer.

	gt X_{Mg}	gt X_{Mn}	gt X_{Ca}	Mn+Ca / X bi	bi X_{Mg}	bi X_{Ti}	bi X_{Alvi}	Ti+Alvi / X bi	gt-bi Kd_{Mg-Fe}
V448-3r*	.017	.354	.205	.559	.130	.047	.117	.164	.119
c*	.011	.348	.209	.557					.071
V450-1r	.019	.266	.228	.494	.095	.063	.056	.119	.185
c	.019	.271	.220	.491					.185
V465r	.068	.195	.300	.495	.407	.046	.068	.114	.107
c	.080	.207	.305	.512					.126

Temperature Estimates (°C)

	G+A(1977)	T (1976)	F + S (1978) 3kb	F + S (1978) 5kb	F + S (1978) 6.5kb	I + M (1985a) 3kb	I + M (1985a) 5kb	I + M (1985a) 6.5kb
V448-3r	459	480	454	463	466	652	658	663
c	373	389	345	352	355	511	517	521
V450-1r	318	580	585	592	598	772	780	786
c	331	580	585	592	598	771	778	785
V465r	505	459	429	437	440	601	608	613
c	555	492	469	478	481	660	667	672

G+A = Goldman and Albee (1977)
T = Thompson (1976)
F+S = Ferry and Spear (1978)
I+M = Indares and Martignole (1985a)

found with coexisting chlorite + quartz + carbonate + mica, hence Plyusnina's geothermobarometer is not strictly applicable to these rocks. Indeed, application of this calibration to the present samples, although yielding reasonable temperatures ranging from ca. 450-550°C, provided spurious pressure estimates ranging from <2kb to 7kb for samples along and to the north of the CTIF, and pressures of ~4kb to >8kb for samples in domain G (south of the CTIF).

Church (1978) compiled analyses of coexisting amphibole, garnet and clinopyroxene from the literature, and, using Raheim and Green's (1974) garnet-clinopyroxene geothermometer as a basis, indirectly evaluated the temperature dependence of Mg-Fe partitioning between coexisting amphibole and garnet. Coexisting amphibole and garnet associated with GS2 fabrics have been analyzed in deformed jotunite gneiss (unit 3B; V194-4), pelitic metatexite (unit 1C; V580-2, V580-3), monzodiorite of the BMIS (unit 6B; V523, V683-3) and Michael gabbro (V554-2). With the exception of V554-2, which has a relatively high distribution coefficient, the coexisting amphiboles and garnets show a regular distribution of Mg/(Mg+Fe2+)ratios (Fig. 4-25), suggesting that equilibrium is approached in these samples. Application of Church's geothermometer yields the following results:

Sample	lnKd	T (°C)
V194-4	2.062	505
V580-2	2.394	480
V580-3	2.094	510
V523	2.187	495
V683-3	1.962	540
V554-2	1.661	580

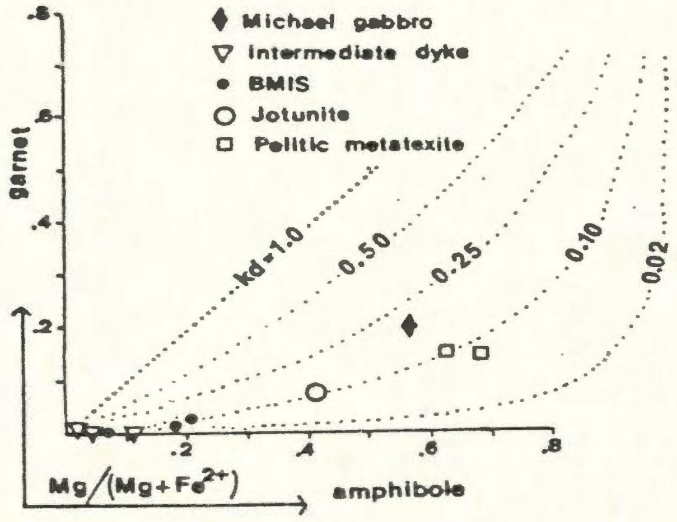

Figure 4-25. Plot showing the distribution of $Mg/(Mg+Fe^{2+})$ between coexisting garnet and amphibole associated with Grenvillian fabrics. Kd lines are after Kretz (1961).

$$\text{where } Kd = \frac{X_{Mg}^{amph}\,(1-X_{Mg}^{gt})}{X_{Mg}^{gt}\,(1-X_{Mg}^{amph})}$$

Of these samples, V194-4 and V554-2 show the best correspondence with garnet-biotite temperature estimates (cf. Table 4-15). Sample V523 yields a temperature some 30-60C higher than that determined from the garnet-biotite calibrations. Low temperatures determined for the deformed metapelite (V580-2, V580-3) probably reflect disequilibrium between hornblende and garnet in the samples (see below).

Graham and Powell (1984) have recently calibrated a garnet-amphibole Fe-Mg exchange geothermometer against Ellis and Green's (1979) garnet-clinopyroxene geothermometer using published data on coexisting garnet, hornblende, and clinopyroxene in various medium- to high-grade metamorphic rocks. The calibration is applicable to low-Mn garnet + hornblende bearing assemblages equilibrated below 850°C. Two samples of pelitic metatexite (unit 1C, samples V580-2, V580-3) and one sample of Michael gabbro (V554-2) contain low-Mn garnets associated with Grenvillian fabrics. Application of Graham and Powell's geothermometer to these specimens, assuming ternary (Ca + Mg +Fe) garnets and using the 13CNK amphibole recalculation scheme (see section 4.3.7C) to estimate ferric iron in the amphibole, yields the following results for core compositions:

Sample	lnKd	TC
V554-2	1.664	572
V580-2	2.392	382
V580-3	2.092	478

$$\text{where } Kd = \left(\frac{X_{Fe}^{gt}}{X_{Mg}^{gt}}\right) \Big/ \left(\frac{X_{Fe}^{amph}}{X_{Mg}^{amph}}\right)$$

Temperature estimates for garnet rim compositions for the three samples is within 5°C of these values, except in V580-3 (T = 456°C).

The low temperature estimates provided by the samples of deformed pelitic metatexite likely suggest disequilibrium between garnet and amphibole, since in these samples both minerals coexist but do not form a paragenesis. The ca. 572°C temperature estimate provided by deformed Michael gabbro, is consistent with both Church's calibration of the amphibole-garnet geothermometer, and with various calibrations of the garnet-biotite geothermometer (Table 4-15). Temperature estimates determined for this sample (V554-2), which is characterized by touching spindle-shaped fabric-forming hornblende and subidiomorphic garnet (see Fig. 4-13A), are thus considered to closely approximate Grenvillian conditions south of the CTIF.

Microprobe analyses of plagioclase and K feldspar from five samples of granitoid rocks were obtained using a defocussed (10-15um) electron beam. Although coarsely perthitic feldspars are locally present, the K feldspar most typically associated with Grenvillian fabrics is grid-twinned microcline. Consequently the problems encountered during analysis of perthitic pre-Grenvillian feldspars were avoided. Three of the five analysed samples are

intermediate garnetiferous dykes (V257-8; V683-3; V710-2); a fourth sample (V434) is garnetiferous biotite granite (unit 6E). A fifth sample (V450-1), which lacks a discernible Grenvillian fabric, is granodioritic gneiss (unit 5A) from the northern Groswater Bay Terrane (Bluff Head orthogneiss). All five specimens, which were sampled south of the CTIF, cluster near the 400°C contour on Stormer's (1978) diagram (Fig. 4-26). This result indicates: (1) significant reequilibration of two-feldspar-bearing assemblages south of the CTIF to relatively low temperatures during the Grenvillian orogeny; and (2) significant recrystallization of the Bluff Head orthogneiss during the Grenvillian orogeny, even where south-dipping Grenvillian L-S fabrics are not evident in these rocks.

4.3.9 Summary

The effects of the Grenvillian orogeny define a zonal distribution of structures and metamorphic mineral assemblages north to south across the study area. Two major south-dipping Grenvillian high-strain zones, which coincide with the Benedict and Cut Throat Island faults, separate three structural domains. The northern domain (domain M) is characterized by locally-occurring Grenvillian shear and (or) brittle fracture zones marked by greenschist-facies assemblages. The southern boundary of this zone, the Benedict Fault, is marked by mylonites developed in granitoids and metabasite layers. Both greenschist-facies and epidote amphibolite-facies (here characterized by the presence of hornblendic amphibole) assemblages occur in these zones. Epidote amphibolite-facies rocks characterize locally-occurring Grenvillian high-strain zones which partially overprint pre-Grenvillian fabrics across a 3km wide transitional zone (domain T), whose southern border coincides with the CTIF. Like the Benedict Fault, the

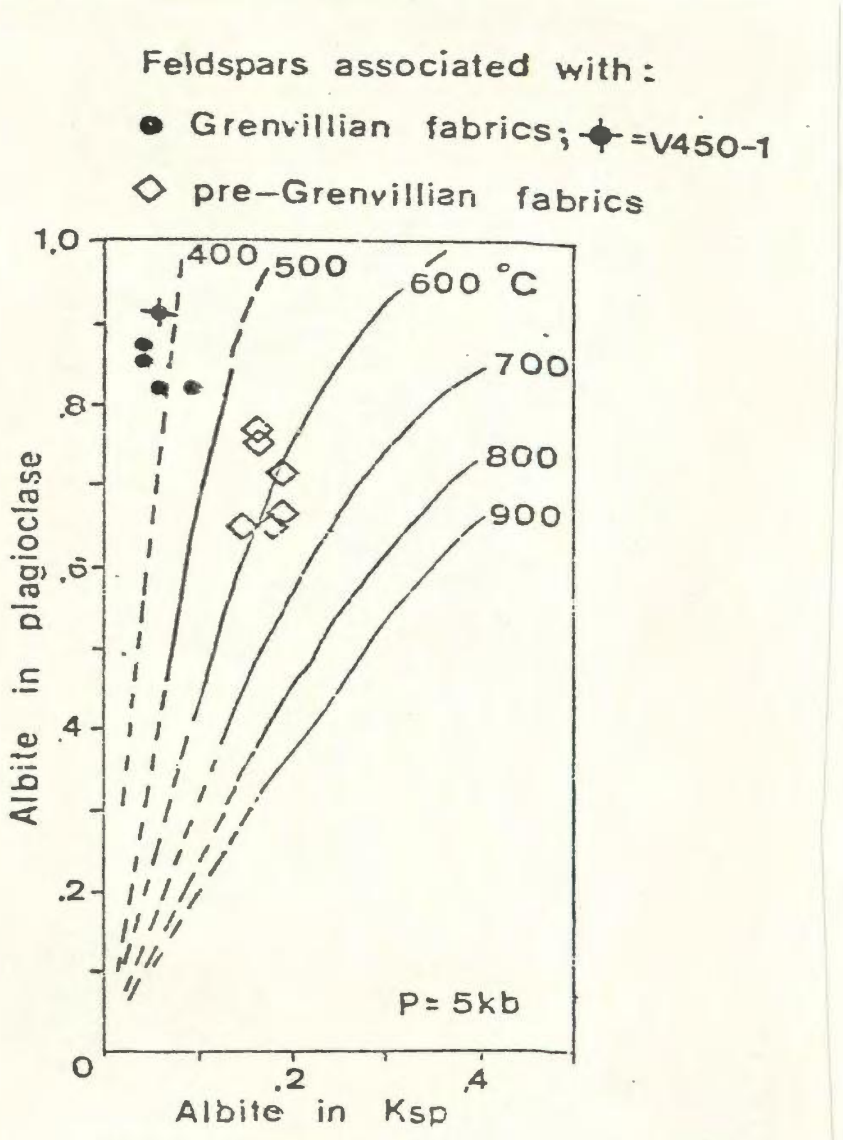

Figure 4-26. Partitioning of Na between coexisting plagioclase and K feldspar from various lithologies containing Grenvillian and pre-Grenvillian fabrics. Temperature contours are from Stormer (1977). Sample V450-1 is from the Bluff Head orthogneiss (unit 5A). See text.

CTIF is characterized by both greenschist-facies and epidote-amphibolite facies assemblages, although here calcic plagioclase occurs rather than albite. The CTIF also coincides with the southernmost occurrence of actinolitic amphibole in the area. Immediately south of the CTIF, garnet appears as a stable phase in epidote amphibolite-facies assemblages.

The distribution of these assemblages thus indicates a southward increase in the grade of Grenvillian metamorphic mineral assemblages. The Grenvillian metamorphic (PT) gradient has been telescoped by foreland- (north-) directed thrusting along the Benedict and Cut Throat Island faults.

Established geothermobarometers have limited applicability to these Grenvillian assemblages. Various calibrations of the garnet-biotite geothermometer yield temperature estimates averaging between 520-630°C, while the garnet-amphibole geothermometer estimates temperatures ranging from 430-580°C, and the two-feldspar geothermometer provides significantly lower results, which cluster around 400°C. Elimination of samples lacking evidence for textural equilibrium and of those containing high Ca-Mn garnets narrows the most probable range of temperatures associated with the development of Grenvillian fabrics south of the CTIF to ca. 550 $\pm$ 30°C.

4.4 CORONITIC AND NON-CORONITIC GABBROIC ROCKS

A variety of coronitic and non-coronitic gabbroic rocks occur in the Smokey archipelago. Many of these contain variable amounts of olivine and have well-preserved igneous textures, features which distinguish them from older, more strongly recrystallized metabasites. Although somewhat diverse in their mode of occurrence, the units in question all postdate members of the WBIGC and the Bluff Head orthogneiss, and therefore are interpreted to have escaped medium- to high-grade pre-Grenvillian metamorphism. Conversely (with one possible exception, unit 11), all pre-date the Grenvillian orogeny, although Grenvillian effects on the gabbroic rocks are not always easily identifiable. Four groups of gabbroic rocks are described here. They are (1) the Michael gabbro (unit 10); (2) the Adlavik gabbro (unit 7); (3) olivine diabase (unit 11); and (4) the uncorrelated layered gabbroids of the Pottles Bay dyke (unit 12).

Coronitic textures were examined in four samples (V436, V505-2, V554-2, V740) of Michael gabbro from various locations in the study area, and in two samples (V458, V459) of the layered coronitic gabbroic Pottles Bay dyke (Fig. 2-1) and a third sample (V472) from a similar dyke west of Bluff Head. In addition, a sample (V519-2) of the non-coronitic rectiplanar olivine gabbro dyke (unit 11) extending east-southeastward from Abliuk Bight through Marks and Cut Throat Island (Fig. 2-1), was included for comparison. Only one specimen (V635-1) of the Adlavik gabbro was noted to contain olivine + plagioclase. This was examined for comparison with a specimen (V555) of coronitic Adlavik gabbro interpreted to have originally contained olivine + plagioclase (the latter is still present) sampled south of the Benedict Fault.

To facilitate comparison between these four types of gabbroic rocks, different types of coronitic textures occurring in these samples are summarized in tabular form (Table 4-17). In addition, phases interpreted as primary igneous relicts have been distinguished, and the compositions of zoned plagioclase is described in each sample.

Five types of corona textures have been distinguished among these samples. Textural types A and B (Table 4-17) are associated with well-preserved igneous textures. The remaining corona textural types (C, D, E) overprint these igneous textures, and are considered to have developed during a later period of recrystallization.

Primary igneous phases in the samples include plagioclase, clinopyroxene, orthopyroxene, olivine, biotite and ilmenite. Compositions of the mafic phases expressed in end-member components are summarized in Table 4-18. Secondary coronitic minerals include orthopyroxene and amphibole (both fibrous), and biotite in textural types A and B, and biotite, garnet, quartz, calcite, cummingtonite and hornblende in types C, D, and E. Analyses of these minerals in typical examples of each textural type of corona are presented in Appendix C.

Corona type A comprises narrow, double coronas developed between olivine and zoned plagioclase. The inner corona (adjacent to olivine) consists of colourless, fibrous hypersthene with a Mg/(Mg+Fe+Mn) ratio ranging from 0.5 to 0.65. The outer corona (adjacent to plagioclase) consists of pale green, fibrous pargasitic amphibole. The fibrous minerals in both coronas have nucleated at a high angle to the corona borders. In places, extremely fine-grained, green spinel

Table 4-17. Mineralogy of different textural types of coronitic and non-coronitic metabasites.

Sample	Igneous Phases	Corona Type	Plagioclase (mol.% An) Core	Int.	Rim
V436	pl+ilm	B,C,D,E	59	54	42
V505-2	pl+ol+cpx+ilm	A,B	63	61	31
V554-1	pl+ol+cpx+ilm	A,B	52	52	29
V740	pl+ol+cpx+ilm	A,B	55	57	40
V458	pl+ol+cpx+opx+ilm	A,B	62	54	43
V459	pl+cpx+ilm	B,C,D,E	59	58	48
V472	pl+cpx+ilm	B,C,D,E	10	10	12
V519-2	pl+ol+cpx+ilm	---	61	50	28
V555	pl+opx+cpx+bi	D,E	66	49	51
V635-1	pl+cpx+ol+opx+ilm	---	38	42	38

Corona Mineralogy

A: ol - opx (± sp) - amph - pl
B: ilm - bi - amph
C: (skeletal) ilm - bi - gt - pl
D. gt replacing pl
E. cumm - hbl; (hbl + qz ± ct) - hbl

Note: sequence from centre outwards;
igneous-appearing phases are underscored

Sample Locations:

V436, headland west of East Pompey I.;
V505-2, islet SW of Run By Guess I.; V554-1,
Indian Harbour; V740, SW corner of Ice Tickle I.;
V458 and V459, Pottles Bay dyke; V472, 1km west of
Bluff Head; V519-2, SE corner of Abliuk Bight;
V555, west side, East Pompey Island;
V635-1, 2km west of Emily Harbour.

Table 4-18. End-member compositional parameters of selected mafic igneous phases in coronitic and non-coronitic gabbroic rocks.

[1] Olivine (mol.% Fo)

V505-2	64.6
V554-1	41.9
V458	55.9
V519-2	39.4
V635-1	42.7
V740	41.4

[2] Clinopyroxene

	Wo	En	Fs
V505-2	27.3	49.0	23.7
V554-1	34.7	41.9	23.4
V458*	36.4	45.0	18.6
V458**	44.2	41.7	14.1
V459	47.7	39.2	13.1
V472	43.6	31.2	25.2
V519-2	38.2	45.8	16.0
V635-1	39.6	42.5	17.9

[3] Orthopyroxene

	Wo	En	Fs	Mg/(Mg+Fet)
V458	1.9	60.6	37.5	0.62
V555	insuff. Ca***			0.68
V635-1	1.8	59.0	39.2	0.61

* subophitic clinopyroxene
** clinopyroxene blebs in orthopyroxene
*** insufficient Ca for recalculation

hercynite?) occurs between the coronas, or scattered within the outer layer of fibrous amphibole. Mongkoltip and Ashworth (1983) described similar reaction rims in olivine gabbros in Scotland, and, by invoking a limited degree of mobility Al and Si, presented a series of balanced reactions which closely approximated the volumes of corona minerals observed in their samples. They concluded that the coronas are the result of a subsolidus olivine-plagioclase reaction that occurred during slow, retrograde cooling of the olivine gabbros. The following (balanced) reaction is inferred for the development of type A coronas:

6 olivine + 2 anorthite + 1 albite + 1 H2O =

7 orthopyroxene + 1 spinel + 1 pargasite

Corona type B consists of biotite $\pm$ amphibole mantling ilmenite, the latter commonly showing a distinctive dendritic habit. The biotite lacks the fibroradial character of type A coronas, and has a distinctive reddish-brown colour. A thin discontinuous outer shell consisting of pale green, unoriented, very fine grained amphibole is locally present. The dendritic habit of the ilmenite may imply development from a magnetite-ulvospinel solid solution, which underwent subsequent Fe removal during the development of the mantling corona phase(s). Similar biotite-mantled ilmenite has been described by Grieve and Gittins (1975). Although these authors did not present an interpretation of the texture, Esbensen (1978) described amphibole-mantled ilmenite from Norway, which he interpreted as a product of deuteric alteration during magmatic cooling. The amphiboles described in both papers are brown, the Norwegian example being a titaniferous ferropargasite, and in this regard are different from that in the present example. There is no apparent means to ascertain whether the biotite mantling ilmenite in

the Michael gabbro is a late magmatic phase or records an influx of K-bearing metasomatic fluids. Emslie (1983) implied that reddish-brown biotite in the gabbro is an igneous phase.

Corona type B, which has an outer rim of scattered garnets, also differs from type C in the habit of biotite. In the former corona type, biotite occurs as a continuous, reddish-brown rind on the ilmenite; in the latter, biotite forms discrete, medium-grained unoriented brown flakes. In places, subidiomorphic garnets are scattered at the outer margin of the biotite-rich shell. Garnets also occur enclosed by zoned plagioclase, or along the interface between plagioclase and hornblende + quartz symplectites. Both occurrences comprise a second category of overprinting texture (type D). Similar textural occurrences of garnet in metagabbros have been described by Barink (1984), who suggested that the garnet-forming reaction was synchronous with the replacement of clinopyroxene by hornblende + quartz, and proceeded by the solid solution reaction:

H2O+cpx'+hbl'+plag'+Fe-Ti oxides' = gt+cpx"+hbl"+plag"+
Fe-Ti oxides"+qz

where (') and (") indicate different compositions of the same solid solution minerals on either side of the equation.

A broadly similar type of coupled reaction may be invoked for the coronites from Smokey, although there is no evidence for the secondary formation of clinopyroxene.

Garnets in textural types C and D show a restricted compositional range both within and between samples. In the Michael gabbro and the Pottles Bay dyke (and similar layered dykes west of Bluff Head), the garnets are almandine-

(55-66%)) and grossular- (15-28%) rich, with lesser quantities of pyrope (10-15%) and minor spessartine (1-7%) (Appendix C). Presumably, both garnetiferous textural types (C and D) developed under similar conditions, possibly contemporaneously. In contrast to the restricted range of garnet compositions shown by the Michael gabbro and the Pottles Bay dyke, a sample (V555) of coronitic Adlavik gabbro (unit 7) from East Pompey Island contains rare subidiomorphic garnets markedly richer in pyrope (32%) with lesser almandine (54%) and grossular (11%) contents, and similar amounts of spessartine (3%) (Appendix C). Compositional contrasts of the garnets in V555 versus those in the other samples probably reflect bulk rock compositional control, given the textural similarity in these samples.

Corona type E comprises amphibole-rich patches, in which colourless aggregates of cummingtonite are mantled by green hornblende. Individual grains of cummingtonite in the core of these aggregates commonly have hornblende mantles. Elsewhere, green hornblende grains and grain aggregates enclose intergrowths of quartz + hornblende $\pm$ calcite. In the literature, cummingtonite has been observed to have replaced both orthopyroxene (Austrheim and Robins, 1981) and olivine (Mongkoltip and Ashworth, 1983). In the present study, both primary and secondary orthopyroxene are in a pristine state of preservation in coronites with one exception (V555). Sample V555 contains subophitic orthopyroxene mantled by cummingtonite. In the other samples, however, cummingtonite is interpreted to have formed at the expense of olivine prior to being partly resorbed by hornblendic amphibole. This texture has been noted in a layered, coronitic gabbro dyke west of Bluff Head (sample V471) and in the

Michael gabbro (V436). Patches of hornblende intergrown with quartz ± calcite are interpreted to have developed at the expense of clinopyroxene.

The significance of garnets in coronitic gabbros is somewhat controversial. Although generally regarded as indicating moderate or high pressure conditions (see below), it is possibly also sensitive to bulk-rock compositional parameters, particularly oxidation ratios (Emmett, 1982). In this context, it is interesting to note that garnets are absent in type A coronas. The restriction of garnets to two of the three overprinting corona types (C and D) may be significant. Grieve and Gittins (1975) noted that garnetiferous orthopyroxene-amphibole coronas were restricted to samples showing "a high degree of corona development" (Ibid., p. 298), implying samples which had been significantly hydrated. Such may be the case in the present example; type C and E coronas do not occur in the same samples characterized by orthopyroxene - amphibole reaction rims (type A).

The various corona textures, particularly type A, outlined above, correspond with relatively low pressure ($\leq$ ca. 5kbar) corona gabbros described in the literature, and are consistent with the descriptions given by Emslie (1983) for occurrences of Michael gabbro in the general vicinity of the study area. With higher total pressure or lower P(H2O), clinopyroxene, and subsequently garnet, occurs in or near the outer amphibole shell in these coronas. Pressure estimates for two-pyroxene ± spinel and garnet double and triple reaction rims separating olivine and plagioclase range from ca. 6kb to >8kbar (Johnson and Essene, 1982). In this regard, it is interesting to note that Emslie (1983) observed the progressive development of type A coronas from an early stage of (1) hypersthene - intergrown clinopyroxene + amphibole - fine garnet, to (2) olivine-free (replaced

by the inner corona) hypersthene - clinopyroxene ± orthopyroxene ± amphibole - sodic plagioclase - coarse garnet coronas southward from the Grenville Front. This transition in corona types may be inferred to record an increase in pressure towards the interior of the orogen.

The following observations summarize salient features of coronitic and non-coronitic gabbroic rocks in the study area:

(1) similar coronitic textures are found in diverse gabbroids in domain G, including massive dykes with well-defined chilled margins (the Michael gabbro), and layered gabbroids lacking chilled margins (the Pottles Bay dyke);

(2) coronitic rocks are restricted to the region (domain G) south of the CTIF; non-coronitic equivalents of (e.g.) the Adlavik gabbro (unit 7) occur farther to the north;

(3) the main period of coronite development was succeeded by further recrystallization, characterized by the formation of garnet in plagioclase, and the variable development of relatively sodic plagioclase.

Observation (1) suggests that the double coronas separating plagioclase and olivine did not develop during cooling of the gabbros immediately following crystallization (e.g. Sorensen, 1978) since it would be rather fortuitous for these diverse gabbroic rocks of varying ages to have all been intruded at crustal levels (and therefore PT conditions) conducive to the development of type A coronas. Rather, these coronas (e.g. textural types A and B) probably developed during regional cooling of the crust now exposed south of the CTIF (observation 2).

Overprinting textures (types C, D, E; observation 3) may have developed in response to Grenvillian metamorphism. However, the absence of oriented mineral

fabrics in the coronites precludes the possibility of making correlations with structural events recorded in the relatively ductile rocks enclosing the gabbroids. Such an interpretation is consistent with the metamorphic grade associated with Grenvillian metamorphism in the southern part of the study area; alternatively, it is also consistent with the passive retrogression of the WBIGC described in section 4.2. Perhaps most significant to the model of Grenvillian tectonothermal activity in the area is the observation that the coronites are restricted to domain G, which coincides with medium-pressure Grenvillian parageneses. This is consistent with the portrayal of the CTIF as a thrust fault which has exhumed deeper crustal levels in the interior of the Grenville Province against lower grade rocks farther to the north.

4.5 AGE OF METAMORPHISM AND RELATIONSHIPS BETWEEN THE PRE-GRENVILLIAN LITHOSTRUCTURAL DOMAINS

On the basis of field observations alone, the conclusions which may be drawn concerning the age of pre-Grenvillian metamorphism in the study area are rather limited. In contrast, however, features developed during different phases of the Grenvillian orogeny are readily distinguished in the field, and relations between Grenvillian structural domains M, T and G are relatively well understood and form the basis for a rather simple thrusting model (see sections 3.3.3, 4.3.6) for the late tectono-metamorphic evolution of this portion of the Grenville Front zone.

The age of Grenvillian metamorphism has not been directly (i.e. isotopically) dated in the present study. However, it is clear that metamorphism coincident with deformational events GD1, GD2 and GD3 occurred after ca. 1.4Ga, the approximate age of intrusion of the Michael gabbro, and may be attributed to the Grenvillian orogeny. This is supported by a K-Ar (muscovite) age of ca. 917 $\pm$ 11Ma (927Ma using Steiger and Jager's, 1977, decay constant) for a "granite gneiss" (unit 3B?) from Mundy Island (Grasty et al., 1969). Although south-dipping shear zones transecting the Michael gabbro and its host rocks may readily be identified as Grenvillian features, problems are encountered when interpreting metamorphic mineral assemblages lacking a preferred dimensional orientation which can be readily correlated with a specific deformational event.

Relationships between the three pre-Grenvillian lithostructural domains are not fully understood. This results largely from the masking of early tectono-

metamorphic features by the heterogeneous development of Grenvillian fabrics, particularly in the southern part of the study area, and from a paucity of good exposure in areas critical to the interpretation of these domains (e.g. along their margins).

Particularly problematic is the age of pre-Grenvillian amphibolite-facies metamorphism. Amphibolite-facies assemblages occur in all three lithostructural domains, and include: (1) passively-retrogressed members of the WBIGC; (2) the Bluff Head orthogneiss; and (3) the Makkovik trend in the BMIS.

Before addressing these specific examples, it is worthwhile to summarize the data available for the pre-Grenvillian domains. The following arguments center first on the relations between the development of the Makkovik trend in the BMIS and the passive retrogression of the WBIGC, then on relations between the BMIS and gneisses of the Groswater Bay Terrane, and finally on the early metamorphic history of the WBIGC and the Bluff Head orthogneiss.

Contact relationships demonstrate that high-grade metamorphism of the WBIGC predates the Benedict Mountains Intrusive Suite, and therefore also predates the Makkovik trend fabrics developed in the Suite. The upper age limit of the Makkovik trend in the BMIS is constrained by the ca. 1.9Ga Rb-Sr isotopic ages determined for jotunitic and dioritic-tonalitic gneisses of the WBIGC, while the lower age limit is constrained by the ca. 1.6 Ga age determined for discordant bodies of layered ferrodiorites-ferrosyenites (unit 9) (see section 2.8.1), and may be approximated by the isotopic age (ca. 1.8Ga; section 2.8.2) determined for the synkinematic (?) quartz monzodiorite-granodiorite (unit 6A) of the BMIS.

Passive retrogression of the WBIGC formed middle amphibolite-facies mineral assemblages in mafic rocks (e.g. hornblendic amphibole + oligoclase ± biotite) similar to those preserved in mafic enclaves outlining the Makkovik trend in the BMIS. In most cases, however, retrogression of the granulites shows no apparent relation to the Makkovik trend. Indeed, the WBIGC, as outlined in Figure 3-1, shows an east-west orientation, oblique to the Makkovik trend, and there is no evidence that this orientation may be due to rotation of the granulites en masse during the Grenvillian orogeny.

Translation of early fabrics into parallelism with the Makkovik trend may have occurred in small (cm- to hm-scale) enclaves. This is consistent with the preferential development of the Makkovik trend along ~1km wide north-northeast trending belts in the BMIS in the northern portion of the study area.

In certain cases, gneissic fabrics in rocks correlated with the WBIGC parallel the Makkovik trend. The sporadic occurrence of (quartz) diorite gneiss inclusions (unit 2) in the BMIS between Fairy Island and Cape Rouge support the correlation of dioritic gneiss at the latter locality with similar gneisses (unit 2) within the WBIGC. This correlation is further supported by the similarity in the isotopic composition of dioritic gneiss from Cape Rouge (sample V774) with samples of unit 2 from the WBIGC (see Fig. 2-5, and Table A-3, Appendix A.3). The dioritic gneiss at Cape Rouge occurs as a 0.5km-wide enclave in foliated biotite granite (unit 6E) of the BMIS. The internal gneissic foliation of the enclave parallels the north-northeast trending fabric of the granite. Small (<50cm long), gneissic and non-gneissic mafic enclaves in the granite at this locality contain the assemblage hornblende + oligoclase ± biotite, identical to

large dioritic gneiss enclave. In this case, the present mineralogy of the dioritic gneiss (but not the gneissic fabric itself) and the orientation of the large gneissic enclave may be attributed to the development of the Makkovik trend in the granite.

The similarity of the metamorphic grade between retrogressed members of the WBIGC and the metabasites outlining the Makkovik trend suggests that early high-grade assemblages were, at least locally, retrograded to middle amphibolite-facies during the development of the NNE-trending fabric in the BMIS. It is not certain whether the progressive passive retrogression of the WBIGC westward across the study area may be wholly attributed to this event, however. Resolution of this problem should focus on the isotopic dating of various minerals, in particular amphiboles, from foliated and massive portions of both domains.

The predominance of GF1 folds near Bluff Head underscores the extent of Grenvillian reworking of gneissic rocks in this portion of the Groswater Bay Terrane. The degree of Grenvillian recrystallization of these gneisses is further emphasized by the similarity of metamorphic temperature estimates for the Bluff Head orthogneiss (ca. 500°C) compared with those determined for Grenvillian fabrics developed elsewhere in domain G (ca. 550 $\pm$ 30°C; see section 4.3.8). Pre-Grenvillian features critical to an understanding of the relationship between this domain, the BMIS, and the WBIGC have thus been obscured during the Grenvillian orogeny. The relationship between the Bluff Head orthogneiss and the BMIS will be considered first.

Contact relations between the BMIS and the Groswater Bay Terrane are

masked in the vicinity of Bluff Head by the development of Grenvillian structures. Furthermore, the isotopic ages determined for orthogneiss of the Groswater Bay Terrane and foliated to massive plutonic rocks of the BMIS overlap in the range 1680-1610Ma (see section 1.3). Although the Bluff Head orthogneiss has not been isotopically dated, the similarity of these rocks compared with orthogneisses elsewhere in the Groswater Bay Terrane support their correlation, and the gneisses near Bluff Head are inferred to have a similar "age".

It is difficult to reconcile the overlapping isotopic ages determined for the Groswater Bay Terrane orthogneisses and the BMIS without (1) invoking significant resetting of older isotopic ages (thus far undetermined) in the Groswater Bay Terrane orthogneisses to give the determined age of ca. 1680-1610Ma, or (2) envisioning a major fault between the two terranes. Insufficient data are available to conclusively demonstrate the first possibility, and evidence for a major fault is lacking. Contrasts in the fabrics noted between narrow (up to 100m-wide) bands of schistose megacrystic granodiorite (unit 6A) within the granodioritic gneiss (unit 5A) near Bluff Head strongly suggest that the granodiorite postdates the gneissic fabric-forming event characterizing the enclosing rocks, although intrusive contacts have not been observed. It is therefore inferred that the Bluff Head orthogneiss (and orthogneisses of the Groswater Bay Terrane in general) were metamorphosed prior to the emplacement of the BMIS, but were subsequently isotopically reset at ca. 1.65Ma.

The relationship between the gneissic fabrics characteristic of the Bluff Head orthogneiss and the WBIGC is also unclear: are they both related to a single, common tectono-metamorphic episode, or does each gneissic domain have a

separate, unrelated, early orogenic history? Few lithologic correlations between the two domains are presently known. For instance, although charnockite (unit 3A?) at Bluff Head (see Fig. 2-1) contains relict, coronitic textures indicating retrogression, the mineral assemblage garnet + clinopyroxene forming at the expense of orthopyroxene and plagioclase noted in this charnockite is texturally and mineralogically dissimilar to retrograded jotunite-charnockite (unit 3B) within the WBIGC. More comparable is the isolated presence in both domains of pre-migmatitic hornblende + biotite + microcline $\pm$ plagioclase-bearing "metabasites" containing clinopyroxenes of similar composition (Table 4-19). The significance of these "metabasites" warrants their description in some detail.

Examples of these "metabasites" have been identified on the southwest corner of Mundy Island (in the WBIGC) and approximately 4km northeast of Bluff Head (in the Bluff Head orthogneiss). In both cases, the metabasites are pre-migmatitic, occurring as boudinaged, discontinuous layers attenuated parallel to the gneissic fabric of the host rocks, and infiltrated by leucosomes from the same.

The host rock of the Mundy Island occurrence is retrograded jotunitic gneiss (unit 3B), which forms a swath extending through Mundy Island to Run By Guess Island. A characteristic of this band of retrograded jotunitic gneiss is the presence of meter-scale, green-brown patches of unretrograded material in which metamorphic orthopyroxene $\pm$ clinopyroxene is preserved. This latter observation demonstrates (1) that granulite facies was attained, and (2) that the gradation from granulite-facies gneisses (particularly in the White Bear Islands) to amphibolite-facies gneisses farther to the west in the WBIGC records retrogression

Table 4-19. Bulk rock and clinopyroxene compositions from pre-migmatitic metabasites from the Granulite Complex (sample V132-2) and the Bluff Head orthogneiss (sample V463).

	V132-2		V463	
	Bulk Rock	CPX	Bulk Rock	CPX
SiO2	49.4	54.28	50.5	54.06
TiO2	0.49	0.01	0.59	0.03
Al2O3	10.9	1.18	11.9	1.26
Cr2O3	nd	0.09	nd	0.02
FeO*		5.88		6.92
Fe2O3**	9.80		9.52	
MnO	0.23	0.32	0.17	0.28
MgO	13.83	14.99	11.05	14.05
CaO	6.68	22.23	11.12	22.33
Na2O	0.82	0.55	2.07	0.61
K2O	4.45	0.01	2.22	0.00
P2O5	0.09	nd	0.19	nd
LOI	1.36	nd	1.06	nd
total	99.05	99.54	100.39	99.56
Si		2.002		2.003
Alvi		0.053		0.058
Ti		0.000		0.001
Cr		0.003		0.001
*Fe2+		0.181		0.215
Mg		0.824		0.776
Mn		0.010		0.009
Ca		0.879		0.887
Na		0.039		0.044
K		0.000		0.000
Mg/(Mg+Fe)		0.819		0.783
Mol.%				
Jadeite		4.43		4.02
Ti-Tschermak		0.08		0.03
Ca-Tschermak		0.48		0.55
Wollastonite		44.49		44.00
Enstatite		39.20		41.60
Ferrosilite		11.28		9.66

* all Fe as Fe2+ in clinopyroxene analyses
** all Fe as Fe3+ in whole rock analyses
Note: each clinopyroxene analysis is the average of 9 analyses (3 analyses performed on 3 different grains).

and hydration rather than a primary metamorphic gradient. The pre-migmatitic nature of the clinopyroxene-bearing metabasites identified on Mundy Island is thus taken as evidence that these metabasites recrystallized under granulite facies conditions, despite the absence of orthopyroxene in the samples studied. It is worth noting in this regard that pre-migmatitic metabasites containing clinopyroxene + biotite occur in the same outcrops as two-pyroxene + biotite-bearing metabasites elsewhere in the WBIGC.

The metabasite sample (V132-2) from the WBIGC at Mundy Island contains the assemblage hornblende + microcline + biotite + clinopyroxene. The rock is melanocratic, with a colour index of ~85. Clinopyroxene (<5%) occurs as relict cores enclosed by green hornblende.

The pre-migmatitic metabasite sampled north of Bluff Head contains the same assemblage, but also includes plagioclase (An21). The rock is more leucocratic (colour index ~ 55). Clinopyroxene in this sample (V463) is relatively abundant (~15%), and occurs in the cores of green amphibole grains.

Analyses of the bulk composition of the metabasites and their clinopyroxenes are presented in Table 4-18. Note the compositional similarity of the clinopyroxenes in both samples.

Although these clinopyroxene- and microcline-bearing metabasites may well be correlated on the basis of their distinctive mineralogy and their occurrence as pre-migmatitic layers alone, it is not necessary for the present argument to demonstrate that they belong to the same suite of early mafic dykes. Indeed, the differing Na2O and CaO contents of the metabasites might be considered

evidence that these rocks are not correlative.

What is significant with regard to the early metamorphic history of the WBIGC and the Bluff Head orthogneiss is that both domains contain pre-migmatitic metabasites with metamorphic clinopyroxenes of very similar composition. This evidence supports-but does not prove given the control of oxygen fugacity on clinopyroxene compositions (Spear, 1981)-the conclusion, preferred here, that both domains shared an early, common tectono-metamorphic history. Indeed, it is plausible that the Bluff Head orthogneisses may originally have contained granulite facies assemblages, subsequently wholly retrograded to amphibolite facies.

CHAPTER 5
DISCUSSION AND CONCLUSIONS

Many of the controversial aspects of Grenvillian geology have arisen as a consequence of problems common to polymetamorphic terranes, in particular, those concerning the age and grade of metamorphic events and the extent of structural, metamorphic and isotopic reworking during the younger orogeny.

The key to interpreting the effects of the Grenvillian orogeny lies in the distinction between Grenvillian and pre-Grenvillian tectono-metamorphic features, a distinction achieved in eastern Labrador by using the Neohelikian Michael gabbro as a time marker. To this end, it is worthwhile to summarize briefly the findings described in Chapters 1 to 4.

This study has focussed on four key aspects of the geology of the Smokey archipelago: (1) the stratigraphy of pre-Grenvillian gneissic and intrusive rocks; (2) pre-Grenvillian and Grenvillian structures; (3) pre-Grenvillian and Grenvillian metamorphism; and (4) the absolute age of key lithologies.

The zonal distribution of Grenvillian S- and L-S fabrics and associated metamorphic mineral assemblages noted in a north to south transect provides the basis for the structural subdivision of the study area. The Grenvillian structural domains are separated by two major east- to southeast-trending, south-dipping high-strain zones. The more northerly high-strain zone is the Benedict Fault, which coincides with the Grenville Front in eastern Labrador; the other major high-strain zone is the Cut Throat Island Fault (CTIF), which occurs some 3km to the south of the Benedict Fault.

The northern domain (domain M) locally contains Grenvillian shear zones

with greenschist-facies assemblages. A transitional domain (domain T), between the Benedict and Cut Throat Island faults, is characterized by garnet-free, greenschist- to lower amphibolite facies assemblages, whereas in domain G, immediately to the south of the CTIF, garnetiferous epidote amphibolite- to lower amphibolite-facies assemblages characterize Grenvillian L-S fabrics. Both greenschist and garnet-free epidote amphibolite-facies assemblages occur along the Benedict and Cut Throat Island Faults. Contrasting assemblages and compositions of metamorphic minerals associated with Grenvillian fabrics in domains M, T and G indicate that these faults are metamorphic breaks. Both faults are interpreted as thrusts, which have telescoped the southward-increasing Grenvillian metamorphic gradient. Temperature estimates in domain G suggest that Grenvillian metamorphism occurred at ca. 550 $\pm$ 30°C. The compositions of amphiboles associated with Grenvillian fabrics to the north of the CTIF are indicative of low-pressure metamorphism, whereas amphiboles to the south of the CTIF are indicative of medium-pressure metamorphism. The characterization of the areas to the north and south of the CTIF as regions of relatively low- and high-pressure Grenvillian metamorphism, respectively, is supported by the restriction of garnetiferous parageneses to domain G.

Grenvillian fabrics overprint a variety of relatively high-grade, pre-Grenvillian fabrics typifying three pre-Grenvillian lithostructural domains identified in the area. Two of these domains (the White Bear Islands Granulite Complex (WBIGC) and the Bluff Head orthogneiss) are dominated by medium- to high-grade gneissic rocks, while the third (the Benedict Mountains Intrusive Suite (BMIS)) is characterized by foliated to gneissose granitic rocks.

The highest grade rocks are found in the WBIGC, which demonstrably predates the BMIS. The WBIGC is postulated to share a common early structural-metamorphic history with the Bluff Head orthogneiss since both domains locally contain distinctive microcline-bearing, pre-migmatitic metabasites with very similar compositions of clinopyroxene. A unique set of PT determinations for peak metamorphism of the WBIGC could not be determined. Relatively high PT estimates of 830-860°C and 7-8Kbar were derived using the two-pyroxene geothermometer and the pressure-sensitive nature of of alumina solubility in orthopyroxene coexisting with garnet. Relatively low PT estimates of ca. 685°C and 4.6Kbar were determined using the garnet-orthopyroxene (-plagioclase-quartz) geothermobarometer. If the higher PT estimates are valid, then pre-Grenvillian retrogression of the WBIGC occurred some 150°C and 2Kbar less than the granulite-facies event, and probably records diachronous metamorphism in the area. If the lower PT estimates are valid, then retrogression of the WBIGC did not follow profound cooling and uplift of the granulites, but rather involved significant hydration only, and may be a late manifestation of the granulite-facies event. Granulite-facies metamorphism in the area was probably achieved under conditions intermediate between both sets of estimates.

Retrogression of the WBIGC occurred at conditions estimated at ca. 650$\pm$ 50°C and 5.5 $\pm$ 1.5Kbar, prior to the development of Grenvillian L-S fabrics. In contrast, the few mineral assemblages useful as geothermometers in the Bluff Head orthogneiss yield temperature estimates of ca. 500°C, closely comparable to estimates of Grenvillian metamorphic temperatures in the southern portion of the study area. These temperature estimates indicate that the garnet-biotite and two-

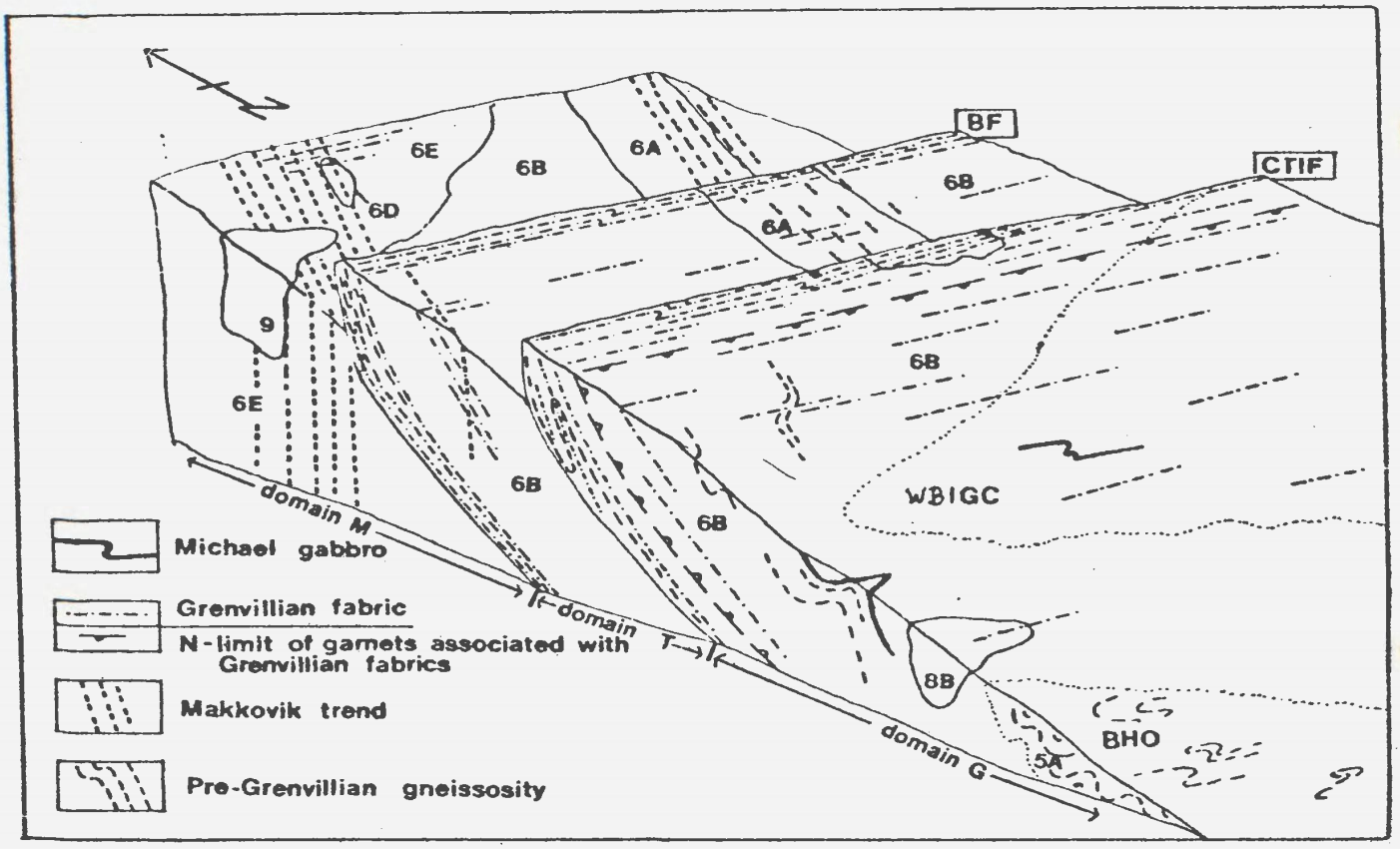

Figure 5-1. Block diagram summarizing salient geological features of the Smokey archipelago. Indicated are: the Benedict Fault (BF), the Cut Throat Island Fault (CTIF), the approximate boundaries of the White Bear Islands Granulite Complex (WBIGC) and the Bluff Head orthogneiss (BHO), and the approximate distribution of major rock units, identified by their respective unit numbers.

feldspar assemblages used for the temperature determinations crystallized during the Grenvillian orogeny.

The Grenville Front on the Labrador coast thus may be portrayed as a zone of polyphase, heterogeneous structural overprinting and retrogression of higher grade, pre-Grenvillian fabrics. Foreland-directed thrusting occurred along two major high-strain zones, which juxtapose crustal blocks of contrasting metamorphic grade and Grenvillian fabric development. Key features of the Grenville Front at Smokey are portrayed in a block diagram in Figure 5-1. This model is broadly consistent with the general features of the Grenville Front summarized earlier (see section 1.3), particularly with regard to the characteristic association of south-dipping thrust faults in the Grenville Front zone.

The model for the Grenville Front in eastern Labrador presented here has several features in common with the Front as described elsewhere, particularly at Coniston, Ontario (LaTour, 1979, 1981; see section 1.3). These include the following salient points:

(1) the Grenville Front coincides with major high-strain zones;

(2) these high-strain zones were active during the Grenvillian orogeny

(3) the high-strain zones represent metamorphic as well as structural breaks;

(4) crustal blocks characterized by medium-grade Grenvillian mineral assemblages have been thrust over crustal blocks containing low-grade mineral assemblages.

The latter point is particularly significant. At neither location is there

evidence suggesting that the faults defining the Grenville Front have developed by profound differential uplift of the crust. These faults, although associated with sufficient reverse dip-slip displacement to juxtapose rocks of discernably different metamorphic grade, probably have relative vertical displacements of no more than a few kilometers. Unfortunately, resolution of geobarometers in both areas is insufficient to make any but the most general estimates in this regard. It must be emphasized that late Grenvillian (e.g. ~post-peak metamorphic) reverse motion along the faults is responsible for the telescoping of the Grenvillian metamorphic gradient, and hence the coincidence of the high strain zones with metamorphic discontinuities. Peak Grenvillian metamorphism may be attributed to earlier foreland-directed translation along these thrust faults (or other thrusts farther to the south), which led to crustal thickening and metamorphism at depth. In this regard, the Lake Melville Terrane, which was thrust northwards along the Grenvillian Rigolet thrust zone (Gower and Owen, 1984), is likely responsible for the Grenvillian metamorphic gradient in the Smokey area.

With regard to the separation of Grenvillian from pre-Grenvillian features, the Smokey area, unlike Coniston, is fortuitously graced with a widespread and easily identifiable intrusive time marker, the Michael gabbro. These dykes place a lower age of ca. 1.4Ga on any structures deforming them. Three phases of deformation attributable to the Grenvillian orogeny have been identified from locally-occurring refolded folds, and, together with a comparison of metamorphic mineral assemblages in a north to south transect across the area, provide a broad geological data base for tracing the evolution of the Grenvillian orogeny in this area. Early Grenvillian folds (GF1), which are north-verging near the CTIF, were

deformed about south-southeast-plunging axes during the main phase (GD2) of reverse-movement along the Benedict and Cut Throat Island Faults. Whether either or both faults developed during GD1 is unclear, although this remains a possibility. These faults did not develop along pre-Grenvillian structures; the lineated schistose to mylonitic fabric associated with both faults overprints north- to northeast-trending pre-Grenvillian fabrics of the Makkovik Province. Late dextral shear (GD3) along both faults appears to be limited to a hectometer-scale at most. Thus, the portrayal of the Grenville Province as a broad zone of dextral shear (e.g. Baer, 1977) does not apply to this area.

Comparing Gower and Owen's (1984) regional-scale subdivision of eastern Labrador with the tectonic model of the Grenville Province proposed by Rivers and Chown (in press), the Benedict Mountains Intrusive Suite (BMIS) north of the Benedict Fault constitutes an autochthonous terrane. The BMIS south of the Benedict Fault, together with the Groswater Bay Terrane (including the Bluff Head orthogneiss and the WBIGC in the Smokey archipelago) comprise the parautochthon in this scheme, and the Lake Melville Terrane may constitute an allochthon, although insufficient data are presently available from this area to justify direct analogy with the allochthons identified in western Labrador.

It is interesting to speculate whether the preservation of pre-Grenvillian K-Ar isotopic ages in mafic dykes from the Mealy Mountains anorthosite massif, which led Emslie (1983) to suggest that Grenvillian metamorphism in this area is of low-grade, constitutes evidence for the late Grenvillian tectonic emplacement of these plutonic rocks. In a recent contribution, Emslie et al. (1984) presented new K-Ar (hornblende) isotopic data for gabbro and amphibolite from the Mealy

Mountains indicating that regional heating in this area did not exceed 535 $\pm$ 45°C after ca. 1.40-1.53Ga B.P. Nonetheless, Grenvillian K-Ar isotopic ages of 951Ma and 955-964Ma were determined for hornblende from the deformed and faulted amphibolite country rock of the massif, and for biotite separated from the medium-grained interiors of thick mafic dykes in the massif, respectively. Emslie et al. (1984) note that latter (biotite) ages need not imply significant regional heating during the Grenvillian orogeny, but probably record cooling through an argon blocking temperature of ca. 300°C in this mineral. Emslie et al. (1983) suggestion that the 951Ma hornblende age records the effects of frictional heating in the fault zone, but allows that rocks northeast of the fault were metamorphosed to temperatures exceeding 535°C prior to the Grenvillian orogeny.

Emslie et al.'s (1983) isotopic data suggest that the tectonic model of Rivers and Chown (in press) may apply to eastern, as well as to western Labrador. The retention of pre-Grenvillian K-Ar (hornblende) ages from rocks intruded by the Mealy dykes suggests that the Mealy Mountains massif is allochthonous, and was not implicated in the widespread effects of Grenvillian orogenesis noted farther to the northeast. The Mealy Mountains massif was probably emplaced to its present position during the Grenvillian orogeny.

Summarizing the features described above, the northern part of the Grenville Province in eastern Labrador is characterized by:

(1) a boundary dominated by foreland-directed Grenvillian thrust faults, which juxtapose parautochthonous rocks comprising crustal slabs metamorphosed at ca. 1.0Ga against correlatable rock units lacking a pervasive Grenvillian tecotonothermal imprint in the Foreland zone;

(2) a telescoped Grenvillian metamorphic gradient, spanning greenschist facies in the Foreland zone to amphibolite facies in parautochthonous domains south of the Front;

(3) the presence of relatively high-grade pre-Grenvillian metamorphic mineral assemblages variably overprinted and/or retrogressed by Grenvillian tectono-metamorphic activity;

(4) the presence of discrete thrust-bound domains (allochthons) in the interior of the Grenville Province, comprising rocks of distinctive metamorphic grade, lithology, structural orientations, and gravity and aeromagnetic signature.

Together, these features are indicative of a prolonged orogenic history in the Grenville Province. LaTour (1979), who reviewed the principal tectonic models proposed for the Grenvillian orogeny (e.g. Wynne-Edwards, 1972, 1976; Dewey and Burke, 1973; Baer, 1976, 1977), concluded that the data base at Coniston could not adequately favour or contradict any particular model. The same conclusion applies to the present study, principally due to the restricted size of the area investigated. Perhaps most significant, however, is the portrayal of the Grenville Front in western Labrador, at Smokey, and at Coniston as a well-defined zone of thrusting. Together with the recent identification of allochthonous terranes in the interior of the orogen, this provides evidence of significant crustal thickening during the Grenvillian orogeny. Such features are characteristic of the margins of orogenic belts, and are a key component of the plate tectonic models currently being applied to various Phanerozoic mobile belts.

REFERENCES

Abbey, S. (1970): Analysis of rocks and minerals by the A.A.S., Geol. Surv. Can. Bull 1968.

Ahmad, R. and Wilson, C.J.L. (1982): Microstructural relationships of sillimanite and "fibrolite" at Broken Hill, Australia. Lithos 15, 49-58.

Allaart, J.H. (1976): Ketilidian mobile belt of West Greenland. In Geology of Greenland (A. Escher and W.S. Watt, eds.). Gronlands Geologiske Undersogelse, pp. 120-151.

Archibald, D., and Farrar, E. (1979): 40Ar/39Ar mineral ages from the Walker-Benedict granodiorite, Central Mineral Belt, Labrador. Department of Mines and Energy, Newfoundland and Labrador, unpublished report, 12 pp.

Armbruster, T., and Bloss, F.D. (1980): Channel CO2 in cordierites. Nature 286, 140-141.

Austrheim, H., and Robins, B. (1981): Reactions involving hydration of orthopyroxene in anorthosite-gabbro. Lithos 14, 275-281.

Baer, A.J. (1976): The Grenville Province in Helikian times: a possible model of evolution. Phil. Trans. R. Soc. Lond. A. 280, 499-515.

Baer, A.J. (1977): The Grenville Province as a shear zone. Nature 267, 337-338.

Baker, D.J. (1980): The metamorphic and structural history of the Grenville Front near Chibougamau, Quebec. Unpublished PhD thesis, Univer sity of Georgia.

Barink, H.W. (1984): Replacement of pyroxene by hornblende, isochemically balanced with replacement of plagioclase by garnet, in a metagabbro of upper-amphibolite grade. Lithos 17, 247-258.

Bell, T.H. (1978): Progressive deformation and reorientation of fold axes in a ductile mylonite zone; the Woodroffe thrust. Tectonophysics 44, 285-320.

Binns, R.A. (1965): The mineralogy of metamorphosed basic rocks from the Willyama complex, Broken Hill district, New South Wales, Parts 1 and 2. Min. Mag. 35, 306-326, 561-587.

Bohlen, S.R., and Essene, E.J. (1979): A critical evaluation of two-pyroxene thermometry in Adirondack granulites. Lithos 12, 335-345.

Bohlen, S.R., and Essene, E.J. (1980): Evaluation of coexisting garnet-biotite, garnet-clinpyroxene, and other Mg-Fe exchange thermometers in Adirondack granulites: Summary. Geol. Soc. Am. Bull. 91, 107-109.

Bowen, N.L. (1940): Progressive metamorphism of siliceous limestone and dolomite. J. Geology 48, 225-274.

Brooks, C. (1982): Supplement to the third report on the geochronology of Labrador. Unpublished report to the Dept. of Mines and Energy, Newfoundland and Labrador, 23pp.

Brooks, C. (1983): Fourth report on the geochronology of Labrador. Unpublished report to the Dept. of Mines and Energy, Newfoundland and Labrador, 42pp.

Brooks, C., Hart, S.R., and Wendt, I. (1972): Realistic use of two-error

regression treatments as applied to rubidium-strontium data. Reviews of Geophysics and Space Physics 10, 551-577.

Brown, E.H. (1977): The crossite content of Ca-amphibole as a guide to pressure of metamorphism. J. Petrol. 18, 53-72.

Bryant, B. and Reed, J.C. (1969): Significance of lineation and minor folds near major thrust faults in the southern Appalachian and the British and Norwegian Caledonides. Geol. Mag. 106, 412-429.

Buddington, A.F. (1965): The origin of three garnet isograds in Adirondack gneisses; Mineral. Mag. 34, 71-81.

Buddington, A.F. (1966): The occurrence of garnet in the granulite-facies terrane of the Adirondack highlands-a discussion. J. Petrology 7, 331-335.

Busch, W., Schneider, G., and Mehnert, K.R. (1974): Initial melting at grain boundaries. Part II. Melting in rocks of granodioritic, quartzdioritic, and tonalitic composition. N. Jb. Miner. Mh. v. 8, 345-370.

Calon, T.J., and Hibbs, D.C. (1980): Structure of an area along the boundary of the Letitia Lake Group and Seal Lake Group, Central Labrador. in C.F. O'Driscoll and R.V. Gibbons (eds.) Current Research, Dept. of Mines and Energy, Newfoundland and Labrador, Report 80-1, p. 177-181.

Chinner, G.A. (1960): Pelitic gneisses with varying ferrous/ferric ratios from Glen Clova, Angus, Scotland. J. Petrology 2, 312-323.

Chown, E.H. (1984): Mineralization controls in the Aphebian formations, Chibougamau, Mistassini and Otish areas. in Chibougamau-Stratigraphy

and Mineralization. Can. Instit. of Mining and Metallurgy, Spec. Vol. 34, p. 229-243.

Church, W.R. (1978): Eclogite-bearing amphibolites from the Appalachian mobile belt, northwest Newfoundland: dry versus wet metamorphism: a discussion. J. Geology 86, 655-659.

Clark, A.M.S. (1979): Proterozoic deformation and igneous intrusions in part of the Makkovik Subprovince, Labrador. Precambrian Res. 10, 95-114.

Daignault, R., and Allard, G.O. (1984): Evolution tectonique d'une portion du sillon de roches vertes de Chibougamau. in Chibougamau-Stratigraphy and Mineralization. Can. Instit. of Mining and Metallurgy, Spec. Vol. 34, p. 212-228.

Dallmeyer, R.D. (1974): The role of crystal structure in controlling the partitioning of Mg and Fe2+ between coexisting garnet and biotite. Am. Mineral. 59, 201-203.

Dallmeyer, R.D., and Rivers, T. (1983): Recognition of extraneous argon components through incremental-release 40Ar/39Ar analysis of biotite and hornblende across the Grenvillian metamorphic gradient in southwestern Labrador. Geochim. Cosmochim. Acta 47, 413-428.

Daly, R.A. (1902): The geology of the northeast coast of Labrador. Bulletin of the Museum of Comparative Zoology, Harvard Univ., v. 38. Geol. Ser., v. 5, Nr. 5, p. 205-269.

Davidson, A. (1984): Identification of ductile shear zones in the southwestern

Grenville Province of the Canadian Shield, in A. Kroner and R. Greiling (eds.): Precambrian Tectonics Illustrated, E. Schweizerbart'sche Verlagsbuchhandlung, Stuttgart, p. 263-279.

Davidson, A., Culshaw, N.G., and Nadeau, L. (1982): A tectono-metamorphic framework for part of the Grenville Province, Parry Sound region, Ontario, in Current Research, Part A, Geol. Surv. Canada, Paper 82-1A, 175-190.

DeWaard, D. (1965a): The occurrence of garnet in the granulite-facies terrane of the Adirondack highlands. J. Petrology 6, 165-191.

DeWaard, D. (1965b): A proposed subdivision of the granulite-facies. Am. J. Sci. 263, 455-461.

Dewey, J.F. and Burke, K.C.A. (1973): Tibetan, Variscan, and Precambrian basement reactivation: products of continental collision. J. Geology 81, 683-692.

Donath, F.A. and Parker, R.B. (1964): Folds and folding. Geol. Soc. Amer. Bull. 75, 45-62.

Douglas, G.V. (1953): Notes on localities visited on the Labrador coast in 1946 and 1947. Geol. Surv. Can., Paper 53-1.

Dymek, R. (1983): Titanium, aluminium and interlayer cation distributions in biotite from high-grade gneisses, West Greenland. Am. Mineral. 68, 380-399.

Ellis, D.J., and Green, D.H. (1979): An experimental study of the effect of Ca

upon garnet-clinopyroxene exchange equilibria. Contrib. Mineral. Petrol. 71, 13-22.

Emmett, T.F. (1982): The petrography and geochemistry of corona-bearing dolerites from the Jotun Nappe, central southern Norway. Mineral. Mag. 46, 43-48.

Emslie, R.F. (1976): Mealy Mountains complex, Grenville Province, southern Labrador, in Current Research, Part A. Geological survey of Canada Paper 76-1A, 165-170.

Emslie, R.F. (1983): The coronitic Michael gabbros, Labrador: assessment of Grenvillian metamorphism in northeastern Grenville Province. in Current Research, part A. Geological Survey of Canada, Paper 83-1A, p. 139-145.

Emslie, R.F., Loveridge, W.D., and Stevens, R.D. (1984): The Mealy dykes, Labrador: petrology, age, and tectonic significance. Can. J. Earth Sci. 21, 437-446.

Ermanovics, I.F., Korstgard, J., and Bridgwater, D. (1982): Structural and lithological chronology of the Archean Hopedale block and the adjacent Proterozoic Makkovik Subprovince, Labrador. In Current Research, Part B, Geol. Surv. Can. Paper, 82-1B, p. 153-165.

Esbensen, K.H. (1978): Coronites from the Fongen gabbro complex, Trondheim region, Norway: role of water in the olivine-plagioclase reaction. N. Jb. Miner. Abh. 132, 113-135.

Eskola, P. (1920): The mineral facies of rocks. Norsk. Geol. Tidsskr. 6,

143-194.

Eskola, P. (1939): Die enstehung der Gesteine. Springer-Verlag, Berlin.

Essene, E.J. (1982): Geologic thermometry and barometry. in Characterization of metamorphism through mineral equilibria, Reviews in Mineralogy, Mineral. Soc. Amer., Vol. 10, p. 153-206.

Fahrig, W.F., and Larochelle, A. (1972): Paleomagnetism of the Michael gabbro and possible evidence of the rotation of Makkovik Subprovince. Can. J. Earth Sci. 9, 1287-1296.

Fahrig, W.F., and Loveridge, W.D. (1981): Rb-Sr study of the Michael gabbro, Labrador. In Current Research, Part C, Geol. Surv. Can. Paper, 81-1C, p. 99-103.

Ferry, J.M., and Spear, F.S. (1978): Experimental calibration of the partitioning of Fe and Mg between biotite and garnet. Contrib. Mineral. Petrol. 66, 113-117.

Field, D., and Raheim, A. (1980): Secondary geologically meaningless Rb-Sr isochrons, low 87Sr/86Sr initial ratios and crustal residence times of high-grade gneisses. Lithos 13, 295-304.

Field, D., and Raheim, A (1981): Age relationships in the Proterozoic high-grade gneiss regions of southern Norway. Precambrian Research 14, 261-275.

Finnerty, A.A., and Boyd, F.R. (1983): Evaluation of thermobarometers for garnet peridotites. Geochim. Cosmochim. Acta 48, 15-27.

Ganguly, J., and Saxena, S. (1984): Mixing properties of aluminosilicate garnets:

constraints from natural and experimental data, and applications to geothermobarometry. Am. Mineral. 69, 88-97.

Gasparik, T. (1984): Two-pyroxene thermobarometry with new experimental data in the system CaO-MgO-Al2O3-SiO2. Contrib. Mineral. Petrol. 87, 87-97.

Ghent, E.D. (1976): Plagioclase-garnet-Al2SiO5-quartz: a potential geobarometer-geothermometer. Amer. Mineralogist 61, 710-714.

Ghent, E.D. (1977): Application of activity-composition relations to displacement of a solid-solid equilibrium. Anorthite = grossular + kyanite + quartz. in H.J. Greenwood (ed.): Application of Thermodynamics to Petrology and Ore Deposits, Mineralogical Association of Canada, Short course vol. 2.

Ghent, E.D., Robbins, D.B., and Stout, M.Z. (1979): Geothermometry, geobarometry, and fluid compositions of metamorphosed calc-silicates and pelites, Mica Creek, British Columbia. Amer. Mineralogist 64, 874-885.

Gil Ibarguchi, J.I., and Martinez, F.J. (1982): Petrology of garnet-cordierite-sillimanite gneisses from the El Tormes thermal dome, Iberian Hercynian foldbelt (W Spain). Contrib. Mineral. Petrol. 80, 14-24.

Goldman, D.S., and Albee, A.L. (1977): Correlation of Mg/Fe partitioning between garnet and biotite with 180/160 partitioning between quartz and magnetite. Am. J. Sci. 277, 750-767.

Gower, C.F. (1981): The geology of the Benedict Mountains, Labrador [13/J northeast and 13/I northwest]. Dept. of Mines and Energy, Newfoundland

and Labrador, Report 81-3, 26pp.

Gower, C.F., Noel, N., and Gillespie, R.T. (1983): Groswater Bay 1:100,000 Map Sheet. Mineral Development Division, Government of Newfoundland and Labrador, Map 83-43.

Gower, C.F., Noel, N., and Van Nostrand, T. (in prep): Geology of the Paradise River region, Grenville Province, eastern Labrador.

Gower, C.F., and Owen, V. (1984): Pre-Grenvillian and Grenvillian lithotectonic regions in eastern Labrador-Correlations with the Sveconorwegian orogenic belt in Sweden. Can. J. Earth Sci. 21, 678-693.

Gower, C.F., Owen, V., and Finn, G. (1982): The geology of the Cartwright region, Labrador, in Current Research, Mineral Development Division, Department of Mines and Energy, Government of Newfoundland and Labrador Report 82-1, 122-130.

Gower, C.F., Ryan, A.B., Bailey, D.G., and Thomas, A. (1980): The position of the Grenville Front in eastern and central Labrador. Can. J. Earth Sci., v. 17, p. 784-788.

Gower, C.F. (1984): Geology of the Double Mer White Hills and surrounding region, Grenville province, eastern Labrador. in Current Research, Newfoundland Department of Mines and Energy, Mineral Development Division, Report 84-1, p. 68-79.

Graham, C.M. and Powell, R. (1984): A garnet-hornblende geothermometer: calibration, testing, and application to the Pelona Schist, Southern

California. J. Metamorphic Geol. 2, 13-31.

Grasty, R.L., Rucklidge, J.C., and Elders, W.A. (1969): New K-Ar age determinations on rocks from the east coast of Labrador. Can. J. Earth Sci. 6, 340-344.

Greenwood, H.J. (1963): The synthesis and stability of anthophyllite. J. Petrology 4, 317-351.

Grew, E.S. (1981): Granulite-facies metamorphism at Molodezhnaya Station, East Antarctica. J. Petrology 22, 297-336.

Grieve, R.A.F. and Gittens, J. (1975): Composition and formation of coronas in the Hadlington gabbro, Ontario, Canada. Can. J. Earth Sci. 12, 289-299.

Harley, S.L., and Green, D.H. (1982): Garnet-orthopyroxene barometry for granulites and peridotites. Nature 300, 697-701.

Harley, S.L. (1984a): An experimental study of the partitioning of Fe and Mg between garnet and orthopyroxene. Contrib. Mineral. Petrol. 86, 359-373.

Harley, S.L. (1984b): The solubility of alumina in orthopyroxene coexisting with garnet in FeO-MgO-Al2O3-SiO2 and CaO-FeO-MgO-Al2O3-SiO2. J. Petrology 25, 665-696

Harley, S.L. (1984c): Comparison of the garnet-orthopyroxene geobarometer with recent experimental studies, and applications to natural assemblages. J. Petrology 25, 697-712

Hodges, K.V., and Spear, F.S. (1982): Geothermometry, geobarometry and the Al2SiO5 triple point at Mt. Moosilauke, New Hampshire. Amer.

Mineralogist 67, 1118-1134.

Holdaway, M.J., and Lee, S.M. (1977): Fe-Mg cordierite stability in high-grade pelitic rocks based on experimental, theoretical, and natural observations. Contrib. Mineral. Petrol. 63, 175-198.

Holland, T.J.B., and Richardson, S.W. (1979): Amphibole zonation in metabasites as a guide to the evolution of metamorphic conditions. Contrib. Mineral. Petrol. 70, 143-148.

Holt, R.W., and Wightman, R.T. (1983): The role of fluids in the development of a granulite facies transition zone in S India. J. geol. Soc. Lond. 140, 651-656.

Hormann, P.K., Raith, M., Raase, P., Ackermand, D., and Seifert, F. (1980) The granulite complex of Finnish Lappland: petrology and metamorphic conditions in the Ivalojoki-Inarijarvi area. Geol. Surv. Finland Bull. 308, 1-95.

Hsu, K.J. (1968): Selected phase relationships in the system Al-Mn-Fe-Si-O; a model for garnet equilibria. J. Petrology 9, 40-83.

Hynes, A. (1982): A comparison of amphiboles from medium- and low-pressure metabasites. Contrib. Mineral. Petrol. 81, 119-125.

Indares, A., and Martignole, J. (1984): Evolution of P-T conditions during a high-grade metamorphic event in the Maniwake area. Can. J. Earth Sci. 21, 853-863.

Indares, A., and Martignole, J. (in press): Biotite-garnet geothermometry in

granulite facies: the influence of Ti and Al in biotite. Amer. Mineralogist

Indares, A., and Martignole, J. (in press): Biotite-garnet geothermometry in granulite facies: evaluation of equilibrium criteria. Can. Mineralogist

Johnson, C.A. and Essene, E.J. (1982): The formation of garnet in olivine-bearing metagabbros from the Adirondacks. COntrib. Mineral. Petrol. 81, 240-251.

Kline, S.W. (1984): Iron-rich hornblende plus albite in low-pressure metabasites, Chibougamau, Quebec. Can. Mineralogist 22, 391-399.

Kranck, E.H. (1939): Bedrock geology of the seaboard region of Newfoundland-Labrador. Nfld. Geol. Surv., Bull 19, 44pp.

Kranck, E.H. (1947): Indications of movement of the earth-crust along the coast of Newfoundland-Labrador. Bull. de la Commission geologique de Finland, Nr. 140, p. 89-96.

Kranck, E.H. (1953): Bedrock geology of the seaboard of Labrador between Domino Run and Hopedale, Newfoundland. Geol. Surv. Can., Bull. 26, 41 pp.

Kretz, R. (1961): Some applications of thermodynamics to coexisting minerals of variable composition. Examples: orthopyroxeene-clinopyroxene and orthopyroxene-garnet. J. Geol. 69, 361-387.

Krogh, T.E. (1983): Unpublished report to the Dept. of Mines and Energy, Newfoundland and Labrador.

Laird, J. (1980): Phase equilibria in mafic schist from Vermont. J. Petrology 21,

1-37.

Laird, J. (1982): Amphiboles in metamorphosed basaltic rocks: greenschist facies to amphibolite facies. In Amphiboles: Petrology and Experimental Phase Relations (D.R. Veblen and P.H. Ribbe, eds.), Reviews in Mineralogy, Min. Soc. Am., v. 9B, p. 113-137.

Laird, J., and Albee, A.L. (1981): Pressure, temperature, and time indicators in mafic schist: their application to reconstructing the polymetamorphic history of Vermont. Am. J. Sci. 281, 127-175.

LaTour, T.E. (1979): The nature and origin of the Grenville Front near Coniston, Ontario: a reinterpretation. Unpubl. Ph.D. thesis, Univ. Western Ontario.

LaTour, T.E. (1981): Metamorphism and geothermometry near Coniston, Ontario: a clue to the tectonic evolution of the Grenville Front. Can J. Earth Sci. 18, 884-898.

Leake, B.E. (compiler) (1978): Nomenclature of Amphiboles. Mineral. Mag. 42, 533-563.

Lee, S.M., and Holdaway, M.J. (1977): Significance of Fe-Mg cordierite stability relations on temperature, pressure, and water pressure in cordierite granulites. In The Earth's Crust: its Nature and Physical Properties (J.G. Heacock, ed.). Am. Geophys. Union. Mon. 20, 79-94.

Leiber, O.M. (1860): Notes on the geology of the coast of Labrador. Report of the United States Coast Survey for 1860.

Lister, G.S. and Price, G.P. (1978): Fabric development in a quartz-feldspar mylonite. Tectonophysics 49, 37-78.

Lof, P. (1983): Elsevier's Mineral and Rock Table, Elsevier Publ. Co. Inc., N.Y.

Lonker, S. (1980): Conditions of metamorphism in high-grade pelitic gneisses from the Frontenac Axis, Ontario, Canada. Can. J. Earth Sci. 17, 1666-1684.

Lumbers, S.B. (1975): Geology of the Burwash area, districts of Nipissing, Parry Sound, and Sudbury. Ontario Division of Mines, Geological Report 116, 158pp.

Martignole, J., and Nantel, S. (1982): Geothermobarometry of cordierite-bearing metapelites near the Morin anorthosite complex, Grenville Province, Quebec. Can. Mineralogist 20, 307-318.

Martignole, J., and Schriver, K. (1973): Effect of rock composition on appearance of garnet in anorthosite-charnockite suites. Can. J. Earth Sci. 10, 1132-1139.

Martignole, J., and Sisi, J.C. (1981): Cordierite-garnet-H20 equilibrium: a geological thermometer, barometer and water fugacity indicator. Contrib. Mineral. Petrol. 77, 38-46.

Mehnert, K.R. (1968): Migmatites and the Origin of Granitic Rocks. Elsevier Publ. Co., Copenhagen, 393pp.

Mehnert, K.R., Busch, W., and Schneider, G. (1973): Initial melting at grain boundaries of quartz and feldspar in gneisses and granulites. N. Jb. Miner.

Mh. v. 4, 165-183.

Miyashiro, A. (1979): Metamorphism and Metamorphic Belts. George Allen and Unwin, London, 492pp.

Mongkoltip, P. and Ashworth, J.R. (1983): Quantitative estimation of an open-system symplectite forming reaction: restricted diffusion of Al and Si in coronas around olivine. J. Petrology 24, 635-661.

Newton, R.C., and Haselton, M.T. (1981): Thermodynamics of the garnet-plagioclase - Al2SiO5 - quartz geothermometer. in Thermodynamics of Minerals and Melts. Springer-Verlag, p. 131-147.

Newton, R.C., and Perkins, D. III (1982): Thermodynamic calibration of geobarometers based on the assemblages garnet-plagioclase-orthopyroxene (clinopyroxene)-quartz. Am. Mineralogist 67, 203-222.

Newton, R.C., and Wood, B.J. (1979): Thermodynamics of water in cordierite and some petrologic consequences of cordierite as a hydrous phase. Contrib. Mineral. Petrol. 68, 391-405.

Nunn, G.A.G., Noel, N., and Culshaw, N. (1984): Geology of the Atikonak Lake area, Grenville province, western Labrador. in Current Research, Newfoundland Department of Mines and Energy, Mineral Development Division, Report 84-1, p. 30-41.

Owen, V., Gower, C.F., and Finn, G. (1983): Table Bay 1:100,000 Map Sheet. Mineral Development Division, Department of Mines and Energy, Newfoundland and Labrador, Map 83-46.

Owen, V., and Rivers, T. (1983): Geology of the Smokey archipelago, Grenville Front Zone, Labrador. In Current Research, Part A, Geol. Surv. Can., Paper 83-1A, p. 153-161.

Owen, V., Rivers, T., and Gower, C.F. (in prep.): The Grenville Front on the Labrador coast.

Packard, A.S. (1891): The Labrador coast. New York, N.D.C. Hodges (publisher), 513 pages.

Percival, J.A. (1983): High-grade metamorphism in the Capleau-Foleyet area, Ontario. Amer. Mineralogist 68, 667-686.

Perkins, D. III, and Newton, R.C. (1981): Charnockite geobarometers based on coexisting garnet-pyroxene-plagioclase-quartz. Nature 292, 144-146.

Perkins, D. III, Essene, E.J., and Marcotty, L.A. (1982): Thermometry and barometry of some amphibolite-granulite facies rocks from the Otter Lake area, southern Quebec. Can. J. Earth Sci. 19, 1759-1774.

Plyusnina, L.P. (1982): Geothermometry and geobarometry of plagioclase-hornblende bearing assemblages. Contrib. Mineral. Petrol. 80, 140-146.

Powell, R. (1978): The thermodynamics of pyroxene geotherms. Phil. Trans. R. SOc. Lond. A283, 457-469.

Powell, R. (1985): Geothermometry and geobarometry: a discussion. J. geol. Soc. London 142, 29-38.

Raase, P. (1974): Al and Ti contents of hornblende, indicators of pressure and temperature of regional metamorphism. Contrib. Mineral. Petrol. 45,

231-236.

Raheim, A., and Green, D.H. (1974): Experimental determination of the temperature and pressure dependence of the Fe-Mg partition coefficient for coexisting garnet and clinopyroxene. Contrib. Mineral. Petrol. 48, 179-203.

Raith, M., Raase, D., Ackermand, D., and Lal, R.K. (1983): Regional geothermobarometry in the granulite facies terrane of south India. Trans. R. Soc. Edinburgh (Earth Sciences) 73, 221-244.

Ramsay, D.H. (1979): Analysis of rotation of folds during progressive deformation. Geol. Surv. Am. Bull., v. 90, p. 732-738.

Ramsay, J.G. (1981): Tectonics of the Helvetic nappes. in Thrust and Nappe Tectonics, International Conference (McClay, K.R. et al., eds.), Spec. Publ. Geol. Soc. Lond. No. 9, p. 293-309.

Ramsay, J.G. (1967): Folding and Fracturing of Rocks, 568pp., McGraw-Hill, New York.

Ramsay, J.G., Casey, M., and Kligsfield, R. (1982): Role of shear in development of the Helvetic fold-thrust belt of Switzerland. Geology 11, 439-442.

Rhodes, S. and Gayer, R.A. (1977): Non-cylindrical folds, linear structures in the X direction and mylonite developed during translation of the Caledonian Kalak Nappe Complex of Finnmark. Geol. Mag. 114, 329-341.

Rivers, T. (1983a): Progressive metamorphism of pelitic and quartzofeldspathic rocks in the Grenville Province of western Labrador-tectonic implications

of bathozone 6 assemblages. Can. J. Earth Sci. 20, 1791-1804.

Rivers, T. (1983b): The northern margin of the Grenville province in western Labrador-anatomy of an ancient orogenic front. Precambrian Res. 22, 41-73.

Rivers, T., and Nunn, G.A.G. (in press): A reassessment of the Grenvillian orogeny in western Labrador.

Rivers, T., and Chown, E.H. (in prep.): The Grenville orogen in eastern Quebec and western Labrador-definition, identification and tectonometamorphic relationships of autochthonous, parautochthonous and allochthonous terranes.

Robinson, P., Spear, F.S., Schumacker, J.C., Laird, J., Klein, C., Evans, B.W., and Doolan, B.L. (1982): Phase relations of metamorphic amphiboles: natural occurrence and theory. in D.R. Veblen and P.H. Ribbe (eds.), Amphiboles: Petrology and experimental phase relations, Mineral. Soc. Amer. Reviews in Mineralogy, V. 9B, p. 1-227.

Simpson, C., and Schmid, S.M. (1983): An evaluation of criteria to deduce the sense of movement in sheared rocks. Geol. Soc. Am. Bull., v. 94, p. 1281-1288.

Sorensen, K. (1978): Are coronas cooling products? Rapp. Gronlands geol. Unders. 89, 113-114.

Spear, F.S. (1981): An experimental study of hornblende stability and compositional variability in amphibolite: Am. J. Sci. 281, 697-734.

Steiger, R.H., and Jager, E. (1977): Subcommission on geochronology: convention on the use of decay constants in geo- and cosmochronology. Earth Planet. Sci. Lett. 36, 359-362.

Stevenson, I.M. (1970): Rigolet and Groswater Bay map-areas, Newfoundland (Labrador). (13J, 13I). Geol. Surv. Can., Paper 69-48.

Stephenson, N.C.N. (1979): Coexisting garnets and biotites from Precambrian gneisses of the south coast of Western Australia. Lithos 12, 73-87.

Stephenson, N.C.N. (1984): Two-pyroxene thermometry of Precambrian granulites from Cape Riche, Albany-Fraser Province, western Australia. J. Metamorphic Petrology 2, 297-314.

Stormer, J.C. (1975): A practical two-feldspar geothermometer. Amer. Mineralogist 60, 667-674.

Stormer, J.C. (1977): Two-feldspar geothermometry, geobarometry in mesozonal granitic intrusions: three examples from the Piedmont of Georgia. Contrib. Mineral. Petrol. 63, 51-64.

Streckeisen, A. (1976): To each plutonic rock its proper name. Earth-Science Reviews 13, 1-33.

Taylor, F.C. (1971): A revision of Precambrian structural provinces in northeastern Quebec and northern Labrador. Can. J. Earth. Sci. 8, 579-584.

Thomas, A., Culshaw, N., Mannard, G., and Whelan, J.G. (1984): Geology of the Lac Ghyvelde-Lac Long area, Grenville province, Labrador and

Quebec. in Current Research, Newfoundland Department of Mines and Energy, Mineral Development Division, Report 84-1, p. 42-52.

Thompson, A.B. (1976): Mineral reactions in pelitic rocks: II. Calculations of some P-T-X(Fe-Mg) phase relations. Am. J. Sci. 276, 425-454.

Treloar, P.J. (1981): Garnet-biotite-cordierite thermometry and barometry in the Cashel thermal aureole, Connemara, Ireland. Mineralogical Mag. 44, 183-189.

Troger, W.E. (1971): Optische Bestimmung der gesteinsbilden der Minerale. T.1, Stuttgart, Schweizerbart, 259pp.

Turner, F.J. (1981): Metamorphic Petrology: Mineralogical, Field, and Tectonic Aspects. McGraw-Hill, New York, (2nd ed.) 524pp.

Wanless, R.K., Stevens, R.D., Lachance, G.R., and Delabio, R.N. (1972): Age determinations and geological studies. K-Ar isotopic ages, Report 10; Geol. Surv. Canada, Paper 71-2.

Wanless, R.K., Stevens, R.D., Lachance, G.R>, and Delabio, R.N. (1973): Age determinations and geological studies, Report 11; Geol. Surv. Canada, Paper 73-2.

Wardle, R.J. and Staff, Labrador Section (1982): The Trans-Labrador Batholith; a major pre-Grenvillian feature of the eastern Grenville Province. In Grenville Workshop, 1982, program with abstracts, p. 11. Ottawa-Carleton Centre for Geoscience Studies.

Wells, P.R.A. (1977): Pyroxene thermometry in simple and complex systems.

Contrib. Mineral Petrol. 62, 129-139.

Wells, P.R.A. (1979): Chemical and thermal evolution of Archaean sialic crust, southern West Greenland. J. Petrology 20, 187-226.

Whitney, P.R. (1978): The significance of garnet "isograds" in granulite facies rocks of the Adirondacks, in Metamorphism in the Canadian Shield, Geol. Surv. Canada Paper 78-10, p. 357-366.

Williams, G.D. (1978): Rotation of contemporary folds into the X direction during overthrust processes in Laksefjord, Finnmark. Tectonophysics, v. 48, p. 29-40.

Winkler, H.G.F. (1979): Petrogenesis of Metamorphic Rocks. Springer-Verlag, New York, (5th ed.) 348pp.

Wood, B.J. (1974): The solubility of alumina in orthopyroxene coexisting with garnet. Contrib. Mineral. Petrol. 46, 1-15.

Wood, B.J., and Banno, S. (1973): Garnet-orthopyroxene and orthopyroxene-clinopyroxene relationships in simple and complex systems. Contrib. Mineral. Petrol. 42, 109-124.

Wynne-Edwards, H.R. (1972): The Grenville Province, in: Price, R.A., and Douglas, R.J.W. (eds.): Variations in tectonic styles in Canada. Geol. Assoc. Canada Spec. Pap. 11, p. 263-334.

Wynne-Edwards, H.R. (1976): Proterozoic ensialic orogenesis: the millipede model of ductile plate tectonics. Am. J. Sci. 276, 927-953.

APPENDIX A
ANALYTICAL METHODS

Representative specimens of major rock units and various ages of metabasites were sampled for analytical work in three areas: (1) whole rock major and trace element goechemistry; (2) Rb-Sr isotopic dating on seven rock units (units 2, 3A, 6A, 6B, 6E, 7, and 9); and (3) mineral analyses, employing the electron probe microanalyser (microprobe).

A.1 SAMPLE COLLECTION AND PREPARATION

The majority of specimens described in this study, those numbered with a "V" prefix, were sampled by the author. Dr. Charles F. Gower generously provided other samples, those numbered with a "CG79" prefix, from the Smokey archipelago.

Specimens for major and trace element and isotopic analysis were reduced to gravel size fragments in the field, after removal of weathered surfaces. Between 0.5kg and 2kg of fresh material were kept for analysis, larger amounts being selected in the case of relatively coarse grained rocks. The samples were subsequently crushed to 1-3mm size chips, and the coarsest grained samples were coned and quartered, each fraction subsequently being pulverized to -200 mesh in a tungsten carbide Siebtechnik shatter box. The shatter box was scoured with silica and cleaned with water and with methanol between samples. The -200 mesh powders were used in the subsequent analyses.

Specimens for mineral analysis were selected primarily for the purpose of estimating conditions of Grenvillian and pre-Grenvillian metamorphism. In the former case, Grenvillian high strain zones were sampled in a variety of lithologies,

and special attention was paid to garnet and (or) amphibole bearing shear zones. Specimens for the study of pre-Grenvillian metamorphism were selected from the least retrograded members of the Granulite Complex, in particular, pelitic metatexite (unit 1C) and jotunitic-charnockitic gneiss (unit 3A). Whole rock major element analyses were performed on a number of the specimens chosen for mineral analysis in order to ascertain the influence of bulk rock compositions on mineralogy and mineral compositions.

A.2 MAJOR AND TRACE ELEMENT ANALYSES

Major element analyses were obtained by atomic absorption spectrometry (AA) using a Perkin-Elmer digitized spectrometer. The analyses were performed by G. Andrews of the Department of Earth Sciences, MUN, and were run in sets of 24 per day, including replicate analyses. A sample weight of 0.1000g was selected for analysis. The samples were dissolved in a solution of 5ml HF, 50ml saturated H3BO3 and 145ml H2O heated on a steam bath for approximately 12 hours prior to analysis. P2O5 was determined by colourimetry (Maxwell, 1968) and loss on ignition (LOI) was determined after heating approximately 1.5g of sample at ~1000C for 2-3 hours in a muffle furnace. Between-sample precision estimated from six replicate analyses is as follows: SiO2 ($\pm$ 0.37%; TiO2 $\pm$ 9.26%; Al2O3 $\pm$ 1.34%; Fe2O3 $\pm$ 1.36%; MnO $\pm$ 1.00%; CaO $\pm$ 0.17%; Na2O $\pm$ 0.79%; K2O $\pm$ 1.35%; P2O5 $\pm$ 10.74%. Relatively poor precision for TiO2 and P2O5 is attributed to the small quantities of these oxides in the samples. All iron is expressed as Fe2O3 in these analyses.

Accuracy of the A.A. analyses has been determined through the repeated analysis of various rock standards. Analysis of granodiorite standard GSP-1 has yielded the following results:

	Published Value*	No. of Analyses	Mean (wt.%)	Standard Deviation
SiO2	67.27	7	68.65	0.60
TiO2	0.65	7	0.60	0.08
Al2O3	15.18	7	14.77	0.22
Fe2O3	4.26	8	4.22	0.07
CaO	2.06	8	1.94	0.07
MgO	0.98	7	0.96	0.03
Na2O	2.77	8	2.74	0.06
K2O	5.50	6	5.44	0.12
MnO	0.04	8	0.04	0.01

* = Abbey (1970)

Trace element analyses were performed using a Phillips 1450 X-ray fluorescence spectrometer autocalibrated against international rock standards G-2 and PCC-1. Powdered rock samples weighing 10g were mixed with 1.3g of phenol formaldehyde binder, pressed into a pellet under 50MPa for 1 minute, and fused for 10-12 minutes at 200C. The precision of the trace element analyses has been estimated from the results of repeated analyses of standard G2, which was run regularly with the unknown samples. Average results of 12 replicate analyses of G2 in ppm are, with one standard deviation in brackets: Pb 31.5 (3.37); Th 28.1 (3.26); U 1.75 (2.0); Rb 167.4 (2.74); Sr 457.4 (4.66); Y 10.70 (1.65); Zr 299.60 (3.23); Nb 12.0 (0.60); Zn 85.0 (2.56); Cu 25.8 (1.53); Ni 8.0 (1.8); La 43.3 (3.00); Ba 1872.4 (20.2); V 39.2 (2.63); Ce (84.5 (5.12); Cr 15.0 (2.32); Ga 20.6 (1.30).

Appendix A.2.1 Major and trace element geochemistry of the Granulite Complex.

Note: Zero values for FeO are for those samples in which all iron is expressed as Fe_2O_3

A.2.1a Pelitic metatexite (unit 1C)

	V207	V172
SiO2	64.70	68.90
TiO2	.80	.67
Al2O3	14.70	13.50
Fe2O3	6.75	6.57
FeO	0.00	0.00
MnO	.08	.08
MgO	3.32	2.64
CaO	1.79	2.28
Na2O	2.17	2.54
K2O	4.10	2.59
P2O5	.07	.01
LOI	.75	.82
Total	99.23	100.60
Pb	23	15
Th	29	0
U	8	0
Rb	122	101
Sr	275	261
Y	33	28
Zr	154	217
Nb	11	19
Zn	63	20
Cu	11	12
Ni	57	48
La	37	17
Ba	1614	602
V	144	124
Ce	55	31
Cr	96	97
Ga	17	15

Appendix A.2.1 (Continued)

A.2.1b Dioritic-tonalitic gneiss (unit 2)

	V325-1	V581-1	V588-1	CG-339	V774	V211-1	V213
SiO2	64.00	46.00	68.80	58.10	57.90	72.70	68.10
TiO2	.56	1.68	.33	.74	.74	1.52	.80
Al2O3	16.90	17.40	16.30	16.40	17.10	11.20	11.80
Fe2O3	5.34	12.43	2.64	3.09	7.37	5.09	7.26
FeO	0.00	0.00	0.00	4.18	0.00	0.00	0.00
MnO	.07	.14	.02	.15	.11	.05	.07
MgO	1.27	5.74	.79	4.71	3.31	2.29	3.03
CaO	3.62	8.68	4.78	6.53	5.64	1.44	2.11
Na2O	3.56	2.86	3.98	3.18	4.26	2.15	2.26
K2O	4.01	1.70	1.20	1.65	2.75	2.94	2.31
P2O5	.13	.87	0.00	.33	.26	.09	.05
LOI	.43	.50	.55	1.25	.93	.41	.22
Total	99.89	98.00	99.39	100.31	100.37	99.88	98.01
Pb	14	4	13	7	3	17	7
Th	2	0	19	5	13	6	3
U	4	0	0	15	0	0	0
Rb	142	54	28	65	103	127	99
Sr	349	1021	518	832	805	142	137
Y	23	46	4	38	26	18	27
Zr	186	170	215	125	118	185	219
Nb	7	15	3	5	12	12	13
Zn	76	156	28	92	72	64	88
Cu	16	49	14	2	22	8	39
Ni	4	30	0	47	9	33	52
La	18	18	20	25	8	23	23
Ba	974	1367	181	418	923	881	579
V	89	244	43	138	137	110	136
Ce	40	66	45	147	33	34	42
Cr	4	3	16	177	5	73	97
Ga	21	23	18	20	19	12	19

Appendix A.2.1 (Continued)

A.2.1c Jotunitic-charnockitic gneiss (unit 3A) and its retrograded equivalent (unit 3B)

	unit 3A							unit 3B		
	V74-1	V193-3	V193	V526-1	V585	V586	V579-1	V194-3	V220	V526-2
SiO2	58.10	68.10	61.80	69.30	62.20	62.70	62.00	61.70	68.50	68.10
TiO2	.81	.35	.60	.42	.78	.59	.99	.80	.36	.40
Al203	18.30	15.70	20.30	15.00	17.10	16.10	13.20	18.00	15.30	15.20
Fe203	6.03	3.39	2.78	3.00	5.53	5.79	9.56	4.45	2.90	2.70
FeO	0.00	0.00	0.00	0.00	0.00	0.00	0.00	0.00	0.00	0.00
MnO	.10	.06	.04	.05	.08	.09	.09	.05	.05	.05
MgO	2.33	1.30	1.07	.85	2.36	2.78	4.04	1.62	1.31	.71
CaO	4.57	3.27	5.09	2.22	4.47	4.70	2.42	3.75	3.05	2.08
Na20	4.49	3.50	5.37	3.53	4.07	3.74	2.73	4.68	3.44	3.63
K20	3.36	4.24	2.34	4.73	3.12	3.35	3.03	3.13	4.31	5.16
P205	.18	.11	.09	.09	.25	.25	.02	.16	.12	.11
LOI	.41	.21	.50	.88	.38	.38	.15	.30	.63	.99
Total	98.68	100.23	99.98	100.07	100.34	100.47	98.23	98.64	99.97	99.13
Pb	8	9	10	23	15	10	10	16	10	23
Th	0	0	0	7	8	2	9	5	5	3
U	3	0	0	0	5	2	0	2	1	0
Rb	87	71	34	121	63	66	91	89	83	138
Sr	853	564	858	452	723	727	369	661	711	444
Y	35	20	6	9	19	21	40	17	12	10
Zr	182	99	116	193	179	139	288	208	103	203
Nb	11	6	5	6	10	8	11	12	3	9
Zn	79	44	38	41	74	70	137	65	34	33
Cu	24	13	21	17	16	30	9	14	18	22
Ni	3	0	0	1	6	11	65	0	0	1
La	12	15	13	10	20	9	24	29	20	14
Ba	1869	1154	467	1473	1195	1247	1233	863	1844	1426
V	98	47	32	29	80	95	193	44	40	22
Ce	36	33	28	34	51	32	47	59	41	30
Cr	0	4	0	0	27	27	130	0	4	0
Ga	23	19	24	13	19	17	17	26	15	18

Appendix A.2.1 (Continued)

A.2.1d Biotite + hornblende ± pyroxene monzonitic gneiss (unit 4)

	V26	V310-1	V711-2
SiO2	68.10	67.00	71.4
TiO2	.30	.31	.31
Al2O3	16.10	16.50	14.4
Fe2O3	2.77	3.16	2.04
FeO	0.00	0.00	0.00
MnO	.04	.05	0.04
MgO	.79	.84	0.61
CaO	2.66	2.67	2.02
Na2O	4.43	3.63	3.47
K2O	3.81	4.77	4.54
P2O5	.09	.12	0.09
LOI	.87	.61	0.98
Total	99.96	99.66	99.90
Pb	13	14	22
Th	5	0	4
U	2	3	0
Rb	75	122	127
Sr	614	595	340
Y	9	15	9
Zr	174	253	152
Nb	4	11	17
Zn	42	39	27
Cu	14	20	8
Ni	0	0	0
La	18	11	35
Ba	1153	1374	1156
V	31	30	60
Ce	28	20	18
Cr	0	0	9
Ga	17	20	23

Appendix A.2.2 Major and trace element geochemistry of the Benedict Mountains Intrusive Suite.

Note: Zero values for FeO are for those samples in which all iron is expressed as Fe_2O_3.

A.2.2a K-feldspar megacrystic biotite ± hornblende quartz monzodiorite-granodiorite (unit 6A)

	V192	V294	V340	V393-1	V333-1	V40	V546-1	CG-344	CG-366	CG-377
SiO2	74.00	69.40	71.50	70.50	71.30	69.90	71.00	65.09	72.50	70.6
TiO2	.20	.31	.28	.40	.13	.29	.20	.42	.25	0.32
Al2O3	14.10	15.30	15.20	14.70	15.10	15.90	15.20	17.50	14.60	15.25
Fe2O3	1.60	2.81	1.89	2.46	1.80	3.15	2.08	1.59	.55	0.60
FeO	0.00	0.00	0.00	0.00	0.00	0.00	0.00	1.91	1.23	1.45
MnO	.02	.04	.04	.05	.05	.05	.04	.06	.03	0.04
MgO	.38	.74	.53	.61	.39	.83	.53	.94	.47	0.64
CaO	1.65	2.00	1.66	1.92	1.53	2.48	1.86	3.28	1.72	2.29
Na2O	3.14	3.63	3.96	3.59	4.28	4.12	3.74	4.29	3.91	4.32
K2O	4.46	4.64	4.05	4.12	4.03	3.30	5.21	4.08	4.49	3.83
P2O5	.05	.08	.04	.09	.07	.08	.16	.42	.06	0.07
LOI	.28	.43	.79	.44	.68	.28	.45	.13	.88	0.85
Total	99.88	99.38	99.94	98.88	99.36	100.38	100.47	99.71	100.69	100.26
Pb	15	18	20	22	17	22	23	12	22	12
Th	15	4	9	4	11	9	6	6	12	6
U	0	0	1	0	7	3	0	7	26	13
Rb	76	102	144	91	148	85	156	87	144	100
Sr	473	620	370	475	396	570	406	756	384	552
Y	6	11	22	8	27	15	11	8	12	7
Zr	122	148	143	124	117	137	121	222	121	124
Nb	4	6	22	7	13	8	14	2	11	2
Zn	18	42	29	43	35	49	32	52	22	27
Cu	18	17	8	0	20	18	13	2	2	2
Ni	0	0	0	0	0	5	0	16	18	10
La	21	25	19	21	17	21	14	38	30	31
Ba	1277	1391	889	1020	903	1109	1027	1825	721	1039
V	11	24	18	26	19	36	18	38	17	7
Ce	47	57	33	27	33	39	27	194	168	130
Cr	0	0	0	0	0	5	5	5	5	5
Ga	12	20	19	19	18	17	17	23	19	18

Appendix A.2.2 (Continued)

A.2.2a (Continued)

	unit 6A					
	V628	V766	V274-1	V260	V427	V428
SiO2	72.00	70.30	66.00	70.60	66.70	66.30
TiO2	.32	.26	.35	.49	.36	.48
Al2O3	14.60	14.50	16.50	14.30	16.30	15.90
Fe2O3	2.04	2.90	3.47	2.98	2.81	3.21
FeO	0.00	0.00	0.00	0.00	0.00	0.00
MnO	.04	.05	.04	.04	.06	.07
MgO	.50	.88	.95	.36	.88	1.12
CaO	1.73	2.14	2.76	1.53	2.44	2.43
Na2O	4.31	4.09	3.92	3.41	4.15	4.52
K2O	4.80	4.44	4.25	6.37	3.95	4.04
P2O5	.06	.10	.13	.04	.14	.17
LOI	.64	.48	.56	.57	.58	.50
Total	101.04	100.14	98.93	100.69	98.37	100.47
Pb	25	15	6	27	18	20
Th	16	23	0	17	10	10
U	2	0	0	1	6	3
Rb	144	150	87	164	120	150
Sr	416	340	785	190	547	357
Y	18	23	7	57	19	63
Zr	164	111	186	471	179	273
Nb	10	10	4	21	13	30
Zn	48	35	53	41	49	66
Cu	21	13	12	23	14	10
Ni	0	0	0	1	0	4
La	19	10	23	86	23	40
Ba	1078	705	1647	672	1194	774
V	16	27	37	11	25	39
Ce	43	30	38	167	46	74
Cr	0	5	0	0	6	0
Ga	18	15	20	18	19	18

Appendix A.2.2 (Continued)

A.2.2b Hornblende + biotite monzodiorite-monzonite (unit 6B)

	V9-4	V32	V44-4	V113-1	V164	V225-2	V226	V237	V255-1	V257	V257-6	V293
SiO2	66.70	61.10	61.20	65.90	64.40	62.40	64.70	61.90	68.90	63.60	66.40	62.30
TiO2	.34	.64	.85	.38	.33	.62	.64	.52	.49	.98	.40	.55
Al2O3	16.10	16.40	17.00	17.10	15.90	16.80	15.00	17.50	14.70	15.20	16.10	16.00
Fe2O3	3.39	7.01	6.25	3.90	4.05	5.31	5.47	5.29	3.33	6.87	4.26	5.35
FeO	0.00	0.00	0.00	0.00	0.00	0.00	0.00	0.00	0.00	0.00	0.00	0.00
MnO	.07	.12	.14	.07	.08	.11	.08	.10	.07	.10	.08	.08
MgO	.35	.72	.67	1.21	.25	.42	.93	2.18	.76	1.08	.17	2.44
CaO	1.43	2.37	2.16	2.66	1.56	2.02	2.09	4.87	1.82	2.86	1.70	4.02
Na2O	4.64	4.00	4.65	4.26	4.02	4.30	3.70	4.61	4.27	3.71	4.40	3.62
K2O	6.22	6.74	6.50	4.80	6.78	7.06	5.92	2.57	4.44	5.63	6.56	3.22
P2O5	.06	.13	.15	.12	.05	.10	.19	.19	.18	.23	.04	.24
LOI	.41	.21	.43	.43	1.23	.54	.52	.57	1.06	.49	.67	.38
Total	99.71	99.44	100.00	100.83	98.65	99.68	99.24	100.30	100.02	100.75	100.78	98.20
Pb	29	26	30	14	27	32	21	16	31	15	32	5
Th	7	0	0	1	4	6	0	3	13	0	10	1
U	2	5	3	0	0	5	0	0	1	0	0	3
Rb	137	154	112	115	165	179	151	102	205	141	147	97
Sr	173	178	253	619	150	157	229	757	303	276	104	621
Y	41	67	60	26	77	77	70	34	45	68	97	31
Zr	493	705	775	191	587	623	673	116	208	710	595	115
Nb	16	21	23	10	34	33	26	12	26	28	35	12
Zn	50	113	99	52	87	100	74	72	67	101	105	67
Cu	18	19	13	21	13	11	21	26	15	20	16	16
Ni	0	3	0	0	0	4	2	3	6	1	0	8
La	50	36	48	28	40	102	41	29	27	37	125	18
Ba	857	861	1605	1240	777	722	1095	978	835	1209	553	992
V	1	8	0	50	2	3	22	85	25	33	0	87
Ce	89	70	84	51	77	164	69	42	57	84	233	46
Cr	0	0	0	0	0	0	0	3	0	0	0	18
Ga	23	25	24	19	23	25	24	18	21	21	28	18

Appendix A.2.2 (Continued)

A.2.2b (Continued)

---------unit 6B-------

	V415	V506	V759	V776
SiO2	61.50	62.60	68.40	67.40
TiO2	.68	.58	.55	.28
Al2O3	18.80	16.80	15.50	15.60
Fe2O3	3.85	4.98	3.47	4.34
FeO	0.00	0.00	0.00	0.00
MnO	.06	.09	.06	.08
MgO	1.47	1.97	.99	.13
CaO	3.51	4.42	2.49	1.68
Na2O	4.98	4.34	4.01	4.38
K2O	3.53	3.58	4.80	6.50
P2O5	.19	.21	.16	.01
LOI	.64	.42	.52	.37
Total	99.21	99.99	100.95	100.77
Pb	11	17	21	27
Th	8	2	16	13
U	0	1	0	0
Rb	133	105	96	137
Sr	522	697	400	68
Y	23	29	18	76
Zr	278	148	261	589
Nb	13	14	12	34
Zn	66	64	55	95
Cu	22	26	16	15
Ni	4	6	4	1
La	20	11	26	91
Ba	921	1383	1348	331
V	42	74	32	0
Ce	39	40	56	165
Cr	0	2	0	0
Ga	24	18	18	24

A.2.2c Leucocratic biotite + hornblende granodiorite-granite

----------unit 6C----------

	V120	V112-1	V238-2	V447-1	V447-2
SiO2	77.20	73.30	74.80	75.40	77.30
TiO2	.03	.14	.05	.13	.13
Al2O3	12.10	13.90	12.80	12.50	11.90
Fe2O3	1.09	1.83	1.51	1.09	.82
FeO	0.00	0.00	0.00	0.00	0.00
MnO	.02	.04	.02	.03	.02
MgO	.10	.19	.09	.23	.19
CaO	.41	.99	.73	.67	.58
Na2O	3.07	3.60	3.14	3.42	3.29
K2O	5.60	5.85	6.00	5.46	5.21
P2O5	.04	.07	.01	.03	.02
LOI	.58	.26	.47	.79	1.12
Total	100.24	100.17	99.62	99.75	100.58
Pb	33	23	60	18	21
Th	30	16	27	33	32
U	1	5	0	1	2
Rb	178	180	223	195	207
Sr	49	125	84	66	48
Y	15	12	68	18	9
Zr	97	193	105	104	84
Nb	7	9	15	11	7
Zn	15	26	42	14	9
Cu	16	29	20	16	12
Ni	0	0	0	0	0
La	31	29	23	32	22
Ba	81	789	211	202	148
V	3	3	0	10	2
Ce	60	59	46	50	46
Cr	0	0	0	0	0
Ga	13	16	21	14	13

Appendix A.2.2 (Continued)

A.2.2d Megacrystic hornblende + biotite quartz monzodiorite-granodiorite (unit 6D)

	V577-1	V727	V728	V730	V731	V309	V772
SiO2	65.70	63.80	65.10	66.80	64.80	66.10	64.00
TiO2	.35	.33	.45	.43	.38	.27	.71
Al2O3	15.60	16.90	16.40	16.00	16.30	17.10	17.50
Fe2O3	3.51	2.96	4.22	3.82	4.25	3.23	4.80
FeO	0.00	0.00	0.00	0.00	0.00	0.00	0.00
MnO	.07	.06	.08	.07	.07	.05	.16
MgO	1.43	1.15	1.65	1.52	1.60	1.04	1.37
CaO	3.36	2.30	3.53	3.12	3.74	2.67	3.22
Na2O	4.44	3.93	4.33	4.00	4.43	4.00	5.25
K2O	3.48	6.41	3.27	3.86	2.86	4.62	2.86
P2O5	.12	.11	.16	.15	.19	.13	.18
LOI	.88	.49	1.48	.57	.95	.64	.20
Total	98.94	98.44	100.67	100.34	99.57	99.85	100.25
Pb	18	22	15	13	14	13	17
Th	10	6	6	9	10	0	9
U	2	0	0	0	1	0	1
Rb	112	139	100	94	79	126	81
Sr	598	718	628	647	627	657	381
Y	22	13	23	13	20	30	24
Zr	116	98	148	137	158	127	221
Nb	13	7	14	7	10	13	13
Zn	49	42	58	47	51	39	87
Cu	19	13	24	23	23	43	22
Ni	2	1	0	0	1	2	0
La	10	14	15	13	14	13	18
Ba	964	2990	1077	1395	807	1669	1701
V	50	52	58	49	59	47	33
Ce	27	35	39	46	44	28	41
Cr	0	0	0	2	0	1	0
Ga	16	14	18	15	18	23	18

Appendix A.2.2 (Continued)

A.2.2e Biotite quartz monzonite-granite (unit 6E)

	V735	V734-1	CG311	CG300	V243-3	CG-263	V255-2	V574-1	V333-2	V385-1	V725	V732
SiO2	72.40	69.70	72.80	72.10	68.50	70.40	75.10	69.70	73.50	74.20	71.90	71.00
TiO2	.33	.40	.28	.25	.36	.47	.13	.36	.28	.16	.21	.20
Al2O3	13.20	15.00	13.95	15.10	14.70	14.55	12.70	15.00	14.50	12.80	13.90	14.30
Fe2O3	1.51	2.60	.56	.53	3.56	.60	1.60	2.32	1.99	1.94	1.73	1.98
FeO	0.00	0.00	1.70	1.46	0.00	2.55	0.00	0.00	0.00	0.00	0.00	0.00
MnO	.05	.07	.05	.04	.05	.08	.03	.05	.04	.03	.04	.05
MgO	.52	.84	.22	.22	.41	.44	.07	.71	.19	.06	.46	.59
CaO	1.30	2.02	.92	.94	1.42	1.04	.75	1.98	.93	.99	1.24	1.64
Na2O	3.75	4.21	4.05	4.70	3.92	4.92	3.43	4.14	4.77	2.93	3.72	3.90
K2O	4.48	4.29	5.81	5.99	5.84	4.87	5.41	4.56	3.73	5.66	5.08	4.51
P2O5	.03	.11	.01	0.00	.13	0.00	.01	.12	.01	.01	.10	.05
LOI	.54	1.02	.88	.48	.51	.60	.50	1.26	.45	.47	.84	.76
Total	98.11	100.26	101.23	101.81	99.40	100.52	99.73	100.20	100.39	99.25	99.22	98.98
Pb	18	19	30	44	30	37	40	22	22	56	18	24
Th	11	10	24	17	11	14	68	16	8	62	11	46
U	0	6	5	3	6	3	8	4	0	5	2	6
Rb	110	132	226	269	184	179	184	105	91	340	111	112
Sr	196	369	76	111	139	146	76	371	102	57	253	323
Y	7	17	42	42	77	109	18	8	41	185	7	9
Zr	95	148	372	271	418	553	220	140	208	211	109	120
Nb	7	9	27	27	31	59	8	4	7	86	3	7
Zn	31	50	40	41	43	80	27	40	33	43	28	34
Cu	16	15	0	0	14	0	14	16	9	15	13	14
Ni	0	2	41	51	0	66	0	0	0	4	0	0
La	14	25	123	79	63	124	41	16	27	60	13	23
Ba	567	967	320	455	614	615	298	1094	323	229	723	819
V	10	21	0	7	9	18	0	23	3	0	14	17
Ce	28	49	341	282	117	361	93	38	65	122	33	41
Cr	0	2	0	0	0	0	0	0	0	0	5	0
Ga	10	17	22	26	21	23	16	15	22	19	12	15

Appendix A.2.3 Major and trace element geochemistry of gabbroids correlated with the Adlavik Intrusive Suite (?) (unit 7)

	V149	V177-1	V178-1	V416-2	V416-3	V302-2	CG329	V768	V562	V597-8	V670
SiO2	49.50	47.50	43.20	49.80	48.70	49.20	46.50	52.10	44.10	53.10	50.00
TiO2	.16	.31	1.78	.80	1.20	.48	.50	.31	.30	1.18	1.01
Al2O3	4.17	26.80	15.20	12.60	17.40	10.60	6.60	14.50	6.30	17.00	21.20
Fe2O3	8.14	4.47	18.42	10.78	10.32	8.30	1.48	8.30	12.72	9.68	7.95
FeO	0.00	0.00	0.00	0.00	0.00	0.00	8.37	0.00	0.00	0.00	0.00
MnO	.15	.06	.21	.20	.17	.14	.18	.13	.18	.14	.10
MgO	19.75	1.70	7.07	9.20	7.21	13.82	19.19	10.23	26.60	4.27	2.77
CaO	14.90	12.08	11.44	13.02	10.24	10.75	13.95	10.44	6.76	6.60	9.84
Na2O	.53	2.87	1.72	1.99	2.83	2.18	.75	1.93	1.04	3.77	3.83
K2O	.22	1.01	.94	.55	1.39	1.33	.32	1.05	.65	2.83	1.50
P2O5	.03	.14	.23	.10	.12	.20	.02	.05	.08	.49	.87
LOI	1.20	2.77	.70	.96	.95	1.25	1.58	1.64	1.23	.34	.44
Total	98.75	99.71	100.91	100.00	100.53	98.25	99.44	100.68	99.96	99.40	99.51
Pb	1	0	0	0	0	4	5	0	5	10	4
Th	0	0	0	0	0	0	3	12	8	8	2
U	0	0	0	0	0	0	0	0	0	0	0
Rb	8	24	27	4	45	27	5	28	16	91	50
Sr	123	1699	983	486	732	535	190	653	274	680	1084
Y	10	7	18	29	36	18	12	13	8	31	27
Zr	22	25	38	99	140	52	14	27	32	138	39
Nb	1	4	7	5	12	6	0	3	2	7	6
Zn	42	34	93	99	119	61	35	62	85	88	68
Cu	69	18	25	53	15	32	31	23	13	24	26
Ni	156	0	0	43	14	215	91	50	521	14	0
La	11	17	18	18	20	15	0	0	2	8	11
Ba	143	627	694	218	447	469	136	280	283	988	709
V	173	123	537	250	265	149	201	120	118	130	128
Ce	8	11	30	18	27	18	70	12	8	41	25
Cr	2091	0	0	20	0	911	1830	312	1336	29	0
Ga	6	24	14	16	18	12	5	13	9	18	21

Note: Zero values for FeO are those samples in which all iron is expressed as Fe_2O_3

Appendix A.2.4 Major and trace element geochemistry of clinopyroxene-bearing plutonites

A.2.4a Layered clinopyroxene-bearing monzonite-syenite (unit 8A)

	V629-2	V597-1	V62	V3
SiO2	66.30	68.40	58.70	65.40
TiO2	.52	.40	.87	.77
Al2O3	14.00	15.50	17.00	14.40
Fe2O3	5.63	2.73	7.36	5.34
FeO	0.00	0.00	0.00	0.00
MnO	.10	.05	.15	.10
MgO	.39	.56	.83	.79
CaO	2.14	1.72	3.50	1.99
Na2O	3.72	4.41	5.07	3.58
K2O	6.15	5.76	5.30	6.00
P2O5	.09	.19	.28	.13
LOI	.61	.38	.21	.74
Total	99.65	100.10	99.27	99.24
Pb	28	14	25	26
Th	1	12	0	3
U	1	0	0	0
Rb	131	158	124	136
Sr	107	293	263	186
Y	95	20	79	102
Zr	675	185	288	674
Nb	35	8	32	43
Zn	128	32	119	102
Cu	17	14	15	12
Ni	0	0	0	0
La	42	13	48	71
Ba	892	1006	1604	909
V	8	13	0	16
Ce	100	40	101	128
Cr	0	0	0	0
Ga	23	14	27	21

Appendix A.2.4 (Continued)

A.2.4b Massive to foliated clinopyroxene-bearing monzonite unit (unit 8B)

	V306	V302-1	V765	V760	V762	V453-1	V743-2	V763-2	V303	CG-395	CG-753	CG-757
SiO2	59.90	58.80	55.70	60.90	63.10	57.10	52.00	57.50	59.90	56.80	57.50	59.40
TiO2	.76	.92	.74	.80	.76	.73	1.50	.59	.64	2.35	.69	.68
Al203	18.00	17.60	16.60	16.70	15.50	16.80	18.10	16.70	18.80	17.15	16.93	15.80
Fe203	6.53	7.03	8.26	5.60	5.28	7.42	9.16	7.61	5.54	2.96	1.98	3.12
FeO	0.00	0.00	0.00	0.00	0.00	0.00	0.00	0.00	0.00	4.54	4.38	2.59
MnO	.13	.14	.15	.13	.09	.13	.09	.14	.10	.14	.13	.10
MgO	2.11	2.22	4.38	1.97	2.05	3.63	3.75	3.90	1.67	3.66	3.08	4.17
CaO	5.10	3.84	7.42	3.90	3.88	6.57	7.44	6.59	4.61	6.72	5.69	4.28
Na20	4.44	4.72	4.02	4.63	3.99	4.01	3.70	4.07	5.75	4.05	4.18	4.54
K20	3.05	4.26	2.05	4.08	3.84	2.28	1.65	2.47	2.43	2.35	2.94	3.86
P205	.33	.36	.33	.26	.29	.36	.83	.31	.24	.31	.30	.20
LOI	.41	.55	.44	.33	.92	.35	.77	.50	.21	.90	.77	.83
Total	100.76	100.44	100.09	99.30	99.70	99.38	98.99	100.38	99.89	101.93	98.57	99.57
Pb	11	10	9	12	19	8	5	14	3	12	9	25
Th	2	0	8	2	19	6	2	1	0	6	6	13
U	1	2	0	0	1	0	0	3	0	28	33	22
Rb	64	65	47	79	110	67	47	82	32	65	70	152
Sr	639	693	829	478	578	798	1232	769	788	0	691	468
Y	31	35	28	29	35	31	26	26	28	31	28	13
Zr	114	308	57	146	241	77	125	90	251	76	86	147
Nb	9	22	6	11	16	10	11	6	13	3	2	12
Zn	82	109	90	72	70	79	119	79	75	74	61	25
Cu	24	14	46	22	19	47	36	41	11	38	32	2
Ni	0	5	14	0	5	8	4	13	6	33	22	21
La	27	37	13	12	22	16	19	15	50	33	24	15
Ba	1351	1747	929	1563	1106	810	1444	1112	1074	1026	1076	1161
V	93	81	163	76	77	143	173	140	69	156	124	20
Ce	47	63	43	43	66	45	54	46	69	108	70	166
Cr	0	0	37	3	11	22	6	36	0	30	15	5
Ga	20	22	20	17	20	17	22	16	22	20	19	20

Appendix A.2.5 Major and trace element geochemistry of layered clinopyroxene-bearing ferrodiorite-ferrosyenite (unit 9)

	V341-2	V119-1	V497	V535	V538	V540	V737	V330
SiO2	62.80	62.00	55.50	65.00	61.90	64.70	58.40	60.90
TiO2	.69	.57	1.11	.42	.98	.70	1.31	.72
Al2O3	14.00	13.60	16.70	14.20	14.60	13.80	15.10	15.50
Fe2O3	10.40	9.79	9.15	6.76	7.93	6.40	9.36	8.43
FeO	0.00	0.00	0.00	0.00	0.00	0.00	0.00	0.00
MnO	.30	.31	.14	.20	.19	.16	.22	.21
MgO	.10	.12	3.17	.09	.90	.60	1.13	.58
CaO	2.74	2.51	5.44	1.89	2.50	1.93	2.92	2.56
Na2O	3.81	4.03	4.05	4.91	4.73	4.54	4.95	5.24
K2O	5.66	5.34	3.29	5.58	5.33	5.61	5.44	5.25
P2O5	.03	.02	.49	0.00	.30	.15	.38	.21
LOI	.23	.02	.98	.31	.66	.85	.45	.41
Total	100.76	98.31	100.02	99.36	100.02	99.44	99.66	100.01
Pb	12	34	14	21	39	28	25	40
Th	17	17	5	27	13	18	8	14
U	3	5	1	2	0	3	5	9
Rb	116	153	107	142	135	135	103	175
Sr	34	41	641	37	150	104	176	63
Y	115	170	36	158	132	149	148	140
Zr	1488	1295	138	1082	1078	1261	1299	673
Nb	25	61	8	50	39	42	48	47
Zn	202	226	98	177	159	148	240	201
Cu	11	11	22	12	12	11	12	13
Ni	0	2	2	1	0	0	1	1
La	197	126	13	289	65	116	51	66
Ba	107	131	1193	80	953	610	1593	471
V	0	0	116	0	11	11	9	0
Ce	386	265	51	530	151	220	131	140
Cr	0	0	0	0	0	0	0	0
Ga	28	38	19	32	29	26	25	31

Nore: Zero values for FeO are for those samples in which all iron is expressed as Fe_2O_3

Appendix A.2.6 Major and trace element geochemistry of olivine-bearing mafic rocks (units 10, 11)

	V505-1	V505-2	V519-1	V519-2	V554-1
SiO2	47.50	47.30	45.60	46.80	47.70
TiO2	2.25	2.05	2.96	2.99	2.40
Al2O3	14.70	15.60	13.00	13.20	15.50
Fe2O3	14.99	14.27	16.88	16.42	15.74
FeO	0.00	0.00	0.00	0.00	0.00
MnO	.19	.17	.26	.21	.19
MgO	6.63	6.67	6.41	5.62	5.60
CaO	8.28	8.35	8.09	8.42	7.86
Na2O	2.77	2.76	2.92	2.85	2.95
K2O	1.24	1.16	1.35	1.50	1.21
P2O5	.40	.40	.69	.82	.53
LOI	1.45	.11	1.68	1.03	.08
Total	100.40	98.84	99.84	99.86	99.76
Pb	5	14	5	11	10
Th	1	4	5	4	6
U	0	3	3	0	1
Rb	28	28	48	35	29
Sr	287	311	351	383	314
Y	45	46	42	48	55
Zr	233	214	227	264	264
Nb	12	9	20	18	11
Zn	131	117	118	104	148
Cu	36	40	46	36	36
Ni	83	93	45	26	56
La	15	17	16	20	12
Ba	589	538	468	617	635
V	265	221	390	323	239
Ce	54	60	61	68	56
Cr	104	114	59	29	52
Ga	19	22	20	18	20

V505-1 = Michael gabbro (unit 10); chilled margin
V505-1 = Michael gabbro (unit 10); centre of dyke
V554-1 = Michael gabbro (unit 10); centre of dyke
V519-1 = non-coronitic olivine gabbro (unit 11); chilled margin
V519-2 = non-coronitic olivine gabbro (unit 11); centre of dyke

Note: Zero values for FeO are for those samples in which all iron is expressed as Fe_2O_3

A.3 RUBIDIUM-STRONTIUM GEOCHRONOLOGY AND ANALYTICAL RESULTS

Rubidium-strontium ratios were obtained on pressed powder pellets using a Phillips 1450 X-ray flourescence spectrometer calibrated against international rock standards. Cycles of 10 to 20 runs were employed for each sample, the higher number of replicate analyses being used on mafic rocks (e.g. unit 7).

Samples were prepared for Sr separation in groups of ten, including one duplicate and one blank for each 20 samples. Depending upon the Rb-Sr ratio of the sample, 0.5 to 1.0g of sample were dissolved in 10-15ml of HF and 2ml of HClO4 and evaporated to dryness on a hot plate at ca. 150C. Then, 10-15ml HF were added and the sample was again dried. The sample was redissolved first in 10-15ml 2N HCl and 2ml HClO4 and dried, and then was redissolved again in 10-15ml of 2N HCl and evaporated to dryness. After being redissolved in 5ml warm 2N HCl and diluted with distilled water, the sample was ready for strontium separation in ion exchange columns.

Borosilicate glass columns measuring 18 X 1cm were filled to a height of 15cm with 100 to 200 mesh rexyn 101 cation resin. The resin was preconditioned with 30ml of 2N HCl, and the samples were lead onto the columns through funnels lined with size 1 filters. Increments of 2N HCl totalling 85ml were passed through the columns to remove other ions, and discarded. The strontium was stripped from the columns with 20ml of 2N HCl. The final eluant was evaporated to one drop and stored in a vial. The sample was loaded with 2-3 microlitres of H3PO4 onto a degassed tantalum filament and heated until dried. The samples were analysed in groups of six on a Vacuum Generators Micromass 30B mass

spectrometer using a Faraday detector. Data were collected in blocks of five cycles. The mean of each block of five cycles was determined, and blocks with a 1-sigma error greater than 2 in the fourth decimel place were rejected. The mean of the remaining blocks was determined, and the data were accepted if the uncertainty of the mean was ≤ 2 in the fourth decimel place at the 2-sigma level. The data for the seven isochrons are presented in Table A-3. 87Sr/86Sr ratios are reported to six decimel places with 1-sigma errors; Rb/Sr ratios are reported to 3 decimal places. The Rb/Sr ratios are assumed to have a 1% (relative) analytical error. Duplicates were analysed for high Rb/Sr samples for each isochron in order to determine analytical precision. These replicate analyses demonstrate that the 87Sr/86Sr determinations are precise to ≤ 1 in the fourth decimel place, and all replicate analyses are within the reported 1-sigma errors. The Rb/Sr determinations are precise to ≤ 8 in the second decimel place.

The Rb/Sr and 87Sr/86Sr ratios were regressed by the weighted linear least squares method according to their analytical error. A decay constant of 1.42 x 10^{-11} /yr (Seiger and Jager, 1977) was adopted. Analytical errors associated with 87Sr/86Sr ratios were expressed at the 1-sigma level in the regression, and an error of 1% (relative), which exceeds the precision stated above, was assumed for Rb/Sr ratios. The accuracy of the Rb/Sr determinations was determined from repeated runs of standard G2 (see section A.2). The accuracy of the 87Sr/86Sr analyses was determined by repeated runs of standard NBS-987 strontium carbonate. Thirteen replicate analyses of this standard yield an average of value of .710249 $\pm$ .000008 (1-sigma).

TABLE A-3. Rubidium-strontium compositional data.

	$^{87}Sr/^{86}Sr \pm 10^{6}\sigma$		Rb/Sr	ppmSr	Location	
[1] Ferrosyenite-ferrodiorite (unit 9)						
V119-1	.954093	36	10.925	41	54°37'30"N	57°19'00"W
V119-1d	.954050	63	10.902	40		
V341-2	.936708	73	9.982	41	54°37'30"	57°19'00"
V497	.712979	22	.462	670	54°34'00"	57°16'20"
V538	.760969	39	2.387	161	54°34'45"	57°21'45"
V540	.791809	25	3.433	112	54°35"30"	57°24'00"
V736	1.004111	54	12.946	29	54°37'15"	57°25'30"
V737	.739866	38	1.582	177	54°36'20"	57°26'00"
[2] Biotite granite (unit 6E)						
V255-2	.876507	67	6.961	76	54°33'25"	57°10'00"
V255-2d	.876431	79	7.085	75		
V725	.733041	41	1.204	267	54°40'00"	57°30'00"
V732	.727468	82	0.975	342	54°39'45"	57°30'05"
V735	.742511	19	1.602	205	54°39'00"	57°26'50"
[3] Quartz monzodiorite-granodiorite (unit 6A)						
CG79-344	.711756	60	.332	766	54°27'25"	56°55'08"
CG79-366	.730820	90	1.063	393	54°27'47"	57°14'38"
CG79-377	.716752	60	.512	561	54°28'13"	57°18'10"
V192	.715418	60	.467	472	54°31'00"	57° 9'00"
V264	.710538	17	.282	889	54°28'40"	57°19'30"
V264d	.710536	31	.282	897		
V333-1	.730741	55	1.081	396	54°35'00"	57° 8'00"
V340	.732177	89	1.130	370	54°33'00"	57° 9'30"
[4] Adlavik(? Gabbro (unit 6))						
V149	.706504	36	.178	123	54°27'30"	57°13'00"
V178-1	.704185	17	.079	982	54°31'30"	57°12'30"
V241	.712153	43	.376	680	54°33'20"	57°11'40"
V302-2	.706452	17	.145	535	54°26'50"	57°24'00"
V597-8	.711383	19	.378	693	54°32'40"	57°16'00"
V597-8d	.711367	52	.370	690		
V637	.708361	44	.245	273	54°34'30"	57°17'00"
V670	.706133	20	.125	1108	54°34'30"	57°17'00"

TABLE A-3 (Continued)

	$^{87}Sr/^{86}Sr \pm 10^{6}\sigma$		Rb/Sr	ppmSr	Location	
[5] Hornblende + Biotite Monzodiorite-Monzonite (unit 6B)						
V009-4	.761143	53	2.288	173	54° 29'25"N	57° 14'00"W
V032	.765224	48	2.515	178	54° 29'30"	57° 13'00"
V119-2	.720132	35	.637	583	54° 37'30"	57° 19'00"
V164	.780179	61	3.186	150	54° 29'00"	57° 19'00"
V164d	.780124	92	3.182	151		
V225-2	.784599	52	3.299	157	54° 29'30"	57° 11'30"
V255-1	.751639	47	1.963	303	54° 33'25"	57° 10'00"
V257-6	.803820	115	4.099	104	54° 29'30"	57° 14'00"
V257-6d	.803845	93	4.089	104		
V293	.715145	49	.451	620	54° 28'00"	57° 20'00"
V341-1	.716274	16	.522	579	54° 36'00"	57° 19'10"
[6] Jotunitic-charnockitic gneiss (unit 3A)						
V193	.706221	42	.113	858	54° 27'30"	56° 56'45"
V193d	.706250	89	.117	860		
V193-3	.712323	32	.350	585	54° 27'30"	56° 56'45"
V526-1	.721893	49	.727	488	54° 27'45"	57° 18'00"
V526-1d	.721770	36	.727	490		
V579-1	.722854	39	.666	376	54° 28'30"	56° 58'30"
V586	.709390	46	.247	765	54° 29'00"	56° 57'30"
V687	.707830	76	.181	938	54° 28'20"	57° 19'50"
[7] Dioritic-tonalitic gneiss (unit 2)						
CG79-339	.708590	86	.225		54° 28'52"	57° 2'20"
V211-1	.776895	54	2.596	142	54° 27'30"	56° 54'00"
V213	.764756	105	2.097	137	54° 27'25"	56° 53'00"
V213d	.764860	51	2.113			
V325-1	.733164	39	1.177	349	54° 28'00"	57° 16'40"
V379-2	.773360	26	2.542	149	54° 24'30"	57° 6'10"
V588-2	.707869	57	.169	571	54° 29'00"	57° 1'30"
V774	.711640	32	.358	835	54° 39'00"	57° 34'00"

*d = duplicate analysis

A.4 MINERAL ANALYSES

Mineral analyses were obtained using a fully automated JEOL JXA-50A wavelength dispersive electron microprobe with Krisel control, equiped with three spectrometers and a Digital Equipment Corporation PDP-11 computer with a teleprinter. The microprobe was operated with a beam current of 22 nanoamps and an accelerating voltage of 15kV. Counts were made for 30 seconds or to a maximum of 60,000. A beam diameter of 1-2 micrometers was employed for all minerals except for perthitic feldspars, for which a defocussed (10-15 micrometers) beam was used. Bence-Albee corrections were employed in data reduction, and analyses were performed using a variety of calibrations based on appropriate standards. Values of the homogeneity index (sigma ratio) presented along each analysis provided a quantitative means for determining whether analytical differences recorded between grains or within grains (e.g. zoned crystals) were valid given the analytical capability of the machine.

Analytical errors associated with the mineral analyses determined with the electron microprobe have been evaluated by noting the extent to which analyses performed on the clinopyroxene "FCPX" varied from the composition published for this standard. This standard, among others, was analysed routinely during operation of the microprobe. The data presented in Table A-4-1 are based on FCPX analyses determined at 20 different sittings at the microprobe, and give an idea of the probable range of analytical errors associated with the analyses presented in Tables A-4-2 to A-4-10. It should be noted that the analytical error associated with elements occurring in minor or trace quantities in a given mineral will be significantly higher than in minerals in which the element is a major

TABLE A-4. Analytical errors associated with repeated analyses of clinopyroxene standard FCPX using the electron microprobe.

	Na	Mg	Al	Si	Ca	Ti	Mn	Fe
x (error)	.04	.39	.22	.52	-.08	-.11	-.03	-.02
σ (error)	.17	.33	.19	1.53	.34	.13	.04	.35
FCPX (std)	1.27	15.47	7.86	49.85	17.75	.83	.14	6.17
Avg. 20	1.31	15.86	7.64	50.37	17.67	.72	.11	6.15
Avg. + 1σ	1.48	16.19	7.83	51.90	18.01	.85	.18	6.50
Avg. - 1σ	1.14	15.53	7.45	48.84	17.33	.59	.07	5.80

constituent. The potassium content in FCPX is too small for the averaging process to be statistically significant for this element.

Microprobe analyses are unable to distinguish ferric from ferrous iron, and total iron in the analyses in Tables A-4-2 through A-4-10 is expressed as FeO. Electroneutrality has been assumed for analyses of all ferromagnesian minerals except for biotite, and charge imbalances in these minerals have been assumed to result from the presence of Fe2O3. Charge balancing in this manner is inappropriate for biotite, which may contain significant site vacancies (e.g. Percival, 1983). Two recalculation schemes are presented for amphibole analyses (Tables A-4-5, A-4-6). These are discussed in Chapter 4.3.

The mineralogy of all samples for which mineral analyses are presented is listed in Appendix B.

Appendix A.4.1 Orthopyroxene Analyses.

Unit Number	Analysis Number
1C	12,13,14,21
2	4
3A	1,2,3,8,9,10,11,15,16,20
pre-migmatitic metabasites	5,6,7,17,18,19

	1		2	3	4	5	
	rim	core				rim	core
SiO_2	50.54	50.29	50.28	49.44	52.14	53.28	51.68
TiO_2	0.11	0.86	0.11	0.07	0.07	0.12	0.14
Al_2O_3	0.61	0.62	0.64	0.40	1.23	0.72	0.98
Cr_2O_3	nd	nd	nd	nd	0.00	0.03	0.04
FeO	33.05	32.30	29.42	32.39	23.95	23.93	24.56
MnO	0.77	0.75	0.97	1.71	0.78	0.75	0.75
MgO	16.14	15.93	17.62	15.38	22.15	22.47	22.32
CaO	0.52	0.59	0.50	0.79	0.57	0.45	0.47
Na_2O	nd	nd	nd	nd	0.07	0.04	0.00
	101.74	101.34	99.54	100.18	100.96	101.79	100.94
	Number of ions on the basis of 6 oxygens						
Si	1.953	1.946	1.957	1.952	1.944	1.965	1.934
Aliv	0.028	0.028	0.029	0.019	0.054	0.031	0.043
Alvi	0.000	0.000	0.000	0.000	0.000	0.000	0.000
Ti	0.003	0.025	0.003	0.002	0.002	0.003	0.004
Cr	--	--	--	--	0.000	0.001	0.001
Fe^{3+}	0.002	0.004	0.007	0.000	0.000	0.001	0.002
Fe^{2+}	1.066	1.042	0.951	1.069	0.747	0.737	0.767
Mn	0.025	0.025	0.032	0.057	0.025	0.023	0.024
Mg	0.930	0.919	1.022	0.905	1.231	1.235	1.245
Ca	0.022	0.024	0.021	0.033	0.023	0.018	0.019
Na	--	--	--	--	0.005	0.003	0.000
	(3)*	(4)	(3)	(3)	(3)	(3)	(3)

( )* = number of analyses

analysis 1: V585, in contact with cpx

analysis 2: V586 coexists with cpx

analysis 3: V687 coexists with cpx

analysis 4: V581-1 coexists with cpx

analysis 5: V580-8, in contact with cpx

	6		7		8	9	10	11
	rim	core	rim	core				
SiO_2	52.07	53.30	52.74	52.48	49.49	47.45	49.35	51.41
TiO_2	0.06	0.14	0.04	0.03	0.10	0.02	0.05	0.18
Al_2O_3	0.87	0.89	0.39	0.47	0.50	0.30	0.34	0.53
Cr_2O_3	0.06	0.04	nd	nd	nd	nd	nd	nd
FeO	23.21	22.96	27.30	26.35	38.17	45.89	36.59	31.33
MnO	0.71	0.67	0.82	0.76	1.19	2.98	1.55	1.06
MgO	22.72	22.78	20.52	20.74	10.99	5.08	11.14	15.57
CaO	0.41	0.64	0.42	0.48	0.70	0.83	0.77	1.21
Na_2O	0.00	0.02	nd	nd	nd	nd	nd	nd
	100.11	101.44	102.23	101.31	101.14	102.55	99.79	101.29
	Number of ions based on 6 oxygens							
Si	1.951	1.964	1.968	1.969	1.979	1.966	1.986	1.982
Aliv	0.038	0.036	0.017	0.021	0.021	0.015	0.014	0.018
Alvi	0.000	0.002	0.000	0.000	0.002	0.000	0.002	0.006
Ti	0.002	0.004	0.001	0.001	0.003	0.001	0.002	0.005
Cr	0.002	0.001	--	--	--	--	--	--
Fe^{3+}	0.000	0.000	0.001	0.000	0.001	0.000	0.000	0.000
Fe^{2+}	0.727	0.708	0.851	0.827	1.275	1.590	1.231	1.010
Mn	0.023	0.021	0.026	0.024	0.040	0.105	0.053	0.035
Mg	1.269	1.251	1.141	1.160	0.655	0.314	0.684	0.895
Ca	0.016	0.025	0.010	0.019	0.030	0.037	0.033	0.050
Na	0.000	0.000	--	--	--	--	--	--
	(2)*	(2)	(3)	(3)	(4)	(4)	(3)	(4)

( )* = number of analyses

analysis 6: V580-8, in contact with cpx

analysis 7: V194-2, in contact with cpx

analysis 8: V376

analysis 9: V470-2

analysis 10: V526-1

analysis 11: V193

	12	13		14		15	
		rim	core	rim	core	rim	core
SiO_2	47.03	48.52	47.29	49.21	47.27	51.47	49.89
TiO_2	0.20	0.09	0.10	0.04	0.08	0.02	0.04
Al_2O_3	6.11	5.75	6.50	4.85	5.96	1.21	2.13
FeO	29.53	25.55	27.54	25.07	27.69	31.96	33.22
MnO	0.29	0.46	0.61	0.43	0.55	0.33	0.37
MgO	17.10	18.55	17.53	19.84	17.37	15.96	15.08
CaO	0.07	0.09	0.13	0.06	0.12	0.13	0.16
Na_2O	nd	nd	nd	nd	nd	nd	nd
	100.33	99.01	99.70	99.50	99.04	101.08	100.89
	Number of ions on the basis of 6 oxygens						
Si	1.812	1.856	1.818	1.868	1.831	1.979	1.939
Aliv	0.188	0.144	0.182	0.132	0.169	0.021	0.061
Alvi	0.090	0.115	0.113	0.086	0.104	0.034	0.037
Ti	0.006	0.003	0.003	0.001	0.002	0.001	0.001
Fe^{3+}	0.002	0.000	0.000	0.000	0.007	0.000	0.000
Fe^{2+}	0.950	0.817	0.886	0.796	0.890	1.028	1.080
Mn	0.009	0.015	0.020	0.014	0.018	0.011	0.012
Mg	0.982	1.058	1.005	1.123	1.003	0.915	0.874
Ca	0.003	0.004	0.005	0.002	0.005	0.005	0.007
Na	--	--	--	--	--	--	--
	(3)*	(5)	(3)	(4)	(4)	(4)	(4)

( )* = number of analyses

analysis 12: V207, coexists with garnet + cordierite
analysis 13: V210-1, in contact with garnet + cordierite
analysis 14: V210-1, in contact with garnet + cordierite
analysis 15: V221, in contact with garnet

	16		17		18		19
	rim	core	rim	core	rim	core	
SiO_2	52.62	52.58	54.37	52.67	54.36	54.70	51.22
TiO_2	0.04	0.09	0.01	0.02	0.03	0.06	0.04
Al_2O_3	0.35	0.29	0.65	0.52	0.90	0.95	0.40
Cr_2O_3	0.00	0.00	0.00	0.01	0.16	0.17	0.00
FeO	28.56	28.03	23.67	23.78	19.58	19.58	31.53
MnO	0.91	0.82	0.72	0.76	0.64	0.52	1.39
MgO	18.47	18.22	22.57	22.43	25.10	25.04	15.96
CaO	0.52	0.70	0.57	0.53	0.38	0.68	0.96
Na_2O	0.00	0.02	0.03	0.03	0.01	0.03	0.07
	101.47	100.75	102.59	100.75	101.16	101.73	101.57
	Number of ions on the basis of 6 oxygens						
Si	1.990	11.998	1.982	1.964	1.973	1.974	1.975
Aliv	0.010	0.002	0.018	0.023	0.027	0.026	0.018
Alvi	0.005	0.011	0.010	0.000	0.012	0.014	0.000
Ti	0.001	0.003	0.000	0.001	0.001	0.002	0.001
Cr	0.000	0.000	0.000	0.000	0.005	0.005	0.000
Fe^{3+}	0.003	0.000	0.002	0.001	0.000	0.000	0.000
Fe^{2+}	0.900	0.891	0.720	0.741	0.594	0.591	1.017
Mn	0.029	0.026	0.022	0.024	0.020	0.016	0.045
Mg	1.041	1.032	1.226	1.247	1.358	1.347	0.917
Ca	0.021	0.029	0.022	0.021	0.015	0.026	0.040
Na	0.000	0.001	0.002	0.002	0.001	0.002	0.005
	(3)*	(3)	(3)	(4)	(3)	(3)	(3)

( )* = number of analyses

analysis 16: V526-3A in contact with cpx
analysis 17: V526-3B in contact with cpx
analysis 18: V580-7 in contact with cpx
analysis 19: V711-2 coexists with cpx

	20		21
	rim	core	
SiO_2	49.00	47.01	47.94
TiO_2	0.16	0.07	0.05
Al_2O_3	1.91	3.71	6.07
FeO	31.81	34.00	27.62
MnO	0.30	0.35	1.00
MgO	15.66	14.25	17.31
CaO	0.21	0.19	0.11
Na_2O	nd	nd	0.02
	99.05	99.58	100.13

Number of ions on the basis of 6 oxygens

Si	1.933	1.869	1.837
Aliv	0.067	0.131	0.163
Alvi	0.022	0.042	0.111
Ti	0.005	0.002	0.001
Fe^{3+}	0.001	0.009	0.003
Fe^{2+}	1.049	1.121	0.882
Mn	0.010	0.012	0.032
Mg	0.921	0.844	0.989
Ca	0.009	0.008	0.005
Na	--	--	0.001
	(5)*	(3)	(4)

( )* = number of analyses

analysis 20 : V579-1, in contact with garnet
analysis 21 : V580-12, coexists with garnet + cordierite

Appendix A.4.2 Clinopyroxene Analyses.

Unit Number	Analysis Number
2	4
3A	1,2,3,8,9,10
pre-migmatitic metabasites	5,6,7,11,12,13,14,15,16

	1		2	3	4	5	
	rim	core				rim	core
SiO_2	52.42	53.17	52.80	52.08	52.63	53.88	53.49
TiO_2	0.22	0.23	0.20	0.11	0.17	0.29	0.50
Al_2O_3	1.21	1.31	1.48	0.95	1.76	1.61	1.77
Cr_2O_3	0.00	0.02	0.00	0.00	0.00	0.09	0.08
FeO	11.71	12.70	11.51	12.78	8.71	7.31	8.41
MnO	0.25	0.32	0.40	0.55	0.33	0.23	0.27
MgO	12.60	12.22	13.06	11.79	14.48	14.82	14.30
CaO	22.38	21.64	21.97	21.46	21.97	22.95	22.41
Na_2O	0.43	0.42	0.50	0.48	0.54	0.30	0.18
	101.22	102.03	101.92	100.20	100.59	101.48	101.41
	Number of ions based on 6 oxygens						
Si	1.960	1.972	1.956	1.975	1.951	1.966	1.960
Aliv	0.040	0.028	0.044	0.025	0.049	0.034	0.040
Alvi	0.013	0.030	0.020	0.018	0.028	0.035	0.037
Ti	0.006	0.006	0.006	0.003	0.005	0.008	0.014
Cr	0.000	0.001	0.000	0.000	0.000	0.003	0.002
Fe^{3+}	0.000	0.001	0.000	0.000	0.000	0.001	0.000
Fe^{2+}	0.366	0.393	0.357	0.405	0.270	0.222	0.258
Mn	0.008	0.010	0.013	0.018	0.010	0.007	0.008
Mg	0.702	0.676	0.721	0.667	0.800	0.806	0.781
Ca	0.897	0.860	0.872	0.872	0.873	0.897	0.880
Na	0.031	0.030	0.036	0.035	0.039	0.021	0.013
	(3)*	(3)	(4)	(4)	(3)	(3)	(3)
Mol%							
Wo	45.1	43.9	44.0	44.4	44.1	45.7	44.7
En	35.8	35.1	37.0	34.0	41.3	42.2	41.2
Fs	19.1	21.0	19.0	21.6	14.5	12.1	14.1

( )* = number of analyses

analysis 1: V585, in contact with opx
analysis 2: V586
analysis 3: V687
analysis 4: V581-1
analysis 5: V580-8, in contact with opx

	6		7		8	9
	rim	core	rim	core		
SiO_2	53.64	53.07	54.13	54.26	52.78	52.61
TiO_2	0.35	0.41	0.06	0.70	0.08	0.07
Al_2O_3	1.75	1.89	0.71	0.99	2.19	1.97
Cr_2O_3	0.11	0.12	0.11	0.06	nd	nd
FeO	7.41	8.09	8.28	8.52	11.97	11.48
MnO	0.18	0.28	0.28	0.27	0.93	0.96
MgO	14.40	14.49	14.44	14.40	11.46	12.26
CaO	22.92	22.78	21.86	21.41	21.61	22.64
Na_2O	0.21	0.25	0.30	0.32	nd	nd
	100.97	101.38	100.17	100.93	101.02	101.99
	Number of ions on the basis of 6 oxygens					
Si	1.967	1.948	2.003	2.003	1.972	1.951
Aliv	0.033	0.052	--	--	0.028	0.049
Alvi	0.043	0.029	0.034	0.046	0.068	0.038
Ti	0.010	0.011	0.002	0.002	0.002	0.002
Cr	0.003	0.003	0.003	0.002	--	--
Fe^{3+}	0.000	0.002	--	--	0.004	0.000
Fe^{2+}	0.227	0.246	0.256	0.263	0.370	0.356
Mn	0.006	0.009	0.009	0.008	0.029	0.030
Mg	0.787	0.793	0.796	0.792	0.638	0.678
Ca	0.901	0.896	0.867	0.847	0.865	0.900
Na	0.015	0.018	0.022	0.023	--	--
	(3)*	(3)	(3)	(3)	(2)	(2)
Mol%						
Wo	46.0	45.1	44.8	44.0		
En	41.7	41.5	41.4	41.7		
Fs	12.3	13.4	13.8	14.3		

( )* = number of analyses

analysis 6: V580-8, in contact with opx
analysis 7: V194-2, in contact with opx
analysis 8: V471-2, associated with biotite
analysis 9: V471-2, associated with biotite + garnet

	10		11		12		13
	rim	core	rim	core	rim	core	
SiO_2	52.10	52.29	53.10	51.18	51.99	53.33	52.01
TiO_2	0.09	0.02	0.04	0.03	0.21	0.23	0.08
Al_2O_3	0.68	0.50	1.07	0.98	1.45	1.39	0.88
Cr_2O_3	0.00	0.00	0.01	0.00	0.17	0.21	0.02
FeO	10.03	10.26	8.14	8.44	6.55	6.11	12.32
MnO	0.26	0.38	0.32	0.32	0.23	0.18	0.47
MgO	13.50	13.37	15.31	15.12	15.63	15.66	11.73
CaO	22.00	21.82	22.42	21.54	24.18	24.31	22.57
Na_2O	0.36	0.30	0.42	0.39	0.18	0.20	0.43
K_2O	0.01	0.00	0.00	0.00	0.00	0.00	0.00
	99.03	98.94	100.83	98.00	100.59	101.62	100.51
Number of ions based on 6 oxygens							
Si	1.976	1.986	1.961	1.950	1.924	1.944	1.969
Aliv	0.024	0.014	0.039	0.044	0.063	0.056	0.031
Alvi	0.006	0.008	0.007	0.000	0.000	0.004	0.008
Ti	0.003	0.001	0.001	0.001	0.006	0.006	0.002
Cr	0.000	0.000	0.000	0.000	0.005	0.006	0.001
Fe^{3+}	0.002	0.000	0.002	0.000	0.001	0.002	0.000
Fe^{2+}	0.316	0.326	0.249	0.269	0.202	0.186	0.390
Mn	0.008	0.012	0.010	0.010	0.007	0.006	0.015
Mg	0.763	0.757	0.843	0.859	0.862	0.849	0.662
Ca	0.894	0.888	0.887	0.880	0.959	0.950	0.916
Na	0.026	0.022	0.030	0.029	0.013	0.014	0.032
K	0.000	0.000	0.000	0.000	0.000	0.000	0.000
	(3)*	(3)	(3)	(3)	(3)	(3)	(3)
( )* = number of analyses							
Mol%							
Wo	45.0	44.8	44.3	43.4	46.5	47.0	46.1
En	38.5	38.2	42.5	42.7	43.0	43.3	33.5
Fs	16.5	17.0	13.2	13.9	10.5	9.7	20.5

analysis 10: V526-3A, in contact with opx
analysis 11: V526-3B, in contact with opx
analysis 12: V580-7, in contact with opx
analysis 13: V711-2, coexists with opx

	14	15	16
SiO_2	53.69	53.84	51.26
TiO_2	0.04	0.000	0.66
Al_2O_3	0.56	1.61	1.48
Cr_2O_3	0.02	0.00	0.00
FeO	10.19	7.19	13.53
MnO	0.50	0.32	0.50
MgO	13.06	14.54	11.00
CaO	23.68	23.25	22.11
Na_2O	0.30	0.80	0.73
K_2O	0.00	0.00	0.00
	102.04	101.55	101.27

Number of ions based on 6 oxygens

Si	1.982	1.968	1.938
Aliv	0.018	0.032	0.062
Alvi	0.006	0.037	0.004
Ti	0.001	0.000	0.019
Cr	0.001	0.000	0.000
Fe^{3+}	0.000	0.000	0.000
Fe^{2+}	0.315	0.220	0.428
Mn	0.016	0.010	0.016
Mg	0.719	0.792	0.620
Ca	0.937	0.911	0.896
Na	0.021	0.057	0.054
K	0.000	0.000	0.000
	(2)*	(2)	(2)

( )* = number of analyses

Mol%

Wo	47.1	46.9	45.5
En	36.2	41.1	31.7
Fs	16.7	11.9	22.8

analysis 14: V42-1
analysis 15: V463
analysis 16: V041-2

Appendix A.4.3. Garnet Analyses (Garnets associated with pre-Grenvillian fabrics)

Unit Number	Analysis Number
1C	1,2,3,4,5,6,7,8,9,10,11,15,16
3A	12,13,14
5A,B	17(?),18,19,20

	1		2		3		4	
	rim	core	rim	core	rim	core	rim	core
SiO_2	36.21	36.22	37.92	37.93	37.87	38.19	38.52	37.45
TiO_2	0.00	0.00	0.02	0.00	0.01	0.00	0.00	0.00
Al_2O_3	21.18	21.33	22.16	22.09	21.92	22.10	21.31	21.38
FeO	32.99	34.72	31.35	31.61	31.11	31.06	28.33	28.98
MnO	2.39	1.88	0.92	0.91	2.15	2.15	8.07	7.82
MgO	2.97	4.09	6.78	7.01	6.98	6.81	4.29	4.86
CaO	4.00	1.93	1.13	1.15	1.20	1.16	0.71	0.91
	99.74	100.17	100.37	100.70	101.24	101.47	101.23	101.40
	Number of ions based on 24 oxygens							
Si	5.862	5.834	5.932	5.917	5.900	5.925	6.065	5.921
Aliv	0.138	0.166	0.068	0.083	0.100	0.075	--	0.079
Alvi	3.904	3.884	4.020	3.980	3.926	3.968	4.022	3.907
Ti	0.000	0.000	0.002	0.000	0.001	0.000	0.000	0.000
Fe^{3+}	0.014	0.006	0.016	0.009	0.000	0.007	--	0.002
Fe^{2+}	4.453	4.661	4.086	4.116	4.054	4.024	3.731	3.830
Mn	0.328	0.257	0.122	0.120	0.284	0.283	1.077	1.047
Mg	0.717	0.982	1.581	1.630	1.621	1.575	1.007	1.145
Ca	0.694	0.333	0.189	0.192	0.200	0.193	0.120	0.154
	(3)*	(4)	(5)	(5)	(6)	(7)	(4)	(4)
Mol%								
pyr	11.8	16.1	25.7	26.7	26.8	25.9	16.9	19.1
alm	71.4	74.2	69.2	68.1	65.1	66.2	62.9	60.7
gros	11.3	5.4	2.9	3.1	3.1	3.2	2.6	2.5
spes	5.4	4.2	1.9	2.0	4.7	4.6	18.1	17.5

( )* = number of analyses

analysis 1: V172, garnet in contact with biotite

analysis 2: V207, garnet associated with biotite

analysis 3: V210-1, garnet in contact with idiomorphic biotite

analysis 4: V211-2

	5		6		7		8	
	rim	core	rim	core	rim	core	rim	core
SiO_2	38.55	38.59	37.50	36.82	36.53	37.08	40.13	40.82
TiO_2	0.00	0.02	0.00	0.00	0.02	0.01	0.00	0.00
Al_2O_3	20.90	21.21	22.26	22.17	20.43	20.84	20.88	21.14
FeO	31.18	30.07	28.34	29.64	32.42	31.66	28.72	28.31
MnO	2.20	2.05	2.40	2.46	0.73	0.67	0.55	0.44
MgO	6.21	7.08	8.31	7.70	6.48	7.53	10.53	9.79
CaO	1.14	1.17	1.55	1.36	0.83	0.87	0.05	0.66
	100.18	100.19	100.36	100.15	97.44	98.66	100.86	101.16
	Number of ions based on 24 oxygens							
Si	6.067	6.037	5.837	5.788	5.944	5.923	6.118	6.186
Aliv	--	--	0.163	0.212	0.056	0.077	--	--
Alvi	3.946	3.949	3.923	3.897	3.863	3.849	3.871	3.963
Ti	0.000	0.002	0.000	0.000	0.002	0.001	0.000	0.000
Fe^{3+}	--	--	0.000	0.000	0.001	0.000	--	--
Fe^{2+}	4.105	3.935	3.682	3.892	4.411	4.230	3.662	3.588
Mn	0.293	0.272	0.316	0.328	0.101	0.091	0.071	0.056
Mg	1.457	1.651	1.928	1.804	1.571	1.793	2.393	2.211
Ca	0.192	0.196	0.259	0.229	0.145	0.149	0.008	0.107
	(4)*	(4)	(4)	(3)	(4)	(4)	(2)	(3)
Mol%								
pyr	25.0	28.1	31.4	29.3	26.7	30.4	42.5	39.0
alm	66.6	63.9	59.2	61.7	69.1	65.5	56.1	58.1
gros	3.3	3.3	4.2	3.6	2.4	2.5	0.1	1.9
spes	5.0	4.6	5.2	5.3	1.7	1.5	1.3	1.0

( )* = number of analyses

analysis 5: V580-1B

analysis 6: V580-16, garnet with cordierite mantle

analysis 7: CG-79-347, garnet associated with biotite

analysis 8: CG-79-347, garnet resorbed by cordierite

	9		10		11	
	rim	core	rim	core	rim	core
SiO_2	37.82	36.82	38.16	38.07	37.56	38.55
TiO_2	0.01	0.00	0.01	0.02	0.00	0.00
Al_2O_3	21.42	22.17	21.14	20.83	19.75	19.88
FeO	31.62	29.64	29.87	30.65	33.60	33.30
MnO	2.75	2.46	1.58	1.89	2.46	2.25
MgO	6.42	7.70	8.79	7.76	5.14	5.53
CaO	1.30	1.36	1.04	1.21	1.25	0.95
	101.34	100.15	100.59	100.43	99.76	100.46
	Number of ions based on 24 oxygens					
Si	5.922	5.788	5.937	5.967	6.040	6.166
Aliv	0.078	0.212	0.063	0.033	--	--
Alvi	3.876	3.897	3.815	3.817	3.385	3.835
Ti	0.001	0.000	0.001	0.002	0.000	0.000
Fe^{3+}	0.005	0.000	0.002	0.002	--	--
Fe^{2+}	4.136	3.892	3.885	4.017	4.520	4.419
Mn	0.365	0.328	0.208	0.251	0.335	0.302
Mg	1.498	1.804	2.038	1.813	1.232	1.308
Ca	0.218	0.229	0.173	0.203	0.215	0.162
	(2)*	(3)	(4)	(3)	(3)	(3)
Mol%						
pyr	25.3	29.3	35.0	31.4	21.9	23.4
alm	64.9	61.7	58.4	60.7	68.3	68.2
gros	3.7	3.6	2.9	3.5	3.8	2.9
spes	6.2	5.3	3.6	4.3	6.0	5.4

( )* = number of analyses

analysis 9: V580-16, same garnet as analysis 6, rim analysis adjacent to biotite inclusion

analysis 10: V580-12, garnet resorbed by cordierite

analysis 11: V580-12, garnet associated with biotite

	12		13		14	
	rim	core	rim	core	rim	core
SiO_2	38.59	38.81	37.50	37.36	37.62	38.06
TiO_2	0.02	0.04	0.00	0.02	0.01	0.01
Al_2O_3	19.57	20.15	20.68	20.65	20.33	20.51
FeO	25.11	24.44	36.40	35.53	34.14	31.16
MnO	6.61	7.83	1.74	1.48	1.24	1.24
MgO	3.46	2.79	3.67	4.46	3.87	4.83
CaO	7.01	7.52	1.58	1.53	1.72	1.61
	100.37	101.58	101.57	101.03	98.93	97.42
	Number of ions on the basis of 24 oxygens					
Si	6.130	6.103	5.974	5.956	6.083	6.153
Aliv	--	--	0.026	0.044	--	--
Alvi	3.795	3.840	3.858	3.838	3.959	4.063
Ti	0.002	0.005	0.000	0.002	0.001	0.001
Fe^{3+}	--	--	0.000	0.004	--	--
Fe^{2+}	3.336	3.215	4.850	4.734	4.617	4.214
Mn	0.889	1.043	0.235	0.200	0.170	0.170
Mg	0.819	0.654	0.871	1.060	0.933	1.164
Ca	1.193	1.267	0.270	0.261	0.298	0.279
	(3)*	(4)	(4)	(3)	(3)	(3)
Mol%						
pyr	14.90	11.66	14.95	18.19	16.04	19.84
alm	47.24	47.15	76.38	73.90	75.91	72.51
gros	21.65	22.51	4.63	4.44	5.10	4.73
spes	16.17	18.60	4.03	3.43	2.92	2.89

analysis 12: V471-2, coexists with clinopyroxene
analysis 13: V221, in contact with orthopyroxene
analysis 14: V579-1, in contact with orthopyroxene

	15		16		17	
	rim	core	rim	core	rim	core
SiO_2	37.79	38.17	37.96	38.21	39.78	38.07
TiO_2	0.00	0.00	0.02	0.00	0.00	0.00
Al_2O_3	22.17	22.17	21.68	22.04	20.61	20.42
FeO	30.97	30.52	31.25	31.61	28.88	29.84
MnO	2.25	2.32	2.05	2.01	2.19	2.31
MgO	6.98	6.99	6.98	6.64	8.56	7.98
CaO	1.21	1.19	1.18	1.14	0.91	1.15
	101.37	99.04	101.12	101.65	100.93	99.77
based on 24 oxygens						
Si	5.878	5.919	5.922	5.928	6.130	5.999
Aliv	0.122	0.081	0.078	0.072	(-.130)	0.001
Alvi	3.944	3.973	3.910	3.960	3.874	3.793
Ti	0.000	0.000	0.002	0.000	0.000	0.000
Fe^{3+}	0.000	0.006	0.002	0.000	0.000	0.002
Fe^{2+}	4.029	3.953	4.076	4.102	3.722	3.933
Mn	0.296	0.305	0.271	0.264	0.286	0.308
Mg	1.618	1.616	1.623	1.536	1.966	1.874
Ca	0.202	0.198	0.197	0.190	0.150	0.194
	(3)	(3)	(3)	(3)	(3)	(4)
Mol%						
pyr	26.53	26.55	27.12	25.37	35.00	32.94
alm	65.30	65.18	65.05	67.13	57.23	58.24
gros	3.31	3.19	3.26	3.07	2.68	3.41
spes	4.86	5.01	4.53	4.36	5.09	5.42

( )* = number of analyses

analysis 15: V210-1, in contact with orthopyroxene

analysis 16: V210-1, in contact with orthopyroxene

analysis 17: V210-1, in contact with cordierite

	18		19		20		21	
	rim	core	rim	core	rim	core	rim	core
SiO_2	37.18	37.58	36.66	36.07	37.26	37.32	37.25	38.66
TiO_2	0.00	0.00	0.03	0.10	0.04	0.04	0.02	0.04
Al_2O_3	19.99	20.18	19.00	18.59	18.65	18.85	18.77	18.64
FeO	39.04	38.35	19.93	20.15	22.79	23.08	22.26	21.43
MnO	1.20	1.61	16.04	15.84	12.06	12.38	9.11	9.79
MgO	3.07	3.38	0.20	0.12	0.25	0.25	0.92	1.04
CaO	1.13	0.89	7.34	7.53	8.17	7.95	11.11	11.36
	101.61	101.99	99.20	98.40	99.22	99.87	99.44	100.96
	Number of ions on the basis of 24 oxygens							
Si	5.982	6.001	6.052	6.025	6.126	6.105	6.068	6.174
Aliv	0.018	--	--	--	--	--	--	--
Alvi	3.774	3.801	3.750	3.686	3.742	3.740	3.672	3.683
Ti	0.000	0.000	0.004	0.013	0.005	0.005	0.002	0.005
Fe^{3+}	0.000	--	--	--	--	--	--	--
Fe^{2+}	5.254	5.123	2.752	2.815	3.134	3.158	3.033	2.862
Mn	0.164	0.218	2.243	2.241	1.680	1.716	1.257	1.324
Mg	0.736	0.805	0.049	0.030	0.061	0.061	0.223	0.248
Ca	0.195	0.152	1.298	1.348	1.440	1.394	1.939	1.944
	(2)*	(3)	(5)	(5)	(2)	(2)	(3)	(2)
Mol%								
pyr	12.94	14.11	0.89	0.54	1.13	1.12	4.13	4.70
alm	80.76	79.39	35.31	34.25	41.41	41.92	36.78	33.27
gros	3.42	2.67	23.32	24.26	26.43	25.44	35.80	36.80
spes	2.87	3.82	40.41	40.72	30.95	31.43	23.24	25.13

analysis 18: V201, garnet restricted to leucosome, partly replaced by green biotite

analysis 19: V448-3

analysis 20: V450-1

analysis 21: V465

( )* = number of analyses

Appendix A.4.4. Biotite Analyses (Biotites associated with pre-Grenvillian fabrics)

Unit Number	Analysis Number
1C	1,2,3,4,5,6,7,8
3A	9,10,11
5A,B	12(?),13,14,15

	1	2	3	4	5	6	7	8
SiO_2	37.39	36.48	38.37	38.72	36.79	37.38	37.16	36.36
TiO_2	2.22	3.53	2.32	1.22	3.11	1.97	3.97	4.18
Al_2O_3	15.51	16.27	16.16	18.66	16.33	16.09	16.86	15.15
FeO	21.00	15.84	14.57	15.74	17.35	13.62	16.10	16.92
MnO	0.09	0.03	0.06	0.04	0.03	0.04	0.02	0.04
MgO	11.42	13.70	17.58	13.49	13.34	15.43	12.42	13.36
CaO	0.00	0.00	0.00	0.00	0.00	0.00	0.00	0.00
Na_2O	0.13	0.14	0.22	0.05	0.09	0.09	0.18	0.07
K_2O	10.89	10.96	8.84	9.09	11.19	10.87	9.67	9.88
	98.65	96.95	98.12	97.01	98.23	95.49	96.38	95.96
	Number of ions based on 22 oxygens							
Si	5.583	5.425	5.513	5.625	5.439	5.570	5.507	5.496
Aliv	2.417	2.575	2.487	2.375	2.561	2.430	2.493	2.504
Alvi	0.314	0.278	0.250	0.822	0.286	0.398	0.453	0.169
Ti	0.249	0.395	0.251	0.133	0.346	0.221	0.443	0.471
* Fe^{2+}	2.623	1.970	1.751	1.913	2.145	1.698	1.996	2.118
Mn	0.011	0.004	0.007	0.005	0.004	0.005	0.003	0.005
Mg	2.542	3.037	3.765	2.921	2.940	3.427	2.743	2.980
Ca	0.000	0.000	0.000	0.000	0.000	0.000	0.000	0.000
Na	0.038	0.040	0.061	0.014	0.026	0.026	0.052	0.020
K	2.075	2.080	1.621	1.685	2.111	2.067	1.829	1.887
	(5)**	(6)	(6)	(12)	(5)	(4)	(5)	(3)

*Fe: all iron as Fe^{2+}

( )** = number of analyses

analysis 1: V172

analysis 2: V207

analysis 3: V210-1

analysis 4: V211-2, green biotite

analysis 5: V580-1B

analysis 6: V580-16, biotite enclosed in garnet

analysis 7: CG-79-347, biotite coexists with garnet in leucosome

analysis 8: V580-12

	9	10	11	12	13	14	15
SiO_2	37.63	37.43	36.67	36.79	37.05	34.99	37.94
TiO_2	4.56	3.20	3.34	0.36	2.23	2.90	2.37
Al_2O_3	13.23	14.63	14.42	16.90	15.41	13.60	15.24
FeO	17.73	21.61	21.08	19.71	29.72	32.62	23.70
MnO	0.15	0.04	0.04	0.05	1.51	0.56	0.83
MgO	12.09	11.53	11.18	9.07	2.50	1.92	9.13
CaO	0.02	0.00	0.00	0.00	0.00	0.00	0.00
Na_2O	0.08	0.09	0.08	0.07	0.01	0.04	0.00
K_2O	9.86	11.12	11.06	9.47	9.09	9.16	9.41
	95.35	99.65	97.87	92.42	97.52	95.79	98.62
	Number of ions on the basis of 22 oxygens						
Si	5.714	5.562	5.549	5.774	5.806	5.706	5.696
Aliv	2.286	2.438	2.451	2.226	2.194	2.294	2.304
Alvi	0.083	0.125	0.122	0.902	0.654	0.321	0.394
Ti	0.521	0.358	0.380	0.043	0.263	0.356	0.268
* Fe	2.252	2.686	2.668	2.587	3.896	4.450	2.976
Mn	0.019	0.005	0.005	0.007	0.200	0.077	0.106
Mg	2.736	2.554	2.552	2.122	0.584	0.467	2.043
Ca	0.003	0.000	0.000	0.000	0.000	0.000	0.000
Na	0.024	0.026	0.023	0.021	0.003	0.013	0.000
K	1.910	2.108	2.135	1.896	1.818	1.906	1.803
	(4)**	(5)	(5)	(3)	(3)	(4)	(3)

* Fe: all iron as Fe^{2+}

( )** = number of analyses

analysis 9: V471-2

analysis 10: V221

analysis 11: V579-1

analysis 12: V201, paleosome biotite (garnet restricted to leucosome)

analysis 13: V448-3

analysis 14: V450-1

analysis 15: V465

Appendix A.4.5. Cordierite Analyses (All cordierites are from pelitic metatexite (unit 1C)

	1	2		3	4	5	6	
		rim	core				rim	core
SiO_2	49.61	49.72	49.94	49.87	49.61	49.83	50.10	48.91
TiO_2	0.00	0.00	0.00	0.00	0.00	0.00	0.00	0.00
Al_2O_3	31.12	32.63	32.21	31.18	31.47	31.34	30.07	30.30
FeO	6.18	3.36	5.87	4.54	3.58	4.67	4.35	5.02
MnO	0.11	0.06	0.12	0.25	0.10	0.14	0.03	0.12
MgO	10.43	12.07	10.52	10.75	11.29	10.57	10.75	10.59
CaO	0.00	0.00	0.00	0.00	0.01	0.00	0.00	0.00
Na_2O	0.04	0.06	0.10	0.20	0.09	0.05	0.04	0.06
K_2O	0.01	0.10	0.10	0.06	0.01	0.00	0.00	0.00
	97.50	98.00	98.86	96.87	96.18	96.61	95.34	95.00
	Number of ions on the basis of 18 oxygens							
Si	5.100	5.025	5.058	5.124	5.106	5.127	5.208	5.133
Aliv	0.900	0.975	0.942	0.876	0.894	0.873	0.792	0.867
Alvi	2.871	2.913	2.907	2.904	2.925	2.931	2.895	2.880
Ti	0.000	0.000	0.000	0.000	0.000	0.000	0.000	0.000
Fe^{3+}	0.000	0.000	0.000	0.000	0.000	0.000	0.006	0.000
Fe^{2+}	0.531	0.285	0.498	0.390	0.309	0.402	0.372	0.441
Mn	0.009	0.006	0.009	0.021	0.009	0.012	0.003	0.012
Mg	1.599	1.818	1.587	1.647	1.731	1.620	1.665	1.656
Ca	0.000	0.000	0.000	0.000	0.000	0.000	0.000	0.000
Na	0.009	0.012	0.021	0.039	0.018	0.009	0.009	0.012
K	0.000	0.012	0.012	0.009	0.000	0.000	0.000	0.000
	(6)*	(4)	(3)	(3)	(3)	(3)	(3)	(3)

( )* = number of analyses

analysis 1: V210-1, cordierite surrounded by quartz + feldspar

analysis 2: V210-1, cordierite mantle on garnet

analysis 3: V580-1A, melanosome cordierite

analysis 4: V580-1A, leucosome cordierite

analysis 5: V580-1B, leucosome cordierite

analysis 6: V580-12, cordierite mantle on garnet

	7	8		9	10	
		rim	core		rim	core
SiO_2	49.23	50.23	49.04	50.57	48.77	49.61
TiO_2	0.00	0.00	0.00	0.00	0.00	0.00
Al_2O_3	31.82	32.48	32.39	31.81	30.64	30.90
FeO	5.84	4.55	5.33	3.64	3.63	5.34
MnO	0.19	0.08	0.18	0.02	0.06	0.10
MgO	10.07	11.23	10.42	11.46	11.68	10.55
CaO	0.00	0.00	0.00	0.00	0.00	0.00
Na_2O	0.06	0.07	0.13	0.11	nd	nd
K_2O	0.00	0.00	0.00	0.01	nd	nd
	97.21	98.64	97.49	97.62	94.78	96.49
	Number of ions based on 18 oxygens					
Si	5.067	5.064	5.025	5.124	5.097	5.127
Aliv	0.933	0.936	0.975	0.876	0.903	0.873
Alvi	2.931	2.922	2.940	2.925	2.874	2.895
Ti	0.000	0.000	0.000	0.000	0.000	0.000
Fe^{3+}	0.000	0.000	0.000	0.000	0.000	0.000
Fe^{2+}	0.504	0.384	0.456	0.309	0.318	0.462
Mn	0.018	0.006	0.015	0.003	0.006	0.009
Mg	1.545	1.686	1.593	1.731	1.821	1.626
Ca	0.000	0.000	0.000	0.000	0.000	0.000
Na	0.012	0.015	0.027	0.021	-	-
K	0.000	0.000	0.000	0.000	-	-
	(4)*	(3)	(3)	(7)	(3)	(4)

( )* = number of analyses

analysis 7: V580-16, cordierite surrounded by quartz

analysis 8: V580-16, cordierite mantle on garnet

analysis 9: CG-79-347, cordierite mantle on garnet, analysed within 20 microns of garnet

analysis 10: V210-1, cordierite in contact with garnet

Appendix A.4.6 Feldspar Analyses (Two-feldspar assemblages)

Note: Two tables of feldspar analyses are presented, one lists plagioclase compositions, the other lists the composition of K-feldspar coexisting with the plagioclase. The same analysis numbering sequence is followed in both tables.

[A] Pre-Grenvillian Fabrics

Unit Number	Analysis Number
1C	1,2,3,4,
3A	5
5A,B	6(?),7

[B] Grenvillian Fabrics

AUX(Unit Number)	Analysis Number
6E	8
6B	9
intermediate dykes	10,11

	1	2	3	4	5	6	7	8
SiO_2	59.98	60.77	60.36	63.58	60.96	61.95	65.95	65.51
Al_2O_3	24.36	24.80	24.50	25.80	24.43	23.48	19.32	22.10
FeO	0.02	0.02	0.02	0.03	0.00	0.00	0.02	0.00
CaO	7.02	7.32	7.03	4.64	6.11	5.14	1.61	3.04
Na_2O	7.67	7.99	7.52	8.79	9.13	9.29	11.32	10.81
K_2O	0.21	0.18	0.23	0.03	0.23	0.23	0.12	0.17
	99.26	101.70	99.66	102.80	100.86	100.09	98.34	101.63
	Number of ions on the basis of 32 oxygens							
Si	10.774	10.736	10.788	10.919	10.797	11.008	11.799	11.396
Al	5.159	5.166	5.163	5.224	5.102	4.919	4.075	4.533
Fe	0.003	0.003	0.003	0.004	0.000	0.000	0.003	0.000
Ca	1.351	1.386	1.347	0.854	1.160	0.979	0.309	0.567
Na	2.672	2.737	2.606	2.927	3.136	3.201	3.927	3.647
K	0.048	0.041	0.052	0.007	0.052	0.052	0.027	0.038
	(3)*	(4)	(4)	(6)	(6)	(4)	(5)	(3)
$\frac{Na^{**}}{\Sigma X}$	0.656	0.657	0.651	0.773	0.721	0.756	0.921	0.858
Mol%								
An	33.19	33.28	33.62	22.54	26.68	23.13	7.24	13.33
Ab	65.63	65.74	65.07	77.28	72.13	75.64	92.12	85.78
Or	1.18	0.97	1.31	0.17	1.20	1.23	0.64	0.89

( )* = number of analyses

$\frac{Na^{**}}{\Sigma X} = \frac{Na}{Na+K+Ca}$

analysis 1: V172
analysis 2: V207
analysis 3: V580-1A
analysis 4: CG-79-347
analysis 5: V221
analysis 6: V201
analysis 7: V450-1
analysis 8: V434

	9		10		11
	rim	core	rim	core	
SiO_2	66.13	62.43	67.74	66.90	64.47
Al_2O_3	20.73	21.67	20.67	21.55	21.55
FeO	0.00	0.06	0.07	0.05	0.04
CaO	1.52	2.57	2.18	4.10	4.10
Na_2O	11.12	10.60	11.65	10.73	10.32
K_2O	0.12	0.16	0.02	0.16	0.19
	99.62	97.49	102.33	103.49	100.67
	Number of ions on the basis of 32 oxygens				
Si	11.665	11.327	11.670	11.457	11.360
Al	4.312	4.636	4.199	4.352	4.477
Fe	0.000	0.009	0.010	0.007	0.006
Ca	0.287	0.500	0.402	0.752	0.774
Na	3.804	3.730	3.892	3.563	3.526
K	0.027	0.037	0.004	0.035	0.043
	(4)*	(3)	(3)	(3)	(5)
$\frac{Na^{**}}{\Sigma X}$	0.924	0.874	0.905	0.819	0.812
Mol%					
An	6.98	11.71	9.36	17.29	17.83
Ab	92.37	87.42	90.54	81.90	81.19
Or	0.66	0.87	0.10	0.80	0.98

( )* = number of analyses

$\frac{Na^{**}}{\Sigma X} = \frac{Na}{Na+K+Ca}$

analysis 9: V257-8

analysis 10: V683-3

analysis 11: V710-2

	1	2	3	4	5	6	7	8
SiO_2	64.72	66.50	64.62	65.05	65.95	63.89	65.65	65.80
Al_2O_3	17.70	18.18	17.84	17.61	19.32	19.61	17.96	17.90
FeO	0.02	0.00	0.02	0.02	0.00	0.01	0.04	0.02
CaO	0.23	0.21	0.11	0.13	0.29	0.30	0.00	0.00
Na_2O	2.01	2.11	1.65	1.73	2.15	1.71	0.77	0.61
K_2O	13.69	13.44	13.90	13.54	12.83	13.16	15.54	15.82
	98.37	100.44	98.14	98.08	100.54	98.68	99.96	100.15
	Number of ions on the basis of 32 oxygens							
Si	12.063	12.091	12.065	12.122	11 947	11.828	12.090	12.104
Al	3.890	3.897	3.927	3.869	4.127	4.281	3.900	3.882
Fe	0.003	0.000	0.003	0.003	0.000	0.002	0.006	0.003
Ca	0.046	0.041	0.022	0.026	0.056	0.060	0.000	0.000
Na	0.726	0.744	0.597	0.625	0.755	0.614	0.275	0.218
K	3.256	3.118	3.311	3.220	2.966	3.109	3.652	3.713
	(8)*	(11)	(17)	(8)	(7)	(7)	(5)	(4)
$\frac{Na^{**}}{\Sigma X}$	0.180	0.198	0.152	0.155	0.199	0.162	0.070	0.055
Mol%								
An	1.14	1.05	0.56	0.67	1.49	1.57	0.00	0.00
Ab	18.04	19.06	15.20	16.15	20.00	16.23	7.00	5.54
Or	80.82	79.89	84.24	83.18	78.51	82.19	93.00	94.46

( )* = number of analyses

$$\frac{Na^{**}}{\Sigma X} = \frac{Na}{Na+K+Ca}$$

analysis 1: V172
analysis 2: V207
analysis 3: V580-1A
analysis 4: CG-79-347
analysis 5: V221
analysis 6: V201
analysis 7: V450-1
analysis 8: V434

	9	10	11
SiO_2	67.21	65.36	66.68
Al_2O_3	17.83	17.66	17.85
FeO	0.10	0.13	0.05
CaO	0.00	0.00	0.23
Na_2O	0.64	0.75	1.15
K_2O	16.30	15.68	15.32
	102.08	99.58	101.28
	Number of ions on the basis of 32 oxygens		
Si	12.147	12.104	12.116
Al	3.800	3.856	3.824
Fe	0.015	0.020	0.008
Ca	0.000	0.000	0.045
Na	0.224	0.269	0.405
K	3.759	3.705	3.552
	(7)*	(6)	(6)
$\frac{Na^{**}}{\Sigma X}$	0.056	0.068	0.101
Mol%			
An	0.00	0.00	1.12
Ab	5.63	6.78	10.13
Or	94.37	93.22	88.76

( )* = number of analyses

$\frac{Na^{**}}{\Sigma X} = \frac{Na}{Na+K+Ca}$

analysis 9: V257-8

analysis 10: V683-3

analysis 11: V710-2

Appendix A.4.7. Amphibole Analyses (Amphiboles associated with pre-Grenvillian fabrics)

Unit Number	Analysis Number
2	1,2,6,24
3B	8
5A	15,16,18
6A	3
Discordant mafic dykes	17,19,20,22,23,25,26,27,28
Pre-migmatitic metabasites	10,11,12,13,14,21
Makkovik trend metabasites	4,5,7

	1		2	
	rim	core	rim	core
SiO_2	44.98	45.63	44.78	42.98
TiO_2	0.52	0.40	0.66	1.08
Al_2O_3	8.66	7.93	10.81	10.17
Cr_2O_3	0.00	0.00	0.00	0.00
FeO	21.12	21.05	17.93	18.42
MnO	0.61	0.56	0.59	0.71
MgO	9.17	9.61	9.37	10.24
CaO	12.26	11.88	11.94	12.19
Na_2O	1.60	1.27	1.26	1.33
K_2O	1.33	1.22	1.43	1.46
	100.25	99.55	98.77	98.58

Number of ions based on 23 oxygens

	Fe^{2+}	13CNK	Fe^{2+}	13CNK	Fe^{2+}	13CNK	Fe^{2+}	13CNK
Si	6.858	6.765	6.742	6.688	6.685	6.654	6.498	6.418
Aliv	1.142	1.235	1.258	1.312	1.315	1.346	1.502	1.582
	8.000	8.000	8.000	8.000	8.000	8.000	8.000	8.000
Alvi	0.263	0.151	0.272	0.206	0.588	0.548	0.311	0.208
Ti	0.045	0.044	0.059	0.058	0.074	0.074	0.123	0.122
Fe^{3+}	0.000	0.628	0.000	0.373	0.000	0.214	0.000	0.565
Cr	0.000	0.000	0.000	0.000	0.000	0.000	0.000	0.000
Mg_{2+}	2.153	2.124	2.049	2.032	2.085	2.075	2.308	2.280
Fe^{2+}	2.539	2.610	2.620	2.254	2.239	2.014	2.258	1.735
Mn		0.070		0.076		0.075		0.090
Ca		0.001		0.001				
	5.000	5.000	5.000	5.000	5.000	5.000	5.000	5.000
Fe^{2+}	0.107		0.028				0.071	
Mn	0.071		0.077		0.075		0.091	
Ca	1.822	1.886	1.895	1.952	1.910	1.901	1.838	1.951
Na		0.114		0.048		0.099		0.049
	2.000	2.000	2.000	2.000	2.000	2.000	2.000	2.000
Ca	0.091		0.074				0.137	
Na	0.370	0.251	0.465	0.413	0.365	0.264	0.390	0.336
K	0.234	0.231	0.254	0.252	0.272	0.271	0.282	0.278
	0.695	0.482	0.793	0.665	0.637	0.535	0.809	0.614
	(4)*		(3)		(4)		(3)	
Name:	ferro-hornblende		ferro-edenitic hornblende		edenitic hornblende		magnesian hastingsitic hornblende	

( )* = number of analyses

analysis 1: V123 analysis 2: V325-1

	3		4		5			
	rim		core					
SiO_2	44.93		44.21		42.70		45.21	
TiO_2	1.03		1.18		1.38		1.14	
Al_2O_3	8.31		8.04		9.32		7.63	
Cr_2O_3	0.00		0.00		0.00		0.05	
FeO	21.20		21.54		19.47		19.14	
MnO	0.55		0.68		0.53		0.65	
MgO	7.46		7.93		7.58		9.77	
CaO	11.13		11.55		12.12		11.89	
Na_2O	1.51		1.68		1.53		1.91	
K_2O	1.02		1.10		1.21		1.00	
	97.14		97.91		95.84		98.39	
	Number of ions based on 23 oxygens							
	Fe^{2+}	13CNK	Fe^{2+}	13CNK	Fe^{2+}	13CNK	Fe^{2+}	13CNK
Si	6.914	6.886	6.800	6.762	6.543	6.483	6.839	6.816
Aliv	1.086	1.114	1.200	1.238	1.457	1.517	1.161	1.184
	8.000	8.000	8.000	8.000	8.000	8.000	8.000	8.000
Alvi	0.422	0.388	0.258	0.212	0.227	0.152	0.200	0.171
Ti	0.119	0.118	0.137	0.136	0.159	0.158	0.130	0.130
Fe^{3+}	0.000	0.187	0.000	0.255	0.000	0.425	0.000	0.150
Cr	0.000	0.000	0.000	0.000	0.000	0.000	0.006	0.006
Mg_{2+}	1.711	1.704	1.818	1.808	1.731	1.715	2.203	2.196
Fe^{2+}	2.729	2.531	2.771	2.500	2.883	2.482	2.422	2.264
Mn	0.019	0.072	0.016	0.089		0.068	0.039	0.083
Ca								
	5.000	5.000	5.000	5.000	5.000	5.000	5.000	5.000
Fe^{2+}					0.050			
Mn	0.053		0.073		0.069		0.044	
Ca	1.835	1.827	1.904	1.893	1.881	1.970	1.928	1.922
Na	0.112	0.173	0.023	0.107		0.030	0.028	0.078
	2.000	2.000	2.000	2.000	2.000	2.000	2.000	2.000
Ca					0.109			
Na	0.339	0.276	0.478	0.391	0.455	0.421	0.532	0.480
K	0.200	0.199	0.216	0.215	0.237	0.235	0.193	0.192
	0.539	0.481	0.694	0.606	0.801	0.656	0.725	0.672
	(4)*		(3)		(2)		(2)	
Name:	ferro-hornblende		ferro-edenite		magnesian hastingsitic		ferro-edenite	

( )* = number of analyses
analysis 3: V766 analysis 4: V766-2
analysis 5: V766-3

	6	7	8	9
SiO_2	44.96	44.40	44.96	45.07
TiO_2	1.16	0.72	0.56	0.88
Al_2O_3	7.55	7.56	9.72	8.91
Cr_2O_3	0.00	0.00	0.00	0.00
FeO	19.05	23.53	17.95	17.78
MnO	0.30	0.64	0.35	0.42
MgO	9.86	7.45	10.01	10.56
CaO	10.99	10.35	10.67	10.71
Na_2O	1.18	1.94	1.21	1.32
K_2O	0.83	1.18	0.92	1.03
	95.88	97.77	96.35	96.68

Number of ions based on 23 oxygens

	Fe^{2+}	13CNK	Fe^{2+}	13CNK	Fe^{2+}	13CNK	Fe^{2+}	13CNK
Si	6.924	6.827	6.886	6.776	6.831	6.713	6.838	6.720
Aliv	1.076	1.173	1.114	1.224	1.169	1.287	1.162	1.280
	8.000	8.000	8.000	8.000	8.000	8.000	8.000	8.000
Alvi	0.295	0.179	0.268	0.136	0.572	0.424	0.431	0.285
Ti	0.134	0.132	0.084	0.083	0.064	0.063	0.100	0.098
Fe^{3+}	0.000	0.646	0.000	0.733	0.000	0.797	0.000	0.800
Cr	0.000	0.000	0.000	0.000	0.000	0.000	0.000	0.000
Mg	2.263	2.231	1.722	1.694	2.267	2.228	2.388	2.347
Fe^{2+}	2.454	1.773	2.926	2.271	2.097	1.444	2.081	1.417
Mn		0.039		0.083		0.044		0.053
Ca								
	5.000	5.000	5.000	5.000	5.000	5.000	5.000	5.000
Fe^{2+}	0.146		0.126		0.184		0.175	
Mn	0.039		0.084		0.045		0.054	
Ca	1.814	1.788	1.720	1.693	1.737	1.707	1.741	1.711
Na		0.212	0.070	0.307	0.034	0.293	0.030	0.289
	2.000	2.000	2.000	2.000	2.000	2.000	2.000	2.000
Ca								
Na	0.352	0.135	0.513	0.267	0.323	0.058	0.358	0.092
K	0.163	0.161	0.233	0.229	0.178	0.175	0.199	0.196
	0.515	0.296	0.746	0.496	0.501	0.233	0.557	0.288
	(4)*		(3)		(2)		(3)	
Name:	magnesio-hornblende		ferro-hornblende		magnesio-hornblende		magnesio-hornblende	

( )* = number of analyses

analysis 6 : V774 analysis 7 : V775
analysis 8 : V220 analysis 9 : V687

	10		11		12		13	
SiO_2	44.06		43.46		48.72		45.95	
TiO_2	0.25		1.40		0.54		1.53	
Al_2O_3	10.35		9.37		6.61		9.49	
Cr_2O_3	0.00		0.00		0.03		0.31	
FeO	20.09		22.42		14.87		11.69	
MnO	0.38		0.33		0.24		0.10	
MgO	9.20		7.58		13.04		13.69	
CaO	10.84		10.46		11.55		11.53	
Na_2O	1.28		1.73		1.24		0.98	
K_2O	0.89		1.21		0.72		1.13	
	97.34		97.96		97.56		96.40	
	Number of ions based on 23 oxygens							
	Fe^{2+}	13CNK	Fe^{2+}	13CNK	Fe^{2+}	13CNK	Fe^{2+}	13CNK
Si	6.708	6.562	6.682	6.578	7.179	7.115	6.790	6.727
Aliv	1.292	1.438	1.318	1.422	0.821	0.885	1.210	1.273
	8.000	8.000	8.000	8.000	8.000	8.000	8.000	8.000
Alvi	0.566	0.380	0.381	0.250	0.327	0.253	0.443	0.364
Ti	0.029	0.028	0.162	0.160	0.060	0.060	0.170	0.168
Fe^{3+}	0.000	1.003	0.000	0.717	0.000	0.408	0.000	0.430
Cr	0.000	0.000	0.000	0.000	0.003	0.003	0.036	0.036
Mg_{2+}	2.088	2.042	1.737	1.710	2.864	2.838	3.015	2.987
Fe^{2+}	2.317	1.499	2.720	2.121	1.746	1.409	1.346	1.002
Mn		0.048		0.042		0.029		0.013
Ca								
	5.000	5.000	5.000	5.000	5.000	5.000	5.000	5.000
Fe^{2+}	0.241		0.163		0.087		0.099	
Mn	0.049		0.043		0.030		0.013	
Ca	1.710	1.730	1.724	1.697	1.824	1.808	1.826	1.809
Na		0.270	0.070	0.303	0.059	0.192	0.062	0.191
	2.000	2.000	2.000	2.000	2.000	2.000	2.000	2.000
Ca	0.059							
Na	0.378	0.100	0.446	0.205	0.295	0.159	0.219	0.087
K	0.173	0.164	0.237	0.233	0.135	0.134	0.213	0.211
	0.610	0.269	0.683	0.438	0.430	0.293	0.432	0.298
	(3)*		(2)		(2)		(4)	
Name:	magnesio-hornblende		ferro-hornblende		magnesio-hornblende		magnesio-hornblende	

( )* = number of analyses

analysis 10: V194-3 analysis 11: V526-1
analysis 12: V42-3 analysis 13: V580-8

	14		15			
			rim		core	
SiO_2	46.04		38.84		39.28	
TiO_2	0.48		0.89		1.26	
Al_2O_3	7.24		11.27		10.70	
Cr_2O_3	0.04		0.01		0.00	
FeO	17.36		30.59		30.85	
MnO	0.19		0.80		0.83	
MgO	11.49		1.39		1.43	
CaO	10.48		10.23		10.21	
Na2O	1.45		1.73		1.78	
K_2O	0.73		1.69		1.65	
	95.50		97.44		97.99	
	Number of ions based on 23 oxygens					
	Fe^{2+}	13CNK	Fe^{2+}	13CNK	Fe^{2+}	13CNK
Si	7.033	6.897	6.335	6.223	6.374	6.267
Aliv	0.967	1.103	1.665	1.777	1.626	1.733
	8.000	8.000	8.000	8.000	8.000	8.000
Alvi	0.337	0.176	0.502	0.352	0.421	0.280
Ti	0.055	0.054	0.104	0.107	0.154	0.151
Fe^{3+}	0.000	0.887	0.000	0.814	0.000	0.774
Cr	0.005	0.005	0.001	0.001	0.000	0.000
Mg_{2+}	2.616	2.565	0.338	0.332	0.346	0.340
Fe	2.218	1.288	4.050	3.285	4.079	3.343
Mn		0.025		0.109		0.112
Ca						
	5.000	5.000	5.000	5.000	5.000	5.000
Fe^{2+}	0.231		0.123		0.108	
Mn	0.025		0.111		0.114	
Ca	1.716	1.683	1.766	1.756	1.775	1.810
Na	0.028	0.317	.547	0.244	0.003	0.255
	2.000	2.000	2.000	2.000	2.000	2.000
Ca			0.022		0.063	
Na	0.402	0.105	0.547	0.294	0.557	0.296
K	0.142	0.139	0.352	0.346	0.342	0.336
	0.544	0.244	0.921	0.640	0.899	0.632
	(3)*		(3)		(3)	
Name:	magnesio-hornblende		hastingsite		hastingsite	

( )* = number of analyses

analysis 14 : V711-2 analysis 15: V450-1

	16	17 rim	17 core	18
SiO_2	41.61	41.85	42.18	40.31
TiO_2	0.66	0.94	1.03	0.92
Al_2O_3	11.24	11.30	12.26	11.13
Cr_2O_3	0.03	0.00	0.00	0.00
FeO	22.90	22.20	18.39	23.66
MnO	0.56	0.66	0.39	0.93
MgO	7.31	7.52	9.72	6.69
CaO	11.16	10.89	11.82	10.63
Na_2O	1.90	2.02	1.38	1.77
K_2O	1.55	1.55	1.48	1.57
	98.92	98.93	98.65	97.60

Number of ions based on 23 oxygens

	Fe^{2+}	13CNK	Fe^{2+}	13CNK	Fe^{2+}	13CNK	Fe^{2+}	13CNK
Si	6.404	6.296	6.415	6.310	6.351	6.258	6.335	6.188
Aliv	1.596	1.704	1.585	1.690	1.640	1.742	1.665	1.812
	8.000	8.000	8.000	8.000	8.000	8.000	8.000	8.000
Alvi	0.444	0.302	0.457	0.319	0.528	0.403	0.398	0.203
Ti	0.076	0.075	0.108	0.106	0.117	0.115	0.109	0.107
Fe^{3+}	0.000	0.772	0.000	0.460	0.000	0.674	0.000	1.065
Cr	0.004	0.004	0.000	0.000	0.000	0.000	0.000	0.000
Mg_{2+}	1.677	1.649	1.718	1.690	2.182	2.150	1.567	1.531
Fe^{2+}	2.799	2.126	2.717	2.340	2.173	1.608	2.926	1.973
Mn		0.072		0.085		0.050		0.121
Ca								
	5.000	5.000	5.000	5.000	5.000	5.000	5.000	5.000
Fe^{2+}	0.149		0.129		0.143		0.184	
Mn	0.073		0.086		0.050		0.124	
Ca	1.778	1.810	1.785	1.760	1.807	1.879	1.692	1.748
Na		0.190		0.240		0.121		0.131
	2.000	2.000	2.000	2.000	2.000	2.000	2.000	2.000
Ca	0.063		0.004		0.100		0.098	
Na	0.567	0.367	0.600	0.350	0.403	0.276	0.539	0.395
K	0.304	0.299	0.303	0.298	0.284	0.280	0.315	0.308
	0.934	0.666	0.907	0.648	0.787	0.556	0.952	0.703
	(3)*		(3)		(5)		(5)	
Name:	magnesian hastingsitic hornblende		magnesian hastingsitic hornblende		magnesian hastingsitic hornblende		magnesian hastingsite	

( )* = number of analyses

analysis 16 : V764-5 analysis 17 : V764-7

analysis 18: V764-3

	19		20			
	rim		core			
SiO_2	45.20		43.88		46.88	
TiO_2	0.52		0.59		1.12	
Al_2O_3	11.88		11.57		7.85	
Cr_2O_3	0.01		0.02		0.00	
FeO	17.22		17.05		19.32	
MnO	0.32		0.29		0.63	
MgO	11.45		11.92		10.56	
CaO	10.82		10.88		10.68	
Na_2O	1.61		1.66		1.11	
K_2O	0.41		0.41		0.81	
	99.44		98.27		98.96	
	Number of ions based on 23 oxygens					
	Fe^{2+}	13CNK	Fe^{2+}	13CNK	Fe^{2+}	13CNK
Si	6.606	6.432	6.514	6.321	6.965	6.815
Aliv	1.394	1.568	1.486	1.679	1.035	1.185
	8.000	8.000	8.000	8.000	8.000	8.000
Alvi	0.654	0.426	0.539	0.286	0.341	0.161
Ti	0.057	0.056	0.066	0.064	0.125	0.122
Fe^{3+}	0.000	1.209	0.000	1.363	0.000	0.986
Cr	0.001	0.001	0.002	0.002	0.000	0.000
Mg_{2+}	2.494	2.429	2.637	2.559	2.339	2.290
Fe^{2+}	1.749	0.841	2.117	0.691	2.195	1.364
Mn		0.039		0.035		0.077
Ca						
	5.000	5.000	5.000	5.000	5.000	5.000
Fe^{2+}	0.311		0.361		0.206	
Mn	0.040		0.036		0.079	
Ca	1.649	1.650	1.603	1.680	1.701	1.665
Na		0.350		0.320	0.014	0.313
	2.000	2.000	2.000	2.000	2.000	1.978
Ca	0.046		0.128			
Na	0.456	0.094	0.478	0.144	0.306	
K	0.076	0.074	0.078	0.076	0.154	0.151
	0.578	0.168	0.684	0.220	0.460	0.151
	(4)*		(4)		(3)	
Name:	tschermakitic hornblende		tschermakitic hornblende		magnesio-hornblende	

( )* = number of analyses

analysis 19: V71 analysis 20: V100-2

	21		22		23	
SiO_2	45.84		47.17		39.75	
TiO_2	0.39		0.37		0.68	
Al_2O_3	10.51		8.94		12.69	
Cr_2O_3	0.00		0.19		0.02	
FeO	15.22		13.07		21.22	
MnO	0.28		0.32		0.40	
MgO	12.88		14.35		8.55	
CaO	11.38		11.78		11.31	
Na_2O	1.39		1.11		1.66	
K_2O	1.27		0.88		1.83	
	99.26		98.18		98.11	
	Number of ions based on 23 oxygens					
	Fe^{2+}	13CNK	Fe^{2+}	13CNK	Fe^{2+}	13CNK
Si	6.694	6.570	6.876	6.758	6.150	6.007
Aliv	1.306	1.430	1.124	1.242	1.850	1.993
	8.000	8.000	8.000	8.000	8.000	8.000
Alvi	0.504	0.347	0.412	0.268	0.463	0.266
Ti	0.043	0.042	0.041	0.040	0.079	0.077
Fe^{3+}	0.000	0.883	0.000	0.787	0.000	1.073
Cr	0.000	0.000	0.022	0.022	0.002	0.002
Mg_{2+}	2.804	2.752	3.118	3.064	1.970	1.924
Fe^{2+}	1.649	0.942	1.407	0.780	2.744	1.607
Mn		0.034		0.039		0.051
Ca						
	5.000	5.000	5.000	5.000	5.000	5.000
Fe^{2+}	0.210		0.187			
Mn	0.035		0.040		0.258	
Ca	1.755	1.748	1.773	1.808	1.874	1.830
Na		0.252		0.192		0.170
	2.000	2.000	2.000	2.000	2.000	2.000
Ca	0.026		0.067			
Na	0.394	0.135	0.314	0.116	0.498	0.316
K	0.237	0.233	0.164	0.161	0.361	0.352
	0.657	0.338	0.545	0.277	0.859	0.668
	(3)*		(4)		(3)	
Name:	magnesio-hornblende		magnesio-hornblende		magnesian hastingsite	

( )* = number of analyses

analysis 21 : V132-1 analysis 22 : V132-3
analysis 23 : V132-4

	24		25		26	
	rim	core				
SiO_2	44.79	44.62	40.09		42.77	
TiO_2	1.57	1.98	1.04		1.64	
Al_2O_3	10.50	10.21	10.00		10.62	
Cr_2O_3	0.00	0.00	0.00		0.04	
FeO	13.60	13.60	27.27		15.03	
MnO	0.30	0.34	0.72		0.18	
MgO	12.93	12.64	4.68		11.43	
CaO	10.71	10.98	10.05		11.07	
Na_2O	1.34	1.56	1.89		2.12	
K_2O	1.13	1.21	1.00		0.71	
	96.87	97.14	96.74		95.61	
	Number of ions based on 23 oxygens					
	Fe^{2+}	13CNK	Fe^{2+}	13CNK	Fe^{2+}	13CNK	Fe^{2+}	13CNK
Si	6.650	6.524	6.628	6.542	6.445	6.274	6.516	6.441
Aliv	1.350	1.476	1.372	1.458	1.555	1.726	1.484	1.559
	8.000	8.000	8.000	8.000	8.000	8.000	8.000	8.000
Alvi	0.488	0.327	0.417	0.308	0.341	0.120	0.424	0.327
Ti	0.175	0.172	0.221	0.218	0.126	0.123	0.188	0.186
Fe^{3+}	0.000	0.870	0.000	0.595	0.000	1.220	0.000	0.523
Cr	0.000	0.000	0.000	0.000	0.000	0.000	0.005	0.005
Mg_{2+}	2.861	2.807	2.799	2.763	1.121	1.091	2.596	2.566
Fe^{2+}	1.476	0.787	1.563	1.073	3.412	2.350	1.787	1.370
Mn		0.037		0.042		0.095		0.023
Ca				0.001		0.001		
	5.000	5.000	5.000	5.000	5.000	5.000	5.000	5.000
Fe^{2+}	0.213		0.127		0.255		0.128	
Mn	0.038	0.001	0.043		0.098		0.023	
Ca	1.704	1.672	1.748	1.725	1.647	1.685	1.807	1.786
Na	0.045	0.327	0.082	0.275		0.315	0.042	0.214
	2.000	2.000	2.000	2.000	2.000	2.000	2.000	2.000
Ca					0.084			
Na	0.341	0.052	0.367	0.168	0.589	0.258	0.584	0.405
K	0.214	0.210	0.229	0.226	0.205	0.199	0.138	0.136
	0.555	0.262	0.596	0.394	0.878	0.457	0.722	0.541
	(2)*		(3)		(2)		(2)	
Name:	magnesio-hornblende		magnesio-hornblende		ferro-tschermakitic hornblende		magnesian hastingsitic hornblende	

( )* = number of analyses
analysis 24: V581-1 analysis 25: V113-3
analysis 26: V177-2

	27		28			
	rim		core			
SiO_2	43.97		45.93		41.87	
TiO_2	0.72		0.47		0.84	
Al_2O_3	11.69		9.21		9.78	
Cr_2O_3	0.02		0.22		0.00	
FeO	17.20		15.76		24.34	
MnO	0.36		0.36		0.46	
MgO	11.93		13.94		8.76	
CaO	11.78		12.06		11.58	
Na_2O	1.34		1.12		1.36	
K_2O	1.41		0.87		1.26	
	100.42		99.94		100.25	
	Number of ions based on 23 oxygens					
	Fe^{2+}	13CNK	Fe^{2+}	13CNK	Fe^{2+}	13CNK
Si	6.441	6.297	6.688	6.519	6.393	6.197
Aliv	1.559	1.703	1.312	1.481	1.607	1.803
	8.000	8.000	8.000	8.000	8.000	8.000
Alvi	0.460	0.271	0.270	0.061	0.154	(-.096)
Ti	0.079	0.077	0.051	0.050	0.096	0.093
Fe^{3+}	0.000	1.032	0.000	1.160	0.000	0.628
Cr	0.002	0.002	0.025	0.024	0.000	0.000
Mg	2.605	2.546	3.026	2.950	1.994	1.932
Fe^{2+}	2.107	0.996	1.628	0.712	2.756	2.385
Mn		0.044		0.043		0.058
Ca						
	5.000	5.000	5.000	5.000	5.000	5.000
Fe^{2+}	0.253		0.292		0.352	
Mn	0.045		0.044		0.060	
Ca	1.702	1.807	1.664	1.835	1.588	1.837
Na		0.193		0.165		0.163
	2.000	2.000	2.000	2.000	2.000	2.000
Ca	0.147		0.218		0.307	
Na	0.381	0.179	0.316	0.143	0.403	0.227
K	0.264	0.258	0.162	0.158	0.245	0.237
	0.792	0.437	0.696	0.301	0.955	0.464
	(3)*		(4)		(3)	
Name:	tschermakitic hornblende		magnesio-hornblende		ferro-tschermakite	

( )* = number of analyses

analysis 27 : V150 analysis 28 : V185-2

Appendix A.4.8. Amphibole Analyses (Amphiboles associated with Grenvillian fabrics)

Unit Number	Analysis Number
3B	1
1C	2,3
6B	4,5,6,7
10	14
7	15
intermediate dykes	8,9,10
metabasites	11,12,13,16,17,18,19,20,21,22,23, 24,25

	1	2	3
SiO_2	41.26	45.61	47.31
TiO_2	0.67	0.38	0.26
Al_2O_3	13.54	10.97	10.12
Cr_2O_3	0.01	0.25	0.21
FeO	22.48	14.16	14.54
MnO	0.32	0.50	0.46
MgO	6.43	12.09	13.38
CaO	10.64	11.91	11.54
Na_2O	1.60	1.35	1.28
K_2O	1.80	0.64	0.45
	98.75	97.86	99.55

Number of ions based on 23 oxygens

	Fe^{2+}	13CNK	Fe^{2+}	13CNK	Fe^{2+}	13CNK
Si	6.316	6.209	6.713	6.639	6.820	6.678
Aliv	1.684	1.791	1.287	1.361	1.180	1.322
	8.000	8.000	8.000	8.000	8.000	8.000
Alvi	0.760	0.612	0.617	0.522	0.540	0.362
Ti	0.077	0.076	0.042	0.041	0.028	0.028
Fe^{3+}	0.000	0.783	0.000	0.512	0.000	0.957
Cr	0.001	0.001	0.029	0.029	0.024	0.024
Mg	1.467	1.442	2.652	2.623	2.875	2.815
Fe^{2+}	2.696	2.046	1.660	1.212	1.533	1.716
Mn		0.040		0.061		0.055
Ca						
	5.000	5.000	5.000	5.000	5.000	5.000
Fe^{2+}	0.182		0.083		0.220	
Mn	0.041		0.062		0.056	
Ca	1.745	1.715	1.855	1.858	1.724	1.746
Na	0.032	0.285		0.132		0.254
	2.000	2.000	2.000	2.000	2.000	2.000
Ca			0.024		0.059	
Na	0.443	0.182	0.385	0.249	0.358	0.096
K	0.352	0.346	0.120	0.119	0.083	0.081
	0.795	0.528	0.529	0.368	0.500	0.177
	(2)*		(2)		(2)	
Name:	ferroan pargasite		ferro-hornblende		ferro-hornblende	

( )* = number of analyses

analysis 1: V194-4
analysis 2: V580-2
analysis 3: V580-3

	4				5			
	rim		core		rim		core	
SiO_2	40.69		39.62		41.46		41.15	
TiO_2	0.71		0.62		0.98		0.92	
Al_2O_3	11.85		12.44		11.16		11.58	
Cr_2O_3	0.00		0.00		0.00		0.00	
FeO	30.27		30.66		25.76		25.42	
MnO	0.60		0.56		0.57		0.62	
MgO	1.15		1.16		3.75		3.67	
CaO	10.50		10.48		11.28		11.25	
Na_2O	1.71		1.51		1.57		1.67	
K_2O	2.18		2.24		1.68		1.62	
	99.66		99.29		98.21		97.90	
	Number of ions based on 23 oxygens							
	Fe^{2+}	13CNK	Fe^{2+}	13CNK	Fe^{2+}	13CNK	Fe^{2+}	13CNK
Si	6.443	6.393	6.322	6.236	6.512	6.496	6.477	6.464
Aliv	1.557	1.607	1.678	1.764	1.488	1.504	1.523	1.536
	8.000	8.000	8.000	8.000	8.000	8.000	8.000	8.000
Alvi	0.656	0.589	0.662	0.544	0.579	0.558	0.626	0.609
Ti	0.085	0.084	0.074	0.073	0.116	0.116	0.109	0.109
Fe^{3+}	0.000	0.359	0.000	0.630	0.000	0.111	0.000	0.088
Cr	0.000	0.000	0.000	0.000	0.000	0.000	0.000	0.000
Mg	0.271	0.269	0.276	0.272	0.878	0.876	0.861	0.859
Fe^{2+}	3.988	3.619	3.988	3.406	3.384	3.264	3.347	3.252
Mn		0.079		0.075	0.043	0.075	0.057	0.083
Ca		0.001						
	5.000	5.000	5.000	5.000	5.000	5.000	5.000	5.000
Fe^{2+}	0.021		0.104					
Mn	0.080		0.076		0.033	0.001	0.026	
Ca	1.782	1.767	1.792	1.767	1.899	1.894	1.898	1.894
Na	0.117	0.233	0.028	0.233	0.068	0.105	0.076	0.106
	2.000	2.000	2.000	2.000	2.000	2.000	2.000	2.000
Ca								
Na	0.408	0.288	0.439	0.227	0.410	0.372	0.434	0.403
K	0.440	0.436	0.456	0.450	0.337	0.336	0.325	0.324
	0.848	0.724	0.895	0.677	0.747	0.708	0.759	0.727
	(2)*		(2)		(4)		(2)	
Name:	ferro-pargasitic hornblende		hastingsite		ferro-pargasitic hornblende		ferro-pargasitic hornblende	

( )* = number of analyses

analysis 4: V257-7
analysis 5: V523

	6				7			
	rim		core		rim		core	
SiO_2	40.50		41.87		39.55		40.69	
TiO_2	0.72		1.56		0.86		1.50	
Al_2O_3	11.20		9.30		10.58		9.34	
Cr_2O_3	0.00		0.00		0.00		0.00	
FeO	27.18		28.79		29.76		30.67	
MnO	0.51		0.62		0.56		0.63	
MgO	2.67		3.08		0.78		0.93	
CaO	10.98		10.50		10.53		10.35	
Na_2O	1.46		1.78		1.78		1.72	
K_2O	1.80		1.36		2.18		1.60	
	97.02		98.86		96.58		97.43	
	Number of ions based on 23 oxygens							
	Fe^{2+}	13CNK	Fe^{2+}	13CNK	Fe^{2+}	13CNK	Fe^{2+}	13CNK
Si	6.497	6.468	6.615	6.541	6.496	6.492	6.614	6.579
Aliv	1.503	1.532	1.385	1.459	1.504	1.508	1.386	1.421
	8.000	8.000	8.000	8.000	8.000	8.000	8.000	8.000
Alvi	0.616	0.578	0.348	0.255	0.545	0.540	0.403	0.359
Ti	0.087	0.086	0.185	0.183	0.106	0.106	0.183	0.182
Fe^{3+}	0.000	0.204	0.000	0.512	0.000	0.028	0.000	0.243
Cr	0.000	0.000	0.000	0.000	0.000	0.000	0.000	0.000
Mg	0.638	0.635	0.725	0.717	0.191	0.191	0.225	0.224
Fe^{2+}	3.647	3.427	3.742	3.251	4.088	4.057	4.170	3.905
Mn	0.012	0.070		0.082	0.070	0.078	0.019	0.087
Ca								
	5.000	5.000	5.000	5.000	5.000	5.000	5.000	5.000
Fe^{2+}			0.063					
Mn	0.057		0.083		0.008		0.068	
Ca	1.888	1.880	1.778	1.758	1.853	1.852	1.803	1.793
Na	0.055	0.120	0.076	0.242	0.139	0.148	0.129	0.207
	2.000	2.000	2.000	2.000	2.000	2.000	2.000	2.000
Ca								
Na	0.399	0.332	0.469	0.297	0.428	0.419	0.413	0.332
K	0.368	0.366	0.274	0.271	0.457	0.457	0.332	0.330
	0.767	0.698	0.743	0.568	0.885	0.876	0.745	0.662
	(2)*		(2)		(3)		(3)	
Name:	ferro-pargasitic hornblende		ferro-edenitic hornblende		ferro-pargasitic hornblende		ferro-edenitic hornblende	

( )*- number of analyses

analysis 6: V630 analysis 7: V776

	8		9	
	rim	core	rim	core
SiO_2	37.27	38.38	39.59	38.58
TiO_2	0.38	0.42	0.69	0.65
Al_2O_3	13.99	13.06	13.31	13.31
Cr_2O_3	0.00	0.00	0.00	0.00
FeO	29.93	31.05	26.38	26.89
MnO	0.23	0.23	0.40	0.51
MgO	0.50	0.72	3.33	3.33
CaO	10.92	11.12	10.73	11.05
Na_2O	1.42	1.59	1.76	1.59
K_2O	2.45	2.52	2.26	2.21
	97.09	99.09	98.45	98.12

Number of ions based on 23 oxygens

	Fe^{2+}	13CNK	Fe^{2+}	13CNK	Fe^{2+}	13CNK	Fe^{2+}	13CNK
Si	6.102	6.054	6.182	6.135	6.246	6.188	6.147	6.068
Aliv	1.898	1.946	1.818	1.865	1.754	1.812	1.853	1.932
	8.000	8.000	8.000	8.000	8.000	8.000	8.000	8.000
Alvi	0.803	0.734	0.662	0.596	0.723	0.642	0.647	0.536
Ti	0.047	0.046	0.051	0.050	0.082	0.081	0.078	0.077
Fe^{3+}	0.000	0.361	0.000	0.354	0.000	0.431	0.000	0.588
Cr	0.000	0.000	0.000	0.000	0.000	0.000	0.000	0.000
Mg_{2+}	0.122	0.121	0.173	0.172	0.783	0.776	0.791	0.781
Fe^{2+}	4.028	3.707	4.114	3.797	3.412	3.017	3.484	2.950
Mn		0.031		0.030		0.052		0.068
Ca						0.001		
	5.000	5.000	5.000	5.000	5.000	5.000	5.000	5.000
Fe^{2+}	0.071		0.069		0.069		0.100	
Mn	0.032	0.001	0.031	0.001	0.053		0.069	
Ca	1.916	1,901	1.919	1.904	1.814	1.796	1.831	1.863
Na	0.432	0.098		0.095	0.064	0.204		0.137
	2.000	2.000	2.000	2.000	2.000	2.000	2.000	2.000
Ca	0.019		0.019				0.056	
Na	0.451	0.349	0.497	0.398	0.475	0.330	0.491	0.348
K	0.512	0.508	0.518	0.514	0.455	0.451	0.449	0.443
	0.982	0.857	1.034	0.912	0.930	0.781	0.996	0.791
	(3)*	(3)	(3)		(3)		(3)	
Name:	ferro-paragsite		ferro-pargasite		ferro-pargasite		ferro-pargasite	

( )* = number of analyses

analysis 8: V257-8 analysis 9: V683-3

note: surplus of ions in A-site in analysis 8(core) is likely due to erroneously high FeO and/or SiO_2 determination, this error being propagated through the rest of the stoichiometric calculation

	10		11	
	rim	core	rim	core
SiO_2	38.22	37.38	45.76	48.81
TiO_2	0.17	0.68	0.73	0.83
Al_2O_3	13.35	12.40	9.87	9.22
Cr_2O_3	0.00	0.00	0.00	0.00
FeO	29.01	29.46	13.68	12.90
MnO	0.95	1.11	0.33	0.23
MgO	1.42	1.61	13.18	13.84
CaO	10.03	10.24	11.46	11.43
Na_2O	1.60	1.91	1.54	1.55
K_2O	2.25	2.11	0.69	0.69
	97.00	96.90	97.24	99.50

Number of ions based on 23 oxygens

	Fe^{2+}	13CNK	Fe^{2+}	13CNK	Fe^{2+}	13CNK	Fe^{2+}	13CNK
Si	6.224	6.113	6.147	6.037	6.762	6.661	6.974	6.903
Aliv	1.776	1.887	1.853	1.963	1.238	1.339	1.026	1.097
	8.000	8.000	8.000	8.000	8.000	8.000	8.000	8.000
Alvi	0.788	0.631	0.551	0.398	0.481	0.354	0.527	0.440
Ti	0.021	0.021	0.084	0.083	0.081	0.080	0.089	0.088
Fe^{3+}	0.000	0.821	0.000	0.820	0.000	0.687	0.000	0.188
Cr	0.000	0.000	0.000	0.000	0.000	0.000	0.000	0.000
Mg	0.345	0.339	0.395	0.388	2.903	2.860	2.947	2.917
Fe^{2+}	3.846	3.060	3.970	3.159	1.535	0.979	1.437	1.338
Mn		0.128		0.152		0.040		0.028
Ca								0.001
	5.000	5.000	5.000	5.000	5.000	5.000	5.000	5.000
Fe^{2+}	0.106		0.082		0.156		0.105	
Mn	0.131		0.155		0.041		0.028	
Ca	1.750	1.719	1.763	1.773	1.803	1.788	1.750	1.731
Na	0.013	0.281		0.227		0.212	0.117	0.269
	2.000	2.000	2.000	2.000	2.000	2.000	2.000	2.000
Ca					0.012			
Na	0.492	0.215	0.609	0.371	0.441	0.222	0.312	0.156
K	0.468	0.459	0.443	0.435	0.130	0.128	0.126	0.125
	0.960	0.674	1.052	0.806	0.583	0.350	0.438	0.281
	(2)*		(2)		(2)		(2)	
Name:	hastingsite		hastingsite		magnesio-hornblende		magnesio-hornblende	

( )* = number of analyses

analysis 10: V710-2 analysis 11: V438-4

	12		13	
	rim	core	rim	core
SiO_2	46.43	46.60	45.55	46.93
TiO_2	0.40	0.46	0.33	0.77
Al_2O_3	9.27	9.50	10.82	7.95
Cr_2O_3	0.00	0.00	0.00	0.00
FeO	13.67	14.32	15.77	15.00
MnO	0.29	0.30	0.41	0.41
MgO	12.61	12.69	10.82	12.23
CaO	11.92	12.00	10.74	10.98
Na_2O	1.26	1.43	1.29	1.26
K_2O	0.88	0.87	1.01	0.79
	96.73	98.17	96.74	96.32

Number of ions based on 23 oxygens

	Fe^{2+}	13CNK	Fe^{2+}	13CNK	Fe^{2+}	13CNK	Fe^{2+}	13CNK
Si	6.895	6.848	6.842	6.784	6.811	6.712	7.023	6.932
Aliv	1.105	1.152	1.158	1.216	1.189	1.288	0.977	1.068
	8.000	8.000	8.000	8.000	8.000	8.000	8.000	8.000
Alvi	0.518	0.460	0.487	0.415	0.719	0.592	0.426	0.317
Ti	0.045	0.045	0.051	0.051	0.037	0.037	0.087	0.086
Fe^{3+}	0.000	0.864	0.000	0.391	0.000	0.670	0.000	0.593
Cr	0.000	0.000	0.000	0.000	0.000	0.000	0.000	0.000
Mg	2.791	2.772	2.777	2.753	2.412	2.377	2.728	2.692
Fe^{2+}	1.646	0.822	1.685	1.353	1.832	1.273	1.759	1.260
Mn		0.036		0.037		0.051		0.051
Ca								0.001
	5.000	5.000	5.000	5.000	5.000	5.000	5.000	5.000
Fe^{2+}	0.052		0.074		0.140		0.119	
Mn	0.036		0.037		0.052		0.052	
Ca	1.897	1.884	1.888	1.872	1.721	1.696	1.761	1.738
Na	0.015	0.116	0.001	0.128	0.087	0.304	0.068	0.262
	2.000	2.000	2.000	2.000	2.000	2.000	2.000	2.000
Ca								
Na	0.348	0.244	0.406	0.275	0.287	0.064	0.298	0.099
K	0.167	0.166	0.163	0.161	0.195	0.192	0.151	0.149
	0.515	0.410	0.569	0.436	0.482	0.256	0.449	0.248
	(2)*		(2)		(2)		(3)	
Name:	magnesio-hornblende		magnesio-hornblende		magnesio-hornblende		magnesio-hornblende	

( )* = number of analyses
analysis 12: V560 analysis 13: V453-3

	14		15			
	rim		core			
SiO_2	41.32		41.90		45.41	
TiO_2	1.07		1.05		1.27	
Al_2O_3	13.94		13.90		11.16	
Cr_2O_3	0.00		0.00		0.00	
FeO	19.07		18.95		12.54	
MnO	0.12		0.14		0.19	
MgO	9.08		9.11		13.50	
CaO	11.00		11.00		11.60	
Na_2O	2.20		2.07		1.41	
K_2O	1.43		1.37		1.08	
	99.23		99.49		98.16	
	Number of ions based on 23 oxygens					
	Fe^{2+}	13CNK	Fe^{2+}	13CNK	Fe^{2+}	13CNK
Si	6.198	6.093	6.250	6.145	6.622	6.538
Aliv	1.802	1.907	1.750	1.855	1.378	1.462
	8.000	8.000	8.000	8.000	8.000	8.000
Alvi	0.664	0.517	0.695	0.549	0.541	0.433
Ti	0.121	0.119	0.118	0.116	0.139	0.137
Fe^{3+}	0.000	0.778	0.000	0.771	0.000	0.583
Cr	0.000	0.000	0.000	0.000	0.000	0.000
Mg	2.030	1.996	2.026	1.992	2.934	2.897
Fe^{2+}	2.185	1.575	2.161	1.554	1.386	0.927
Mn		0.015		0.018		0.023
Ca						
	5.000	5.000	5.000	5.000	5.000	5.000
Fe^{2+}	0.208		0.204		0.144	
Mn	0.015		0.018		0.023	
Ca	1.768	1.738	1.759	1.729	1.813	1.790
Na	0.009	0.262	0.019	0.271	0.020	0.210
	2.000	2.000	2.000	2.000	2.000	2.000
Ca						
Na	0.631	0.367	0.580	0.318	0.379	0.184
K	0.274	0.269	0.261	0.256	0.201	0.198
	0.905	0.636	0.841	0.574	0.580	0.382
	(3)*		(3)		(5)	
Name:	magnesian hastingsite		magnesian hastingsite			

( )* = number of analyses

analysis 14: V554-2 analysis 15: V137-5

	16		17			
	rim		core			
SiO_2	45.72		46.75		52.05	
TiO_2	0.50		0.49		0.13	
Al_2O_3	8.89		9.87		4.82	
Cr_2O_3	0.00		0.00		0.00	
FeO	14.46		14.19		11.37	
MnO	0.15		0.13		0.28	
MgO	11.05		12.02		16.52	
CaO	11.22		11.83		12.36	
Na_2O	1.09		1.18		0.56	
K_2O	0.75		0.59		0.26	
	93.83		97.05		98.35	
	Number of ions based on 23 oxygens					
	Fe^{2+}	13CNK	Fe^{2+}	13CNK	Fe^{2+}	13CNK
Si	7.003	6.971	6.902	6.856	7.429	7.339
Aliv	0.997	1.029	1.098	1.144	0.571	0.661
	8.000	8.000	8.000	8.000	8.000	8.000
Alvi	0.608	0.568	0.620	0.563	0.240	0.140
Ti	0.058	0.058	0.054	0.054	0.014	0.014
Fe^{3+}	0.000	0.211	0.000	0.309	0.000	0.562
Cr	0.000	0.000	0.000	0.000	0.000	0.000
Mg_{2+}	2.523	2.511	2.645	2.627	3.514	3.471
Fe^{2+}	1.811	1.632	1.681	1.431	1.232	0.779
Mn		0.019		0.016		0.034
Ca		0.001				
	5.000	5.000	5.000	5.000	5.000	5.000
Fe^{2+}	0.041		0.071		0.125	
Mn	0.019		0.016		0.034	
Ca	1.842	1.833	1.872	1.859	1.841	1.866
Na	0.098	0.167	0.041	0.141		0.134
	2.000	2.000	2.000	2.000	2.000	2.000
Ca					0.50	
Na	0.226	0.155	0.297	0.195	0.155	0.019
K	0.147	0.146	0.111	0.110	0.047	0.046
	0.373	0.301	0.408	0.305	0.702	0.065
	(2)*		(2)		(3)	
Name:	magnesio-hornblende		magnesio-hornblende		actinolitic hornblende	

( )* = number of analyses

analysis 16: V769-3 analysis 17: V769-3

	18		19		20	
SiO_2	48.50		54.96		43.73	
TiO_2	0.68		0.30		1.40	
Al_2O_3	7.06		2.62		10.43	
Cr_2O_3	0.02		0.00		0.00	
FeO	16.58		10.87		20.45	
MnO	0.48		0.34		0.43	
MgO	12.23		16.72		8.68	
CaO	11.38		12.38		11.24	
Na_2O	0.92		0.37		1.39	
K_2O	0.73		0.13		1.05	
	98.58		98.69		98.80	
	Number of ions based on 23 oxygens					
	Fe^{2+}	13CNK	Fe^{2+}	13CNK	Fe^{2+}	13CNK
Si	7.124	7.018	7.754	7.717	6.596	6.498
Aliv	0.876	0.982	0.246	0.283	1.404	1.502
	8.000	8.000	8.000	8.000	8.000	8.000
Alvi	0.346	0.222	0.190	0.151	0.451	0.325
Ti_{3+}	0.075	0.074	0.032	0.032	0.159	0.156
Fe^{3+}	0.000	0.689	0.000	0.219	0.000	0.687
Cr	0.002	0.002	0.000	0.000	0.000	0.000
Mg_{2+}	2.677	2.637	3.516	3.499	1.951	1.922
Fe^{2+}	1.900	1.317	1.262	1.058	2.439	1.855
Mn		0.059		0.041		0.055
Ca						
	5.000	5.000	5.000	5.000	5.000	5.000
Fe^{2+}	0.137		0.021		0.141	
Mn	0.060		0.041		0.055	
Ca	1.791	1.764	1.872	1.863	1.804	1.789
Na	0.012	0.236	0.066	0.100		0.211
	2.000	2.000	2.000	1.963	2.000	2.000
Ca					0.013	
Na	0.250	0.022	0.035		0.407	0.190
K	0.137	0.135	0.023	0.023	0.202	0.199
	0.387	0.157	0.058	0.023	0.622	0.389
	(3)*		(3)		(3)	
Name:	magnesio-hornblende		actinolite		tschermakitic hornblende	

( )* = number of analyses

analysis 18:V191-1 analysis 19:V493-3
analysis 20:V721-2

	21	22	23	24
SiO_2	41.57	49.62	42.35	51.03
TiO_2	1.80	0.34	3.22	0.20
Al_2O_3	13.60	4.77	12.86	2.61
Cr_2O_3	0.00	0.00	0.00	0.00
FeO	17.41	12.31	13.33	15.46
MnO	0.27	0.27	0.27	0.30
MgO	9.23	16.04	11.80	14.70
CaO	11.63	12.34	11.04	11.71
Na_2O	1.62	0.80	11.76	0.57
K_2O	1.37	0.30	0.75	0.17
	98.50	96.79	97.38	96.75

Number of ions based on 23 oxygens

	Fe^{2+}	13CNK	Fe^{2+}	13CNK	Fe^{2+}	13CNK	Fe^{2+}	13CNK
Si	6.235	6.176	7.278	7.172	6.273	6.193	7.558	7.424
Aliv	1.765	1.824	0.722	0.828	1.727	1.807	0.442	0.576
	8.000	8.000	8.000	8.000	8.000	8.000	8.000	8.000
Alvi	0.639	0.557	0.103	(-.015)	0.519	0.410	0.014	(-.128)
Ti	0.203	0.201	0.038	0.037	0.359	0.354	0.022	0.022
Fe^{3+}	0.000	0.438	0.000	0.665	0.000	0.589	0.000	0.816
Cr	0.000	0.000	0.000	0.000	0.000	0.000	0.000	0.000
Mg	2.063	2.044	3.507	3.456	2.605	2.571	3.245	3.188
Fe^{2+}	2.184	1.726	1.352	0.823	1.517	1.042	1.719	1.065
Mn		0.034	0.034	0.034		0.034		0.037
Ca								
	5.000	5.000	5.000	5.000	5.000	5.000	5.000	5.000
Fe^{2+}	0.158				0.135		0.196	
Mn	0.034				0.034		0.038	
Ca	1.940	1.912	1.869	1.851	1.753	1.730	1.859	1.826
Na	0.060	0.088		0.149	0.078	0.270	0.164	0.161
	2.000	2.000	2.000	2.000	2.000	2.000	2.000	1.987
Ca	0.132							
Na	0.228	0.137	0.471	0.317	0.428	0.230		
K	0.056	0.055	0.262	0.259	0.142	0.140	0.032	0.031
	0.224	0.192	0.733	0.576	0.570	0.370	0.032	0.031
	(2)*		(2)		(3)		(3)	
Name:	ferroan pargasite		magnesio-hornblende		tschermakite		actinolitic hornblende	

( )* = number of analyses

analysis 21: V608-2 analysis 22: V608-2
analysis 23: V725-3 analysis 24: V725-3

	25
SiO_2	49.12
TiO_2	0.39
Al_2O_3	6.49
Cr_2O_3	0.00
FeO	14.45
MnO	0.16
MgO	13.72
CaO	11.32
Na_2O	0.59
K_2O	0.43
	96.67

Number of ions based on 23 oxygens

	Fe^{2+}	13CNK
Si	7.244	7.115
Aliv	0.756	0.885
	8.000	8.000
Alvi	0.373	0.225
Ti	0.043	0.042
Fe^{3+}	0.000	0.817
Cr	0.000	0.000
Mg_{2+}	3.016	2.962
Fe^{2+}	1.568	0.934
Mn		0.020
Ca		
	5.000	5.000
Fe^{2+}	0.215	
Mn	0.020	
Ca	1.745	1.757
Na		0.165
	2.000	1.922
Ca	0.044	
Na	0.169	
K	0.081	0.080
	0.294	0.080

(3)

Name: magnesio-hornblende

( )* = number of analyses

analysis 25: V725-2

Appendix A.4.9. Garnet Analyses (Garnets associated with Grenvillian fabrics)

Unit Number	Analysis Number
1C	2,3
3B	1
6A	4
6B	5,6,7,8,9,10
6D	11
6E	12
intermediate dykes	13,14,15
10	16

	1		2		3		4	
	rim	core	rim	core	rim	core	rim	core
SiO_2	38.52	38.81	36.27	36.37	36.42	36.98	37.72	38.36
TiO_2	0.04	0.09	0.02	0.04	0.06	0.04	0.02	0.04
Al_2O_3	20.06	20.04	21.27	21.08	21.30	21.60	20.23	20.04
FeO	23.69	24.85	32.12	32.58	31.86	30.98	27.16	26.41
MnO	5.03	5.62	2.72	3.30	2.36	2.16	10.31	9.30
MgO	1.25	1.25	3.35	3.61	3.46	3.52	1.23	1.19
CaO	11.75	10.11	3.52	2.66	4.65	5.39	5.15	6.45
	100.34	100.77	99.72	99.64	100.11	100.67	101.82	101.79
	Number of ions on the basis of 24 oxygens							
Si	6.118	6.150	5.877	5.883	5.851	5.878	6.033	6.102
Aliv	--	--	0.123	0.117	0.149	0.122	--	--
Alvi	3.875	3.895	3.940	3.904	3.886	3.926	3.848	3.861
Ti	0.005	0.011	0.002	0.005	0.007	0.005	0.002	0.005
Fe^{3+}	--	--	0.003	0.003	0.006	0.000	--	--
Fe^{2+}	3.032	3.294	4.350	4.405	4.275	4.119	3.634	3.514
Mn	0.677	0.755	0.373	0.452	0.321	0.291	1.397	1.253
Mg	0.296	0.295	0.809	0.870	0.829	0.834	0.293	0.282
Ca	2.000	1.717	0.611	0.461	0.801	0.918	0.883	1.100
	(3/9)*	(3/10)	(3/12)	(3/14)	(2/10)	(2/10)	(1/5)	(1/4)
Mol%								
pyr	5.2	5.2	13.3	14.4	13.7	13.7	5.1	5.0
alm	47.3	50.8	70.6	70.5	67.8	66.4	50.1	53.3
gros	35.4	30.3	10.0	7.6	13.1	15.0	15.4	19.4
spes	12.0	13.4	6.1	7.5	5.3	4.8	24.4	22.2

(#/#)* = (# of garnets analysed/total # of analyses)

analysis 1: V194-4
analysis 2: V580-2
analysis 3: V580-3
analysis 4: V546-1

	5		6	7	8		9	
	rim	core			rim	core	rim	core
SiO_2	36.15	37.32	36.55	35.07	38.48	38.24	38.57	38.47
TiO_2	0.02	0.04	0.00	0.00	0.04	0.07	0.10	0.17
Al_2O_3	20.93	20.83	20.63	21.38	20.23	19.98	20.23	20.08
FeO	27.07	22.74	31.24	25.45	24.07	21.06	22.84	21.58
MnO	6.27	7.90	6.98	6.50	5.97	6.26	6.39	6.53
MgO	0.05	0.02	0.09	0.09	0.10	0.06	0.40	0.36
CaO	10.13	11.70	6.33	11.34	11.75	14.18	12.52	13.20
	100.62	100.60	101.82	99.83	100.64	99.85	101.05	100.39
	Number of ions on the basis of 24 oxygens							
Si	5.853	5.974	5.905	5.724	6.127	6.113	6.106	6.115
Aliv	0.147	0.026	0.095	0.276	--	--	--	--
Alvi	3.849	3.915	3.835	3.839	3.925	3.879	3.882	3.879
Ti	0.002	0.005	0.000	0.000	0.005	0.008	0.012	0.020
Fe^{3+}	0.000	0.005	0.000	0.000	--	--	--	--
Fe^{2+}	3.666	3.040	4.222	3.475	3.206	2.816	3.024	2.869
Mn	0.860	1.071	0.955	0.899	0.805	0.848	0.857	0.879
Mg	0.012	0.005	0.022	0.022	0.024	0.014	0.094	0.085
Ca	1.758	2.007	1.096	1.984	2.005	2.429	2.124	2.249
	(1/4)*	(1/3)	(1/4)	(1/8)	(3/9)	(3/9)	(2/8)	(2/9)
Mol%								
pyr	0.2	0.1	0.4	0.3	0.4	0.2	1.6	1.5
alm	56.1	47.9	64.8	52.9	50.3	41.8	45.8	43.3
gros	29.3	33.8	18.6	32.1	35.1	42.8	37.2	39.3
spes	14.3	18.1	16.2	14.5	14.1	15.0	15.1	15.5

(#/#)* = (# of garnets analysed/total # of analyses)

analysis 5: V9-2
analysis 6: V164
analysis 7: V257-1
analysis 8: V257-7
analysis 9: V523

	10		11		12		13	
	rim	core	rim	core	rim	core	rim	core
SiO_2	37.79	37.79	38.39	37.93	38.10	37.93	37.01	37.42
TiO_2	0.06	0.07	0.05	0.05	0.03	0.09	0.00	0.01
Al_2O_3	20.57	20.35	19.05	18.68	20.45	19.47	20.79	20.72
FeO	23.78	23.06	18.68	19.05	18.36	18.54	23.61	23.75
MnO	5.78	6.30	13.87	13.70	16.04	14.75	5.98	7.27
MgO	0.21	0.19	1.06	1.08	0.79	0.85	0.04	0.05
CaO	13.03	12.73	10.35	11.11	8.59	9.69	11.23	10.70
	101.22	100.49	101.45	101.60	102.36	101.32	98.66	99.87
	Number of ions on the basis of 24 oxygens							
Si	6.002	6.037	6.118	6.068	6.026	6.065	6.014	6.025
Aliv	--	--	--	--	--	--	--	--
Alvi	3.854	3.871	3.698	3.591	3.840	3.736	3.997	3.958
Ti	0.007	0.008	0.005	0.006	0.004	0.011	0.000	0.001
Fe^{3+}	--	--	--	--	--	--	--	--
Fe^{2+}	3.159	3.081	2.490	2.549	2.429	2.480	3.209	3.198
Mn	0.778	0.853	1.873	1.857	2.149	1.998	0.823	0.992
Mg	0.050	0.045	0.252	0.258	0.186	0.203	0.010	0.012
Ca	2.218	2.179	1.768	1.905	1.456	1.661	1.956	1.846
	(1/4)*	(1/5)	(1/5)	(1/5)	(1/5)	(1/5)	(3/9)	(3/9)
Mol%								
pyr	0.8	0.8	4.7	4.8	3.2	3.7	0.1	0.2
alm	47.4	46.5	27.6	24.0	33.7	30.0	53.3	51.7
gros	38.2	37.7	32.8	35.9	25.4	29.9	32.7	31.2
spes	15.5	14.8	34.8	35.1	37.5	36.2	13.8	16.8

(#/#)* = (# of garnets analyses/total # of analyses)

analysis 10: V630
analysis 11: V772
analysis 12: V434
analysis 13: V257-8

	14		15	16	
	rim	core		rim	core
SiO_2	37.82	37.88	35.75	37.85	37.47
TiO_2	0.10	0.07	0.02	0.05	0.02
Al_2O_3	20.00	20.05	20.45	21.20	21.38
FeO	21.97	21.98	28.52	28.67	28.38
MnO	8.37	8.93	7.45	2.89	3.35
MgO	0.42	0.46	0.21	3.59	3.87
CaO	12.10	11.51	8.98	6.42	5.86
	100.78	100.88	101.38	100.67	100.33
	Number of ions based on 24 oxygens				
Si	6.042	6.049	5.805	5.979	5.939
Aliv	--	--	0.195	0.021	0.061
Alvi	3.810	3.824	3.720	3.928	3.935
Ti	0.012	0.008	0.002	0.006	0.002
Fe^{3+}	--	--	0.001	0.000	0.004
Fe^{2+}	2.936	2.936	3.873	3.788	3.759
Mn	1.133	1.208	1.025	0.387	0.450
Mg	0.100	0.109	0.051	0.845	0.914
Ca	2.072	1.970	1.563	1.087	0.995
	(1/6)*	(1/4)	(1/4)	(3/9)	(3/10)
Mol%					
pyr	1.7	1.9	0.8	14.2	15.2
alm	41.6	42.0	55.1	60.9	60.6
gros	36.4	34.6	26.5	18.2	16.6
spes	20.0	21.3	17.4	6.5	7.5

(#/#)* = (# of garnets analysed/total # of analyses)

analysis 14: V683-3
analysis 15: V710-2
analysis 16: V554-2

Appendix A.4.10. Biotite Analyses (Biotites associated with Grenvillian fabrics)

Unit Number	Analysis Number
1C	2,3
3B	1
6A	4
6B	5,6,7,8,,9,10
6D	11
6E	12
intermediate dykes	13,14,15
10	16

	1	2	3	4	5	6	7	8
SiO_2	37.53	36.46	37.36	36.38	34.24	34.96	35.28	35.93
TiO_2	3.01	2.22	1.70	2.19	2.13	3.13	2.99	2.73
Al_2O_3	14.92	17.13	16.54	15.95	14.73	13.43	15.64	14.82
FeO	22.70	19.74	19.12	27.58	34.46	36.32	35.01	32.68
MnO	0.23	0.01	0.05	0.53	0.38	0.29	0.32	0.25
MgO	8.92	11.97	12.20	6.59	1.44	1.15	2.14	1.89
CaO	0.02	0.00	0.02	0.00	0.00	0.00	0.00	0.02
Na_2O	0.06	0.04	0.00	0.03	0.07	0.04	0.05	0.03
K_2O	9.19	9.20	10.74	11.04	7.68	9.38	6.85	8.18
	96.58	96.77	97.73	100.29	95.13	98.70	98.28	96.53
	Number of ions on the basis of 22 oxygens							
Si	5.718	5.462	5.566	5.531	5.622	5.625	5.549	5.736
Aliv	2.282	2.538	2.434	2.469	2.378	2.375	2.451	2.264
Alvi	0.398	0.487	0.472	0.390	0.473	0.172	0.449	0.525
Ti	0.345	0.250	0.191	0.250	0.263	0.379	0.354	0.328
* Fe^{2+}	2.893	2.473	2.383	3.507	4.732	4.888	4.606	4.364
Mn	0.030	0.001	0.006	0.068	0.053	0.040	0.043	0.034
Mg	2.026	2.673	2.709	1.493	0.352	0.276	0.502	0.450
Ca	0.003	0.000	0.003	0.000	0.000	0.000	0.000	0.003
Na	0.018	0.012	0.000	0.009	0.022	0.012	0.015	0.009
K	1.786	1.758	2.042	2.142	1.609	1.926	1.375	1.666
	(8)**	(5)	(3)	(5)	(6)	(5)	(7)	(5)

* Fe: all iron as Fe^{2+}

( )** = number of analyses

analysis 1: V194-4
analysis 2: V580-2
analysis 3: V580-3
analysis 4: V546-1
analysis 5: V9-2
analysis 6: V164
analysis 7: V257-1
analysis 8: V257-7

	9	10	11	12	13	14	15	16
SiO_2	35.82	36.20	37.88	38.30	34.54	35.54	35.30	36.67
TiO_2	2.13	2.05	2.65	2.79	1.70	2.85	3.35	3.75
Al_2O_3	15.51	14.81	13.86	15.64	15.27	15.08	14.43	15.50
FeO	30.72	30.83	22.25	24.56	35.02	28.56	33.04	17.94
MnO	0.31	0.32	0.70	0.72	0.27	0.35	0.50	0.03
MgO	4.93	4.21	10.23	7.45	1.07	5.30	2.62	12.48
CaO	0.01	0.00	0.00	0.00	0.05	0.00	0.02	0.02
Na_2O	0.08	0.05	0.06	0.06	0.03	0.09	0.05	0.07
K_2O	8.91	9.07	10.74	9.98	10.00	9.35	8.78	9.83
	98.42	97.54	98.37	99.50	97.95	97.12	98.09	96.29
	Number of ions on the basis of 22 oxygens							
Si	5.575	5.695	5.722	5.726	5.578	5.578	5.595	5.511
Aliv	2.425	2.305	2.278	2.274	2.422	2.422	2.405	2.489
Alvi	0.421	0.442	0.191	0.484	0.485	0.368	0.291	0.258
Ti	0.249	0.243	0.301	0.314	0.206	0.336	0.399	0.424
Fe^{2+}	3.999	4.057	2.811	3.072	4.730	3.749	4.380	2.255
Mn	0.041	0.043	0.090	0.091	0.037	0.047	0.067	0.004
Mg	1.144	0.987	2.303	1.660	0.258	1.240	0.619	2.796
Ca	0.002	0.000	0.000	0.000	0.009	0.000	0.003	0.003
Na	0.024	0.015	0.018	0.017	0.009	0.027	0.015	0.020
K	1.769	1.821	2.070	1.904	2.061	1.872	1.776	1.885
	(5)**	(6)	(4)	(4)	(3)	(5)	(6)	(3)

Fe: all iron as Fe^{2+}

( )** = number of analyses

analysis 9: V523
analysis 10: V630
analysis 11: V772
analysis 12: V434
analysis 13: V257-8
analysis 14: V683-3
analysis 15: V710-2
analysis 16: V554-2

APPENDIX B.

MINERALOGY OF SELECTED SAMPLES FROM THE SMOKEY ARCHIPELAGO

Sample	Unit	Mineralogy	Comments
V9-2	6B	Ksp + pl(An5) + qz + hbl + gt + bi	Gren
V17	M	pl(An19) + bi + ep	
V42-3	M	pl(An27) + bi + cpx + hbl(r) + qz + py	pre-Gn
V71	M	pl(38) + hbl + bi + py	
V100-2	M	pl(An33) + hbl + bi + py	
V113-3	M	pl(An17) + hbl + bi + ep(r) + mu(r)	trachytic
V123	2	pl(An27) + hbl + bi + qz	
V132-1	M	pl(An30) + hbl + ep + bi	
V132-2	M	hbl + bi + Ksp + cpx + qz	pre-Gn
V132-3	M	hbl + pl(An25) + bi + py	
V132-4	M	pl(An27) + hbl + bi + ep(r)	
V137-5	7	hbl + pl(An37) + zs + bi + cpx + mt + py	GHSZ
V150	M	pl(An36) + hbl + bi + ep	
V164	6B	Ksp + pl(An13) + qz + hbl + gt + bi	
V172	1C	pl(An33) + qz + Ksp + bi + gt + py	
V177-2	M	pl(An60) + hbl + bi + py + mt	trachytic
V185-1	M	hbl + pl(An40) + bi + py	pre-Gn
V185-2	M	pl(An24) + hbl + bi + mt + ep	GHSZ
V191-1	6A	pl(An3) + qz + Ksp + bi + ep + sph + + ct + py	BF
V191	M	pl(An3) + bi + ep + hbl + mt + py	BF
V194-2	M	pl(An34) + bi + cpx + opx + zr + hbl(r) + py	pre-Gn
V194-3	3B	pl(An25) + qz + Ksp + bi + hbl + mt + ap	
V194-4	3B	pl(An25) + qz + Ksp + hbl + bi + gt + ep + zr	GHSZ
V201	?5A	Ksp + pl(An23) + bi + gt + mt + py	
V207	1C	pl(An33) + qz + Ksp + bi + gt + opx	
V210-1	1C	pl(An36) + qz + Ksp + bi + cd + gt + opx + mt + py + ilm + sil + fibrol + sp	

ABBREVIATIONS

M = metabasite
int = intermediate dyke
GHSZ = Grenvillian high strain zone
ME = mafic enclave
GS2 = sample contains GS2 fabric
(r) = retrograde phase
pre-Gn = pre-Grenvillian metabasite
--> = core to rim plagioclase zoning
(v) = as veins
BF = sampled along Benedict Fault
CTIF = sampled along Cut Throat Island Fault

Notes: -retrograde phases in pelitic metatexite (unit 1C) are not indicated (see text)
-minerals in each sample are listed in a decreasing order of modal abundance

APPENDIX B. (Continued)

Sample	Unit	Mineralogy	Comments
V211-2	1C	pl(An24) + qz + Ksp + bi + cd + gt + fibrol + mt + py	
V220	3A	pl(An31) + qz + Ksp + cpx + bi + mt + hbl(r)	
V221	3A	pl(An30) + qz + Ksp + bi + gt + opx + mt	
V257-1	6B	Ksp + pl(An3) + qz + hbl + bi + all + mt + py	GHSZ
V257-7	6B	Ksp + qz + pl(An3) + bi + hbl + gt + zirc + ap	GHSZ
V257-8	int	Ksp + qz + pl(An12-->8) + bi + hbl + all + ep + zr	GHSZ
V325-1	2	pl(An31) + bi +hbl + Ksp + mt + cpx	
CG79-347	1C	pl(An22) + bi + qz + cd + Ksp + gt + fibrol + sil + mt	
V376	3A	pl(An26) + qz + Ksp + bi + opx + mt + py + ap + zr	
V434	6E	Ksp + qz + pl(An14) + bi + gt + mu + ep + zr + mt	
V438-4	M	hbl + pl(An24) + bi + qz	GHSZ
V448-3	5A	Ksp + qz + pl(An20) + bi + hbl + gt + mt	
V450-1	5A	Ksp + pl(An7) + qz + bi + gt + all + ep + zr + py	
V453-3	M	pl(An22) + hbl + bi	GHSZ
V463	M	Ksp + hbl + cpx + bi + pl(An21) + py + mt	pre-Gn
V465	5A	Ksp + qz + pl(An16) + bi + hbl + mu + gt + ep + all + mt	
V470-2	?3A	Ksp + qz + pl(An2) + hbl + cpx + mt + py + bi	
V471-2	?3A	Ksp + qz + pl(An12) + mt + bi + gt + cpx	
V493-3	M	act + pl(An1) + zs + sph + bi	BF
V523	6B	Ksp + qz + pl(An17) + bi + hbl + gt + ep	GHSZ
V526-1	6B	pl(An26) + qz + Ksp + bi + hbl + mt	
V526-3A	3A	pl(An26) + qz + cpx + opx + Ksp + bi	
V526-3B	M	cpx + bi + opx + pl(An34)	pre-Gn
V541-2	M	pl(An32) + Ksp + bi + cpx + mt + py	pre-Gn
V546-1	6A	Ksp + qz + pl(An22) + bi + gt + mu	
V554-2	10	hbl + pl(An25) + gt + bi +ilm + qz	GHSZ
V560	M	pl(An21) + hbl + bi	GHSZ
V579-1	3A	pl(An30) + qz + Ksp + bi + gt + opx + mt	
V580-1A	1C	pl(An34) + qz + Ksp + bi + gt + cd + fibrol + mt	
V580-1B	1C	pl(An35) + qz + Ksp + bi + gt + cd + mt + sil + fibrol	
V580-2	1C	pl(An35) + qz + bi + hbl + gt + py	GHSZ
V580-3	1C	pl(An33) + qz + bi + hbl + gt + mt	GHSZ
V580-7	M	pl(An90) + opx + cpx + bi + py + qz	
V580-8	M	pl(An86) + opx + cpx + bi + hbl(r) + mt	pre-Gn
V580-12	1C	pl(An35) + qz + Ksp + bi + cd + gt + mt + opx + sp + fibrol	
V580-16	1C	pl(An33) + qz + Ksp + bi + cd + gt + fibrol + mt + zr	

APPENDIX B. (Continued)

Sample	Unit	Mineralogy	Comments
V581-1	2	pl(An42) + bi + hbl + mt + cpx + opx	
V585	3A	pl(An32) + qz + Ksp + cpx + opx + bi + mt + ap	
V586	3A	pl(An32) + qz + Ksp + bi + cpx + opx + hbl(r) + mt + py + ap	
V608-2	M	pl(An27) + hbl(1) + hbl(2) + ep + qz + mt	
V630	6B	Ksp + qz + pl(An17) + hbl + bi + gt + ep + zr + ct + mt + py	GS 2
V683-3	int	Ksp + qz + pl(An17-->9) + bi + hbl + gt + ep + zr + mt	GS 2
V686	M	pl(An19) + bi + mu + qz(v) + ct(v) + ep	GHS Z
V687	6A	pl(An26) + qz + Ksp + bi + opx + cpx + mt + hbl(r)	
V711-2	M	pl(An24) + hbl + bi + cpx + py	pre-Gn
V714	M	hbl + pl(An29) + bi + qz + ct + zr	
V721-2	M	hbl + bi + pl(An3) + ep + qz + py	BF
V725-2	M	pl(An1) + hbl + ep	
V725-3	M	hbl + act + pl(11)	
V764-3	5B	Ksp + qz + pl(An15) + hbl + bi + ep + mt + sph	
V764-5	M	pl(An4) + bi + hbl + qz + ep + ap	
V764-7	M	pl(An30) + hbl + bi + ap + mu	
V766	6A	Ksp + pl(An20) + qz + bi + hbl + ep + sph + chl(r)	
V766-2	ME	pl(An23) + hbl + bi + py	
V766-3	ME	pl(An21) + hbl + bi + Ksp	
V769-3	M	bi + hbl + pl(An30) + ep + py + mt + ct(v)	CTIF
V772	6D	pl(An17) + qz + Ksp + hbl + bi	
V774	2	pl(An31) + hbl + bi + qz + Ksp	
V775	ME	pl(An20) + hbl + bi + zr + chl	

APPENDIX C.
COMPOSITIONS OF MAFIC MINERALS COMPRISING CORONITIC TEXTURES IN VARIOUS GABBROIC ROCKS

Notes: - Mineral recalculation schemes are as follows: olivine, 4 oxygens; pyroxenes, 6 oxygens; amphibole, 23 oxygens; ilmenite, 6 oxygens; garnet, 24 oxygens; biotite, 22 oxygens.

-descriptions of the corona textural types are presented in section 4.3 and in Table 4-16.

Textural Type A.

	V458			V505-2		
	Olivine	Opx	Amph	Olivine	Opx	Amph
SiO2	35.70	51.64	38.49	37.12	53.97	38.68
TiO2	0.00	0.00	0.02	0.02	0.00	0.09
Al2O3	0.02	1.46	18.16	0.09	0.35	20.32
FeO*	37.66	22.42	15.06	31.17	22.95	13.08
MnO	0.47	0.38	0.23	0.29	0.44	0.17
MgO	27.16	23.71	15.50	32.27	23.34	12.43
CaO	0.02	0.23	11.89	0.23	0.16	10.37
Na2O	nd	nd	0.32	nd	nd	2.88
K2O	nd	nd	0.00	nd	nd	0.00
	101.03	99.84	99.67	101.19	101.21	98.52
Si	.993	1.930	5.600	.996	1.986	5.668
Aliv	.001	.064	2.400	.003	.014	2.332
Alvi	.000	.000	.716	.000	.000	1.179
Ti	.001	.000	.002	.003	.000	.010
Fe2+	.876	.701	1.833	.699	.706	1.603
Mn	.011	.012	.028	.007	.014	.021
Mg	1.125	1.321	3.362	1.290	1.280	2.715
Ca	.001	.009	1.854	.007	.006	1.629
Na	--	--	.090	--	--	.818
K	--	--	.000	--	--	.000
	(3)	(3)	(3)	(3)	(3)	(3)
Mol%						
Fo:	55.93			34.75		

Textural Type A (continued)

	V554-1			V740		
	Olivine	Opx	Amph	Olivine	Opx	Amph
SiO2	32.57	50.76	38.89	33.33	53.77	37.83
TiO2	0.68	0.00	0.06	0.02	0.00	0.05
Al2O3	0.02	0.81	17.35	0.02	0.44	19.46
*FeO	45.34	28.37	17.19	47.97	21.68	11.20
MnO	0.57	0.54	0.15	0.78	0.33	0.12
MgO	18.61	19.28	8.74	19.32	24.07	12.58
CaO	0.02	0.18	10.87	0.02	0.14	11.14
Na2O	0.04	nd	2.23	nd	nd	3.02
K2O	0.00	nd	1.75	nd	nd	0.95
	97.85	99.94	97.23	101.46	100.43	96.35
Si	.991	1.951	5.923	.978	1.982	5.656
Aliv	.001	.037	2.077	.001	.018	2.344
Alvi		.000	1.039	.000	.001	1.086
Ti	.001	.000	.007	.001	.000	.006
Fe2+	1.154	.912	2.285	1.177	.668	1.401
Mn	.015	.018	.019	.019	.010	.015
Mg	.844	1.105	1.984	.845	1.323	2.803
Ca	.001	.007	1.774	.001	.006	1.785
Na	.002	--	.659	--	--	.876
K	.000	--	.340	--	--	.181
	(3)	(3)	(3)	(3)	(3)	(3)
Mol% Fo:	41.9			41.4		

* all Fe as FeO
( ) = number of analyses

APPENDIX C (Continued)

Textural Type B.

	V458			V505-2		
	Ilmenite	Biotite		Ilmenite	Biotite	Amphibole
SiO2	0.02	35.37		0.00	32.96	38.80
TiO2	51.17	5.60		52.57	3.91	0.70
Al2O3	0.09	15.36		0.00	14.77	16.78
Cr2O3	0.02	0.00		0.00	0.00	0.00
*FeO	46.21	12.96		47.08	21.29	19.44
MnO	0.43	0.01		0.69	0.08	0.21
MgO	0.00	16.92		0.16	9.41	6.50
CaO	0.00	0.04		0.00	0.04	10.52
Na2O	0.00	0.18		0.00	0.10	1.93
K2O	0.00	9.87		0.00	8.08	1.59
	97.94	96.31		100.52	90.64	96.47
Si	.001	5.225		.000	5.366	6.005
Al	.005	Aliv 2.676	Al	.000	Aliv 2.634	1.995
		Alvi .000			Alvi .202	1.067
Ti	1.987	.622		1.989	.479	.081
Cr	.001	.000		.000	.000	.000
Fe2+	1.994	1.602		1.980	2.899	2.516
Mn	.019	.001		.029	.011	.028
Mg	.000	3.726		.012	2.284	1.499
Ca	.000	.006		.000	.007	1.745
Na	.000	.052		.000	.032	.579
K	.000	1.861		.000	1.679	.314
	(2)	(3)		(2)	(1)	(2)

* all Fe as FeO
( ) = number of analyses
note: low total in 505-2 biotite analysis is attributed to polishing problems associated with fine coronas enveloping the relatively hard ilmenite.

APPENDIX C. (Continued)

Textural Type C.

	V436		
	Ilmenite	Biotite	Garnet
SiO2	0.00	35.72	38.18
TiO2	42.37	2.39	0.00
Al2O3	0.07	14.05	20.29
*FeO	49.23	21.23	30.47
MnO	0.57	0.04	2.86
MgO	0.12	10.48	2.70
CaO	0.01	0.00	5.24
Na2O	0.00	0.18	0.00
K2O	0.00	7.80	0.00
	92.37	91.89	99.74
Si	.000	5.674	6.116
Al	.070 Aliv	2.326	--
	Alvi	.306	3.949
Ti	1.808	.286	.000
Fe2+	2.336	2.821	4.083
Mn	.027	.005	.388
Mg	.010	2.481	.645
Ca	.001	.000	.900
Na	.000	.055	.000
K	.000	1.581	.000
	(1)	(2)	(2)

* all Fe as FeO
( ) = number of analyses

APPENDIX C. (Continued)

Textural Type D. Garnet analyses.

	V472 core	[a]* rim	V472 core	[b]* rim
SiO2	38.42	37.46	37.54	38.35
TiO2	0.03	0.02	0.03	0.03
Al2O3	20.31	20.31	20.03	20.16
FeO**	30.20	30.44	30.40	30.62
MnO	1.08	1.29	1.08	1.23
MgO	2.94	2.82	2.72	2.64
CaO	7.88	7.90	8.25	8.01
	100.86	100.24	100.05	101.04
Si	6.074	5.990	6.015	6.072
Aliv	(-.074)	.010	(-.015)	(-.072)
Alvi	3.860	3.819	3.799	3.836
Ti	.004	.002	.004	.004
Fe2+	3.994	4.071	4.074	4.055
Mn	.145	.175	.147	.165
Mg	.693	.672	.650	.623
Ca	1.335	1.354	1.417	1.359
	(4)	(4)	(3)	(3)
Mol%				
pyr	12.19	11.70	11.44	11.03
alm	61.77	61.70	61.04	62.00
spes	2.55	3.04	2.58	2.92
gros	23.43	23.52	24.88	24.00

*[a] = 2mm euhedral garnet enclosed in plagioclase (An 22)
*[b] = 1mm euhedral garnet nucleated in plagioclase (An22) along margin of hornblende-mantled igneous clinopyroxene
** all Fe as Fe 2+
( ) = number of analyses

APPENDIX C. (Continued)

Textural Type E.

	V436	
	Cummingtonite	Hornblende
SiO2	54.01	43.73
TiO2	0.05	0.51
Al2O3	0.59	10.29
*FeO	25.89	19.21
MnO	0.57	0.17
MgO	16.08	9.20
CaO	0.67	10.20
Na2O	0.11	1.88
K2O	0.00	0.38
	97.97	95.57
Si	7.959	6.735
Aliv	.041	1.265
Alvi	.062	.603
Ti	.006	.059
Fe2+	3.191	2.475
Mn	.071	.022
Mg	3.532	2.112
Ca	.106	1.683
Na	.031	.561
K	.000	.075
	(1)	(2)

* all Fe as FeO
( ) = number of analyses

APPENDIX D
WET CHEMICAL MINERAL ANALYSIS

A biotite separate from V210-1 (pelitic metatexite; unit 1C) was analysed for major oxides, including FeO and Fe2O3, by atomic absorption spectrophotometry. Caution should be excerised in comparing this analysis with microprobe analyses of biotite from the same sample, given the between-grain variations in biotite compositions characteristic of this unit.

SiO2	37.2
TiO2	3.33
Al2O3	15.9
FeO	11.45
Fe2O3	3.39
MgO	13.96
MnO	0.08
CaO	0.18
Na2O	0.22
K2O	8.78
P2O5	0.01
LOI	4.40
Total	98.90

Number of ions on the basis of 22 oxygens

Si	5.536
Aliv	2.464
Alvi	0.326
Ti	0.373
Fe3+	0.380
Fe2+	1.425
Mn	0.010
Mg	3.097
Ca	0.029
Na	0.063
K	1.667

Fe3+/(Fe3+ + Fe2+) = .210

APPENDIX E. NORMATIVE MINERALOGY OF MAJOR ROCK UNITS

Notes: These CIPW norms (wt. %) were determined from the analyses presented in Appendix A.2. Normative calculations for samples with a "V" prefix were performed for total Fe as Fe2O3; samples with a "CG79" prefix have a known oxidation state.

Abbreviations: Qz-quartz; Or-orthoclase; Ab-albite; An-anorthite; Co-corundum; Di-diopside; Hy-hypersthene; Wo-wollastonite; Ol-olivine; Il-ilmenite; Hm-hematite; Rt-rutile; Sp-sphene (titanite); Ap-apatite, Ne-nepheline; Mt-magnetite

(V-__)	Qz	Or	Ab	An	Co	Di	Hy	Wo	Ol	Il	Hm	Rt	Sp	Ap
3	17.6	36.0	30.8	5.6		1.0	1.5			0.2	5.4		1.6	0.3
9-4	13.0	37.0	39.5	4.8		0.8	0.5			0.2	3.4		0.6	0.1
26	21.3	22.7	37.8	12.7	0.1		2.0			0.1	2.8	0.3		0.2
32	7.1	40.1	34.1	6.9		1.8	1.0			0.3	7.0		1.3	0.3
40	26.7	19.5	34.9	11.8	1.2		2.1			0.1	3.2	0.2		0.2
62	2.6	31.6	43.3	8.0		4.0	0.2			0.3	7.4		1.7	0.7
74-1	6.8	20.2	38.7	20.2			5.9			0.2	6.1	0.2	1.2	0.4
112-1	27.8	34.6	30.5	4.5			0.5			0.1	1.8	0.1		0.2
113-1	15.5	28.3	35.9	12.4	0.3		3.0			0.2	3.9	0.3		0.3
119-1	14.8	32.1	34.7	3.3		0.7		3.2		0.7	10.0	0.6		
119-2	0.3	30.7	48.5	8.1		3.3	1.8			0.2	5.0		1.6	0.5
120	37.1	33.2	26.1	1.8	0.3		0.3				1.1			0.1
132-2	19.8	35.4	29.2	8.6	0.4	2.5				0.1	2.9		0.8	0.3
149		1.3	4.6	8.6		52.2	20.8		3.8	0.3	8.3			0.1
164	14.0	40.3	34.2	5.4		0.1	0.2			0.2	4.1		0.6	0.1
172	35.5	15.3	21.5	11.3	2.4		6.6			0.2	6.6			
178-1	0.4	5.5	14.5	30.9		14.7	10.7			0.5	18.4		3.8	0.5
192	34.8	26.5	26.7	7.9	1.2		1.0				1.6	0.2		0.1
193	9.5	13.9	45.7	24.5			2.7			0.1	2.8	0.5	0.2	0.2
193-3	23.1	25.1	29.6	14.6			3.2			0.1	3.4		0.6	0.3
194-3	12.7	18.8	40.3	17.9	0.5		4.1			0.1	4.5	0.8		0.4
207	28.2	24.6	18.7	8.7	3.7		8.4			0.2	6.9	0.7		0.2
211-1	42.9	17.5	18.3	6.6	2.1		5.7			0.1	5.1	1.5		0.2
213	38.1	14.0	19.6	10.4	1.9		7.7			0.2	7.4	0.7		0.1
220	24.2	25.6	13.7	13.7			3.3			0.1	2.9	0.1	0.6	0.3
225-2	6.5	42.1	36.7	5.7		1.5	0.3			0.2	5.4		1.2	0.2
226	15.9	35.4	31.7	6.9		0.3	2.2			0.2	5.5		1.4	0.5
237	12.9	15.2	39.1	19.5		1.6	4.7			0.2	5.3		1.0	0.4
243-3	20.5	34.9	33.5	5.3			1.0			0.1	3.6		0.7	0.3
257	14.3	33.2	31.3	8.2		1.2	2.2			0.2	6.9		2.2	0.5
257-6	12.6	38.7	37.2	4.8		0.9		0.5		0.2	4.3		0.8	0.1
255-1	22.8	26.5	36.5	7.9			1.9			0.2	3.4	0.4		0.4
255-2	33.1	32.2	29.3	3.3			0.2			0.1	1.6		0.2	
260	23.2	37.6	28.8	4.9		0.7	0.6			0.1	3.0		1.1	0.1
274-1	20.3	25.5	33.7	13.1	0.8		2.4			0.1	3.5	0.3		0.3
293	17.8	19.5	31.3	18.3			6.2			0.2	5.5	0.3		0.6
294	25.6	27.7	31.0	9.5	0.9		1.9			0.1	2.8	0.3		0.2
302-1	4.4	26.3	39.9	13.7		0.3	5.4			0.3	7.0		1.9	0.8
302-2		8.1	19.0	15.7		28.7	9.5		8.9	0.3	8.6		0.8	0.5
303	6.1	14.4	48.9	18.4		0.9	3.8			0.2	5.5		1.3	0.6
306	9.9	18.0	37.4	20.1		0.7	4.9			0.3	6.5		1.5	0.8

Appendix E (Continued)

	Qz	Or	Ab	An	Co	Di	Hy	Wo	Ol	Il	Hm	Rt	Sp	Ap
309	18.4	27.5	34.1	12.5	1.0		2.6			0.1	3.2	0.2		0.3
310-1	21.2	28.5	31.0	12.6	0.8		2.1			0.1	3.2	0.3		0.3
325-1	18.8	23.8	30.3	17.2	0.4		3.2			0.2	5.4	0.5		0.3
330	6.3	31.2	44.5	3.3		3.1		1.0		0.5	8.4		1.2	0.5
333-1	27.7	24.1	36.7	7.2	1.1		1.0			0.1	1.8	0.1		0.1
333-2	29.3	22.0	40.4	4.6	1.0		0.5			0.1	2.0	0.2		
340	29.0	24.1	33.8	8.0	1.4		1.3			0.1	1.9	0.2		0.1
341-2	14.9	33.3	32.1	4.4		0.5		3.0		0.6	10.3		0.9	0.1
385-1	33.7	33.9	25.1	4.9	0.1		0.2			0.1	2.0	0.1		
393-1	29.5	24.7	30.8	9.1	1.1		1.5			0.1	2.5	0.4		0.2
415	10.0	21.2	42.8	16.4	0.9		3.7			0.1	3.9	0.6		0.5
416-2	3.5	3.3	17.0	24.0		30.0	9.2			0.4	10.9		1.4	0.2
416-3		8.3	24.1	30.8		12.4	8.1		3.0	0.4	10.4		2.5	0.3
427	21.8	23.9	35.9	11.5	1.1		2.2			0.1	2.9	0.3		0.3
428	18.5	24.3	38.9	11.2	0.1		2.8			0.2	3.3	0.4		0.4
447-1	33.4	32.6	29.2	2.7			0.5			0.1	1.1		0.2	0.1
447-2	37.0	30.9	28.0	2.3			0.5			0.8		0.3	0.1	
450-2	10.8	39.0	39.7	2.7		1.7		0.3		0.4	4.4		0.8	0.2
453-1	8.6	13.6	34.3	21.3		5.6	6.5			0.3	7.5		1.5	0.8
497	5.7	19.6	34.6	17.8		2.2	6.9			0.3	9.2		2.4	1.2
505-1	3.3	7.4	23.7	24.3		5.8	14.0			0.4	15.2		5.1	0.9
505-2	2.7	6.9	23.7	27.1		4.4	14.8			0.4	14.5		4.6	0.9
506	12.9	21.2	36.9	15.9		2.4	3.8			0.2	5.0		1.1	0.5
519-1	2.3	8.1	25.2	18.7		6.4	13.3			0.6	17.2		6.7	1.6
519-2	4.2	9.0	24.4	19.0		6.4	11.2			0.5	16.6		6.8	1.9
526-1	25.1	18.2	30.1	10.5	0.3		2.1			0.1	3.0	0.4		0.2
526-2	22.4	31.1	31.3	9.8	0.1		1.8			0.1	2.8	0.4		0.3
535	12.8	33.3	42.4			0.5		3.4		0.4	6.8		0.5	
538	9.8	31.7	40.3	2.9		3.9	0.5			0.4	8.0		1.9	0.7
540	14.1	33.6	39.0	0.7		3.3				0.4	6.5		1.3	0.4
546-1	24.8	30.8	31.6	8.2	0.4		1.3			0.1	2.1	0.2		0.4
554-1	4.4	7.2	25.0	25.6		1.9	13.1			0.4	15.8		5.4	1.2
562		3.9	8.9	10.7		17.4	13.3		32.0	0.4	12.9	0.2		0.2
574-1	23.5	27.2	35.4	9.0			1.8			0.1	2.3	0.3	0.1	0.1
577-1	16.7	21.0	38.3	12.6		2.0	2.7			0.2	3.6	0.7		0.3
579-1	23.8	18.3	23.6	12.1	1.1		10.3			0.2	9.8	0.9		
581-1		10.3	24.8	30.4			2.0	13.1	0.4	0.3	12.8		3.8	2.1
585	14.5	18.4	34.5	19.2			5.9			0.2	5.5	0.3	1.0	0.6
586	15.6	19.8	31.6	17.2		2.1	5.9			0.2	5.8		1.2	0.6
588-1	30.1	7.2	34.1	23.3			2.0				2.7	0.1	0.5	
597-1	17.2	34.1	37.4	5.5		0.5	1.1			0.1	2.7		0.9	0.4
597-8	3.1	16.9	32.2	21.3		3.8	8.9			0.3	9.8		2.5	1.1
628	23.0	28.8	37.1	6.4		0.7	0.9			0.1	2.1		0.7	0.1
629-2	17.8	36.7	31.8	3.4		2.1		1.1		0.2	5.7		1.1	0.2
670	0.7	8.9	32.7	36.6		3.0	5.6			0.2	8.0		2.2	2.0
687	2.9	14.4	47.9	22.8		0.4	4.5			0.2	4.9		1.2	0.9
711-2	29.2	27.1	29.7	9.5	0.3		1.5			0.1	2.1	0.3		0.2
725	28.2	30.5	32.0	5.6	0.3		1.1			0.1	1.8	0.2		0.2
726	15.6	23.9	37.3	13.2		1.0	3.6			0.2	4.1		0.8	0.5
727	10.5	38.7	33.9	9.7		0.2	2.8			0.1	3.0		0.7	0.3
728	18.1	19.5	36.9	15.8			4.1			0.2	4.3	0.1	0.6	0.4
730	20.3	22.9	33.9	14.3			3.8			0.2	3.8	0.3	0.1	0.4
731	18.7	17.1	38.0	16.4		0.1	4.0			0.2	4..3		0.8	0.5
732	27.3	27.1	33.6	7.9	0.1		1.5			0.1	2.0	0.2		0.1
734-1	23.8	25.5	35.6	9.5	0.1		2.2			0.2	2.7	0.3		0.2
735	30.8	27.1	32.5	6.1			1.3			0.1	1.5	0.2	0.2	0.1
737	3.9	32.4	42.2	2.9		4.3	0.9			0.5	9.4		2.6	0.9
743-2	5.8	9.9	31.9	28.4			9.5			0.2	9.3	0.4	2.6	2.0
759	20.4	28.3	33.8	10.1			2.5			0.1	3.5		1.1	0.2
760	8.9	24.4	39.6	12.9		2.1	4.0			0.3	5.7		1.6	0.6
762	15.8	23.0	34.2	13.2		1.6	4.4			0.2	5.3		1.6	0.7
763-2	7.6	14.6	34.5	20.0		7.2	6.4			0.3	7.6		1.0	0.7
765	5.9	12.2	34.1	21.3		9.0	6.8			0.3	8.3		1.4	0.8
766	24.4	26.3	34.7	8.1		0.9	1.8			0.1	2.9		0.5	0.2
768	4.5	6.3	16.5	28.1		18.2	17.3			0.3	8.4		0.4	0.1
772	14.1	16.9	44.4	14.8			3.4			0.3	4.8	0.5		0.4
774	7.8	16.3	36.3	19.5		3.7	6.6			0.2	7.4		1.5	0.6
776	14.2	38.3	36.9	3.7		0.7		1.3		0.2	4.3		0.5	

Appendix E (Continued)

(CG79-___)	Qz	Or	Ab	An	Ne	Co	Di	Hy	Wo	Ol	Mt	Il	Hm	Rt	Sp	Ap
243-3	20.5	34.9	33.5	5.3				1.0				0.1			0.7	0.3
263	19.1	28.8	41.7	3.2			1.7	3.8			0.9	0.9				
300	18.9	34.9	39.3	2.4			1.9	1.4			0.8	0.5				
311	24.0	34.2	34.2	2.7			1.5	2.0			0.8	0.5				
329		1.9	5.7	14.0	0.4		45.2			29.5	2.2	1.0				
339	14.9	10.3	28.3	26.9			2.5	11.2				0.6	3.3		1.2	0.8
344	16.6	24.2	36.5	13.6				4.0			2.3	0.8				1.0
366	27.8	26.6	33.2	8.2				2.6			0.8	0.5				0.1
377	24.5	22.8	36.8	11.0				3.3			0.9	0.6				0.2
395	5.2	14.0	34.6	21.3			8.4	10.2			4.3	1.3				0.7
753	5.2	17.8	36.2	19.2			6.3	10.4			2.9	1.3				0.7
757	4.7	23.1	38.9	11.5			6.9	8.6			4.6	1.3				0.5